A LINE-SOURCE METHOD FOR THE MEASUREMENT OF TEMPERATURE AND PRESSURE DEPENDENCE OF ROCK THERMAL CONDUCTIVITY

by

Alvise Sartori

A thesis submitted for the degree of Doctor of Philosophy of the University of London.

Geology Department
Imperial College
London S.W. 7

October, 1983.

A LINE-SOURCE METHOD FOR THE MEASUREMENT OF TEMPERATURE AND PRESSURE DEPENDENCE OF ROCK THERMAL CONDUCTIVITY

Abstract

A transient method for accurate laboratory measurements of the temperature and pressure dependence of the thermal conductivity and diffusivity of crystalline rocks and other poor conductors is described. The method involves heating a cylindrical sample by a thin axial heater wire, and monitoring the resulting temperature increase at points within the rock by a microcomputer. The temperature and pressure dependence of the thermal parameters is investigated by allowing the samples to reach thermal equilibrium in an oven or autoclave before commencing measurements.

Several line-source solutions to the heat equation were derived from a rigorous study of the boundary conditions to provide an accurate description of the temperature field within the rock. A nonlinear least-squares fit of the theoretical results to the experimental data yields absolute values of rock conductivity and diffusivity, and requires no calibration against standard materials.

Conductivity values of several rock specimens and two standard materials are presented in the temperature range 250-570 K. They exhibit the expected temperature dependence and show good agreement with conductivities from a steady-state apparatus at room temperature and with published results for similar types of rock over the whole temperature range. A discussion of the errors and accuracy of the results is given. The results of investigations of rock dehydration during high-temperature measurements and the pressure dependence of granites in the range to 50 MPa are discussed.

ACKNOWLEDGEMENTS

I gratefully acknowledge the assistance of the following during the preparation of this thesis:

Mr. J. Wheildon, the project supervisor, for constant guidance and support.

Dr. A. Thomas-Betts for many useful dicussions and patient reading of the thesis drafts.

Dr. M.F. Francis, Mr. J. Ellis and my contemporaries at the Geophysics Section of the Royal School of Mines for their co-operation.

Mr. N. Bassett, Mr. A. Cheyne, Mr. A. Jackson, Mr. J. Robinson, Mr. K. Jason, Mr. K. Zapalowski, Mr. A. Cameron and Mr. M.A. Adam for much experimental work on the line-source.

Mr. K. O'Hara for counsel about electronics.

The workshop and technical staff of the Geology Department for undertaking many "rush" jobs.

The Department of Mineral Resources Engineering of Imperial College for the use of their high-pressure facilities.

Dr. J. Tester of the Los Alamos Scientific Laboratory for the preparation of two rock samples.

Dr. J.K. Hawkes of the Institute of Geological Sciences for the analysis of the granite samples.

My family for financial and moral support.

Brigitte and Caterina Bluemel for continuous encouragement.

The Society of Exploration Geophysicists for financial backing.

TABLE OF CONTENTS

LIST OF FIGURES

LIST OF TABLES

Chapter 1

INTRODUCTION

1.1 Background.

Hot Dry Rock (HDR) technology requires detailed information on the dependence of the thermal properties of crustal crystalline rocks on temperature, pressure, moisture and mineralogy up to depths of the order of 5 Km. For a given regional heat flow, the crustal thermal conductivty controls the geothermal gradient. Thus the drilling depth required to reach a rock at a given temperature will vary in direct proportion to the mean thermal conductivity of the formation (Wheildon et al., 1980).

In the course of an investigation of the S.W. England thermal anomaly zone by this Department, Francis (1980) calculated a set of extrapolated crustal temperature profiles (Fig. 1.1) based on observed surface values of conductivity for a typical Cornish granite with two different published values for the temperature dependence of conductivity of Westerly and Rockport granites (Birch and Clark, 1940). It will be noticed that for formation temperatures of 180-230 ^{o}C suitable for power production the drilling depth is critically dependent on the temperature dependence of the conductivity. Because drilling costs increase exponentially with depth (Sibbitt et.al, 1979), thermal conductivity characteristics are important in determining costs associated with developing a reservoir. In the performance modelling of a HDR reservoir,

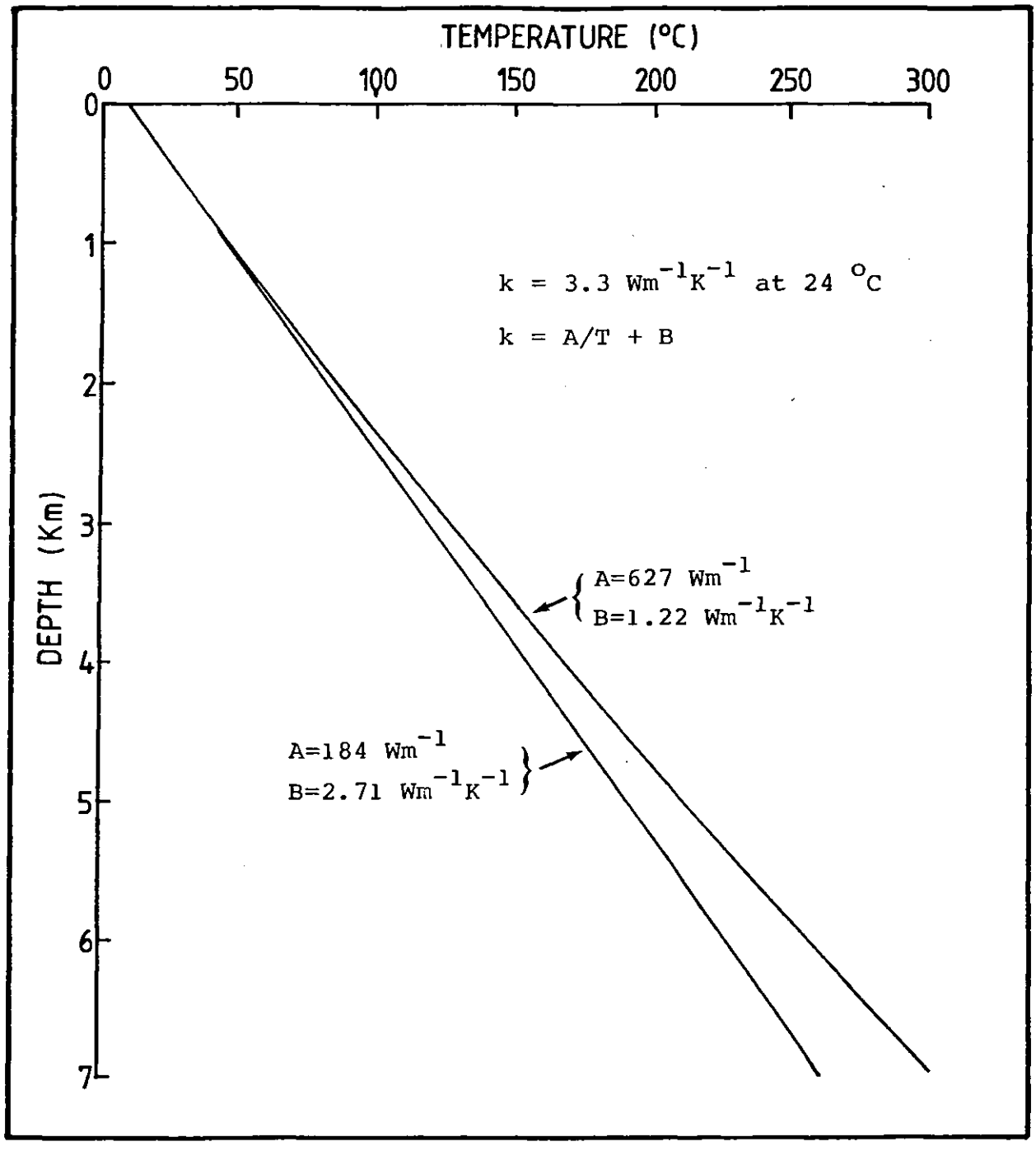

Fig. 1.1 Crustal temperature profiles for exponential function heat-production model and temperature-dependent thermal conductivity. From Francis (1980). The temperature dependence values are from Birch and Clark (1940).

the thermal conductivity will strongly affect the maximum rate of heat extraction, the depletion rate and hence the lifetime of the reservoir.

1.2 Measurement techniques.

The objective of the present work was to develop a simple line-source method for fast measurements of rock thermal conductivities over a range of ordinary and elevated temperatures and pressures. The stimulus to the research was mainly due to previous work on the line-source in this Department by Cheyne (1978), Jackson (1978), Robinson (1979), Bassett (1979), Jason (1980), Zapalowski (1980) and Cameron (1981).

The line-source method was first used by Van der Held and Van Drunen (1949) and Van der Held **et al.** (1953) for the measurement of thermal conductivity of liquids, and later developed, among others, by Jaeger and Sass (1964), Scott **et al.** (1973), Cull (1974), Kieffer **et al.** (1976) and Arakawa and Shinohara (1980).

The present method employed the sample geometry suggested by Cull (1975). Cylindrical samples of rock, which had reached thermal equilibrium in an oven, were heated by means of a thin axial heater wire. The resulting transient temperature increase at points inside the rock was detected by a thermocouple and interpreted to yield values of thermal conductivity and diffusivity. In the development of the method an attempt was made to overcome some of the shortcomings of well-established divided-bar (Beck,1957) and needle-probe methods (Von Herzen and Maxwell, 1959, Woodside and Messmer, 1961), such as the

need for carefully characterized reference materials over wide temperature and pressure ranges. In the present method, absolute values of the thermal paramenters are obtained, thus no calibrations being required. The expensive drilling of long and narrow holes in the crystalline samples needed to accommodate needle-probes was avoided, and the reduced thickness of the heater contributed to minimizing contact-resistance effects. Large specimens could be investigated, thus decreasing grain-size related inaccuracies. The simultaneous determination of conductivity and diffusivity provided a self-checking property in that both these must be of reasonable orders of magnitude.

Some of the difficulties previously encountered in transient thermal conductivity measurements were overcome as follows:

1) Modern analogue and digital techniques were used to perform the relatively fast and accurate measurements of sensor temperature required by all transient methods.

2) New mathematical models were developed to represent accurately the temperature fields within the rock samples. In particular, the thermal contact-resistance between heater and rock had to be investigated in detail.

3) The collection and reduction of the large data samples, a considerable source of error in previous studies, was simplified by the use of a microcomputer, with the added advantage of immediate computation of results.

A short description of this line-source method is given in a paper by Sartori and Francis (1982), reported in

Appendix VI. For a comprehensive account of thermal conductivity measurement techniques see Tye (1969). Various techniques for in situ conductivity and diffusivity measurements are given in Beck **et al.** (1971), Murphy and Lawton (1977) and Lee (1982).

1.3 Units and nomenclature.

Unless otherwise stated, S.I. units will be used throughout this thesis. Table 1.1 gives a list of the most commonly used symbols and their meanings. The occasional departures from this nomenclature will be made explicit in the text.

TABLE 1.1 Nomenclature.

Unless otherwise stated, the following symbols will be used throughout the text:

c	Specific heat capacity
$-Ei(-x)$	Exponential integral
h	Thermal diffusivity
I_n	Modified Bessel function of the first kind and order n
j	Euler's constant
J_n	Ordinary Bessel function of the first kind and order n
k	Thermal conductivity
K_n	Modified Bessel function of the second kind and order n
$L\{f\}=\bar{f}$	Laplace transform of function f
p	Laplace transform variable
Q	Line-source linear power
r	Radial coordinate
t	Time
T	Absolute temperature
v	Temperature rise
$\bar{v}$	Laplace transform of temperature
Y_n	Ordinary Bessel function of the second kind and order n
α	$=r^2/4ht$
ρ	Density

Chapter 2

HEAT CONDUCTION THEORY

The thermal conductivity coefficient k of a solid is most easily defined with respect to the steady-state flow of heat down a long rod with a temperature gradient dT/dx:

$$q = - k \, dT/dx \qquad (1)$$

where q is the flux of thermal energy, or the energy transmitted across unit area per unit time. The thermal diffusivity h is then defined by

$$h = k/\rho c \qquad (2)$$

where ρ is the density and c the heat capacity. c and ρ are not constant for a given material, and their temperature and pressure dependence must be taken into account when applying equation (2).

2.1 Crystalline solids.

The physical mechanisms controlling the transfer of heat in earth materials at normal and elevated temperatures are phonon diffusion, radiation and electron processes. Heat transfer by radiation follows a T^3 relationship (Clark, 1957) and can be assumed to be negligible compared to conduction up to temperatures of about 800 K (Sibbitt, 1979). At the temperatures normally encountered in the upper crust, free electrons do not significantly contribute to transport mechanisms, as testified by the small electrical conductivity of crustal rocks.

In modern solid-state theory, a dielectric solid is regarded as a lattice of closely-coupled atoms. An increase

in vibrational energy in one part of a crystal, associated with an increase in temperature, will be transmitted to the other parts. Heat is here considered as being transmitted by phonons, which are the quanta of energy associated with of the atomic lattice vibration modes.

From the kinetic theory of gases applied to the phonon quasi-particles, the following expression for the thermal conductivity is found (see for example Kittel, 1976):

$$k = \frac{1}{3} cvl \ , \qquad (1)$$

where c is the lattice heat capacity per unit volume

v is the average particle velocity (velocity of sound)

l is the mean phonon free path.

A study of the absolute value of k and its dependence on temperature and pressure requires a knowledge of the parameters v,c,l in equation (1): the velocity v can be assumed to be almost constant (Rosenberg, 1975). The heat capacity c is given to a good approximation by the Debye specific heat function (Kittel, 1976). c is plotted against T/θ in Fig. 2.1, where θ is the Debye temperature, a constant for a given material. At high temperatures, c tends to the constant Dulong-Petit value of 3Nk where N is Avogadro's number and k the Boltzmann constant. It should be noted, however, that θ for Si is about 640 K, so that at normal temperatures the value of c has a slight positive dependence on T. The estimation of the phonon mean free path is complex and requires considerable analysis of phonon scattering mechanisms. These include interaction of phonons with one another (u-processes), scattering by point

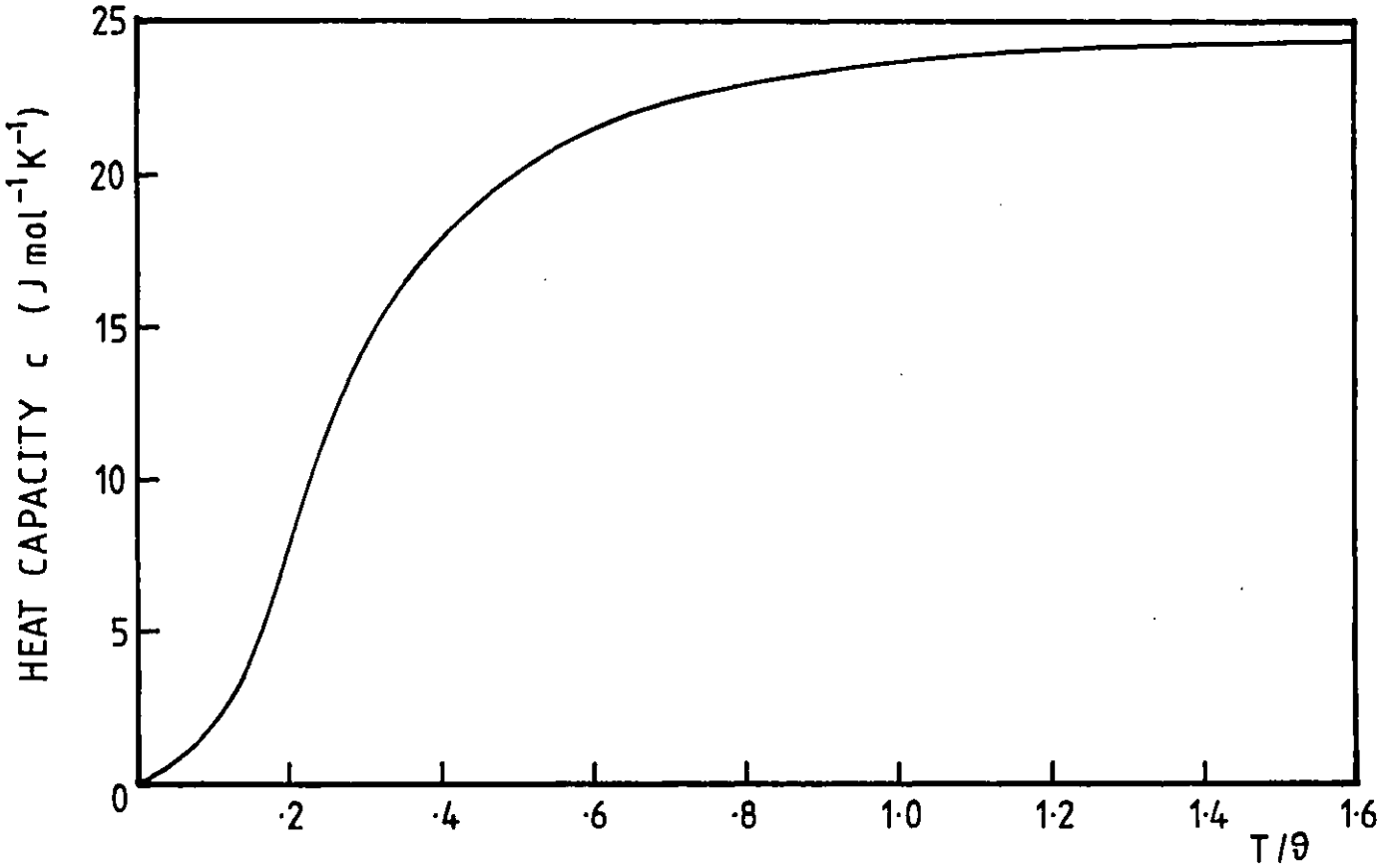

Fig. 2.1 Heat capacity c of a solid according to the Debye approximation. The horizontal scale is the temperature normalized to the Debye temperature θ. The asymptotic value at high values of T/θ is 24.943 J $mol^{-1}K^{-1}$.

defects (impurities) or dislocations and scattering by the boundary of the specimen or crystallite.

Three-phonon interactions are dominant in rock specimens at high temperatures. In this case the conservation laws for the combination of phonons are

$$h\omega_1 + h\omega_2 = h\omega_3 \qquad \text{(energy conservation)} \qquad (2)$$

$$K_1 + K_2 = K_3 + G \qquad \text{(momentum conservation)} \qquad (3)$$

where the w's are the phonon frequencies, the K's the wavevectors $K=2\pi/\lambda$, λ is the phonon wavelength and h the Planck constant. The reciprocal lattice vector G expresses the periodic nature of the lattice, where a phonon with wavevector K is physically equivalent to a phonon with wavevector K+G. The mechanism described by equations (2) and (3) is called an umklapp, or u-process. It causes a reversal of energy flow after a collision (Fig. 2.2), which gives rise to a thermal resistance. Normal or n-processes, in which G=0, also play an important role in establishing thermal equilibrium, but they do not directly contribute to heat conduction.

The probability for the occurrence of a u-process increases with increasing phonon energy and therefore with increasing temperature. At high temperatures, when $T \sim \theta$, nearly all the phonons will have large enough wavevectors to produce u-processes, and the probability will then be proportional to the total number of phonons which are present, which is in turn proportional to T. Hence $l \sim 1/T$, and, substituting in equation (1), we get $k \sim 1/T$.

More rigorous estimates give the conductivity in the form

$$k \propto M a \theta^3 / T \gamma^2 \ , \qquad (4)$$

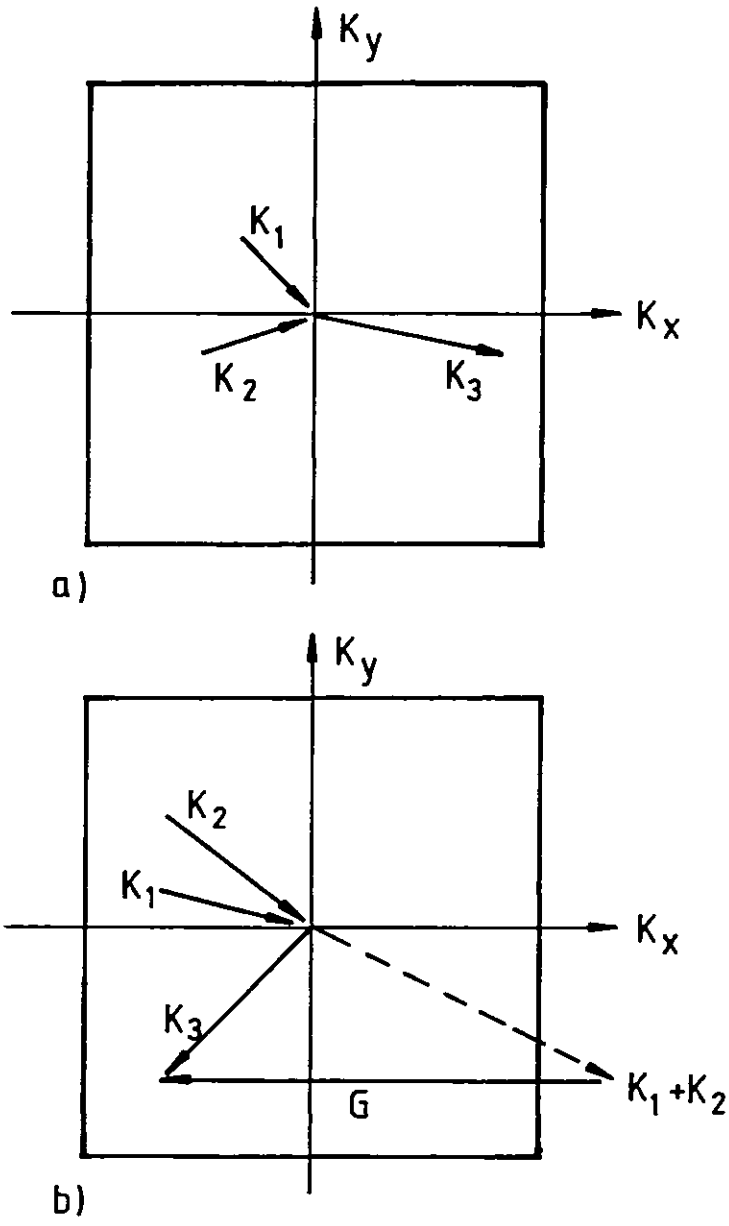

Fig. 2.2 (a) Normal and (b) umklapp phonon collision processes in a two-dimensional square lattice. The square in each figure represents the first Brillouin zone in the phonon K-space; this zone contains all the possible independent values of the phonon wavevector. Note that in the umklapp process (b) the direction of the x-component of the phonon flux has been reversed.

where a^3 is the volume occupied by one atom, M is the atomic weight and γ is the Grueneisen constant. This simple dependence on the properties of a crystal has been deduced, with different constants of proportionality, by many workers (see Berman, 1976). Its experimental applicability to earth materials was confirmed by Birch and Clark (1940), as shown in Fig. 2.3.

Roufusse and Clemens (1974) argued that the phonon mean free path cannot become arbitrarily short as the temperature is increased, but should instead approach a lower limit l_o, which one would expect to be comparable with the linear dimensions of the unit cell of the crystal lattice. The transition from the 1/T dependence to the minimum conductivity is, however, very gradual, and in most minerals it should set in at temperatures above 500 K. Deviations from the inverse temperature dependence would be expected to be appreciable only above 1500 K.

The absolute value of k was calculated by Slack (1977) for crystals with more than one kind of atom and more than one atom per primitive unit cell:

$$k = \frac{3.0 \times 10^{-5} \bar{M} a \theta_o^3}{\gamma^2 n^{2/3}} \qquad (5)$$

where $\bar{M}$ is the mean atomic weight of all the costituent atoms, n is the number of atoms per unit primitive cell, a^3 is the average volume of one atom, and θ_o is the Debye constant taken from low-temperature heat capacity measurements. The agreement with experimental values is fairly good. For quartz (n=9), the calculated and measured thermal conductivities are 20 and 13 $Wm^{-1}K^{-1}$ respectively.

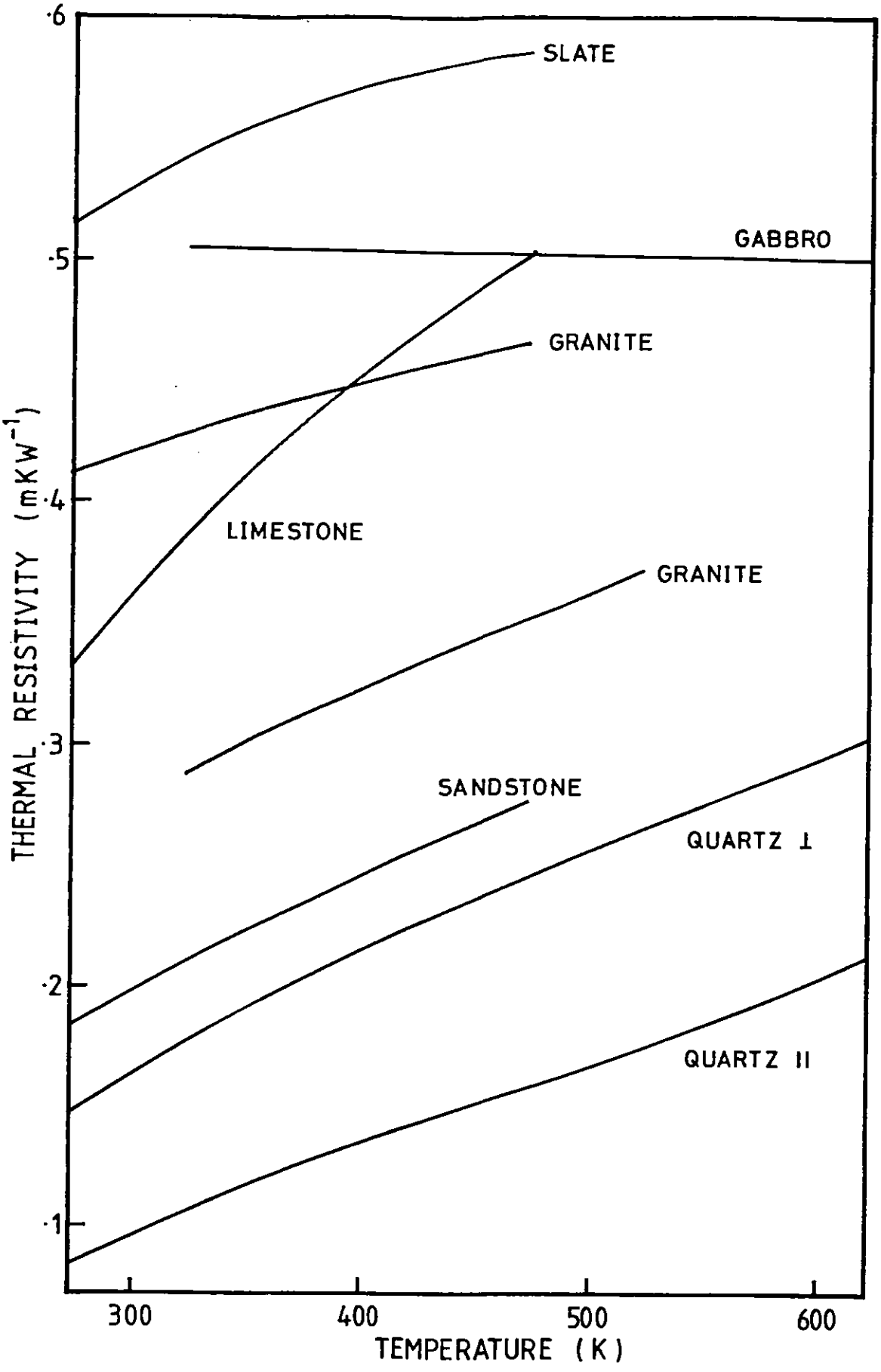

Fig. 2.3 Thermal resistivity (=1/k) of rocks and crystalline quartz. Data from Birch and Clark (1940).

Mooney and Steg (1969) used an equation of the same form as (4) to estimate the pressure dependence of k at high temperatures. The expression they derive, however, is of limited use here as it depends on values for the Grueneisen parameter and its dilatational derivative which are not readily available. The order of magnitude of the expected pressure dependence is best estimated from previous experimental work. Kieffer (1976) reports a measured value of $+1.7 \times 10^{-4}$ MPa^{-1} for the fractional P-dependence of conductivty of crystalline quartz.

The results quoted so far apply only to very pure crystals. In earth materials the conductivity is further affected by phonon scatter from grain boundaries and lattice defects such as point defects and dislocations. Callaway and von Bayer (1960) estimated these effects for small defect concentrations at $T>\theta$ and obtained an expression of the form

$$W = W_{ph} + W_I \qquad (6)$$

where $W=K^{-1}$, and W_{ph}, W_I are the phonon and defect contributions. Cull (1975) used this equation to estimate the pressure dependence of k in olivine with arbitrary defect concentrations of 10 and 50%, and found that the pressure derivative of k was little decreased from the value obtained for a pure crystal.

2.2 Amorphous solids.

It was suggested by Berman (1976) that amorphous solids such as vitreous silica or nylon are ideally suited as thermal conductivity standards because the values found are little dependent on the particular sample used. Kittel (1949) pointed out that the conductivity of glasses decreases with decreasing temperature and that there is much less difference between the conductivities of amorphous solids than there is between the conductivities of crystals.

The temperature dependence of thermal conductivity of amorphous solids can be explained with reference to their molecular structure. The solids considered so far have been crystals which were nearly perfect or contained imperfections within such limits that there was still an underlying regularity in the lattice. In amorphous solids, however, there is no long-range order in the atomic structure (Fig. 2.4). For short wavelengths, the mean free path of equation 2.1(1) is constant because it is limited to the dimensions of the structural atomic units (unit cells) which are of the order of tenths of nanometers. At high temperatures, therefore, the conductivity follows the specific heat and decreases with decreasing temperature. This is in agreement with experimental measurements on fused quartz (Ratcliffe, 1959) and with the results of chapter 5 for fused silica and a ceramic sample.

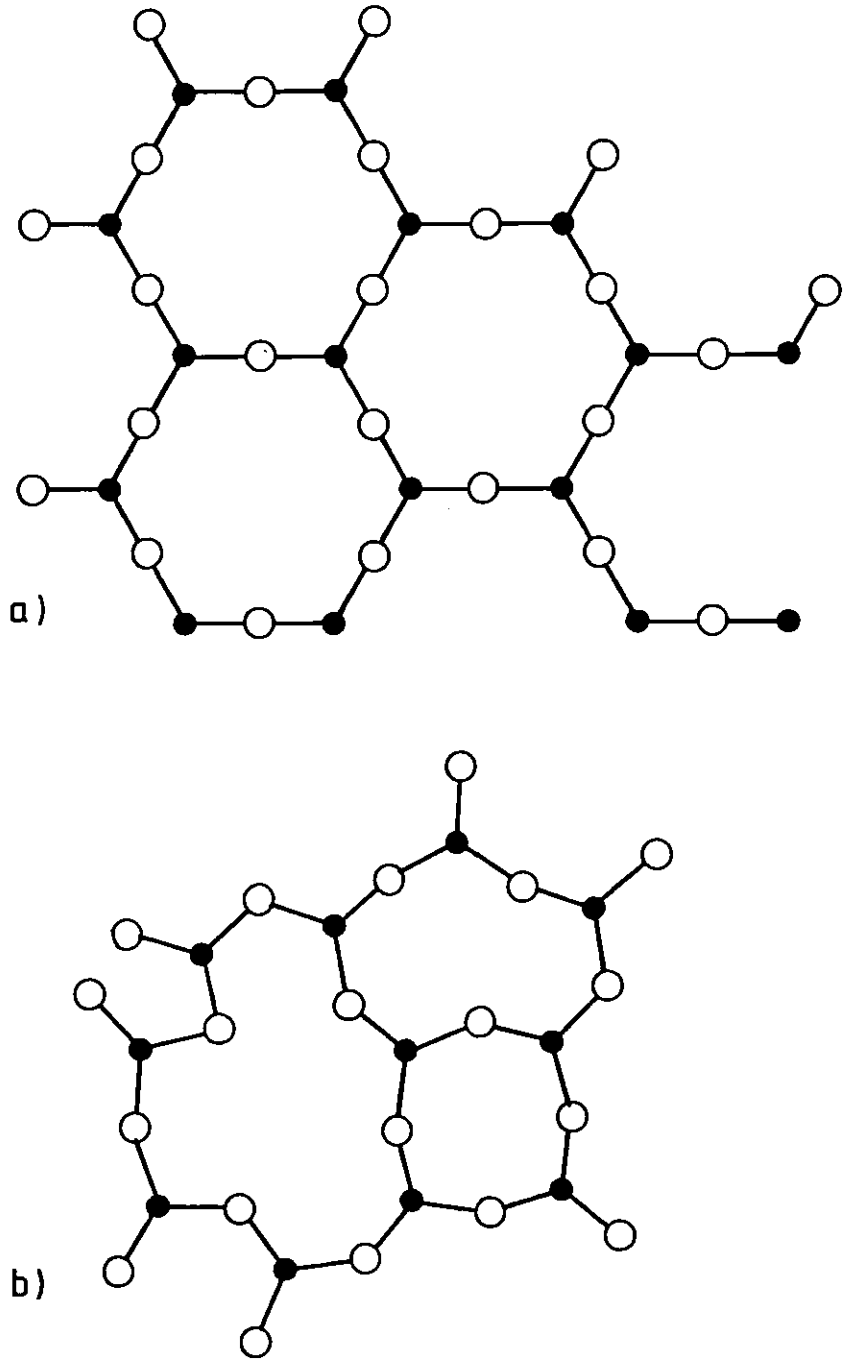

Fig. 2.4 Schematic two-dimensional figures illustrating the difference between a) the regularly repeating structure of a crystal and b) the random network of a glass (From Kittel, 1949).

2.3 Porosity effects.

The problem of relating laboratory conductivity measurements to the in situ values was first analyzed by Clark (1941), who investigated the effects of water saturation and uniaxial compression on a set of samples of widely different porosities. He observed conductivity variations of up to 30% in high-porosity samples, and up to 13% even in a 1.1% porosity marble sample. Even larger variations were reported by Woodside and Messmer (1961) for highly porous rock. Walsh and Decker (1966) made a detailed study of the relationship between porosity, water saturation and confining pressure in compact rock. Some of their conclusions will be summarized here. Two types of cavities can be distinguished in low-porosity rocks. approximately spherical cavities have a negligible effect on the conductivity for porosities of a per cent or so. The elastic behaviour of low-porosity rocks, however, suggests that a large part of the porosity is in the form of very narrow crack-like openings along grain boundaries or cleavage planes which close under external compressive stress. Because of the narrowness of the cracks, many may be required to account for a porosity of even 1%.

To establish the effect of pore fluid, we must find the effective conductivity of a composite material with two isotropic phases, rock and pore fluid. A maximum bound for the effective conductivity k_e of a system composed of a rock matrix of conductivity k and porosity $\eta << 1$, and a fluid of conductivity k' can be estimated from:

$$\frac{k-k_e}{k-k'} = \frac{\eta}{3\epsilon} \qquad (1)$$

where $\varepsilon = k'/k << 1$. Equation (1) describes the system shown in Fig.2.5a, where the solid phase is considered as inclusions in the continuous fluid phase; Fig. 2.5b shows the opposite limiting case in which the fluid is an inclusion of the solid. A more realistic model would be represented by an intermediate case where both rock and fluid form continuous phases. Equation (1) always overestimates the effect of pore fuid: for better accuracy the total porosity η is replaced by the porosity η_c due to cracks. The value of the crack porosity can be found from a plot of the volumetric strain $-\Delta V/V_o$ of a jacketed sample as a function of pressure p. As shown by Walsh (1965) the crack porosity is the intercept on the $\Delta V/V_o$ axis of the linear portion of the pressure-strain curve extrapolated to zero pressure.

A more rigorous study which takes into account a distribution of penny-shaped cracks of various dimensions leads to an improved estimate

$$\frac{k-k_e}{k-k'} = \frac{R\eta_c}{3\varepsilon} \qquad (2)$$

where R is a function of the crack distribution and can be determined experimentally from pressure-volumetric strain curves. Walsh and Decker analyzed two granite samples from Casco, Maine. The results are reported in Table 2.1. Both equation (1) with the value for the crack porosity and equation (2) give deviations in agreement with experimental values for dry samples. For water-saturated samples, the deviations are negligible when compared to the experimental errors.

The pressure dependence of the effective conductivity can be determined from Fig. 2.6, where the intercept η_{c1}

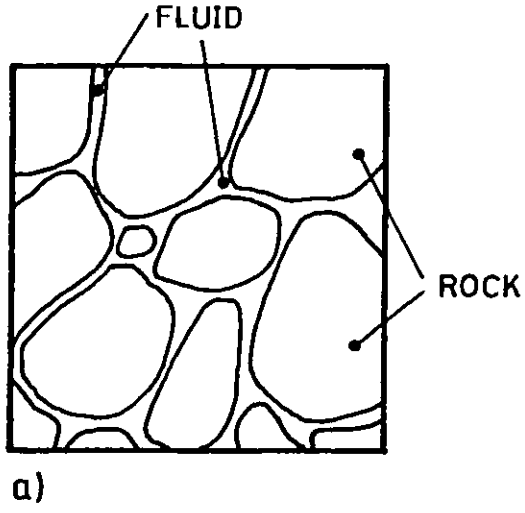

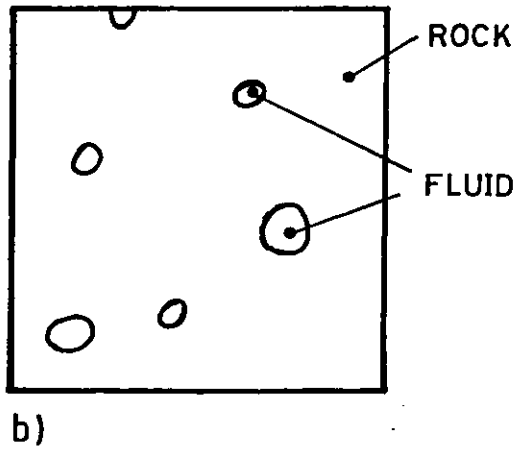

Fig. 2.5 Pore fluid models (from Walsh and Decker, 1966). In a) the pore fluid and in b) the rock form a continuous phase.

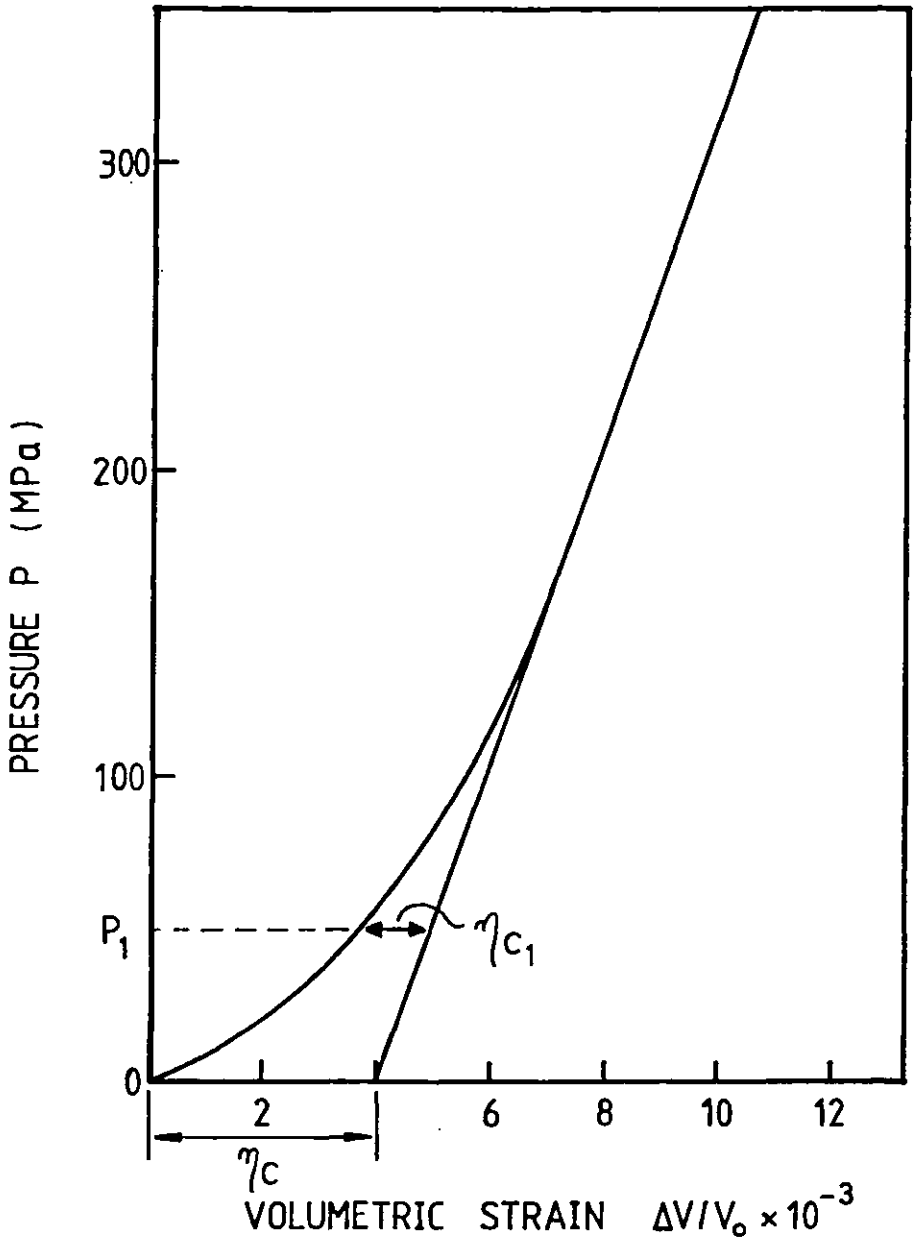

Fig. 2.6 Crack porosity found from pressure-strain data for Casco granite (From Walsh and Decker, 1966). The crack porosity at pressure P_1 is the intercept η_{c1}.

represents the residual crack porosity at pressure P_1. The value η_{c1} is then substituted in equations (1) or (2) to give an estimate of the porosity correction.

TABLE 2.1 Effect of porosity on measured conductivity of granite.

		Dry samples	Wet samples
Equation (1)	η=.007	$\frac{k-k_e}{k_e-k'}$ = 29.5%	1.2%
" "	$\eta=\eta_c$=.004	17	.7
Equation (2)	R=0.86	14.5	.6
Experimental value	1	16	-
" "	2	13	-

The following conductivity values were used:

k(granite)= 3.35 $Wm^{-1}K^{-1}$
k'(air) = 0.026
k'(water) = 0.63

Chapter 3

MATHEMATICAL THEORY

3.1 Introduction.

This chapter presents solutions of the heat equation and techniques for the computation of thermal constants of rock samples from transient measurements of temperature.

It was felt that existing treatments of the problem could not achieve the accuracy required in the present experiments. Much of the theoretical background to the problem has been developed for needle-probe systems having geometries considerably different from the present one (cf. Blackwell, 1954). In particular, the thin heater used here required different sets of boundary conditions in the mathematical solutions. The availability of microcomputers for the fast computation of large data samples allowed a departure from previous "straight line" approaches in which the mathematics is simplified as much as possible in order to make calculations of the thermal constants more manageable. Fairly complex, nonlinear equations could thus be used to represent the temperature fields, resulting in a higher accuracy.

After a cursory presentation of the heat equation and of the theory of the Laplace transform, the main line-source solution is derived in section 3.3. This solution was found to be sufficiently flexible to accurately represent the physical situation, and at the same time simple enough to be manipulated by a microcomputer. Various corrections to this basic equation are then presented in sections 3.4 to 3.8, wich are shown to impose intercorrelated constraints

on the minimum and maximum data-acquistiton times (the sampling window), the diameter and length of the samples, the dimensions of the heater wire, and the amount of permissible contact resistance (in the form of thermal grease, high-temperature cement or adhesive between heater and rock). A nonlinear least-squares method for fitting the equations to the experimental results is then presented in seciton 3.10.

A flowchart highlighting the relationship between the sections of the chapter is shown in Fig.3.0. Readers not interested in the details of the mathematical derivations are referred to section 3.11 for a qualitative account of the results quoted in this chapter.

3.2 The heat equation.

In an infinite isotropic solid of diffusivity h and conductivity k the temperature v satisfies the equation of conduction of heat

$$\nabla^2 v - \frac{1}{h}\frac{\partial v}{\partial t} = -\frac{A}{k} \qquad (1)$$

where A is the heat productivity within the solid, and $h=k/\rho c$, with ρ as the density and c as the specific heat capacity per unit mass of the solid (Carslaw and Jaeger, 1959 - for compactness referrd to as C.J. in the remainder of this chapter). If the heat productivity within the solid is assumed to be zero, equation (1) takes the form

$$\frac{\partial^2 v}{\partial x^2} + \frac{\partial^2 v}{\partial y^2} + \frac{\partial^2 v}{\partial z^2} = \frac{1}{h}\frac{\partial v}{\partial t} \qquad (2)$$

in Cartesian coordinates and

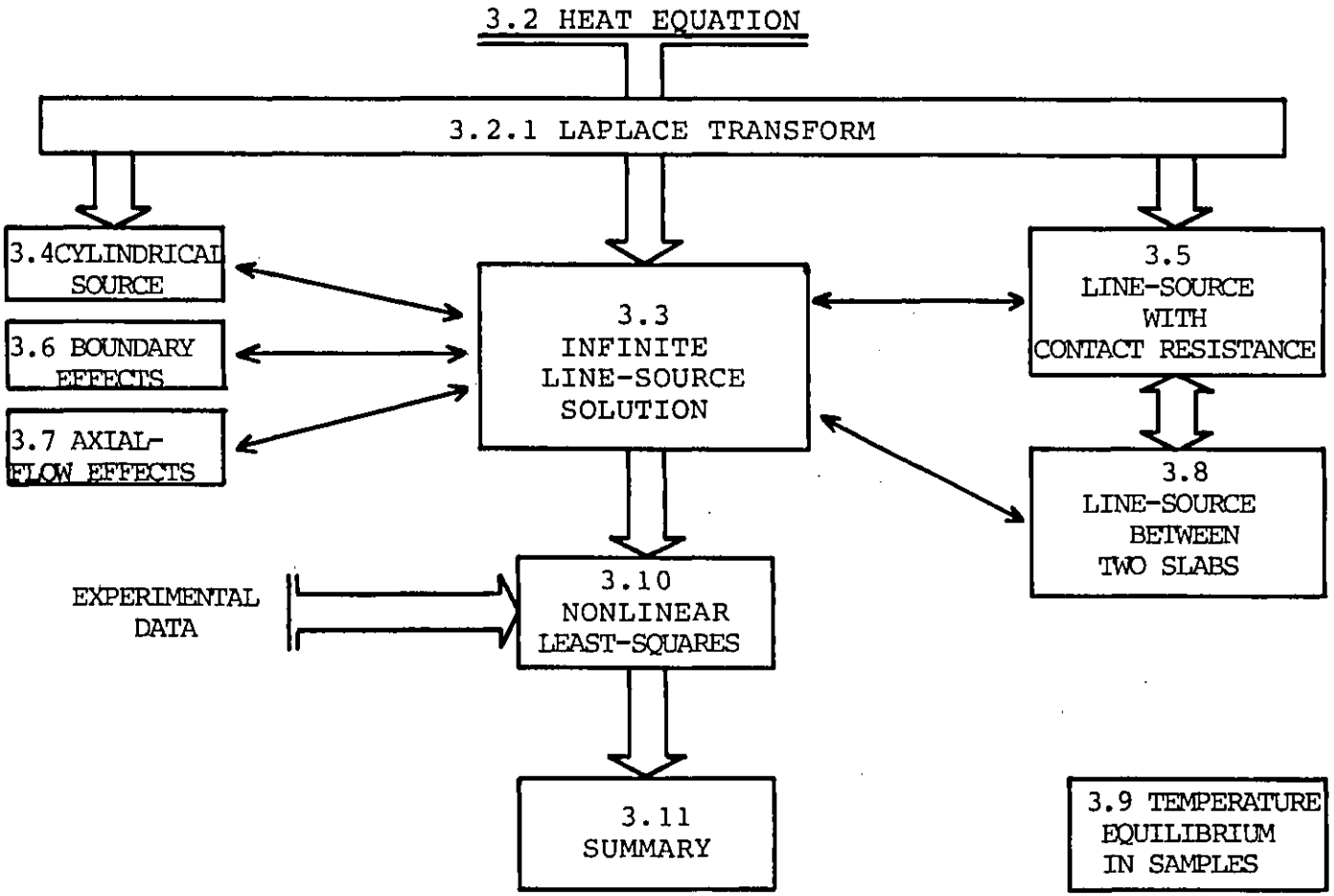

Fig. 3.0 Flowchart of chapter 3.

$$\frac{\partial^2 v}{\partial r^2} + \frac{1}{r}\frac{\partial v}{\partial r} + \frac{1}{r^2}\frac{\partial^2 v}{\partial \theta^2} + \frac{\partial^2 v}{\partial z^2} = \frac{1}{h}\frac{\partial v}{\partial t} \qquad (3)$$

in cylindrical polar coordinates, where r and θ are the radial coordinate and the azimuth angle respectively. The parameters k and h will be assumed constant for any constant value of the ambient temperature. This is not strictly justified as any transient measurement necessarily raises the temperature of a sample, but it simplifies the mathematical treatment. Also, if the heating of the samples is kept small during measurements, the variations in the parameters will be negligible.

In obtaining the subsidiary equations and their boundary conditions (see section 3.2.2), assumptions as to the commutability of certain operators have to be made, so that the solutions obtained in this chapter are not rigorous and must be regarded as purely formal. Strictly speaking, it must be verified that the solutions do satisfy the original differential equations and boundary conditions (Carslaw and Jaeger, 1940). However, the solutions were considered adequate for the purpose of this study.

3.2.1 The Laplace transformation.

In the solution of the heat equation, extensive use will be made of the Laplace transformation defined by

$$L\{v(x,y,z,t)\} = \bar{v}(x,y,z,p) = \int_0^\infty e^{-pt}\, v(x,y,z,t)\,dt \qquad (1)$$

where p is a number with a positive real part and large enough to make the integral in (1) convergent. For example, to solve the partial differential equation in two variables

$$\frac{\partial^2 v}{\partial x^2} - \frac{1}{h}\frac{\partial v}{\partial t} = 0 \qquad (2)$$

the Laplace transformation is applied to (2) to get the "subsidiary" equation

$$\frac{d^2\bar{v}}{dx^2} - \frac{p}{h}\bar{v} = 0 \quad , \tag{3}$$

an ordinary differential equation. Solving (3) subject to the appropriate boundary conditions yields $\bar{v}(x,p)$. $v(x,t)$ can then be found:

1) from tables of transforms (e.g. Bateman Manuscript Project, 1954)

2) by using the inversion theorem of the Laplace transformation

$$v(t) = 1/(2\pi i)\int_{\gamma-i\infty}^{\gamma+i\infty} e^{\lambda t}\,\bar{v}(\lambda)\,d\lambda \tag{4}$$

where γ is to be so large that all the singularities of $\bar{v}(\lambda)$ lie to the left of the line $(\gamma-i\infty\ ,\gamma+i\infty\ )$.

The line integral (4) can usually be put in real form by the use of one of two standard methods:

(i) If $\bar{v}\ (\lambda)$ is a single-valued function of λ with a row of poles along the negative real axis (and possibly other poles also), we complete the contour by a large circle of radius R, not passing through any pole of the integrand (Fig. 3.1). In all the problems in this work the integral over the large circle vanishes in the limit as its radius tends to ∞ . Thus, in the limit, the line integral (4) is equal by Cauchy's theorem to $2\pi i$ times the sum of the residues at the poles of its integrand. This case usually arises in problems of conduction of heat in finite regions.

(ii) In problems of conduction of heat in semi-infinite regions, $\bar{v}(\lambda)$ usually has a branch point at $\lambda=0$. In such cases we use the contour of Fig. 3.2 with a cut along the

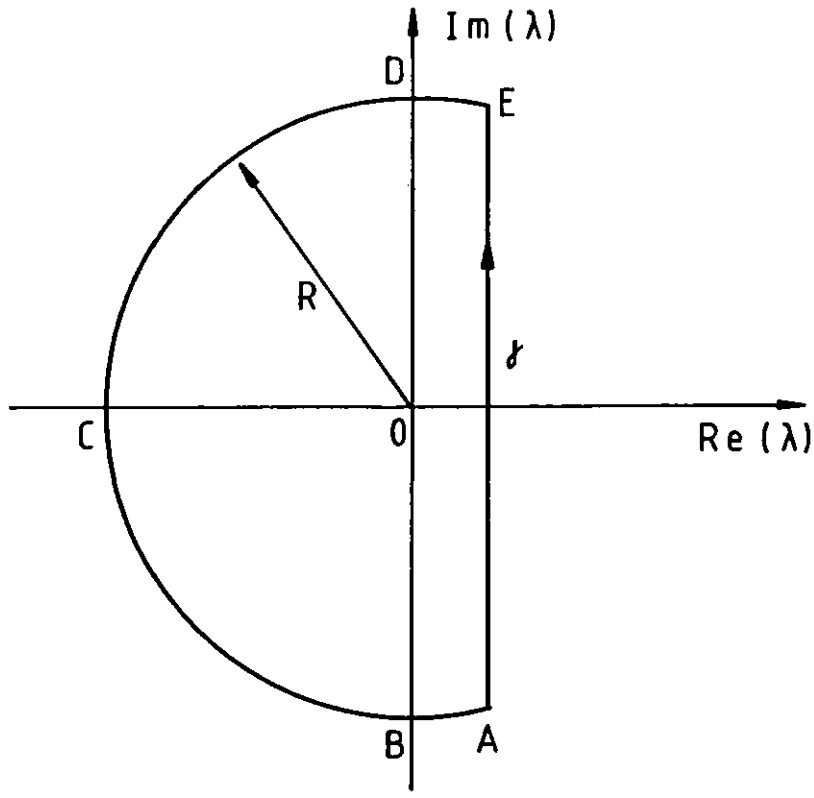

Fig. 3.1 Contour of integration 1.

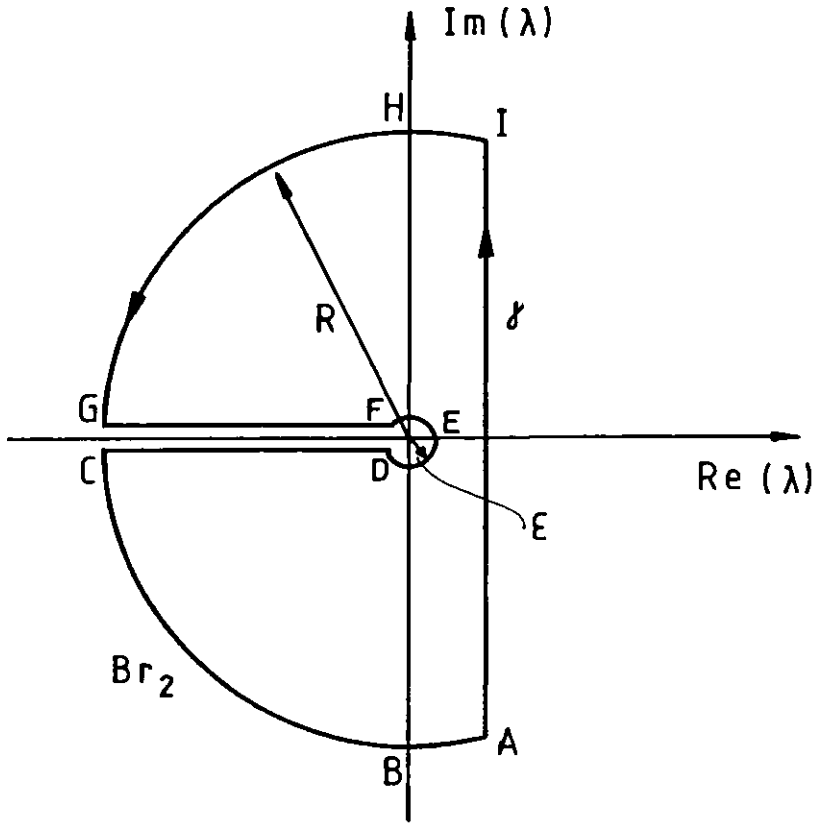

Fig. 3.2 Contour of integration 2:
The Bromwich contour

negative real axis so that $\bar{v}(\lambda)$ is a single-valued function of λ within and on the contour. In the limit as the radius of the large circle tends to infinity the integral round it can be shown to vanish, and the line integral (4) is replaced by a real infinite integral, derived from the integrals along CD and FG, together, possibly, with contributions from the small circle about the origin and any poles of the integrand.

For a more exhaustive account of the Laplace transform and other methods of solution of the heat equation, see C.J. chapter 12.

3.3 Infinite line-source solution.

3.3.1 Ideal case.

The simplest mathematical model for a line-source experiment consists of a thin heater in perfect contact with a large sample. We seek a solution to the one-dimensional heat equation for an infinite line-source along the z-axis transmitting heat at the rate Q per unit length per unit time into an infinite medium for t>0. In cylindrical coordinates

$$\frac{\partial^2 v}{\partial r^2} + \frac{1}{r}\frac{\partial v}{\partial r} = \frac{1}{h}\frac{\partial v}{\partial t} \qquad , t>0 \qquad (1)$$

subject to

$$\lim_{r\to 0} (r\ \partial v/\partial r) = -Q/(2\pi k) \qquad , t>0. \qquad (2)$$

The boundary condition at the surface of a cylindrical heater of radius r requires that the radial component of the heat flux F be the same on both sides of the surface of the heater:

$$F = -k\partial v/\partial r \ . \qquad (3)$$

F is the flux in the outward direction and is related to the linear power Q through the equation $F = Q/(2\pi r)$. Hence

$$Q = -2\pi rk \ \partial v/\partial r \ . \qquad (4)$$

A line-source can be regarded as the limit of a cylindrical source as $r \to 0$. The required boundary condition is then

$$\lim_{r \to 0} (r \ \partial v/\partial r) = -Q/(2\pi k) \ . \qquad (5)$$

A second boundary condition requires that v be bounded as $r \to \infty$.

Laplace transformation of (1) and (2) results in the subsidiary equation

$$\frac{d^2\bar{v}}{dr^2} + \frac{1}{r}\frac{d\bar{v}}{dr} - q^2\bar{v} = 0 \qquad (6)$$

subject to

$$\lim_{r \to 0} (r \ d\bar{v}/dr) = Q/(2\pi kp) \qquad (7)$$

where $q^2 = p/h$, and p is the transformation variable. The general solution of (3) is (MacLachlan, 1955)

$$\bar{v} = AI_o(qr)+BK_o(qr) \ , \qquad (8)$$

where A and B are functions of p, and I_o,K_o are Bessel functions. I_o diverges as $r \to \infty$,thus A=0. Applying the boundary condition (7) to (8) gives

$$\bar{v} = Q \ K_o(qr)/(2\pi kp) \ . \qquad (9)$$

Taking the inverse Laplace transform of this (Bateman Manuscript Project, 1954),

$$v = -\frac{Q}{4\pi K} \ Ei\left(\frac{-r^2}{4ht}\right). \qquad (10)$$

where

$$-Ei(-x) = \int_x^\infty e^{-u}/u \ du \qquad (11)$$

the "exponential integral", a tabulated function (Beyer, 1981). This is a well known result. It was described here only to introduce the Laplace transform method which will be used extensively in subsequent sections.

A power series expression of the exponential integral can be shown to be

$$Ei(-x) = j + \ln x - x + \frac{x^2}{2.2!} - \frac{x^3}{3.3!} + \ldots \qquad (12)$$

where j=0.5772157 is Euler's constant.

A plot of $-Ei(-r^2/4ht)$ against $\ln(ht/r^2)$ is given in figure 3.3. The first two terms of the expansion (12) are often used as an approximation to Ei in equation (10) to determine the thermal constants from a plot of temperature v against ln t, as also shown in figure 3.3. This plot, however, shows that care must be exercised (in the present experiment) in applying this approximation as the error becomes less than 1% only when $ht/r^2>10$. For a rock with $h=1.5\times10^{-6}$ m^2s^{-1} and an offset r=0.003 m, this corresponds to a time of about 60 seconds, which tends to make acquisition times rather long. Also, at such large times the sensitivity decreases as the rate of temperature increase is small. The acquisition time can be reduced considerably if r is made smaller. In the present work, however, a wide range of offsets were used and the series for Ei was computed with a number of terms sufficient to give the required accuracy. Because powers of the parameter h appear in expression (10), a nonlinear least-squares fitting method is required to determine the parameters k and h from the experimental data. This is described in section 3.10.

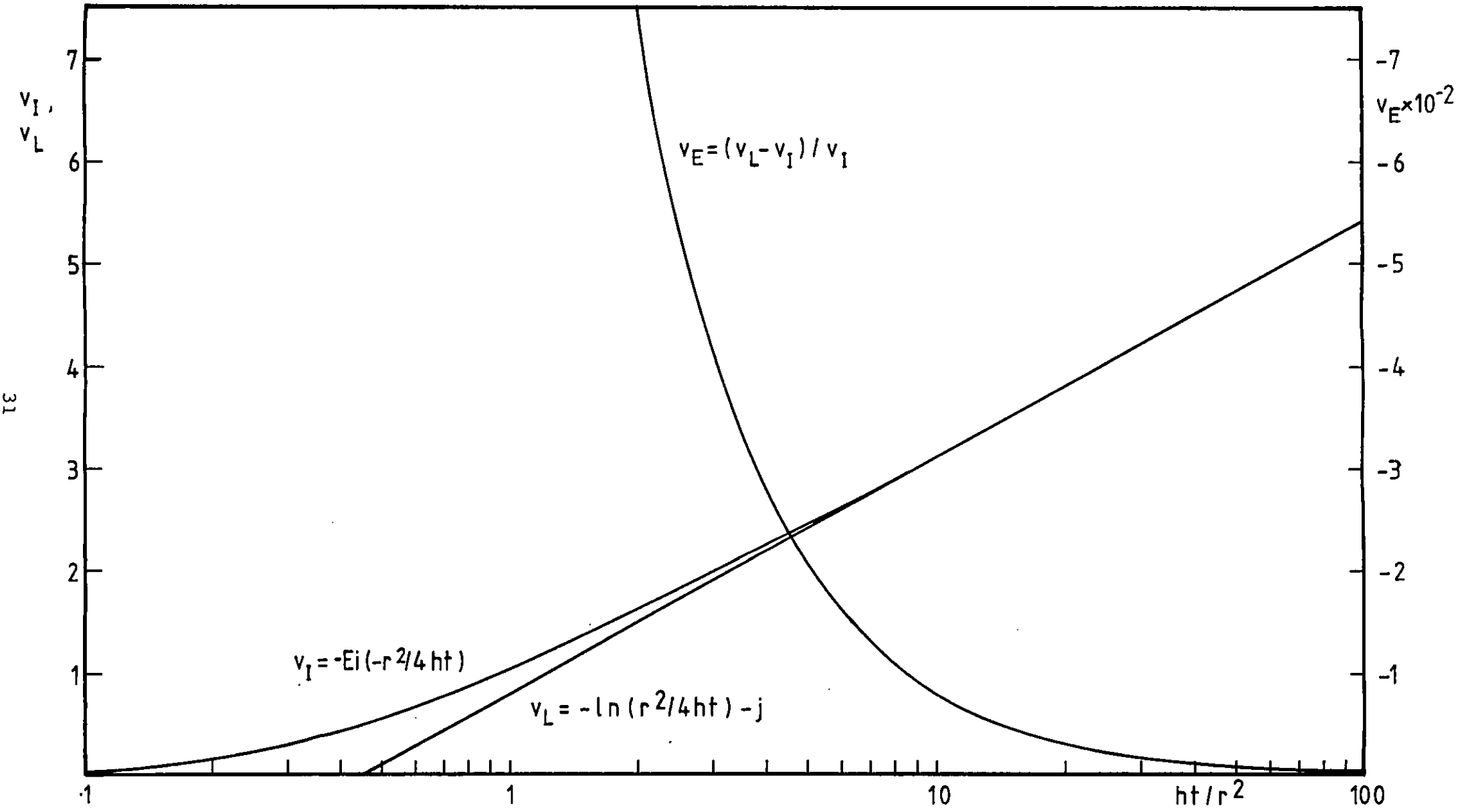

Fig. 3.3 Comparison of exponential integral (v_I) and logarithmic (v_L) solutions.

3.3.2 Maximum gradient solution.

Differentiating equation 3.3.1 (10) with respect to time gives

$$v' = \partial v/\partial t = Q/(4\pi k)\ \exp\{-r^2/(4ht)\} \qquad (1)$$

which has a maximum $v'_m = \partial v/\partial t\Big|_{t_m}$ at $t_m = r^2/4h$. (2)

Substituting in (1),

$$k = Q\ \exp(-1)/(4\pi v'_m t_m)\ . \qquad (3)$$

The conductivity k and diffusivity h can be determined very easily if v'_m and t_m are known (Scott **et al.**, 1973; Cull, 1975). This method, however, is not very accurate in this type of experiment as it relies on the precise determination of just one point on the temperature versus time curve. Better repeatability is achieved by fitting a set of experimental points to a theoretical curve, as described in section 3.3.1. Differentiation of the experimental curve also introduces uncertainty in the value of v'_m, and requires filtering of the high-frequency components to reduce noise. The value of t_m depends on the offset r of the temperature sensor through equation (2). If r is made small, v'_m occurs at a low time, when the shape of the curve is largely dependent on the thickness of the heater and the contact resistance between heater and rock, as shown in sections 3.5 and 3.8. On the other hand, large values of r reduce the overall sensitivity thus making v'_m difficult to determine.

3.4 The cylindrical source.

In the previous sections the heater was assumed to have zero diameter, and no heat capacity. The error introduced by such an assumption will be computed here.

The problem is modelled as follows: consider the region r>a initially at zero temperature, in contact at r=a with a perfect conductor of heat capacity S per unit length of the cylinder. Heat is supplied to the cylinder for t>0 at the rate Q per unit length per unit time. C.J. show that the temperature v at the surface of the cylinder is given by

$$v = \frac{2Q\beta^2}{\pi^3 k}\int_0^\infty \frac{1-\exp(-htu^2/a^2)}{u^3\Delta(u)}\,du \qquad (1)$$

where

$$\Delta(u) = [uJ_o(u)-\beta J_1(u)]^2 + [uY_o(u)-\beta Y_1(u)]^2 , \qquad (2)$$

J_o, J_1, Y_o, Y_1 are Bessel functions, k and h are the conductivity and diffusivity of the medium and $\beta=2\pi a^2 \rho c/S$ is a parameter which is twice the ratio of the heat capacity of an equivalent volume of the medium to that of the perfect conductor. The temperature at the surface of the wire computed using (1) was compared with that given by the simple line-source solution at the same position. The function $(v_I-v)/v$, where v_I is the line-source solution 3.3.1 (10) is plotted in figure 3.4, and decreases rapidly with time. Taking $\rho c=2\times10^6$ $Jm^{-3}K^{-1}$ for a typical rock and $c=4\times10^6$ for a constantan or nichrome heater wire, $\beta=1$ and the error becomes less than 1% when $ht/a^2=50$. For a wire of diameter 3.0×10^{-4} m, and a sample with $h=1.5\times10^{-6}$ m^2s^{-1}, this corresponds to a time of about 1 second.

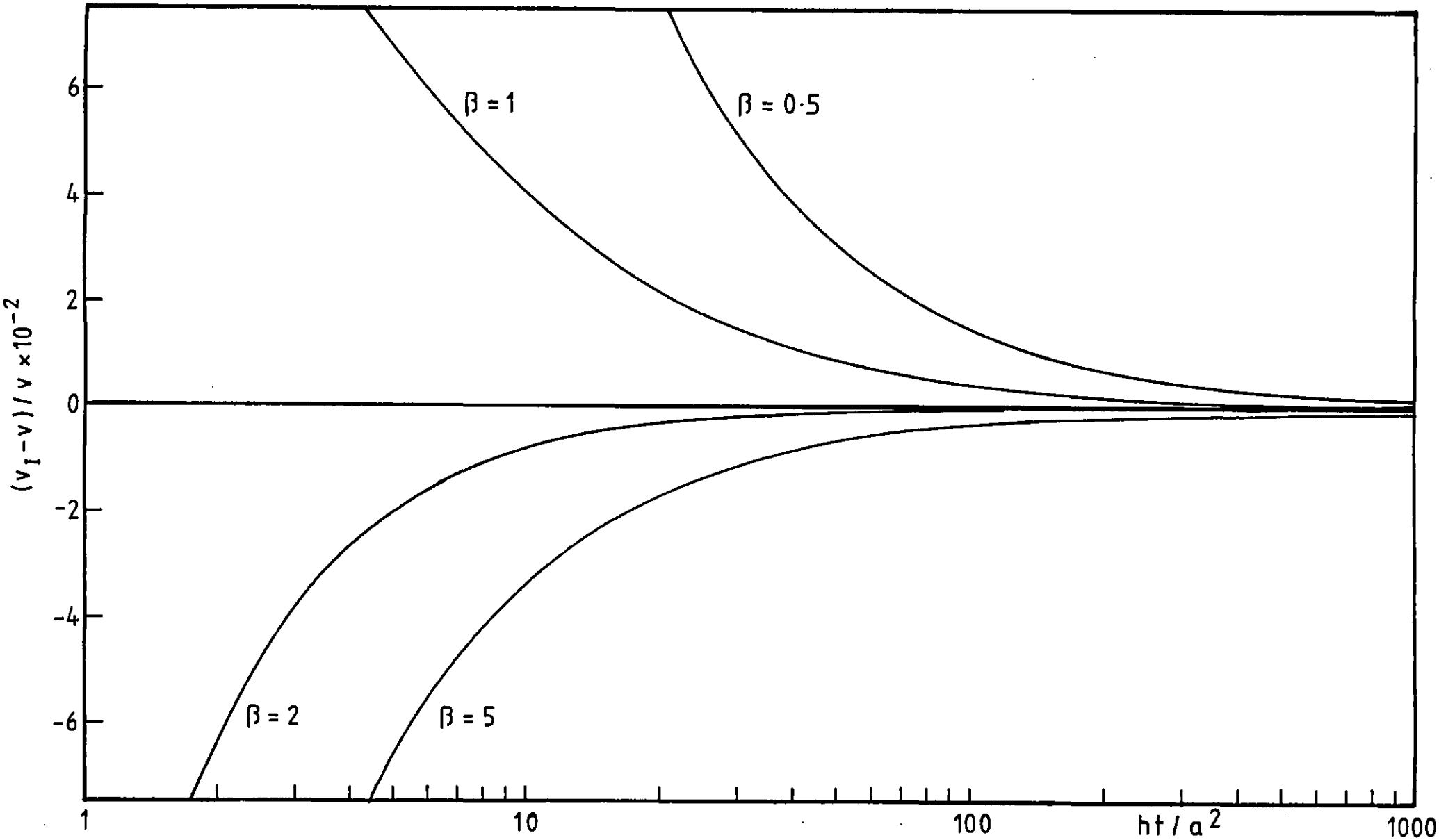

Fig. 3.4 Comparison of cylindrical source and line-source solutions.

3.5 Line-source with contact resistance.

3.5.1 The temperature transform.

In this section an attempt will be made to evaluate the effect of the layer of cement between the heater and the sample. In needle-probe experiments the contact resistance is sometimes modelled by a vanishingly thin resistive coating on a cylindrical heater of finite radius (see for example Blackwell, 1956), Fig. 3.5a. This method, however, is not suitable for modelling the present experiment because the radius of the heater is one order of magnitude smaller than the thickness of the cement. The model by Blackwell (1956) is modified here to include a resistive cylindrical layer of radius b surrounding and concentric with a linear heat source, Fig. 3.5b. The initial temperature is zero and the linear power supplied to the heater is Q for t>0. The temperature sensor is embedded in the rock, i.e. we are looking for a solution in the region r>b. In cylindrical polar coordinates, the subsidiary equations are

$$\frac{d^2\bar{v}_1}{dr^2} + \frac{1}{r}\frac{d\bar{v}_1}{dr} = q_1^2\bar{v}_1 \qquad ,0<r<b \tag{1}$$

$$\frac{d^2\bar{v}_2}{dr^2} + \frac{1}{r}\frac{d\bar{v}_2}{dr} = q_2^2\bar{v}_2 \qquad ,r>b \tag{2}$$

subject to the boundary conditions

$$\bar{v}_1 = \bar{v}_2 \quad \text{and} \quad k_1 d\bar{v}_1/dr = k_2 d\bar{v}_2/dr \quad \text{at } r=b \tag{3}$$

$$\lim_{r\to 0} (r d\bar{v}_1/dr) = -Q/(2\pi k_1 p) \qquad \text{and} \tag{4}$$

$$\bar{v}_2 \text{ bounded as } r\to \infty. \tag{5}$$

Subscript 1 refers to the cement, subscript 2 to the rock and

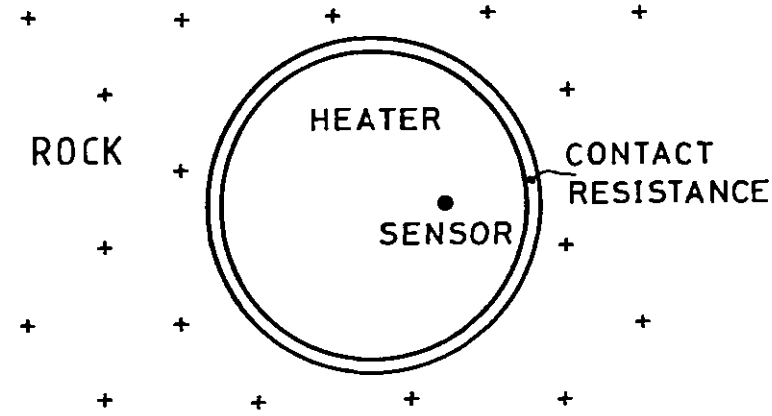

a)

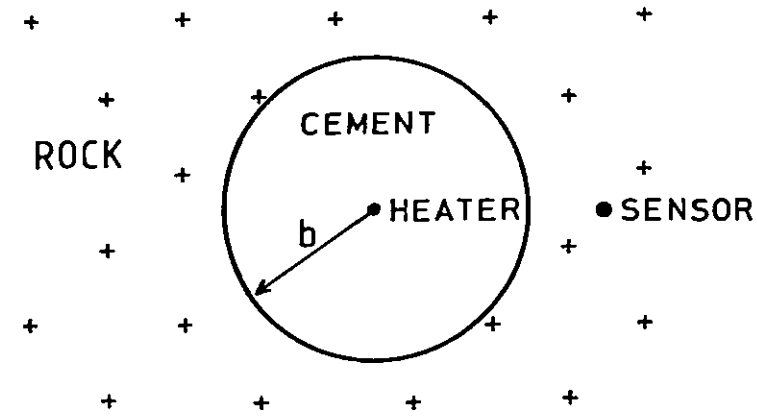

b)

Fig. 3.5 Needle-probe (a) and line-source (b) models. Enlarged cross-sectional views of heater, contact material and sample.

$$q_i^2 = p/h_i \quad , \; i=1,2 \quad . \tag{6}$$

The general solutions of (1) and (2) are

$$\bar{v}_1 = AI_o(q_1 r)+BK_o(q_1 r) \tag{7}$$

$$\bar{v}_2 = CI_o(q_2 r)+DK_o(q_2 r) \tag{8}$$

where A,B,C and D are arbitrary functions of p, and I_o, K_o are Bessel functions. $I_o(p)$ diverges as $p\to\infty$, so equation (5) requires that C=0. Using $I'_o(p)=I_1(p)$ and $K'_o(p)=-K_1(p)$, (4) gives

$$B = Q/(2\pi k_1 p) \; . \tag{9}$$

The boundary conditions (3) and (9) give

$$D = Q/(2\pi bp\Delta \;) \tag{10}$$

with $$\Delta = q_1 k_1 K_o(q_2 b) I_1(q_1 b)+q_2 k_2 K_1(q_2 b) I_o(q_1 b). \tag{11}$$

Thus the Laplace transform of the temperature in the sample is given by

$$\bar{v}_2 = Q\, K_o(q_2 r)/(2\pi bp\Delta) \tag{12}$$

with a similar expression for $\bar{v}_1$.

3.5.2 Exact solution.

By the inversion theorem of the Laplace transform, the temperature in the sample is

$$v_2(t) = 1/(2\pi i)\int_{\gamma-i\infty}^{\gamma+i\infty} \bar{v}_2(p)\; e^{tp}\; dp \quad . \tag{1}$$

To evaluate $v_2(t)$ a standard artifice is employed. Let

$$\bar{v}_2(p) = F(p)/p \; . \tag{2}$$

Then, by a well-known theorem of the Laplace transform (Bateman Manuscript, p.150)

$$v_2(t) = \int_0^t \left\{ \frac{1}{2\pi i} \int_{\gamma-i\infty}^{\gamma+i\infty} F(p) e^{tp}\; dp \right\} \; dt \; . \tag{3}$$

$v_2(p)$ has a branch point at the origin, and the method outlined in 3.2(ii) can be used. The contour of integration can be replaced by the Bromwich contout Br_2 in Fig. 3.2. The portions ABC and GHI of the integral vanish as $R \to \infty$, as does the integral around DEF as $\varepsilon \to 0$.

Setting $p = \sigma e^{-i\pi}$ on the portion CD

$= \sigma e^{i\pi}$ on the portion FG,

where σ is real and positive,

$$\int_{Br_2} F(p)\, e^{tp}\, dp = \int_0^\infty F(\sigma e^{-i\pi})\, e^{-t\sigma}\, d\sigma - \int_0^\infty F(\sigma e^{i\pi})\, e^{-t\sigma}\, d\sigma \tag{4}$$

$$= -2i\int_0^\infty \mathrm{Im}\,\{F(\sigma e^{i\pi})\}\, e^{-t\sigma}\, d\sigma \quad .$$

Setting $x=(\sigma/h_2)^{1/2}$, $h=(h_2/h_1)^{1/2}$, and using

$$K_n(ze^{\pm\pi i/2}) = \pm\, \pi/2\ i\ e^{\mp n\pi i/2}\,[-J_n(z)\pm iY_n(z)] \tag{5}$$

$$I_n\,(z\ e^{\pm\pi i/2}) = e^{\pm n\pi i/2}\ J_n(z) \tag{6}$$

to replace the modified Bessel functions of imaginary argument by ordinary Bessel functions of real argument, equation 3.5.1 (11) becomes

$$\Delta = \pi x\ \Psi(x)/2 + i\pi x\ \Phi(x)/2 \tag{7}$$

where $\Psi(x) = hk_1Y_o(xb)J_1(hxb)-k_2Y_1(xb)J_o(hxb)$ (8)

and $\Phi(x) = hk_1J_o(xb)J_1(hxb)-k_2J_1(xb)J_o(hxb)$ (9)

From equation 3.5.1 (12),

$$\mathrm{Im}\ (F) = \mathrm{Im}\ \{K_o(q_2r)\ \Delta^*/(\Delta\Delta^*)\}\ , \tag{10}$$

where Δ^* denotes the complex conjugate of Δ .

Then equation (3) becomes

$$v_2 = \frac{Qh_2}{\pi^2 b}\int_0^t dt \int_0^\infty \frac{J_o(xr)\ \psi(x)-Y_o(xr)\ \phi(x)}{\psi^2(x)+\phi^2(x)}\ e^{-h_2x^2t}\ dx. \quad (11)$$

Integrating over t,

$$v_2 = \frac{Q}{\pi^2 b}\int_0^\infty (1-e^{-h_2x^2t})\ \frac{J_o(xr)\psi(x)-Y_o(xr)\phi(x)}{x^2\{\psi^2(x)+\phi^2(x)\}}\ dx\ . \quad (12)$$

If $h_1=h_2$, $k_1=k_2$, or in the limit $b\to 0$, this solution reduces to the simple line-source solution 3.3.1 (10).

3.5.3 Approximate solution.

An alternative approximate solution to equation 3.5.2 (12) valid for small values of b will be derived in this section. Assuming that (q_2b) is small, which corresponds either to the large-time solution or the case where b is small (small contact resistance), a solution is derived as a power series in increasing powers of q_2b. Approximating the modified Bessel functions in Eq. 3.5.1 (11) by the first few terms of series in ascending powers of p, (C.J., Appendix III),

$$I_o(z) = 1+z^2/4+... \quad (1)$$

$$I_1(z) = z/2+z^3/16+... \quad (2)$$

$$K_o(z) = -\{\ln(z/2)+j\}\{1+z^2/4+...\}+z^2/4+... \quad (3)$$

$$K_1(z) = 1/2\ \{\ln(z/2)+j\}\{z/2+z^3/16\}-z/4+1/z\ . \quad (4)$$

Substituting in 3.5.1 (11),

$$\Delta = k_2/b\left[1 + b^2/(4k_2)p\ \ln(\beta p)(k_2/h_2-k_1/h_1) + b^2/4\ p(1/h_1-1/h_2) + O(p^2)\right] \quad (5)$$

where $O(p^2)$ represents the terms of order p^2 and higher and $\beta=b^2e^{2j}/(4h_2)$. Making use of the binomial theorem to find Δ^{-1},

$$\bar{v}_2 = QK_o(q_2r)/(2\pi pk_2) \left[1 - b^2/(4k_2)p \ln(\beta p)(k_2/h_2-k_1/h_1) - b^2/4 \ (1/h_1-1/h_2)p + O(p^2) \right]. \quad (6)$$

v_2 can be found from this by applying the inversion theorem to the separate terms of the series. From standard tables (Bateman Manuscript, 1954)

$$L^{-1}\{K_o(q_2r)/p\} = 1/2 \int_\alpha^\infty e^{-u}/u \ du \quad (7)$$

$$L^{-1}\{K_o(q_2r)\} = e^{-\alpha}/2t \quad (8)$$

$$L^{-1}\{pK_o(q_2r)\} = (\alpha-1)e^{-\alpha}/2t^2 \quad (9)$$

where $\alpha=r^2/(4h_2t)$

for the first, third and error terms respectively. In Appendix III the inverse Laplace transform of the second term is shown to be

$$L^{-1}\{K_o(qr)\ln(\beta p)\} = -e^{-\alpha}/(2t) \ \ln[t/(\alpha\beta)] \ . \quad (10)$$

Then, from (6), (7), (8), (9) and (10),

$$v_2 = Q/(4\pi k_2)\left\{ \int_\alpha^\infty e^{-u}/u \ du + b^2/(4k_2)(k_2/h_2-k_1/h_1) \ e^{-\alpha}/t \ \ln[t/(\alpha\beta)] - b^2/4 \ (1/h_1-1/h_2) \ e^{-\alpha}/t + O(\alpha^2) \right\}. \quad (11)$$

If $b=0$, or $k_1=k_2$, $h_1=h_2$, this reduces to the line-source solution 3.3.1 (10). The approximation is valid for $b^2/h_2t \ll 1$ and is often more useful than the exact solution as it easier to evaluate numerically.

A numerical comparison of the exact solution with equation (11) shows good agreement. Fig. 3.6 is a plot of v_E/v_I against h_2t/b^2, where v_E is the sum of the second and third terms in (11), and v_I is the line-source solution with no contact resistance. The values of the conductivities and diffusivities are the following:

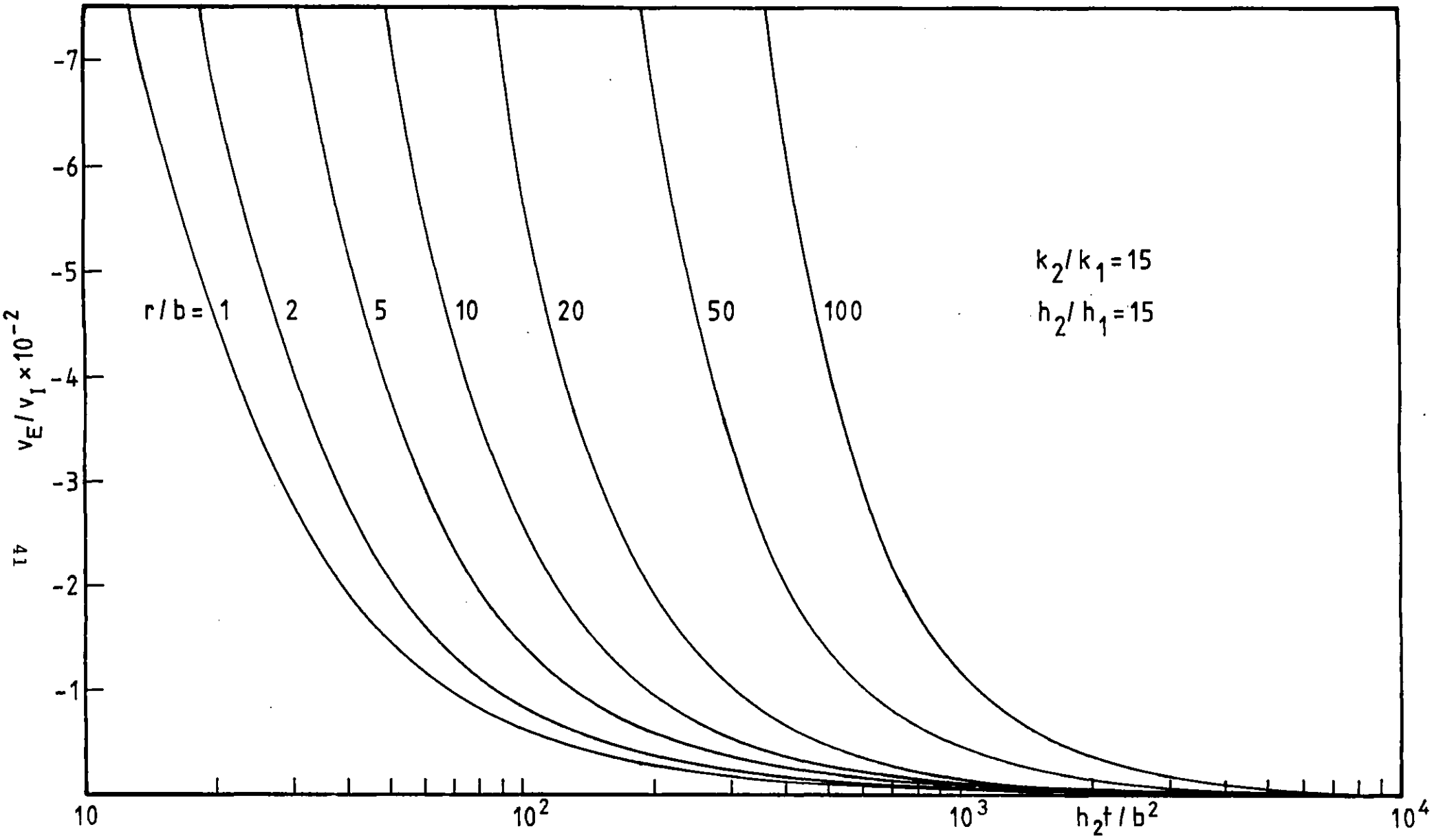

Fig. 3.6 Effect of contact resistance on line-source solution.

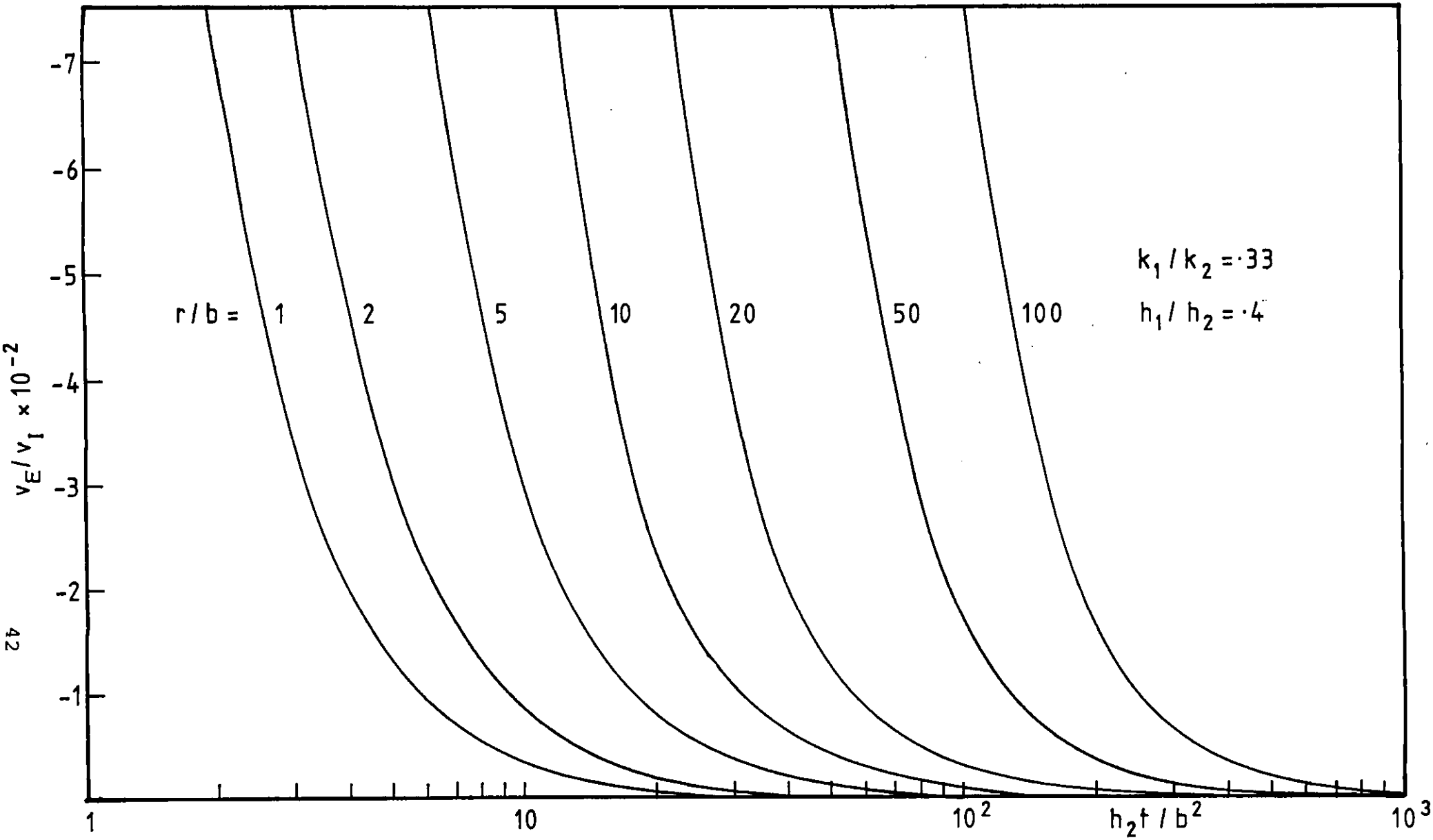

Fig. 3.7 Effect of contact resistance on line-source solution.

k_1=0.2W/mK, h_1=10^{-7} m^2/s, k_2=3, h_2=1.5x10^{-6}, which correspond to a typical granite/epoxy resin interface. Fig. 3.7 is a similar plot with k_1=1.0, h_1=0.6x10^{-6} for a typical granite/fire cement interface.

3.6 Boundary effects.

The effect of reflection of heat from the curved surfaces of a sample will be estimated in this section.

3.6.1 Constant surface temperature.

Consider a linear source emanating heat at the rate Q per unit length per unit time into an infinitely long cylinder with the surface r=b kept at constant temperature. The contact resistance at r=b is assumed to be zero. The differential equation describing the problem is

$$\frac{\partial^2 v}{\partial r^2} + \frac{1}{r}\frac{\partial v}{\partial r} = \frac{1}{h}\frac{\partial v}{\partial t} \quad , \quad 0<r<b,\ t>0 \tag{1}$$

subject to

$$v=0 \quad \text{at } r=b \tag{2}$$

and

$$\lim_{r\to\infty} (r\ \partial v/\partial r) = -Q/(2\pi k) \ . \tag{3}$$

The subsidiary equation is

$$\frac{d^2\bar{v}}{dr^2} + \frac{1}{r}\frac{d\bar{v}}{dr} = q_2\bar{v} \qquad 0<r<b \tag{4}$$

subject to $v=0$ at $r=b$ (5)

and

$$\lim_{r\to 0} (r\ d\bar{v}/dr) = -Q/(2\pi kp) \ . \tag{6}$$

Using the same technique as in 3.3,

$$\bar{v} = \frac{Q}{2\pi k}\frac{1}{p}\ \frac{I_o(qb)K_o(qr)-I_o(qr)K_o(qb)}{I_o(qb)} \tag{7}$$

where the symbols have their usual meaning. An exact solution can be found for v using the Inversion theorem

$$v = 1/(2\pi i) \int_{\gamma-i\infty}^{\gamma+i\infty} \bar{v}(p) e^{pt}\, dp \ . \qquad (8)$$

The integrand is a single-valued function of p with simple poles at zero and on the negative imaginary axis. By the theorem of residues

$$v = 2\pi i \times \text{residues} \ , \text{ or}$$

$$v = \frac{Q}{2\pi k} \sum_i \left[\frac{I_o(qb)K_o(qr) - I_o(qr)K_o(qb)}{\partial / \partial p\{pI_o(qb)\}} \right] e^{pt} \Bigg|_{p=\xi_i} \qquad (9)$$

where the ξ_i's are the poles of the function. Then

$$v = \frac{Q}{2\pi k} \left[\frac{I_o(qb)K_o(qr) - I_o(qr)K_o(qb)}{I_o(qb)} \right]_{p=0}$$

$$+ \sum -\exp(-h^2\alpha_s^2 t) \quad \frac{I_o(i\alpha_s r)K_o(i\alpha_s b)}{\left[p\, d/dp\ I_o(qb)\right]_{p=-h\alpha_s^2}} \qquad (10)$$

where $_s$ is the sth root of $I_o(i\alpha b)=0$ or $J_o(\alpha b)=0$. Then, using

$K_o(z)\ I_1(z) + I_o(z)K_1(z) = 1/z$,

$I_o(zi) = J_o(z)$ and

$I_1(zi) = iJ_1(z)$,

$$v = Q/(\pi k) \left[1/2\ \ln(b/r) - \sum_{s=1}^{\infty} \frac{\exp(-h\alpha_s^2 t)\ J_o(\alpha_s r)}{\alpha_s^2 b^2 J_1^2(\alpha_s b)} \right]. \qquad (11)$$

Fig. 3.8 shows a family of curves $(v_I - v)/v$ plotted against ht/b^2 for several values of b/r. v_I is the line-source solution 3.3.1 (10) in an infinite medium. The set of curves thus represent the error in the simple solution v_I and provide useful information on the relative sizes of b, r and the upper bound of t in the design of experiments. Equation (11) can also be used to yield values of k and h

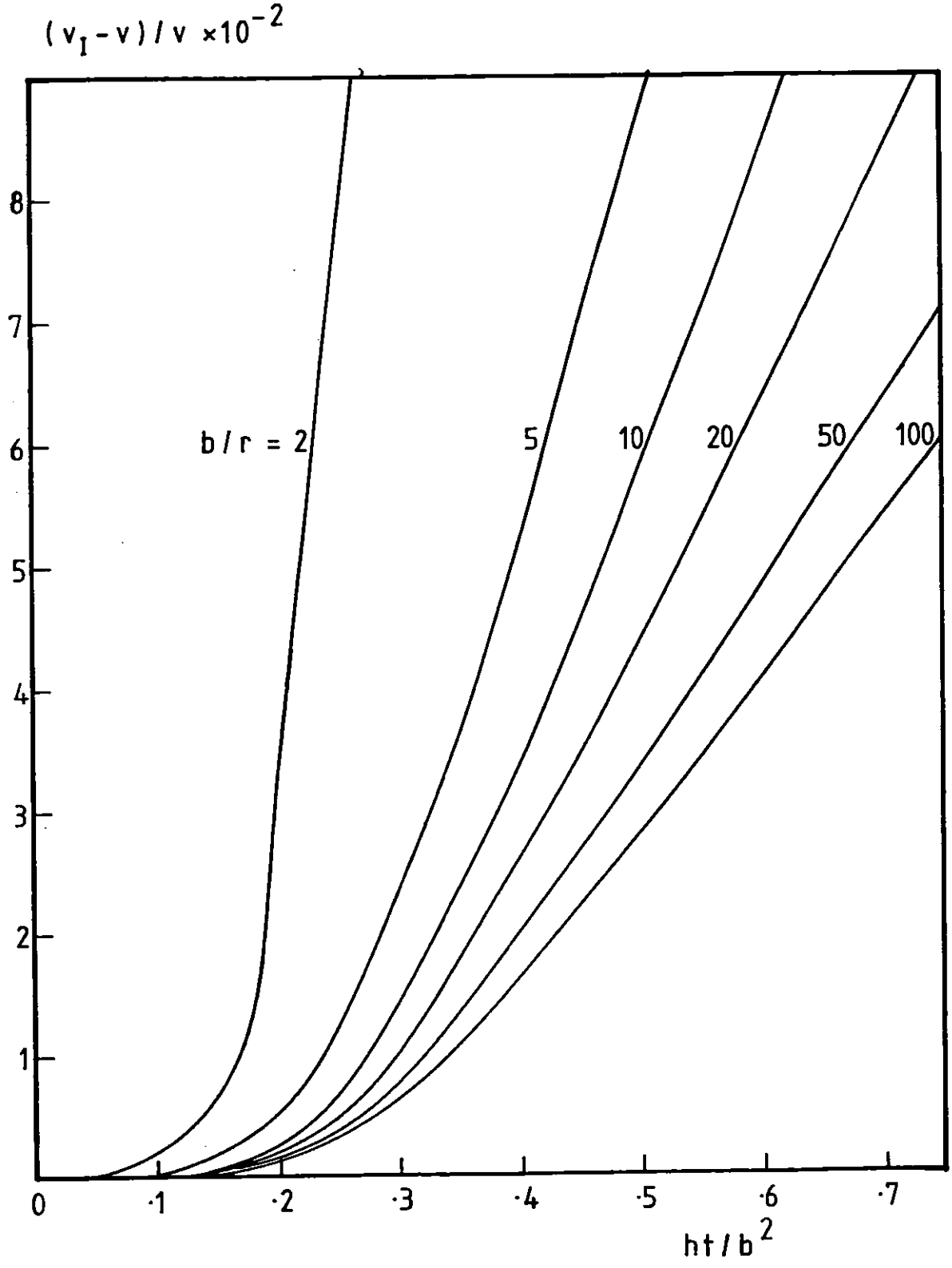

Fig. 3.8 Effect of boundary reflections: zero surface temperature.

(see section 3.10) when equation 3.3.1 (10) is not applicable because of the small size of a sample or to limitations on the upper bound of t.

3.6.2 Zero flux at surface.

The following model represents a sample with zero heat flux across the surface r=b (perfect lagging). The differential equation and boundary conditions are the same as in the previous case, with equation (2) replaced by

$$\partial v/\partial r = 0 , \qquad r=b. \tag{1}$$

The solution in the p-domain is

$$\bar{v} = \frac{Q}{2\pi k} \frac{1}{p} \frac{K_o(qr)I_1(qb)+K_1(qb)I_o(qr)}{I_1(qb)} . \tag{2}$$

Using the inversion theorem,

$$v = \frac{1}{2\pi i} \frac{Q}{2\pi k} \int_{\gamma-i\infty}^{\gamma+i\infty} e^{pt} \frac{K_o(qr)I_1(qb)+K_1(qb)I_o(qr)}{I_1(qb)} dp . \tag{3}$$

The integral has a double pole at the origin and a row of simple poles along the negative imaginary axis. Proceeding in a similar way as in the previous case, the residue at the origin is found to be

$$2ht/b^2 + r^2/(2b^2) - 3/4 + \ln(b/r) . \tag{4}$$

The sum of the remaining residues is

$$-2 \sum_{s=1}^{\infty} \frac{\exp(-\alpha_s ht)\ J_o(\alpha_s r)}{(\alpha_s^2 b^2)\ J_o^2(\alpha_s b)} \tag{5}$$

where the α_s's are the positive roots of $J_1(\alpha b)=0$. The solution is then

$$v = \frac{Q}{2\pi k}\left[\frac{2ht}{b^2} + \frac{r^2}{2b^2} - \frac{3}{4} + \ln(b/r) - 2\sum_{s=1}^{\infty}\frac{\exp(-h\alpha_s^2 t)\, J_o(\alpha_s r)}{[\alpha_s b J_o(\alpha_s b)]^2}\right] \quad (6)$$

Fig. 3.9 shows a family of curves $(v_I - v)/v$ against ht/b^2, where the notation is the same as in 3.6.1. The same general considerations also apply to equation (6). The errors in the two cases have opposite signs, which implies that imperfect stirring of the heating fluid or partial lagging may help reduce the the error in real experiments.

3.7. Axial-flow effects.

In the previous sections the rock samples were assumed to be infinitely long, which resulted in an entirely radial heat flow. The effect of axial flow in a finite-length cylinder will be evaluated here in order to determine the minimum acceptable length for a sample. The relatively simple case of a cylindrical sample of finite length with a non-conductive axial heater is discussed by Blackwell (1953). Jaeger (1955) introduced a useful boundary condition for a cylindrical heater of radius "a" in contact at its surface with a solid. The heater is supposed to be a relatively good conductor so that its temperature is uniform over its cross-section, and there is no contact resistance at the surface. In the usual notation, the boundary condition at r=a is

$$\frac{\partial^2 v}{\partial z^2} + \frac{2k}{ak_1}\frac{\partial v}{\partial r} - \frac{1}{h_1}\frac{\partial v}{\partial t} = -\frac{A}{k_1} \quad (1)$$

where A is the rate of supply of heat to the wire per unit volume. Jaeger (1955) solved the heat equation for a sample of length 2 l and a heater of radius a. The initial temperature is assumed to be zero, the surface $|z|=l$ are

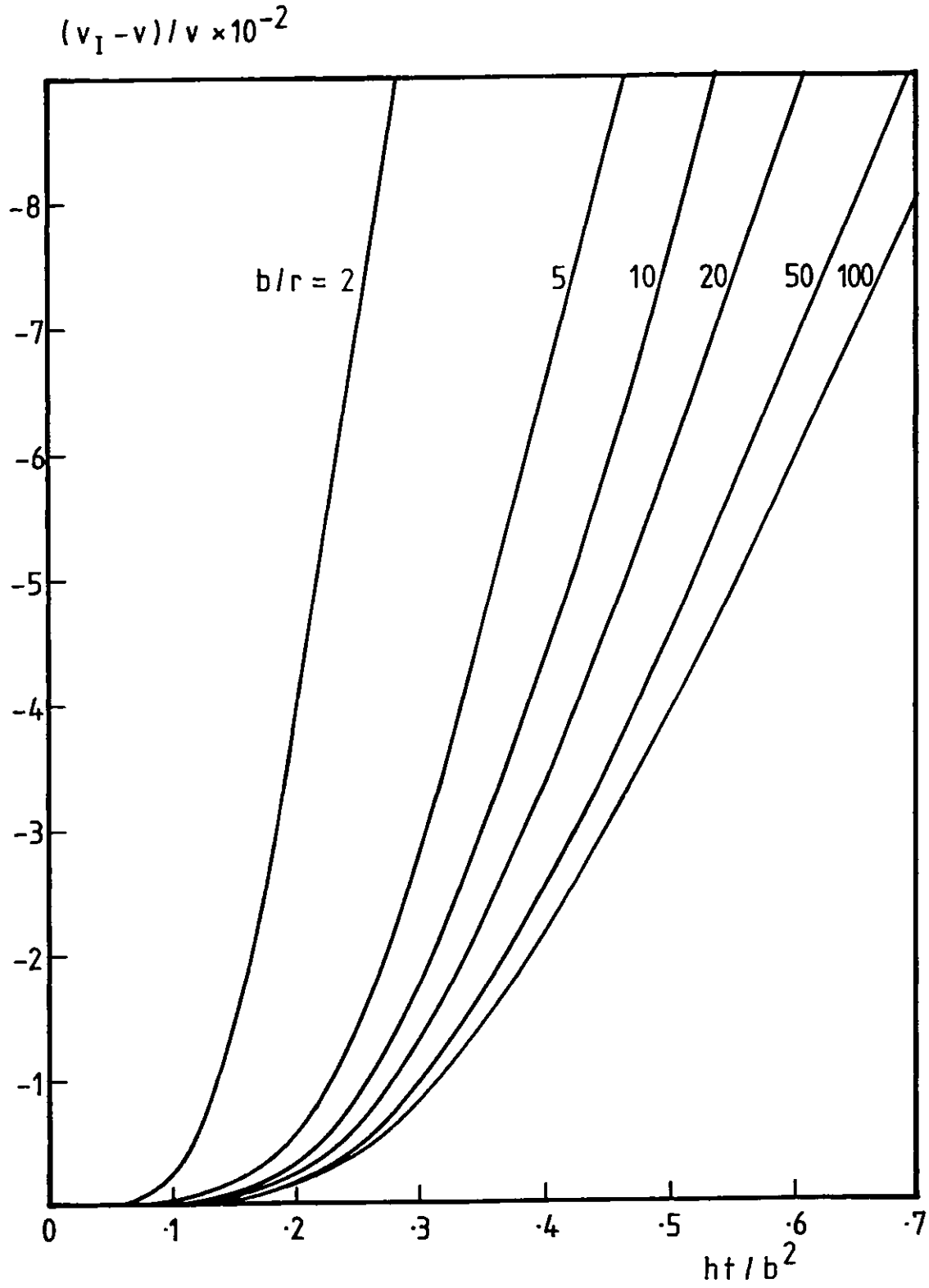

Fig. 3.9 Effect of boundary reflections: zero flux at surface.

maintained at zero temprature for t>0, and the boundary condition (1) holds at r=a. The expression for the temperature at the mid-point of the wire z=0, r=a is shown to be:

$$v(a,0) = \frac{8Q}{\pi^2 k_1}\frac{l^2}{a^2}\sum_{n=0}^{\infty}\frac{(-1)^n K_o(\beta_n)}{(2n+1)^2[(2n+1)\pi^2 K_o(\beta_n)+2\pi l\varepsilon K_1(\beta_n)}$$

$$- \frac{8Q\, h_1^2 k}{\pi^4\, h^2 k_1^2}\sum_{n=0}^{\infty}\frac{(-1)^n}{2n+1}\exp(-h\beta_n^2 t/a^2)\int_0^{\infty}\frac{\exp(-hu^2t/a^2)}{(u^2+\beta_n^2)\Delta_n(u)}\,u\,du \qquad (2)$$

with $\beta_n=(n+1/2)\pi a/l$, (3)

$$\Delta_n(u)=[(b_n-u^2)J_o(u)+uHJ_1(u)]^2 \qquad (4)$$
$$+[(b_n-u^2)Y_o(u)+uHY_1(u)]^2$$

and $b_n=\beta_n^2(h_1-h)/h$, $H=2kh_1/(k_1h)$, $\varepsilon=2k/(ak_1)$. (5)

Equation (2) was evaluated and compared with line-source solution v_I (equation 3.3.1 (10)). The error $(v_I-v)/v$ is plotted in Fig. 3.10. Because of the assumptions made, this is only a rough estimate of the errors involved in a real experiment. For a typical granite with $h=1.5\times10^{-6}$ m^2s^{-1}, t=140 s, $a=10^{-4}$ m, $ht/a^2=2\times10^4$. If the length 2l is 12×10^{-2} m, l/a=600 and the maximum error is well under 1% (Fig. 3.10). If 2 $l=6\times10^{-2}$ m, the error increases to about 1%.

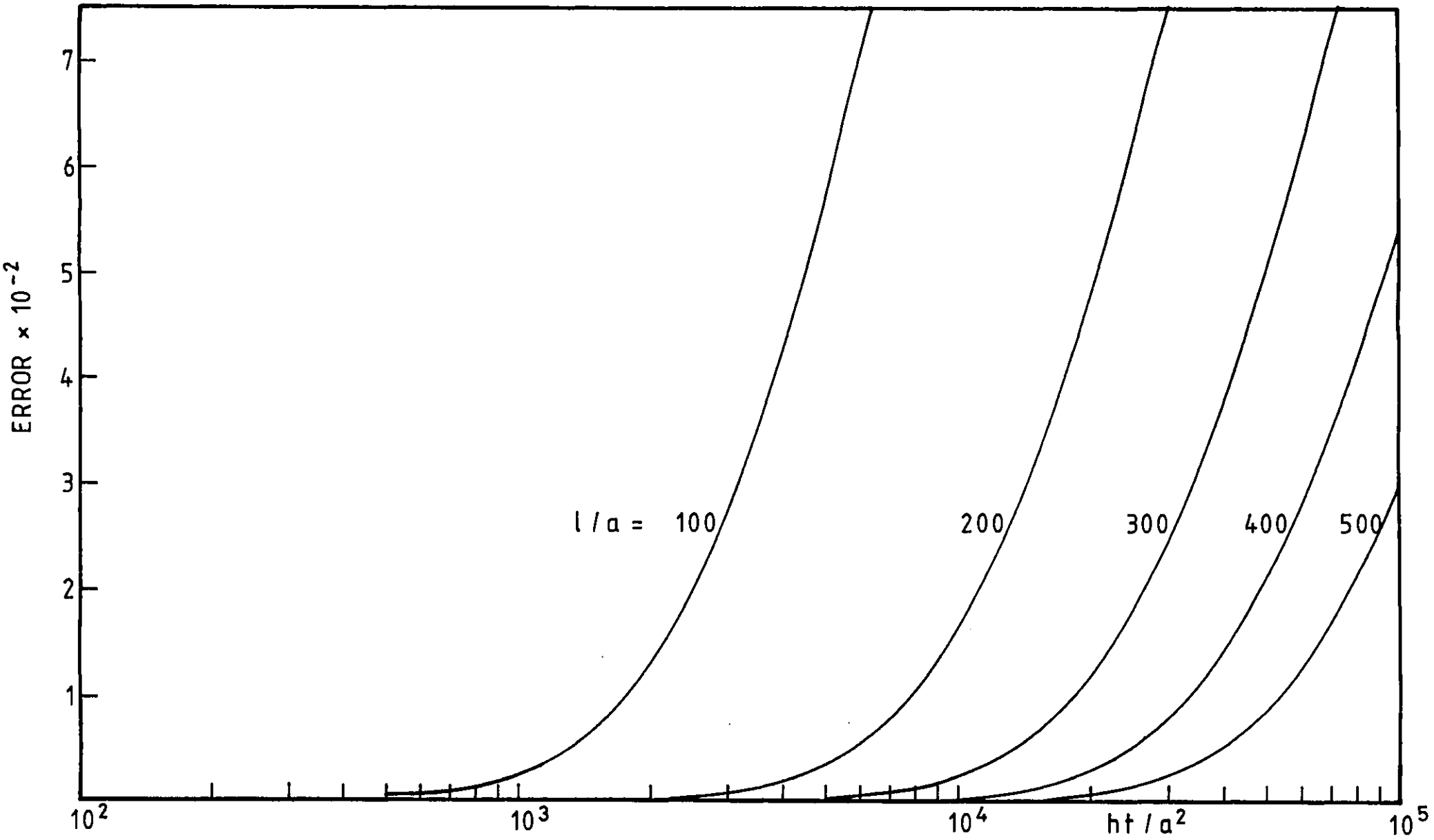

Fig. 3.10 Axial-flow effects on line-source solution.

3.8 Line-source between two slabs.

In the previous sections cylindrical symmetry around the heater was assumed. In this section, a more realistic model is presented which takes into account the layer of cement between the two semi-cylinders of rock. The mathematical solution was derived in collaboration with A. Cameron, and details of the calculations can be found in Cameron (1981).

Fig. 3.11a depicts a sample where the thickness of the cement has been deliberately exaggerated. The model chosen to represent the physical situation is shown diagrammatically in Fig. 3.11b, where medium 1 is the layer of cement of thickness 2a and medium 2 is the rock. The two media are assumed to extend to infinity in the x and y directions. As shown in section 3.6, this is justified provided that a suitable upper bound is chosen for the sampling time. The seemingly unusual choice of axes orientation simplifies the boundary conditions.

The problem can be solved by the use of Green's functions, an account of which is given in C.J., chapter 14. If the heater is assumed to be an instantaneous unit strength point source placed at the origin, the Laplace transforms of the temperature fields will be in the form

$$\bar{v}_1 = \bar{u} + \bar{w}_1 \qquad \text{in medium 1} \qquad (1)$$

$$\bar{v}_2 = \bar{w}_2 \qquad \text{in medium 2} \qquad (2)$$

where u is the Green's function of the heater, and w_1, w_2 have to satisfy the heat equation, to vanish for t=0, and to be such that v_1, v_2 satisfy the boundary conditions. The Green's function of the heater is

$$u = 1/8\ (\pi h_1 t)^{-3/2} \exp\ [-R^2/(4h_1 t)] \qquad (3)$$

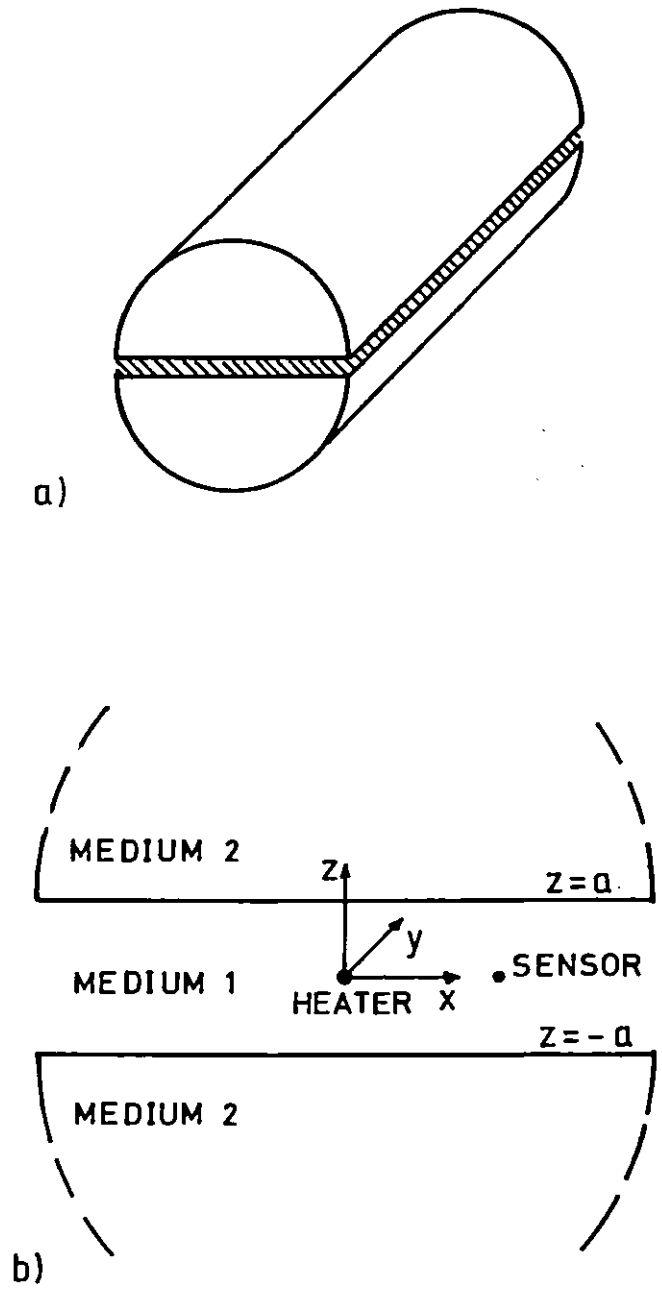

Fig. 3.11 Model for line-source between two infinite slabs with contact resistance. a) View of sample and cement. b) Axis orientation.

where $R=(x^2+y^2+z^2)^{1/2}$. The Laplace transform of this is (C.J., p.372)

$$\bar{u} = (4\pi h_1 R)^{-1} \exp(-q_1 R) \tag{4}$$

where the symbols have their usual meaning. Watson (1952), section 13.47, shows that this can be put in the form

$$\bar{u} = (4\pi h_1)^{-1} \int_0^\infty J_o(\xi r)\xi/\eta_1 \exp(-\eta_1|z|)\, d\xi \tag{5}$$

where $\eta_1^2 = \xi^2+q_1^2$ and $r=(x^2+y^2)^{1/2}$. (6)

The subsidiary equations for $\bar{w}_1$, $\bar{w}_2$ in cylindrical polars are

$$\frac{1}{r^2}\frac{\partial^2\bar{w}_1}{\partial\theta^2} + \frac{\partial^2\bar{w}_1}{\partial r^2} + \frac{1}{r}\frac{\partial\bar{w}_1}{\partial r} + \frac{\partial\bar{w}_1}{\partial z} - q_1\bar{w}_1^2 = 0, \quad |z|<a \tag{7}$$

and

$$\frac{1}{r^2}\frac{\partial^2\bar{w}_2}{\partial\theta^2} + \frac{\partial^2\bar{w}_2}{\partial r^2} + \frac{1}{r}\frac{\partial\bar{w}_2}{\partial r} + \frac{\partial\bar{w}_2}{\partial z} - q_2\bar{w}_2^2 = 0, \quad |z|>a \tag{8}$$

and these are satisfied by

$$\bar{w}_1 = (4\pi h_1)^{-1} \int_0^\infty \xi/\eta_1\, J_o(\xi r)A(\xi)\cosh(\eta_1 z)\, d\xi \tag{9}$$

in medium 1 and by

$$\bar{w}_2 = (4\pi h_2)^{-1} \int_0^\infty \xi/\eta_2\, J_o(\xi r)B(\xi) \exp(-\eta_2|z|)\, d\xi \tag{10}$$

in medium 2. $A(\xi)$ and $B(\xi)$ are arbitrary functions of ξ, with

$$\eta_i = (\xi^2+q_i^2)^{1/2} \quad \text{and} \quad q_i^2 = p/h_i \ , \ i=1,2.$$

The form of the solutions (9) and (10) was suggested by similar expressions given by C.J. in the solution of a related problem (see C.J., p.372). The exponential and hyperbolic functions (both symmetrical in $\eta(z)$) were chosen

to reflect the symmetry of the problem.

The boundary conditions are

$$\bar{v}_1=\bar{v}_2 \ , \qquad |z|=a \quad \text{and} \tag{11}$$

$$k_1 \partial\bar{v}_1/\partial z = k_2 \partial\bar{v}_2/\partial z \ , \qquad |z|=a \ . \tag{12}$$

Applying these to (9) and (10), we get

$$A = \frac{(k_1\eta_1-k_2\eta_2)\exp(\eta_1 a)}{k_2\eta_2\cosh\eta_1 a+k_1\eta_1\sinh\eta_1 a} \tag{13}$$

and

$$\bar{v}_1=(4\pi h_1)^{-1}\int_0^\infty \frac{k_1\eta_1\cosh\eta_1(a-z)+k_2\eta_2\sinh\eta_1(a-z)}{k_1\eta_1\sinh\eta_1 a+k_2\eta_2\cosh\eta_1 a} J_o(\xi r)\xi/\eta_1 d\xi \tag{14}$$

In the z=0 plane (14) simplifies to

$$\bar{v}_1=(4\pi h_1)^{-1}\int_0^\infty \frac{k_1\eta_1\cosh\eta_1 a+k_2\eta_2\sinh\eta_1 a}{k_1\eta_1\sinh\eta_1 a+k_2\eta_2\cosh\eta_1 a}\xi/\eta_1 J_o(\xi r)d\xi \tag{15}$$

The inversion theorem can be applied to this to give an expression for v_1. However, an approximation for small values of $(\eta_1 a)$ simplifies the inversion. This corresponds to the large time solution (Blackwell, 1954) or the case when a is small (cf. section 3.5.3). To the first order in $(\eta_1 a)$,

$$\bar{v}_1 = (4\pi h_1)^{-1} \int_0^\infty \xi J_o(\xi r)\{k/\eta_2+(1-k^2\eta_1^2/\eta_2^2)a\}\, d\xi \tag{16}$$

where $k=k_1/k_2$. This may be written as

$$\bar{v}_1 = \bar{v}^{(1)} + \bar{v}^{(2)} \tag{17}$$

where $\bar{v}^{(1)}$ is the term in a^o and $\bar{v}^{(2)}$ the term linear in a. In what follows it will be assumed that the orders of integration can be freely interchanged. Inverse Laplace

transformation of $\bar{v}^{(1)}$ gives (C.J., p. 372)

$$v^{(1)} = kh_2/[8h_1(\pi h_2 t)^{3/2}] \exp [-r^2/(4h_2 t)] . \quad (18)$$

$\bar{v}^{(2)}$ can be rewritten as

$$\bar{v}^{(2)} = (4\pi h_1)^{-1}$$

$$\int_0^\infty \xi a J_o(\xi r) \{1-\alpha^2 h_2/h_1[1+(h_1-h_2)\xi^2/(h_2\xi^2+p)]\} d\xi. \quad (19)$$

Setting $$H = k^2 h_2 a(h_1-h_2)/(4\pi h_1^2) , \quad (20)$$

and using $$L^{-1} \{1/(h_2\xi^2+p)\} = \exp (-h_2\xi^2 t) , \quad (21)$$

$$L^{-1} \{\text{constant}\} = 0 , \quad (22)$$

we get

$$v^{(2)} = -H\int_0^\infty \xi^3 J_o(\xi r) \exp (-h_2\xi^2 t) d\xi. \quad (23)$$

Using $$d/dt \exp (-h_2\xi^2 t) = -h_2\xi^2 \exp (-h_2\xi^2 t) \quad (24)$$

gives $$v^{(2)} = H/h_2 \, d/dt \int_0^\infty \xi J_o(\xi r) \exp (-h_2\xi^2 t) d\xi. \quad (25)$$

Making use of expression (29) in C.J.,Appenxix III to evaluate the integral,

$$v^{(2)} = H/h_2 \, d/dt \{1/(2h_2 t) \exp [-r^2/(4h_2 t)]\}. \quad (26)$$

The two expressions derived for $v^{(1)}$ and $v^{(2)}$ represent the response to a unit strength instantaneous point source. To get the response for a continuous line-source of strength Q, we have to integrate over time and along the entire y-axis and multiply by the "source strength" $Q/\rho_1 c_1$.

$$v_1 = Q/(\rho_1 c_1)\int_{-\infty}^{\infty}\int_0^t \{v_1(x,y-y',t-t'\} dt' dy' . \quad (27)$$

The final result is

$$v_1 = Q/(4\pi k_2) \int_{\alpha}^{\infty} e^{-u}/u \, du + Qa\varepsilon e^{-\alpha}/[4k_2(\pi h_2 t)^{1/2}] \quad (28)$$

with $\varepsilon = k_1/k_2(1-h_2/h_1)$ and $\alpha = x^2/(4h_2 t)$. (29)

The first term is the well-known line-source solution 3.3.1(10) in a medium of conductivity k_2 and diffusivity h_2. This corresponds to the limiting case where the thermal behaviour of the system is controlled by the rock only and the effect of the layer of cement is negligible. The second term is a first order correction for the layer of cement and tends to zero as time increases. The approximation is valid for $a^2/h_2 t \ll 1$.

Equation (28) can be rewritten as

$$v_1 = v_I + v_E \, , \quad (30)$$

where v_I is the first term and v_E the second, or "error" term. A graph of v_E/v_I against $h_2 t/a^2$ is plotted in Fig. 3.12 for various values of x/a. For a granite sample with k_2=3 $Wm^{-1}K^{-1}$, h_2=1.5x10^{-6} m^2s^{-1} in contact with epoxy resin (k_1=0.2, h_1=10^{-7}), the parameter ε=-0.9; for granite and fire cement (k_1=1, h_1=0.6x10^{-6}), ε=-0.5. In Fig. 3.13, values of v_E/v_I derived in this section are compared with those of 3.5.3 for a granite/fire cement interface with x/a=r/b=10. As expected from the geometry of the models, the correction is always smaller and decreases more rapidly with time in the circular symmetry case.

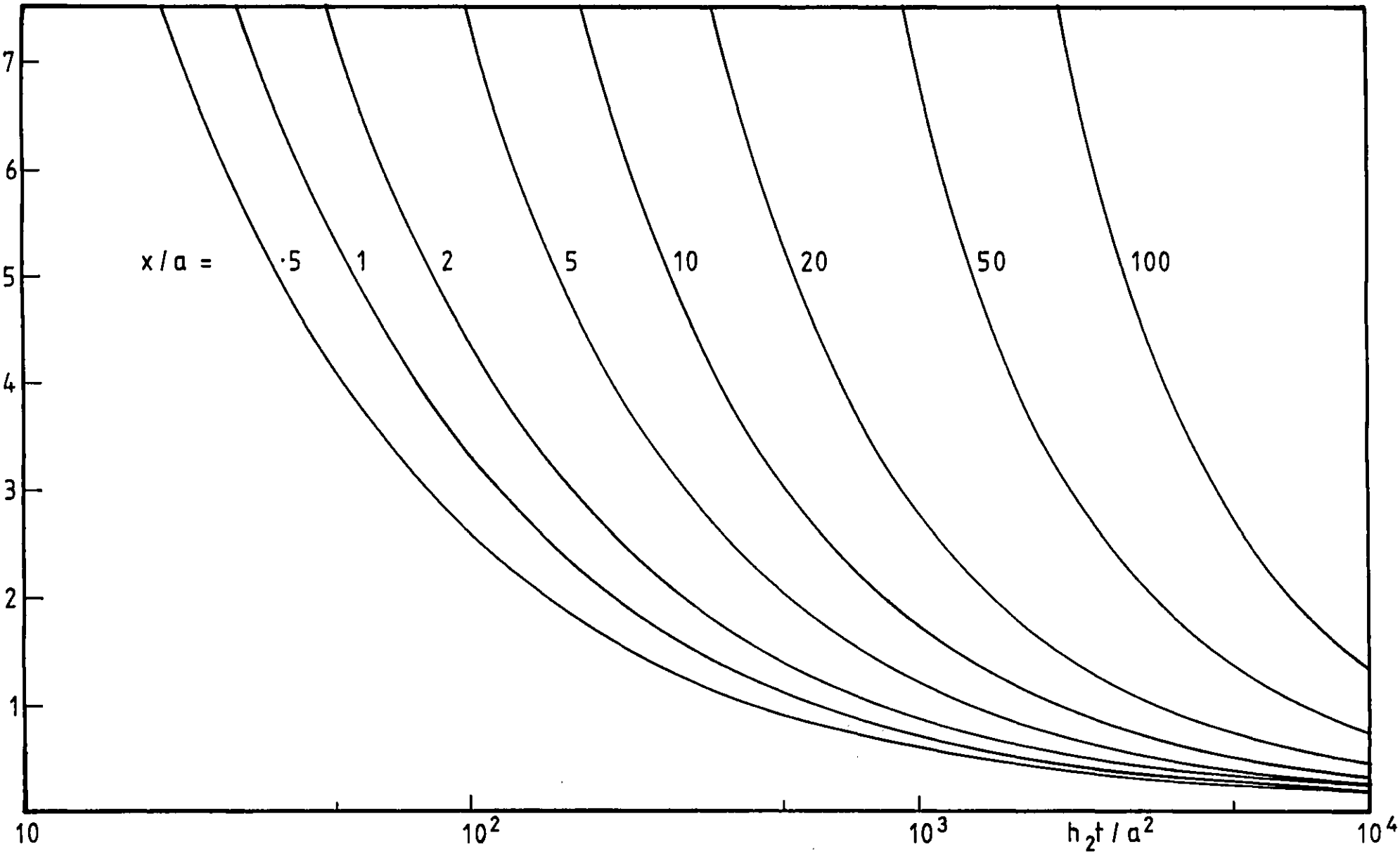

Fig. 3.12 Effect of contact resistance on line-source solution.

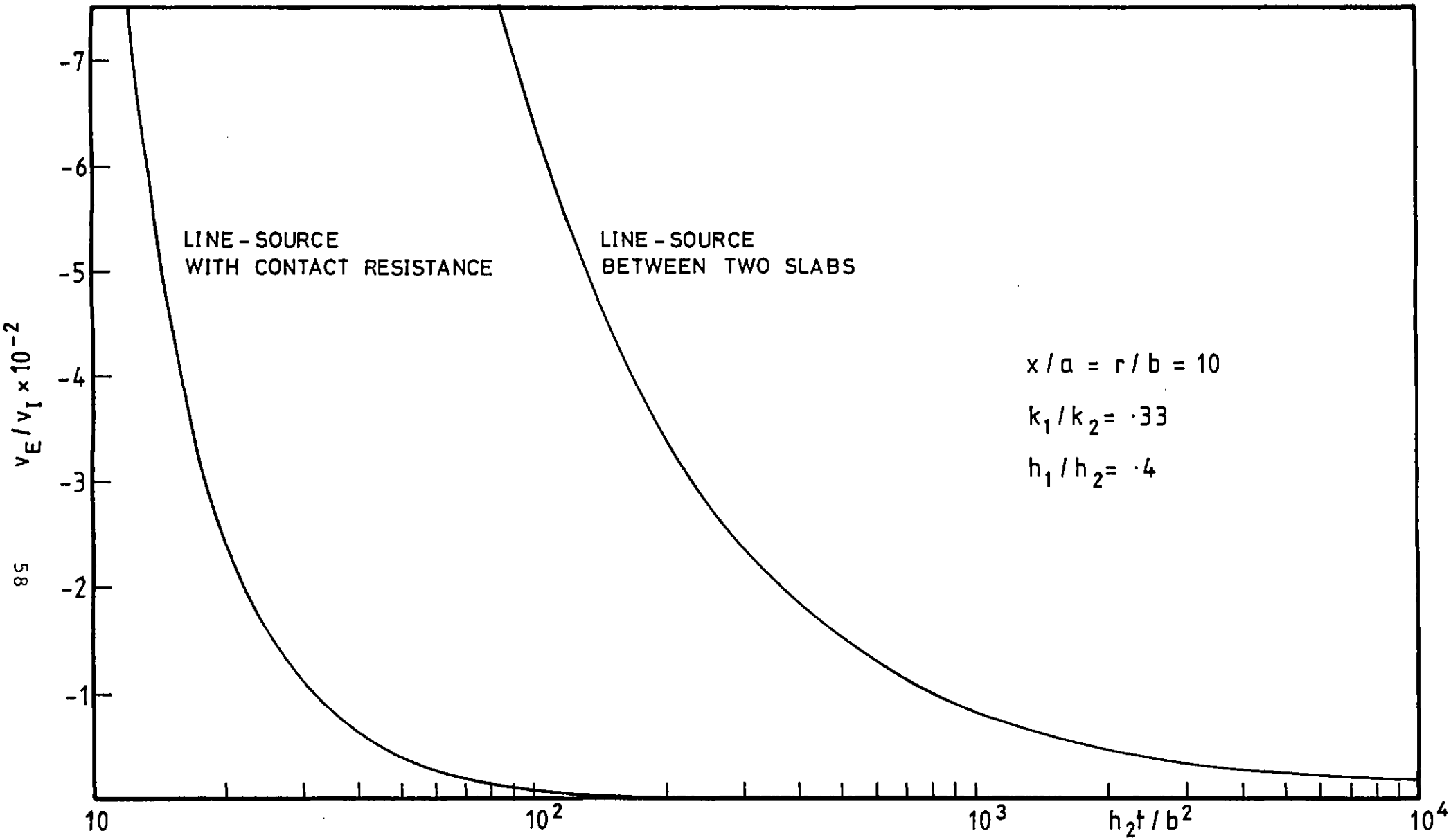

Fig. 3.13 Comparison of two contact resistance models.

3.9. Temperature equilibrium in cylindrical samples.

It is often useful to be able to predict the time a cylindrical sample takes to come to thermal equilibrium when the temperature of the surroundings is altered. In the following analysis the sample is treated as a finite cylinder, and the effect of the heater wire and thermocouple neglected. C.J. show that for a cylindrical sample $|z|<l$, $0<r<a$ initially at zero temperature and with surface temperature v_o, the temperature v at the centre point r=0, z=0 is given by

$$\frac{v}{v_o} = 1 - \frac{8}{\pi}\sum_{n=0}^{\infty}\sum_{m=1}^{\infty}\frac{(-1)^n}{(2n+1)\alpha_m J_1(\alpha_m)}\exp\left\{-ht\left[\frac{\alpha_m^2}{a^2}+\frac{(2n+1)^2\pi^2}{4l^2}\right]\right\} \quad (1)$$

where α_m is the mth root of $J_o(\alpha)=0$. The function $1-v/v_o$ is plotted against ht/b^2 in figure 3.14.

In the analysis above perfect surface contact was assumed. In practice, surface contact resistance and temperature disturbances due to imperfect stirring of the heating fluid will increase the equilibrium time. This is partly offset by the heat flowing into the sample along the heater wire and thermocouples. A treatment which takes into account the effect of a conductive wire is presented in Jaeger (1955).

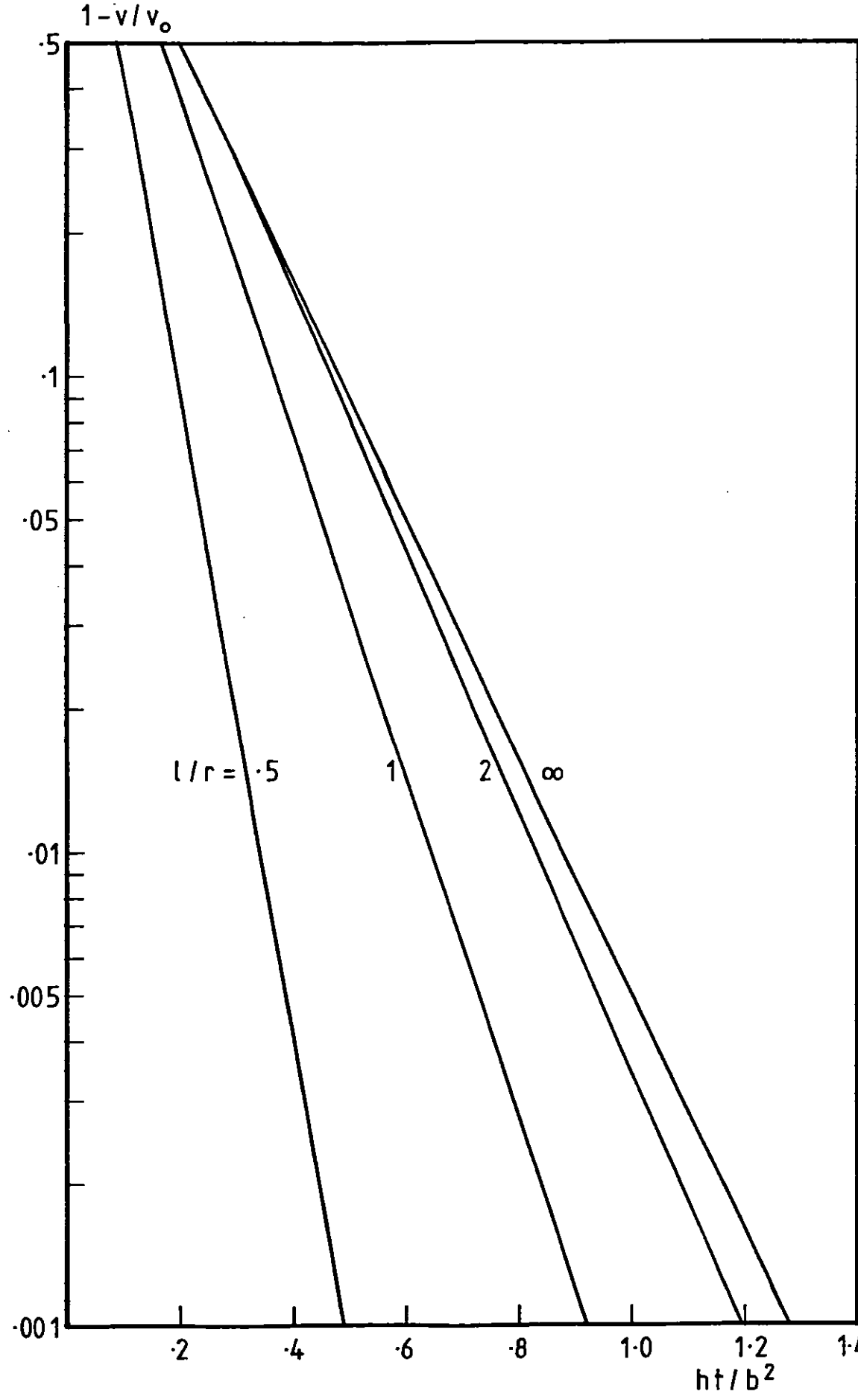

Fig. 3.14 Temperature equilibrium in finite cylindrical sample.

3.10 Nonlinear least-squares.

All the solutions of the heat equation derived in this chapter are of the form:

$$v = v(t_n;k_1,k_2,\ldots,k_p) = v(t_n,\underline{k}) \tag{1}$$

where t_n is treated as a variable and $\underline{k}=(k_1,k_2,\ldots)$ is a vector of parameters k,h,r,... . If the function v is linear in the parameters, it can be written as

$$v(t_n,\underline{k}) = \sum_{r=1}^{\infty} k_r x_{nr} \tag{2}$$

where the x_{nr}'s are known or calculable functions of t_n only. In this simple case, linear least-squares theory (see for example Jenkins and Watts, 1968) provides a way of calculating all the unknown parameters from a fit of equation (2) to a set of experimental points. In general, however, the temperature v is not a linear function of the parameters and a nonlinear least-squares fit is required. The following treatment of the problem is due to Box (1960). Suppose that within a region in the paramenter space in the neighbourhood of the true parameter $\underline{k}^*$ fair accuracy is given by the linear approximation

$$v(t_n,\underline{k}^*) \simeq v(t_n,\underline{k}^o) + \sum_{r=1}^{p} (k_r^o - k_r^*) x_{nr}^o \tag{3}$$

where $$x_{nr}^o = \{ \partial v(t_n,\underline{k})/\partial k_r \}_{\underline{k}=\underline{k}^o} \tag{4}$$

and $\underline{k}^o$ is some point within the region. $\underline{k}^o$ is a set of guessed starting values. Substituting the starting values in the response function, let $\Delta\underline{v}$ be the vector of discrepancies $\Delta v_n = v_n' - v(t_n,\underline{k}^o)$ between the observations v_n' and the calculated responses v. The expectation value of the Δv_n's is then

$$E(\Delta v_n) \simeq \sum_{r=1}^{p} (k_r^o - k_r^*) x_{nr}^o \qquad (5)$$

which is linear model of the same form as equation (2). Treating the Δv_n's as observations, we can by means of ordinary least-squares obtain an estimate $\Delta \underline{k}$ of $\underline{k}^o - \underline{k}^*$. If the functions were linear in the parameters, then the adjusted values $\underline{k}^o + \underline{k}$ for the k_r's would be elements of $\hat{\underline{k}}$, the true least-squares values. Because of nonlinearity, however, $\underline{k}^o + \underline{k}$ does not give $\hat{\underline{k}}$ at once, but a vector of "improved values" which now may be substituted for $\underline{k}^o$ to provide a starting point for a second iteration, and so on. In this way, provided the function v is well-behaved and the starting values of $\underline{k}^o$ are nt too far from the final values, the adjusted values will converge to the least-squares estimates $\hat{\underline{k}}$. The linear theory can then be used to judge adequacy of fit, to obtain an approximate representation of the sum of squares function in the neighbourhood of its minimum, and to find an approximate confidence region.

In some cases the derivatives x_{nr} are obtainable by direct differentiation of v. If this is not practicable, small changes can be made in each of the parameters in turn and the derivatives calculated from the differences. With this device it is necessary only to be able to compute the numerical value of the function v for any given values of t and $\underline{k}$ in order to carry out the iterative process. For the functions derived in this chapter, convergence to the real values $\hat{\underline{k}}$ is fast.

Nonlinear least-squares theory was used in conjunction

with the infinite line-source solution (Eq. 3.3.1 (10)) in most of the experiments to yield values of conductivity and diffusivity from a set of experimental temperatures. The equation is restated here for clarity:

$$v = -Q/(4\pi k)\ Ei(-r^2/4ht) \ . \qquad (6)$$

k and h were chosen as the adjustable parameters. Then $\underline{k}=(k,h)$ with guessed starting values $\underline{k}^o=(k^o,h^o)$. Differentiating (6) with respect to k and h,

$$x^o_{n1} = \partial v/\partial k\Big|_{k=k^o} = -v_n/k^o \qquad (7)$$

$$x^o_{n2} = \partial v/\partial h\Big|_{h=h^o} = Q\ e^{-\alpha}/(4\pi k h^o) \ . \qquad (8)$$

Eq.(5) can be written as

$$E(\Delta v_n) = \Delta k\ \partial v_n/\partial k\Big|_{k=k^o} + \Delta h\ \partial v_n/\partial h\Big|_{h=h^o} \ . \qquad (9)$$

Applying linear least-squares theory to this expression, we obtain estimates of $\Delta\underline{k}=(\Delta k,\Delta h)$:

$$\Delta k = \frac{\sum vk \sum h^2 - \sum kh \sum vh}{\sum k^2 \sum h^2 - (\sum kh)^2} \qquad (10)$$

$$\Delta h = \frac{\sum vh \sum k^2 - \sum kh \sum vk}{\sum k^2 \sum h^2 - (\sum kh)^2} \qquad (11)$$

where v,k,h were substituted for $\Delta v_n, x^o_{n1}, x^o_{n2}$ respectively for clarity. The sums extend over all n's. $k^o+\Delta k, h^o+\Delta h$ are then substitted for k^o, h^o respectively, and the iteration repeated to the required accuracy. The method was also tried in conjunction with equation 3.5.3(11) and three adjustable parameters, but the increased comlexity of the calculations was not offset by a better accuracy, and the method was not pursued.

3.11 Summary of results.

The ideal line-source solution (equation 3.3.1(10)) was found to represent the temperature field within the rock adequately in the experiments, and was used in all calculations of conductivity. Because this equation cannot be inverted to give values of conductivity and diffusivity explicitly, the nonlinear least-squares technique outlined in sections 3.10 is required for calculations of the thermal parameters.

Several factors contribute to departures from the ideal line-source solution, but they can be minimized by a suitable choice of experimental parameters. As shown in section 3.4 the finite thickness of the heater (0.2-0.3 mm) only caused an appreciable departure from the ideal solution in the first second of an experiment, and can be neglected. The contact resistance between heater and rock causes more serious departures from the ideal case at low times, which become progressively less important at larger times, thus imposing a lower bound on the sampling time. The approximate model of section 3.5.3 predicts an error of less than 1% at times greater than 20 s for a typical granite ($k=3$ $Wm^{-1}K^{-1}$, $h=1.5\times10^{-6}$ m^2s^{-1}) in contact with epoxy resin ($k=0.2$, $h=10^{-7}$) and times greater than 30 s for granite/fire cement ($k=1$, $h=0.6\times10^{-6}$). The more realistic model of section 3.8 predicts minimum sampling times of 50 and 25 s respectively.

The finite dimensions of the samples cause heat reflections at the surface at large times and impose an upper bound to the sampling time for a rock specimen of a given diameter. For a lagged sample 6×10^{-2} m in diameter

such time is 180 s (section 3.6.2) and for a sample in a constant temperature environment 150 s (section 3.6.1). As shown in section 3.7, for a maximum sampling time of 150 s, the length of a typical specimen must be at least 6×10^{-2} m for an error of less than 1%.

Temperature equilibrium to within 0.1 K in a sample 6×10^{-2} m in diameter and 0.12 m long subjected to a surface temperature increase of 10 K is reached in 15 minutes (section 3.9). All these figures must be re-calculated referring to the relevant diagrams in this chapter if the size or conductivity of the specimen, the type of adhesive or the sampling window are modified considerably.

Chapter 4

APPARATUS

4.1 Line-source apparatus.

The line-source apparatus, shown schematically in Fig. 4.1, comprises the following main working blocks:

1) A set of rock samples under measurement, provided with an axial heater and thermocouple (only one sample is shown in figure 4.1 for simplicity). A cross-sectional view of a typical sample is given in Fig. 4.2.
2) An oven to maintain the samples at a constant temperature prior to measurements and a set of thermocouples for the measurement of oven temperature.
3) A power supply to energize the linear heaters and ancillary circuits to measure such power.
4) Signal processing apparatus for amplification and filtering of thermocouple voltages.
5) A microcomputer for the acquisition, digitization and recording of sample temperature and power data, control of the heater and real-time data reduction according to the exponential integral solution described in chapter 3.

The apparatus is described in detail in the rest of this chapter.

4.2 Rock samples, ovens and power measurements.

4.2.1 Sample preparation.

All the samples investigated were cylindrical, which led to a simplification of the mathematical modelling. However,

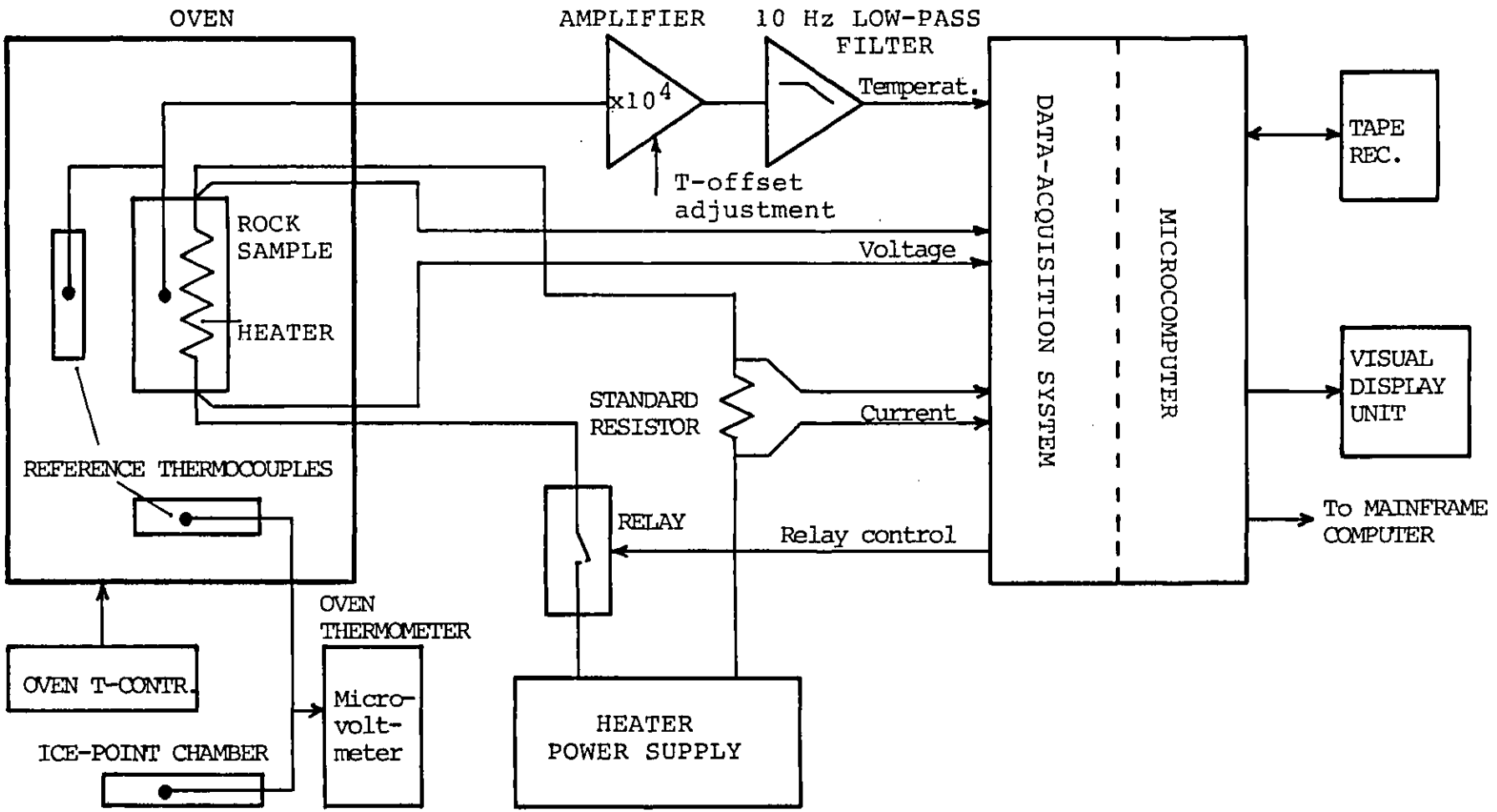

Fig. 4.1 Line-source apparatus.

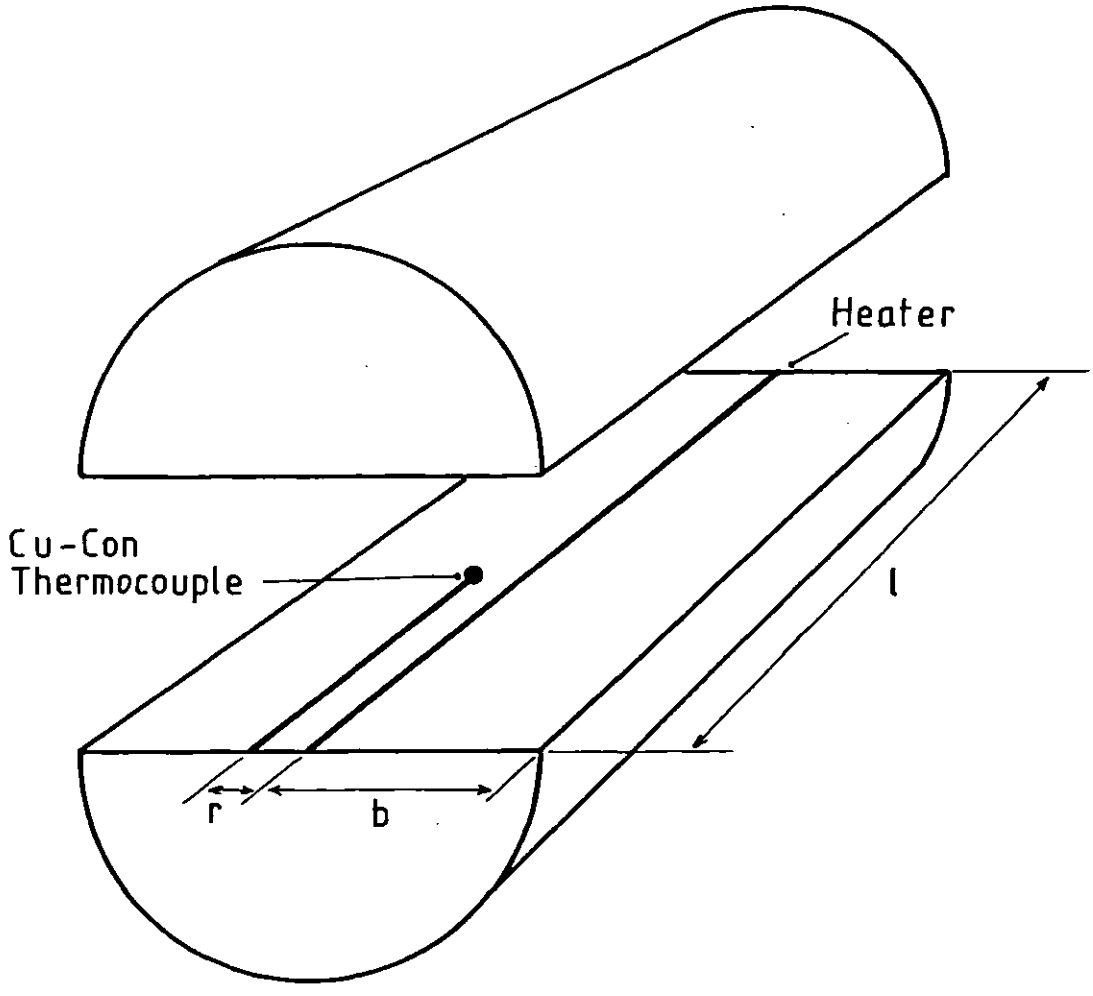

r	THERMOCOUPLE OFFSET	= 1-4 mm
b	SAMPLE RADIUS	= 30-40 mm
l	SAMPLE LENGTH	= 60-120 mm
	APPROX. DIAMETER OF GROOVES	= 0.5 mm

Fig. 4.2 Cross-sectional view of rock sample.

the shape is not critical provided the samples are large enough to satisfy the requirements set out in sections 3.6 and 3.7. Sample preparation was relatively simple: the rock samples were cored (if required) to a diameter of 60-75 mm, the ends cut at right angles to a length of 60-120 mm and the cylinders sliced longitudinally into two semicylinders. Grooves were then scribed into one of the semicylinders to accommodate the nichrome and constantan heater (diameter 0.2-0.3 mm) and one or more copper-constantan thermocouples (wire diameter 0.12 mm - 40 SWG) parallel to the heater. The two semicylinders were then bonded back together with high-temperature epoxy resin, fire cement or zinc oxide-loaded silicone grease if quick dismantling was required. Two high-temperature PTFE-coated leads were welded to either side of the heater for the supply of current and measurement of voltage.

4.2.2. Power measurements.

The heater wires were subjected to very large temperature variations, with a consequent variation in their electrical resistances. Constantan was found to perform better than nichrome under these conditions due to the lower temperature dependence of its electrical resistivity and was used in the later experiments. However, resistance variations of 1% over a temperature range of 250 K were observed even in the constantan wire. To obtain a better accuracy in the power measurements, the voltage across the heater and the current through it were monitored separately, the current being measured as a voltage across

a high-stability resistor of known value. The two signals were digitized separately by the microcomputer and multiplied digitally at the data reduction stage. A check could thus be kept on the variations of electrical resistance with temperature and time. Typical voltages were of the order of 3-5 V, and currents 1-2 A, giving linear power inputs of the order of 30-60 W/m.

The measured thermal conductivity of a sample is directly dependent on the linear power supplied to the heater. The greatest source of error in this parameter is probably due to mis-positioning of the welded joints at either end of the sample. For a sample 100 mm long, an uncertainty of 1 mm in the position of the voltage sensing leads introduces an error of 1% in the measured conductivity. This was taken as the average estimated error in the power measurements.

4.2.3 Ovens.

The samples were maintained at a constant temperature in one of three different temperature-regulated enclosures:

1) A laboratory oven (Gallenkamp OV 150) with automatic on/off temperature control for the temperature range 300 to 470 K. The temperature stability was better than 0.1 K over the duration of one conductivity measurement (Fig. 4.3). Slight temperature gradients existed inside the oven and had to be taken into account. The oven could accommodate up to eight samples on each of three trays.

2) A constant-temperature water/ethyl glycol bath (Colora Ultra Cryostat KT 20 S) for temperatures between 250 and 370 K, with a quoted temperature stability of 0.03 K. It

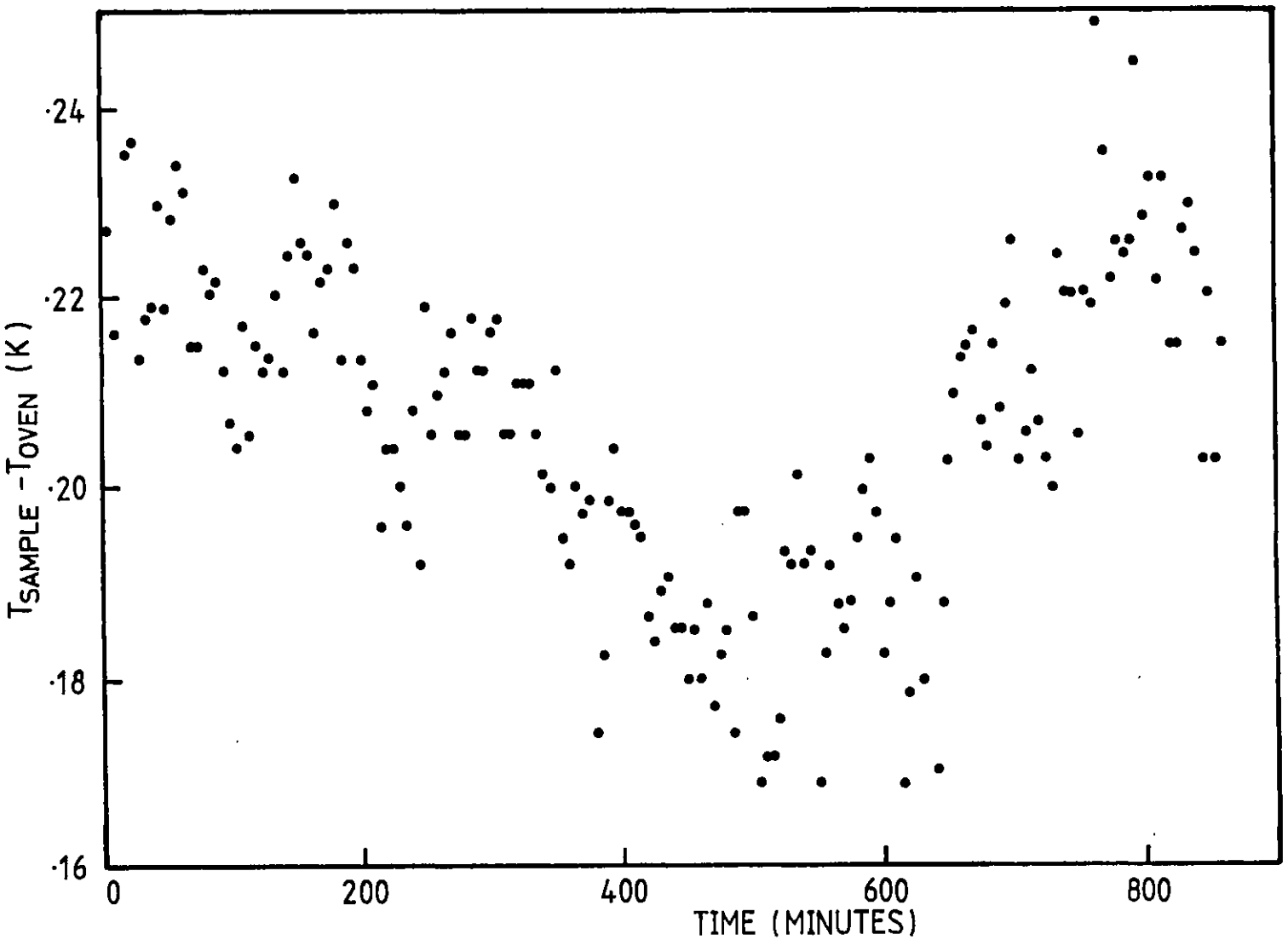

Fig. 4.3 Measured temperature drift in oven (including amplifier drift).

could accommodate up to two samples, which were coated with self-amalgamating tape and wrapped in polythene bags for insulation of the elecrical connections.

3) An autoclave (Fig. 4.4 and 4.5 - modified Chas Cook & Sons 0.75 litre stainless steel high-pressure autoclave) for high temperature and high pressure experiments (up to to 770 K and 50 MPa respectively). It was capable of accommodating one sample in a specially-designed holder. Oil was used as the pressurizing fluid. All the electrical connections were sealed by a high pressure, high temperature gland provided with a magnesium silicate sealing element. A proportional temperature control circuit was designed and built (for details see Appendix I) to give a temperature stability of 0.1 K over a time interval of 200 s.

Temperature equilibrium to within 0.1 K between samples and oven or autoclave was usually reached in 8-12 hours. However, best conductivity results were obtained if the samples were left in the oven at a constant temperature for 20-24 hours. These much larger times than the results of secion 3.9 suggest are accounted for by the extra time the oven itself takes to come to equilibrium. In the cryostat, much shorter equilibrium times (2-4 hours) were possible because of the better mixing and higher thermal conductivity of the heating fluid. Measurements on the same sample could be repeated at intervals of one hour in air and 30-40 minutes in water.

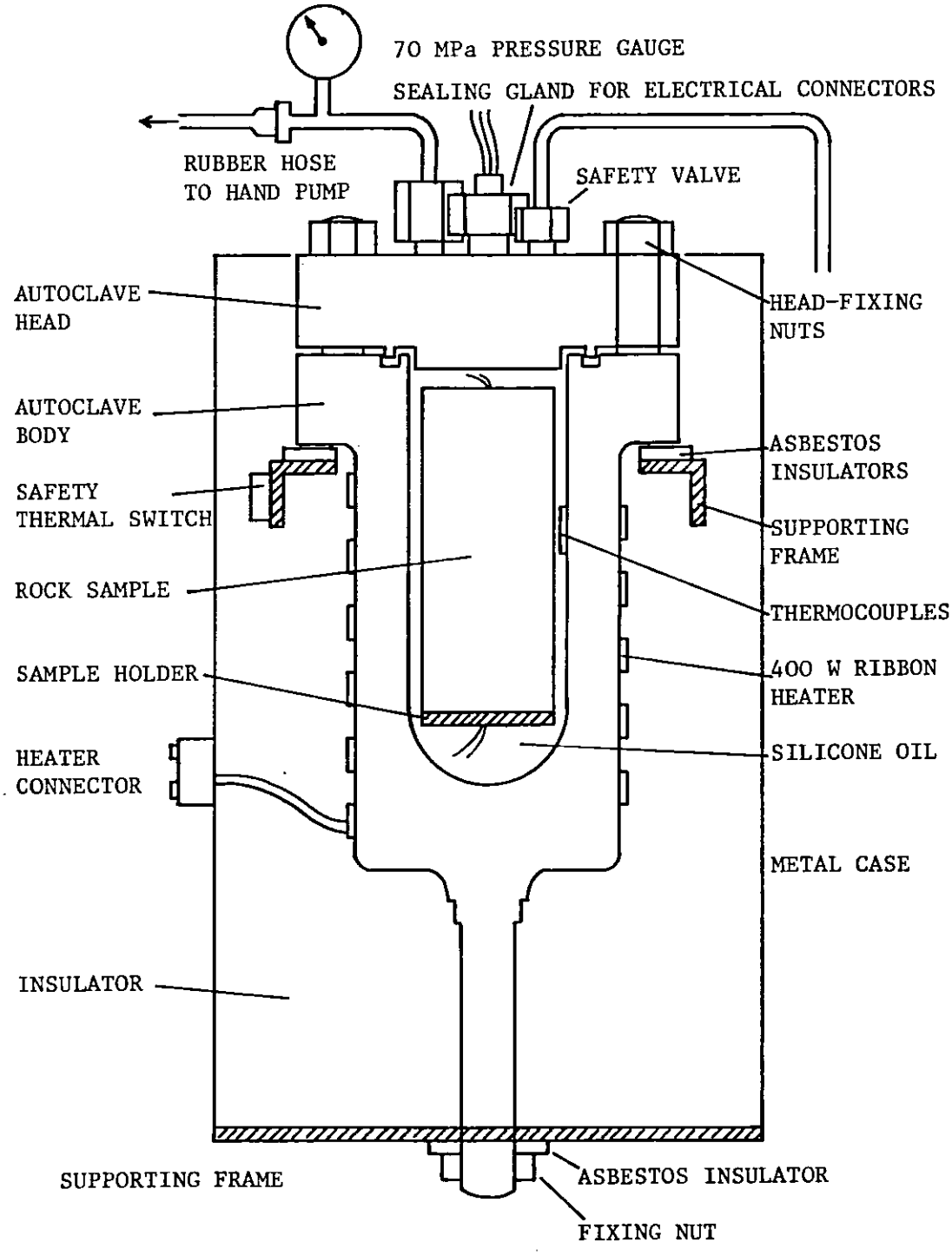

Fig. 4.4 Cross-sectional view of autoclave.

Fig. 4.5 High-pressure equipment.
From left to right are visible the oil pump, the autoclave with the pressure gauge, two rock samples, the microvoltmeter, the heater power supply with the current-sensing standard resistor and the heater relay, the zero-point chamber, the thermocouple amplifier and the autoclave temperature regulator.

HEATER WIRE

4.3 Temperature measurements.

4.3.1 Thermocouples.

T-type copper-constantan (Cu/Cu-43Ni) thermocouples were used throughout the experiments for the measurement of oven and rock temperatures. They were constructed by welding cotton-covered copper and constantan wires from the same batch in a Helium atmosphere.

Thermistors (Robertson **et al.**, 1966; Sachse, 1975) were also considered as temperature sensors because of their high sensitivity at moderate temperatures but were rejected because of the following limitations:

- Low maximum working temperature - about 400 K for the small thermistors needed in the present experiments
- Slower response than thermocouples for the same sensor size
- Need for individual temperature calibrations for each thermistor
- Severe loss of sensitivity at high temperatures
- Drift due to mechanical and thermal shock
- Higher cost than thermocouples.

T-type thermocouples have a range of 80 to 640 K and a high thermoelectric power in the temperature range 270 to 500 K, their sensitivity ranging from 38 μV/K at 270 K to 61 μV/K at 640 K. Due to the rapid oxidation of copper at high temperatures, the maximum working temperature is lower than that of other thermocouple types such as iron-constantan. This was not a limitation in the present experiments as oven and rock temperatures were kept below 600 K at all times.

4.3.2 Thermocouple calibration.

The voltage-temperature characteristic of a T-type thermocouple can be represented by an equation of the form

$$V = aT_c + bT_c^2 + cT_c^3 \qquad (1)$$

between 270 and 570 K, to within 0.2 K (Kinzie, 1973). T_c is the temperature in ^oC and V the output voltage. The constants a, b, c are determined by a cubic least-squares fit to a set of calibration points. Table 4.1 shows the thermoelectric voltage as a function of temperature for the thermocouples used for the transient measurement of rock temperatures as quoted by the manufacturers.

Basset (1979) calibrated three thermocouples from the same batch against a platinum resistance thermometer (Rosemount Engineering Company model WS 104 calibrated to 0.01 K by the National Physical Laboratory) in the range 270-330 K and obtained e.m.f. values very close to those quoted by the manufacturers. A least-squares fit of equation (1) to Basset's data complemented by the data from table 4.1 in the range 330 to 470 K gave the following values for the constants:

$$a=38.736\ \mu V/^oC$$
$$b=0.036\ \mu V/^oC^2 \qquad (2)$$
$$c=1.5\times10^{-7}\mu V/^oC^3\ .$$

All the deviations of the experimental data from the cubic fit are less than 10 μV, or about 0.25 K, which is of the same order of magnitude as the resolution of the data in table 4.1.

The thermocouple sensitivity S(T) is defined as the first derivative of equation (1) with respect to temperature:

TABLE 4.1 E.m.f. values (mV) for copper/constantan thermocouples (B.S. 1828/1921). Manufacturer's data.

°C	0°	100°	200°	300°
0	0	4.24	9.18	14.66
5	0.19	4.47	9.44	14.95
10	0.39	4.70	9.70	15.24
15	0.58	4.94	9.97	15.53
20	0.78	5.18	10.24	15.82
25	0.98	5.41	10.50	16.11
30	1.19	5.65	10.77	16.40
35	1.39	5.89	11.04	16.69
40	1.60	6.14	11.31	16.99
45	1.81	6.38	11.59	17.28
50	2.02	6.63	11.86	17.58
55	2.23	6.88	12.14	17.88
60	2.45	7.13	12.41	18.17
65	2.67	7.38	12.69	18.47
70	2.88	7.63	12.97	18.77
75	3.11	7.88	13.25	19.07
80	3.33	8.14	13.53	19.37
85	3.55	8.40	13.81	19.68
90	3.78	8.66	14.10	19.82
95	4.01	8.92	14.38	20.29

0°C at cold junction.
Tolerances to B.S. 1041/1966: 0°C - 100°C ±1°C
100°C - 400°C ∓1%

$$S(T) = dV/dT = a + 2bT_c + 3cT_c^2 . \quad (3)$$

To obtain a measure of the scatter in sensitivities, a least-squares fit of the linear equation

$$V = a'T + b' \quad (4)$$

to a set of experimental points was performed for three random thermocouples in the range 270 to 330 K. The mean value of a'=41.04 uV/K with a standard deviation of only 0.01 uV/K suggested that the likely scatter in sensitivities was too small to warrant individual calibration for every thermocouple. Equations (1) or (3) and the constants (2) were therefore used to convert voltage readings into temperatures for all thermocouples.

Roeser and Lonberger (1958) indicated that a given couple will maintain its calibration within 0.2 K up to 570 K. Repeated temperature cycling does not cause significant drift (Baxter et. al., 1969). When the e.m.f. of the calibrated thermocouples is compared with reference tables (e.g. Roeser and Dahl, 1938), the calibration output differences are usually proportional to the thermoelectric voltage. In other words, a 10 V error at 1 mV output will double when the output is 2 mV. Kinzie (1973) quotes the accuracy tolerance typical of commercial thermocouples as $\pm$0.8 K between 210 and 370 K and 0.3% of reading between 370 and 470 K. Kinzie also reports a pressure dependence in the thermoelectric potential, whereby increased pressure results in a decreased output. A nearly linear temperature vs. pressure correction curve holds from 0 to 7×10^3 MPa, giving an additive correction of about 5.2×10^{-4} K/MPa when there is a 100 K temperature difference between the

thermocouple junctions. This correction was considered too small to be significant in the present work, and was neglected.

4.3.3 Temperature measurements.

The temperatures of the oven, cryostat and autoclave were measured by a copper-constantan thermocouple. The hot junction was inserted in an aluminium block to smooth out rapid temperature fluctuations, the cold junction being maintained at the ice point in an air-cooled ice point reference chamber (De la Rue Frigistor model 106) with automatic temperature control, quoted temperature accuracy of 0.00 to 0.05 K and temperature stability of $\pm$0.01 K. The resulting e.m.f was measured with a differential voltmeter (Honeywell model 1002 and later Fluke 8860A or Fluke 8050A) to an estimated accuracy of $\pm$10 μV, or about $\pm$0.25 K. The voltage reading was then converted to a temperature value by a microcomputer program making use of the first two terms of equation (1) together with the values in (2) for the constants a and b. The contribution of the cubic term in (1) was found to be negligible for temperatures up to 500 K. The overall acuracy was estimated at about 0.5% due to thermocouple calibration errors plus 0.5% due to the slight temperature gradients in the ovens.

Small diameter thermocouples (0.12 mm wire) were used in the transient measuremnts of the temperature of the rock samples. The thermocouple wires were positioned parallel to the heaters to reduce conductive heat losses along the wires. In this arrangement, the leads run roughly parallel to equithermal surfaces, thereby reducing the distortion of

the temperature field within the rock. The reference junction of the thermocouple was placed in a second aluminium block inside the oven. This proved sufficiently stable for most measurements as the e.m.f.'s of the two junctions were nearly equal and tended to track each other during fluctuations in the oven temperature. The output voltage V of the thermocouple was then a measure of the temperature difference v between the oven and the rock sample, which allowed direct amplification of the signal without the need for a large and accurate offset reference, and a means of testing the thermal equilibrium between oven and sample. The temperature was calculated from the sensitivity S(T) of the thermocouple at the temperature T using the expression

$$v=V/S(T) \ . \qquad (5)$$

For measurements at oven temperatures within $\pm$20 K of the ice point, the ice point chamber was used as the cold junction reference point because of its better stability; a voltage offset was subtracted from the output of the amplifier in order to bring the signal within the range of the data acquisition system.

4.4 Signal processing.

4.4.1 Noise.

The very low voltage levels associated with thermocouples in the high-resolution temperature measurement system required protection against electrical noise. The main types of noise encountered and the steps taken to counteract them are listed below in order of importance (Fig. 4.6):

1) Shot noise and 1/f noise (Motchenbacher and Fitchen, 1973) caused by the semiconductors in the front stage of the thermocouple amplifier contributed most to the overall noise figure. Because they lie in the same frequency range as the signals (Fig. 4.6), they could only be partly reduced by the use of a good thermocouple amplifier with a low noise figure (see section 4.4.2).

2) Electromagnetic interference was reduced by screening of cables and amplifier, avoiding earth loops and using an amplifier and data acquisition system with differential inputs, and by careful design of the power supplies. Filtering of the signals (section 4.4.3) and digital filtering of the data (section 4.4.4) also gave good results as this type of noise has characteristic frequencies higher than those of the signals (Fig. 4.6). The thermocouple wires between the oven and the switches could not be screened. However, noise picked up in this section partly cancelled out because the thermocouple wires ran parallel and close to each other, thus being subjected to electromagnetic fields of roughly equal strength.

3) Thermoelectric noise in the thermocouple connections and

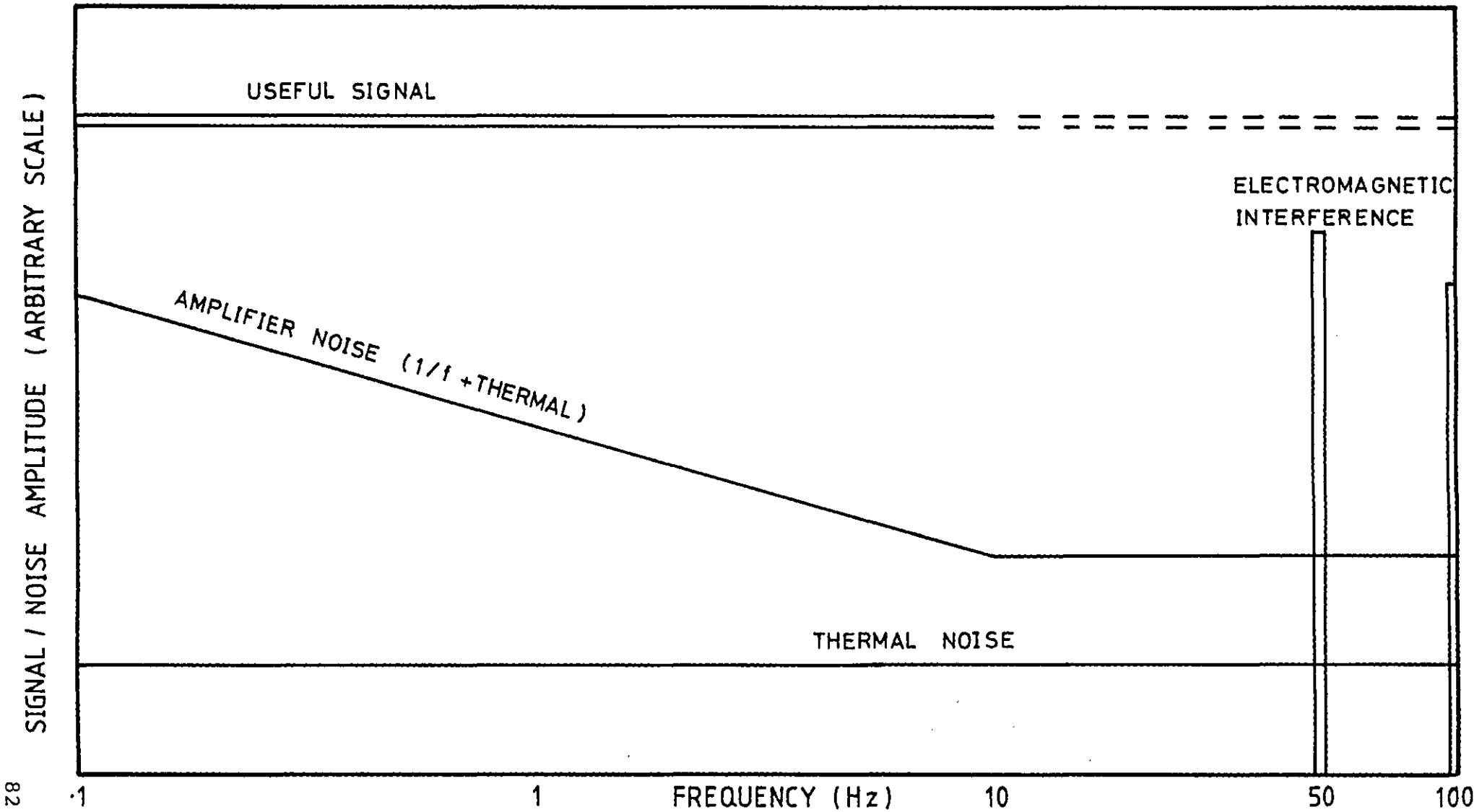

Fig. 4.6 Spectral density of signal and noise (arbitrary units). The amplitudes of the signal and noise are not to scale.

switches was minimized by spreading thermally conductive silicone grease on switches and using compensating cables from the same batch of wire as the thermocouples.

4) Thermal noise. In a resistor of value R, the thermal noise e.m.f. in the frequency range Δf is given by (King, 1966)

$$E = (4kTR\ \Delta f)^{1/2}$$

where $k=1.38 \times 10^{-23}$ J/K is Boltzmann's constant and T the absolute temperature. E was kept to a minimum by reducing the resistance of the thermocouple leads and limiting the signal bandwidth with a low-pass filter (see section 4.4.3).

4.4.2 Thermocouple amplifier.

The thermocouple amplifier is the most critical component in the signal-processing apparatus because of the small voltages involved. It must satisfy the requirements of very low temperature drift, low noise and relatively fast response. A chopper amplifier (Hewlett Packard model 425A) was used in early experiments, but it soon proved inadequate due to its limited bandwidth (0.2 Hz). An amplifier based on an integrated instrumentation amplifier (IA) was then designed and built (see Appendix I) having good frequency response and moderate drift. This was later replaced by an improved amplifier based on an IA (Analog Devices model 606M) offering excellent drift and noise performance (Analog Devices, 1979). Referring to Fig. 4.7, the gain equation of the amplifier is

$$V_{out} = G(V^{+}-V^{-}) + V_{REF}$$

when $V_{sense}=V_{out}$. The gain G, calculated from the formula

$$V_{out} = (1+4x10^5/R_G)\ (V^+ - V^-) + V_{REF}$$

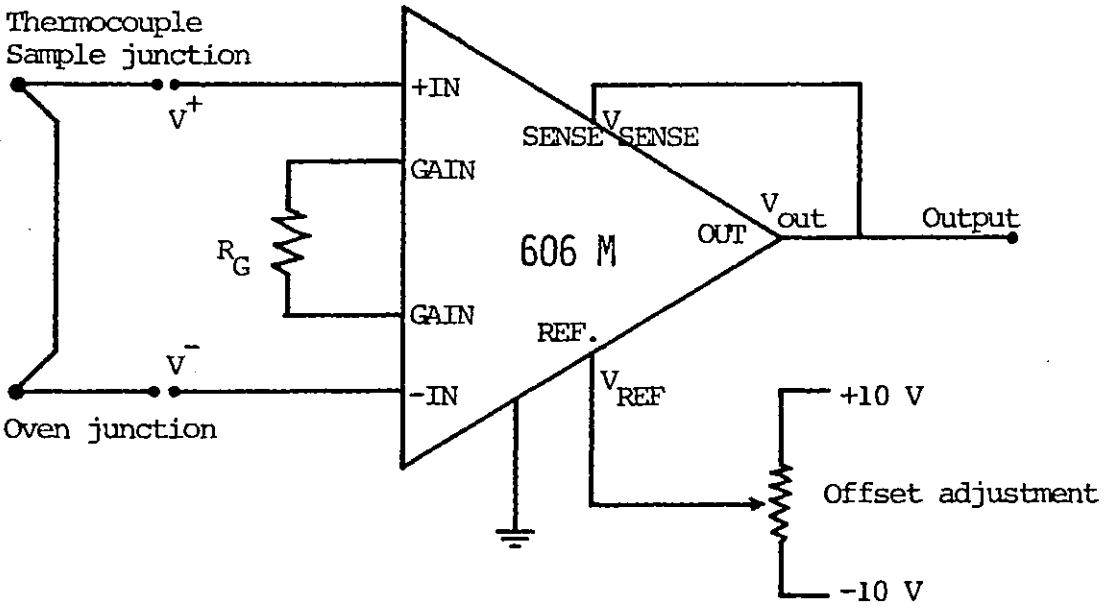

Fig. 4.7 Instrumentation amplifier used as the thermocouple amplifier.

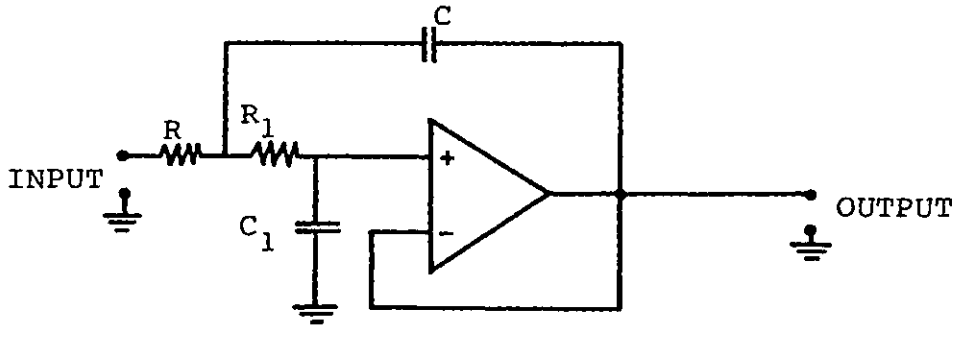

Fig. 4.8 Second-order low-pass filter. Two such sections were cascaded to give the required fourth-order response.

$G=1+4x10^5/R_G$, was set to 10,000 to give a sensitivity of about 0.4 V/K at the output when used in conjunction with copper-costantan thermocouples. V_{REF} had a range of -10 to +10 V and was adjusted before each conductivity measurement to cancel out small voltage differences between the thermocouple junctions.

Table 4.2 shows the main characteristics of the IA: unlike operational amplifiers, the input impedance of both inputs is very high and independent of gain (Riskin, 1979), which keeps electrical loading of the thermocouples low. The high common-mode rejection ratio ensures good amplification of the differential signals (V^+-V^-) and rejection of unwanted common mode signal between either input and ground, thus minimizing the effects of ground loops and electromagnetic interference. The gain accuracy of the amplifier over the frequency range 0.01 to 10 Hz is 0.2%, 0.1% being cotributed by the intrinsic amplifier accuracy and 0.1% by the gain-setting resistor R_G, while the gain nonlinearity is negligible. The temperature fluctuations within the amplifier case over the time of one conductivity run is estimated to be less than 1 K, causing a drift in input voltage of less than 0.2 uV. The severe effect of warm-up drift was eliminated by leaving the amplifier turned on during sets of measurements and by allowing 1-2 hours warm-up time when switching off proved necessary. The wide bandwidth of the IA insured a very flat response well beyond the frequencies of interest. The input voltage noise of 1 uV peak-to-peak was the most serious cause of error and limited the overall accuracy of the

TABLE 4.2 Specifications of Analog Devices Model 606 M instrumentation amplifier used as the thermocouple amplfier (typical at 298 K, gain G=10,000 unless otherwise stated).

Gain range	1 to 10,000
Gain accuracy (G=100)	±0.1% max.
Gain nonlinearity	±0.002%
Input offset voltage:	
warm-up drift, 10 minutes	±5 uV
vs. temperature	±0.25 uV/K max.
vs. supply	±3 uV/V
Input differential current offset:	
vs. temperature	±20 pA/K
Frequency response:	
for 3 dB attenuation	5 KHz
for 0.1% amplitude accuracy	200 Hz
Input voltage noise (0.01 to 10 Hz)	1 uV p-p max.
Common-mode rejection ratio	110 dB
Input impedance	10^9 ohm/3 pF
Reference terminal offset range	±10 V

temperature measurements to about 25 mK. The "high" frequency components of this noise (1 to 10 Hz) are largely smoothed out by the least-squares fit during data reduction, being as likely to cause positive deviations as negative ones, but at the low end of the noise spectrum (0.01 to 1 Hz) the fluctuations have a period of the same order of magnitude as the data collection window and cannot be distinguished from the signal. This directly affects the repeatability of the conductivity results. Also , the amplitude of the amplifier noise has a 1/f behaviour (Fig. 4.6), so that its largest components lie in the critical frequency range. Even lower frequency components are probably present (Motchenbacher and Fitchen, 1973), but their effects are difficult to quantify due to the lack of manufacturer's data.

The new types of integrated "commutating auto-zero" (CAZ) and monolithic chopper amplifiers (Intersil, 1982) are of great interest in low-drift signal processing applications because of their exceptionally low long-term and temperature drift characteristics (down to 200 nV/year and 5nV/K respectively). However, they have narrow bandwidths, high noise figures in the 0.1 to 10 Hz frequency band and tend to produce large spurious voltage spikes. It is likely that, as the technology in this field evolves, commutating amplifiers will become more suitable for fast microvolt-level amplification than those based on conventional techniques.

4.4.3 Low-pass filter.

A low-pass filter was inserted between the thermocouple amplifier and the data-acquisition system to reduce high-frequency amplifier noise and 50 Hz electromagnetic interference. To obtain a wide frequency response with good high-frequency attenuation, a fourth-order Butterworth filter was designed (Daryanani, 1976, Moschytz, 1975). The magnitude of the response function of the filter is

$$H(f) = [\ 1+(f/f_o)^8\ ]^{-1/2}$$

where f is the frequency and f_o=10 Hz is the -3 dB point. The graph of this function, plotted in Fig. 4.9, shows that the low-frequency gain is unity and that the theoretical attenuation is about 56 dB at 50 Hz and 80 dB at 100 Hz. Limiting the bandwidth of the filter to 10 Hz reduces the intrinsic noise of the thermocouple amplifier to less than 1 uV peak-to-peak. To implement the filter, two second-order active filters of the type shown in Fig. 4.8 were cascaded. The circuit diagram of the filter is given in Appendix I.

Low-pass filters introduce a delay in the signal, to obtain a measure of which the response of the filter to a unit step function was calculated. The response function, plotted in Fig. 4.10, is seen to settle to within 1% of the value of the input function in a time of about 0.2 s. This is equivalent to introducing a delay of the same order of magnitude in the output. Assuming a maximum rate of temperature increase of about 10 mK/s in the region of interest, the error in the output due to the filter delay is about 2mK, of the same order of magnitude as the resolution of the thermocouple amplifier. This was

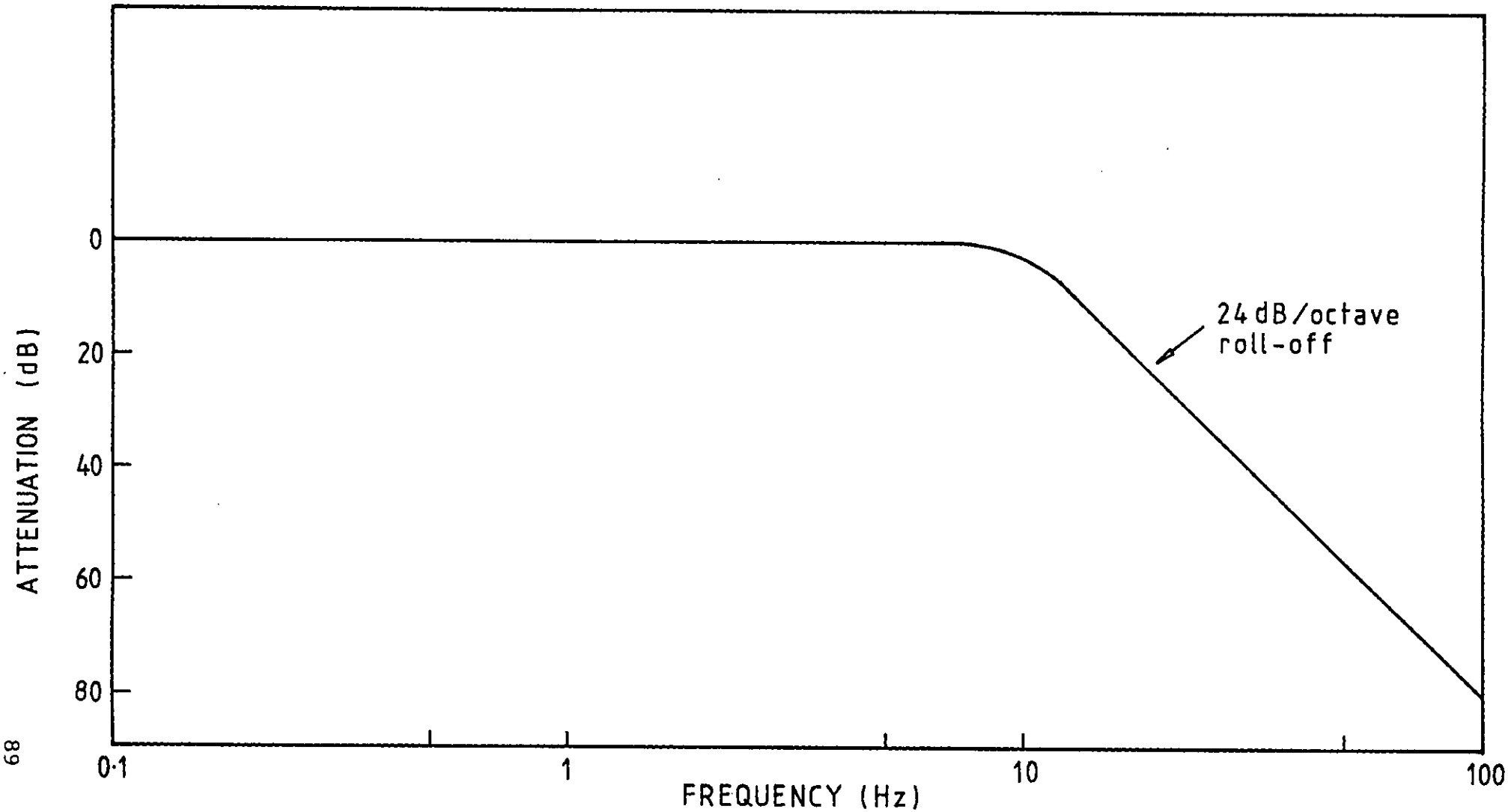

Fig. 4.9 Frequency response of 10 Hz low-pass filter.

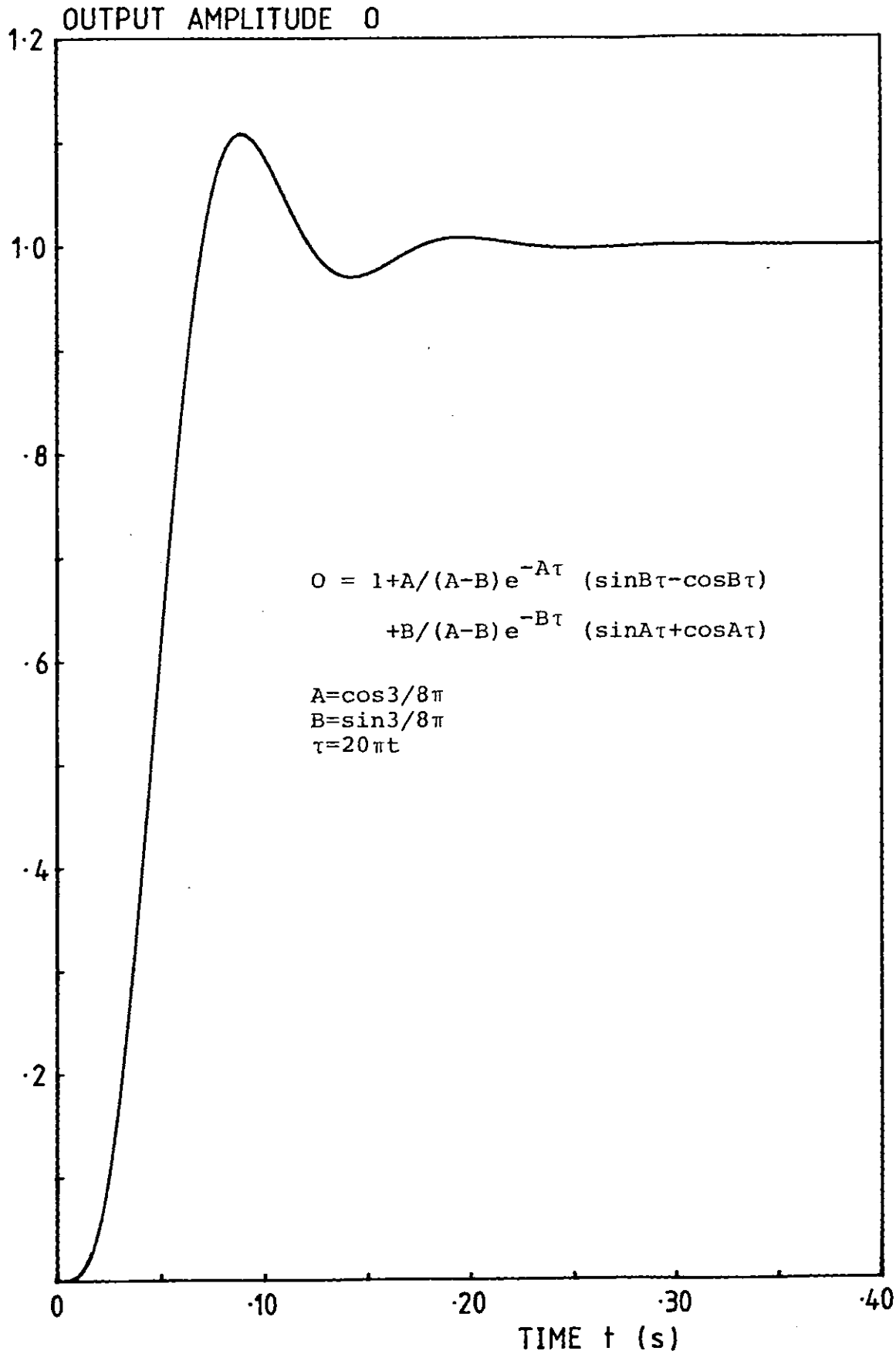

Fig. 4.10 Transient response of fourth-order 10 Hz Butterworth low-pass filter to unit step function.

considered a good tradeoff between the conflicting requirements of fast response and low noise.

4.4.4 Digital filtering.

A digital filter was used for further reduction of the noise in the data. The low-pass filter described in the previous section proved very effective but electromagnetic interference was still injected into the line between the low-pass filter and the data acquisition system (Fig.4.1). Also, as the voltage and current-sensing lines of the heater were not filtered, they were particularly sensitive to electromagnetic interference in the electrically noisy laboratory. The sampling time-window of the data acquisition system was very small (of the order of a few microseconds) so that even fast unwanted transients were recorded. In order to minimize these effects, digital low-pass filtering of the data was attempted at an early stage in the experiments: fast Fourier transformation of the input time series was performed, the high frequency components suppressed above a given cutoff frequency, and the resulting spectrm inverse-transformed (Jenkins and Watts, 1968). Although the results were satisfactory, the procedure was not deemed to be suited to rapid routine data analysis by a simple microcomputer, and therefore was not pursued. A simpler, but effective digital filter was developed instead. A set of 250 data readings taken in rapid succession were averaged over a time interval t'=20 ms equal to the period of the mains voltage. Each reading is the sum of a slowly increasing signal s(t) and periodic

interference of the form $n(t)=A\cos(wt+\Phi)$. As t' is very small, s(t) is nearly linear in the interval (0,t'), so its average value is s(t'/2). Integrating n(t) over (0,t') gives the average interference

$$\langle n\rangle = A\,\frac{\sin(wt'+\Phi) - \sin\Phi}{wt'} \quad . \qquad (1)$$

As shown in figure 4.11, this function has zeroes at $f=w/2\pi=50,\ 100,\ 150,\ldots$ Hz, so that mains-borne interference is completely suppressed together with all its harmonics. Fluctuations in the mains frequency somewhat reduce the effectiveness of the filter. From equation (1), the average noise at the frequency $(w_o+\Delta w)$ close to w_o will be (neglecting the phase)

$$\langle n\rangle(w_o+\Delta w) = A\,\Delta w/w_o \quad , \qquad (2)$$

so for a typical fluctuation $\Delta w/w_o=0.01$ in the mains frequency, the noise attenuation will be about 100. The filter is thus seen to have a small effect on the signal while offering good rejection of electromagnetic interference and some reduction of high-frequency noise.

4.5 The microcomputer.

The main purpose of the microcomputer was to perform the following operations:

1) Analogue-to-digital conversion and temporary storage in memory of transient sample temperature, voltage and current signals from the heater.
2) Switching the power to the rock heater on and off under the control of a programmable timer.
3) Digital reduction of data and calculation of thermal constants.

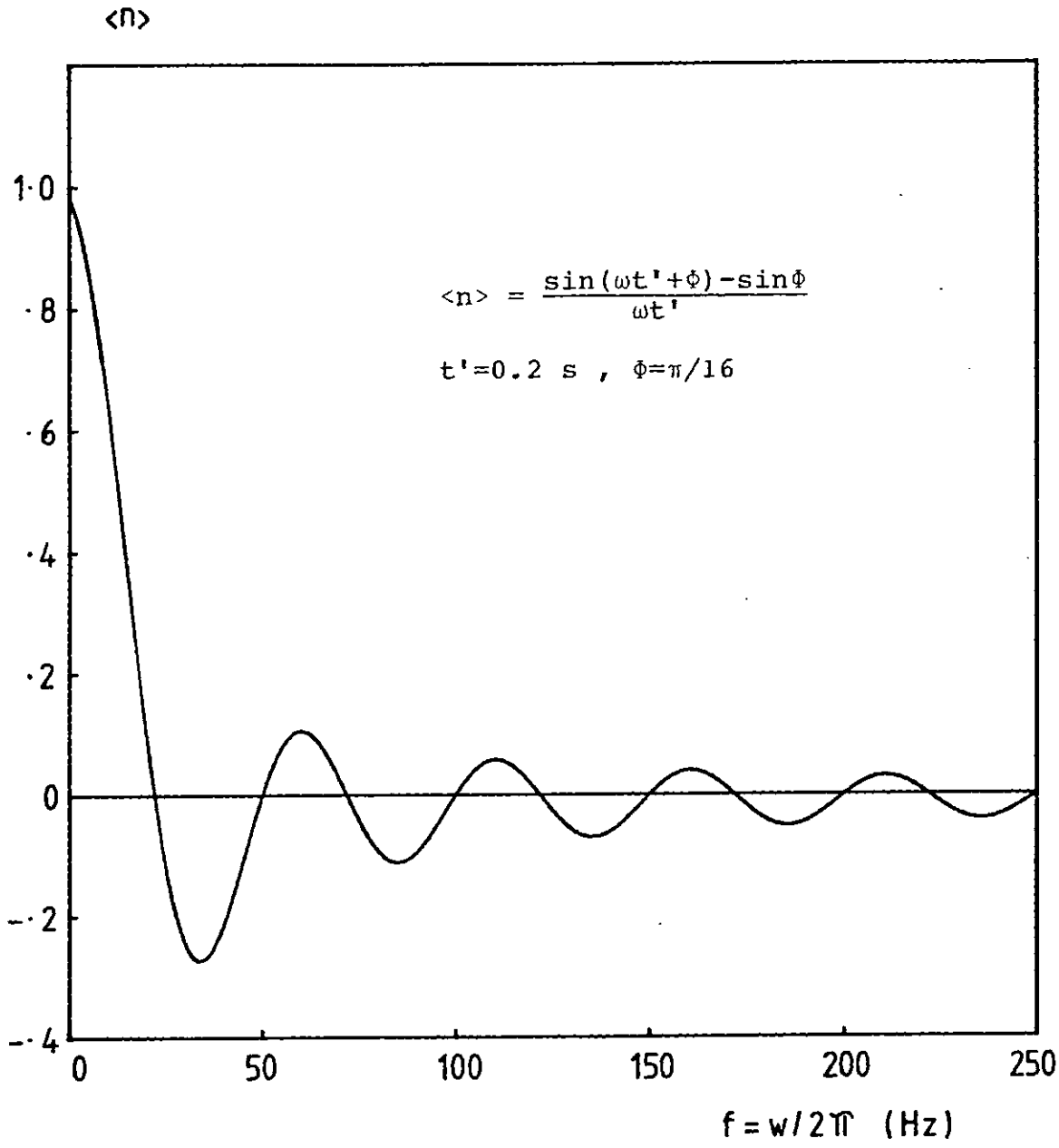

Fig. 4.11 Frequency response <n> of digital filter.

4) Display of data, programs and results on a visual display unit.

5) Permanent storage of data and results on magnetic cassette tape for further analysis.

4.5.1 Hardware.

The microcomputer (Fig. 4.12) was a commercial single-board unit (Nascom 1) expanded and modified to perform the required analogue data capture. The eight-bit central processing unit (CPU - Zilog Z80) performed all the major internal data transfer, input/output, arithmetic and logical functions and communicated with the memory and peripherals via the data, address, and control buses. Temporary storage of data and programs was provided by 16 K-bytes of random-access memory (RAM). The computer monitor, Basic language interpreter, user programs and routines were permanently stored in read-only memory (ROM) and on cassette tape. Programs were inputted and all machine functions controlled from the keyboard. Data and programs were displayed on a visual display unit (VDU). A serial link enabled data transfers to/from a Cyber 176 mainframe computer for fast calculation of time-consuming routines, access to library routines, hard-copy production and alternative storage of large data files on magnetic tape or cards.

Two data-acquisition systems (DAS) were designed and built to perform the analogue data-acquisition and analogue-to-digital conversion (Fig. 4.12). The earlier DAS had a basic resolution of 8 bits (1 part in 256) and is described in Appendix I. Although this resolution was

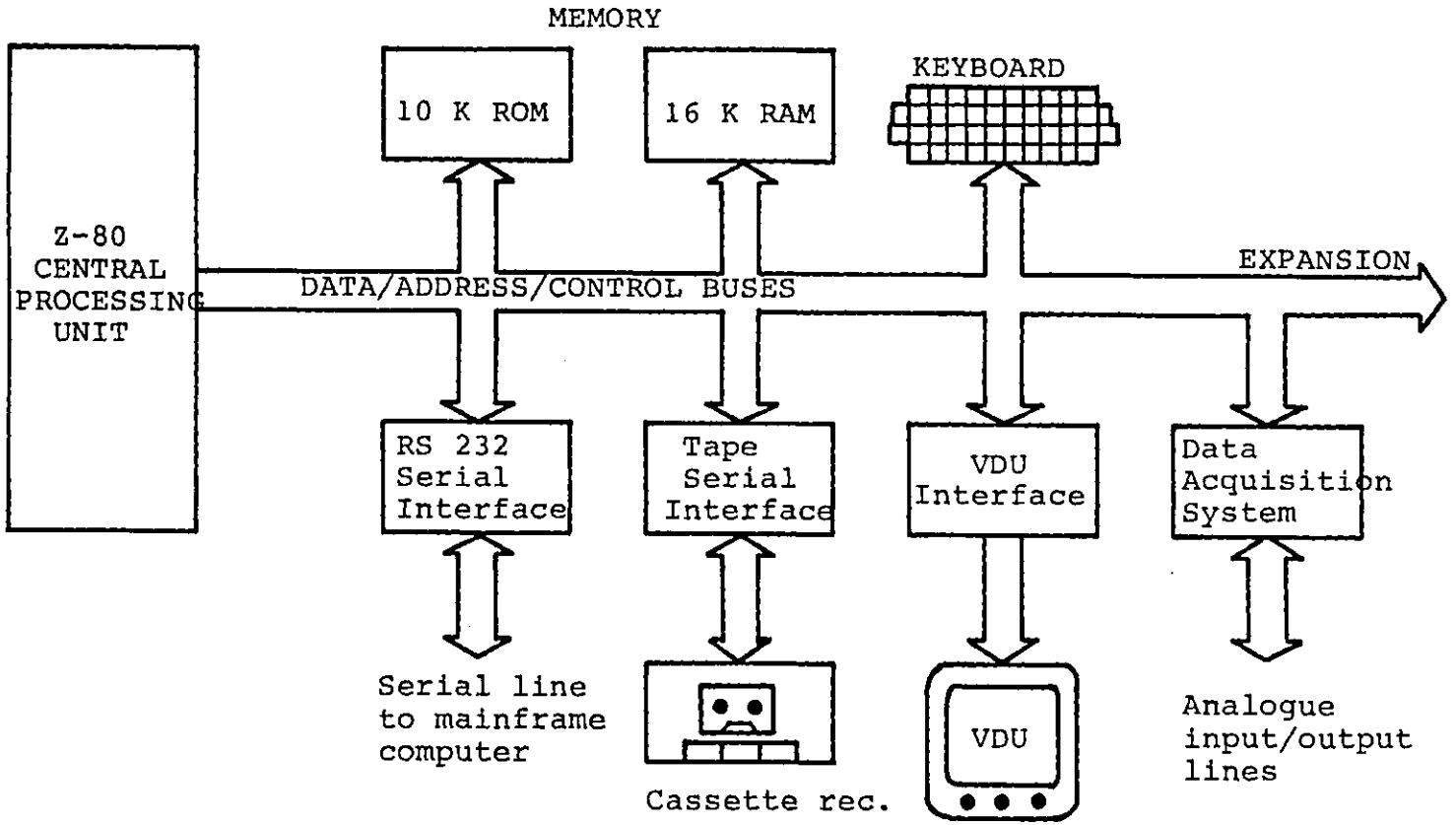

Fig. 4.12 Block diagram of Nascom 1 microcomputer.

adequate for the purposes of the experiments, the dynamic range (the ratio between the largest voltage input and the resolution) was rather limited. For example, if the resolution was set to 0.01 K, the maximum possible temperature rise was only 2.5 K, which was often exceeded in the measurements. For this reason, this DAS was later replaced by an improved version with higher resolution and speed whose main functional blocks are shown in Fig. 4.13. The 8-channel differential multiplexer selected the appropriate signal line. The signal was amplified and sampled at intervals determined by the programmable timer, and converted to digital form by the analogue-to-digital converter with a range of 0 to 5 V (or about 13 K) and a resolution of 12 bits (1 part in 4096) or 1.25 mV, corresponding to a temperature resolution of about 3 mK. The raw data was displayed in binary format to facilitate the setting-up of experiments and to check that the thermocouple and signal conditioning apparatus were in working order. Upon receipt of an "end of conversion" signal, the parallel interface temporarily stored the data, interrupted the CPU and instructed it to transfer the data into the memory. This interface also switched the power to the heater on and off under program control. The salient characteristics of the DAS are reported in Table 4.3: input current and and temperature drift were negligible and the input impedance very high, thus the accuracy was $\pm$0.025% of full scale reading after calibration of the scale factor and adjustment of the zero offset.

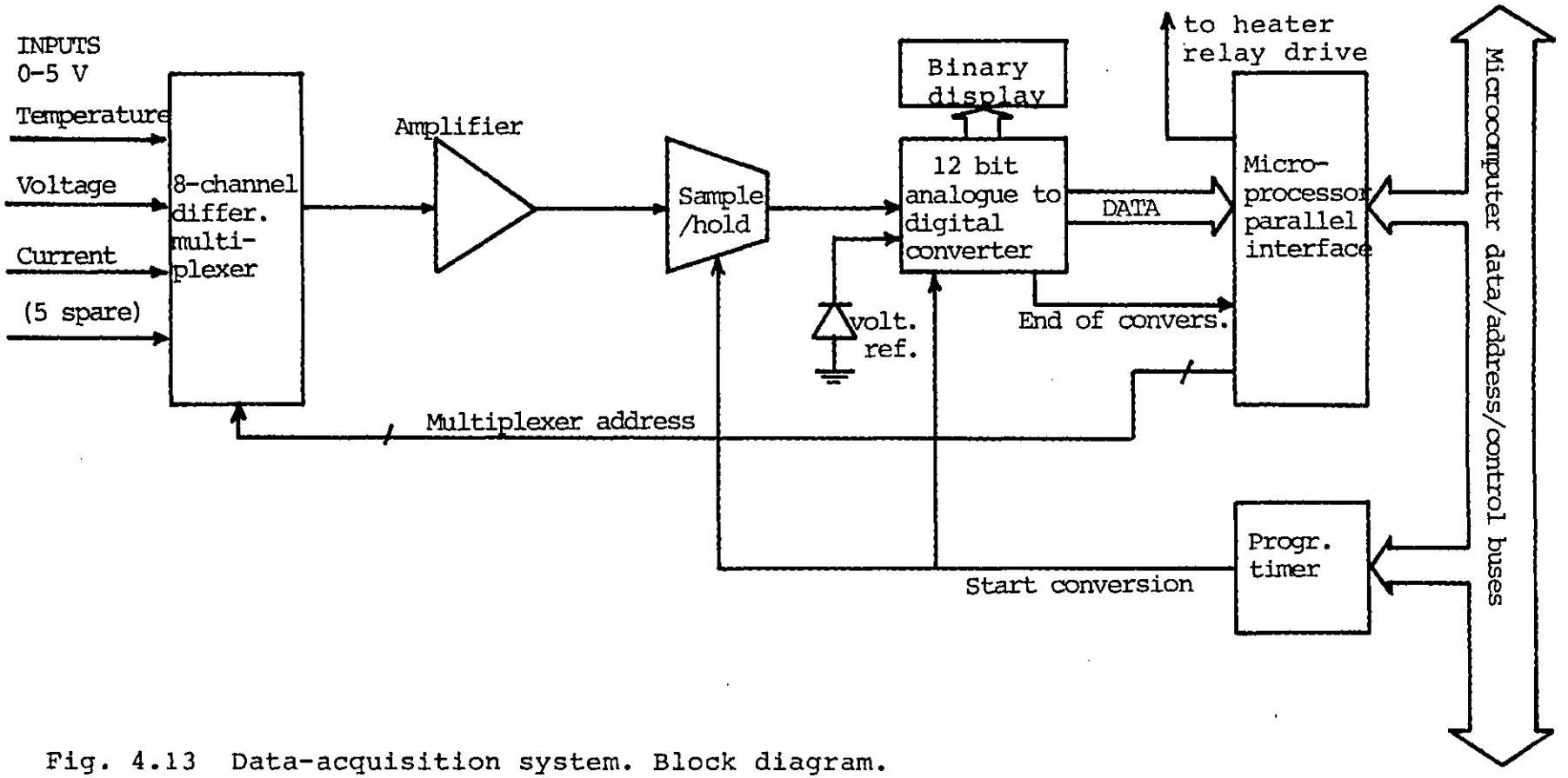

Fig. 4.13 Data-acquisition system. Block diagram.

TABLE 4.3 Characteristics of the data-acquisition system (@ 298 K).

Full-scale differential input voltage	0 to 5.12 V (1.25 mV/bit)
adjustable to	0 to 10.24 V (2.5 mV/bit)
Resolution	12 bits (0.025%)
Accuracy	0.025%
Inherent quantizing error	$\pm$ 1/2 bit
Maximum data-acquisition rate	30,000 samples/s
Data-sampling time window	5 us
Input current	1 nA
Input impedance	10^8 ohm/100pF
Externally adjustable zero offset and scale factor (to calibrate scale)	

4.5.2 Software.

The microcomputer was programmed in machine language in all the cases when high execution speed was required (for example in the data-acquisition routines which required service times of 80-100 μs), in peripheral control, and in interrupt routines requiring immediate attention from the machine and interruption of the current program. The Basic language was used in operations involving floating-point mathematical routines and output to the VDU or printer. The Basic interpreter was much slower in the execution of the programs than the machine language monitor, but eased programming considerably.

The accuracy of the floating-point numbers was limited to 6 decimal digits, which was adequate for most calculations. Although least-squares routines generally require better accuracy, close examination of the nonlinear least-squares method of section 3.10 reveals that the final values of the unknowns are not sensitive to the number of decimal digits employed. To confirm this, several data sets were analyzed both on the microcomputer and a mainframe computer with an accuracy of 18 decimal digits. The same final results were obtained, although in some instances the microcomputer required more iterations than the mainframe computer to achieve the same accuracy in the results. Widely different initial values of the thermal constants were found to lead to identical final values of k and h.

Data collection and automatic calculation of the thermal constants took 2 to 6 minutes, depending on the initial values assigned to the constants and on the number of iterations (usually 2 to 6) required to achieve the target

computational accuracy of 0.1%. As occasional transients in the mains supply caused spurious temperature readings, a routine was incorporated in the microcomputer program to detect and correct temperature readings which did not fit the trend of the temperature curve.

The advantages of performing all the data processing locally were twofold: 1) Data transfers to the mainframe computer were quite slow due to the limitations of the connecting line (30 characters per second). With local processing, results could be obtained in a very short time, and if spurious readings were suspected, the causes could could be searched immediately. Also, data transfers on long lines are an extra source of random errors. 2) The data set analyzed could be made large, with a consequent increase in the accuracy of the results. For example, for a typical experiment with a time window of 60 s and temperature readings taken at intervals of about 0.3 s, over 200 temperature points were analyzed, each point being an average of 250 digitizations. The same number of data points were taken in the heater current and voltage lines.

A flowchart of the line-source programm used in most experiments is shown in Fig 4.14, and a listing in Appendix II. A more comprehensive Fortran/Assembly Language program was developed by M.A. Adam (1983) to run the line-source experiment on a Research Machines microcomputer with facilities for fast printing and storage on magnetic disc of data and results.

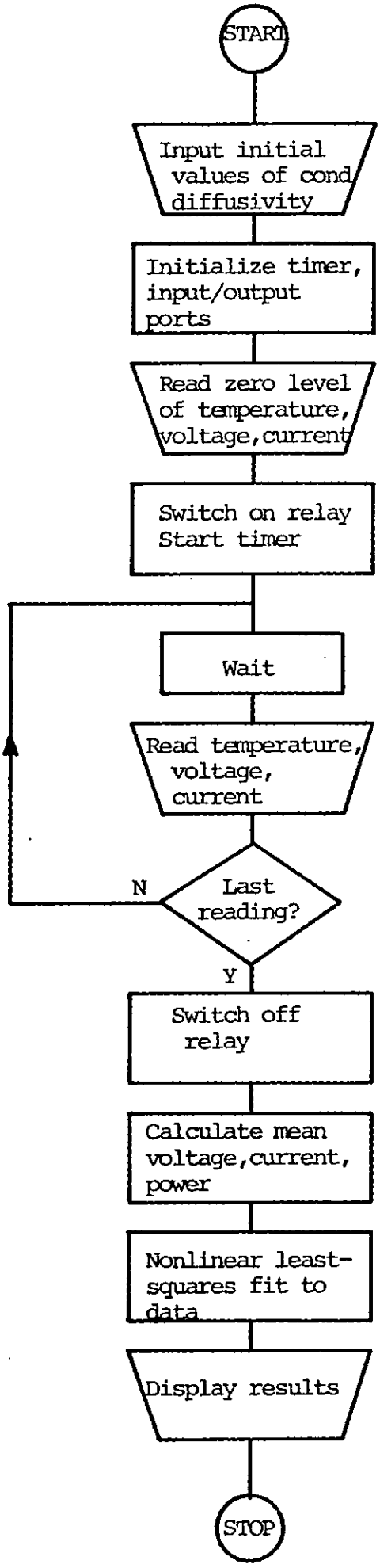

Fig. 4.14 Flowchart of line-source program.

Chapter 5

RESULTS

After a discussion of the expected overall accuracy of the method, thermal conductivity and diffusivity results for various rock types and two standard materials are presented in this chapter.

5.1 Error analysis.

Estimates of the component errors contributing to the total experimental error are given in table 5.1. These are typical values only and are dependent on experimental parameters such as oven regulation, thermocouple offset and sample length. The error introduced by amplifier and reference drift in the transient temperature measurements was estimated from the standard deviation of sets of repeated conductivity measurements at a constant oven temperature and its average value is given for each sample in Appendix IV. It is dependent on oven regulation and amplifier type and increases with increasing sample conductivity. Average values of the standard deviation are about 1.5 and 3% for samples measured in conjunction with the new and old amplifiers respectively. The error in the heater length was derived from the uncertainty in the positioning of the welded joints (section 4.2.2), and the error in the current determination is mainly due to the uncertainty in the measurement of the standard resistor. The fluctuations of Q with time were observed to be less than 0.1 % of the average value during a run. The total

TABLE 5.1 Error components contributing to the total estimated error in measured conductivity and diffusivity.

Param.	Component	Error (%)
v	Amplifier and reference drift	1.5-3
	Thermocouple calibration	1
	Amplifier	0.2
	Filter	0.02
	Data-acquisition system	0.025
Q	Sample length	1
	Voltage	0.025
	Current	1
r		15
t	Zero error	<0.02
	Scale error	<0.01
	Mathematical model	1

Working equation (Eq.3.3.1(10)):

$v = -Q/(4\pi k)\ Ei(-r^2/4ht)$

error in the conductivities, calculated as the sum of all the relevant components in table 5.1 (independent of r), is about 5-6%. However, the contribution of the reference drift is random and cancels out in averaging a large number of readings. The total (systematic) error under these conditions is about 4%.

The error in the thermocouple offset r, due to the finite radius of the thermocouples (0.3-0.5 mm) and the heater wire (0.1-0.2 mm), introduced a systematic error of about 30% in the diffusivity measurements. The random error is also higher than in the conductivity measurements. This can best be illustrated with reference to the logarithmic solution of section 3.3.1 (restated below):

$$v=Q/(4\pi k)\ \{\ln t - j - \ln(r^2/4h)\}. \qquad (1)$$

k and h can be determined by ordinary least squares from the slope and intercept respectively of the curve v against ln t in the interval (t min, t max), Fig. 5.1. The slope will only be affected by the reference drift in the sampling window t min to t max, whereas the intercept is sensitive to reference drift in the whole time interval t=0 to t max. With t max~ 2 tmin , the random error in h can be expected to be about twice that in k, a fact borne out by most results even when the exponential integral solution is used.

The error in the oven and autoclave temperature measurements was estimated to be 1% (section 4.3.3) and that in the pressure measurements about 5%.

A plot of the temperature residuals (the differences

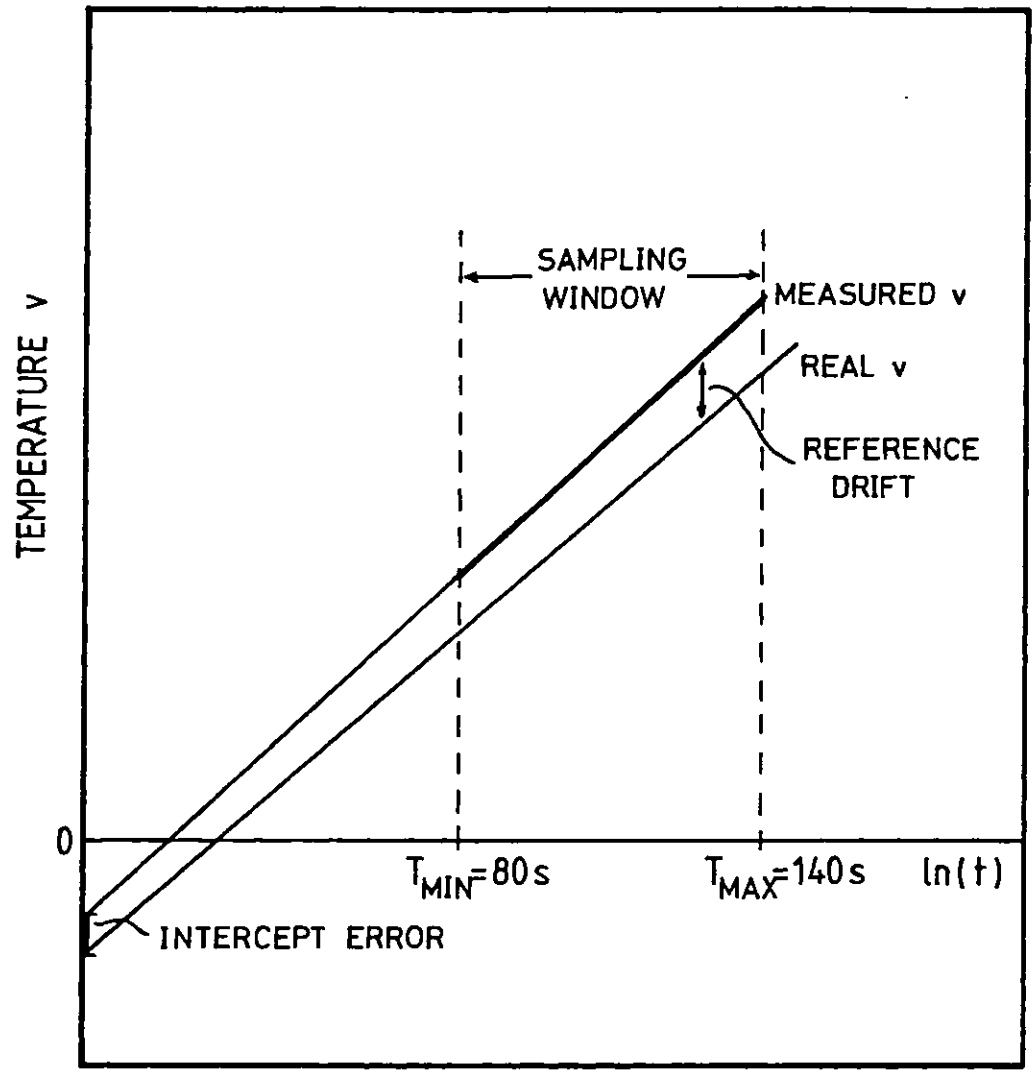

Fig. 5.1 Errors in slope and intercept caused by temperature reference drift. The fractional error in the intercept is larger than that in the slope because of reference drift at times less than t_{MIN}.

between the experimental temperature points and the best fitted curve) is given in figure 5.2. The residuals in the sampling window are less than 3.5 mK with a standard deviation of 1.2 mK and are randomly distributed around the zero level, which confirms the adequacy of the mathematical model.

Some of the rock samples had two thermocouples embedded at different offsets from the heater. By determining the conductivity from both thermocouples, the quality of the mathematical model could be checked. Figures 5.3 to 5.6 show conductivity vs. T plots for four Cornish granite samples having two thermocouples each. Each point is an average of one to four runs, with the error bars representing standard deviations. For most points the error bars of two conductivities from different thermocouples at the same temperature overlap, and the two sets of points for sample M5 are almost undistinguishable. A similar correlation was found in the temperature dependence of the diffusivity results even when the absolute values of h do not compare well due to inaccuracies in the determinations of the offset r. Some samples had to be dismantled at the end of a set of runs to re-measure the offsets, because the thermocouples and heaters had moved slightly during the high-temperature curing of the epoxy resin.

A comparison of the conductivity results for samples M2, M3 and T9 (figures 5.3, 5.4 and 5.6 - measured in conjunction with the old amplifier) and sample M5 (Fig. 5.5 - new amplifier) shows the importance of a very low-drift amplifier in obtaining good-quality results.

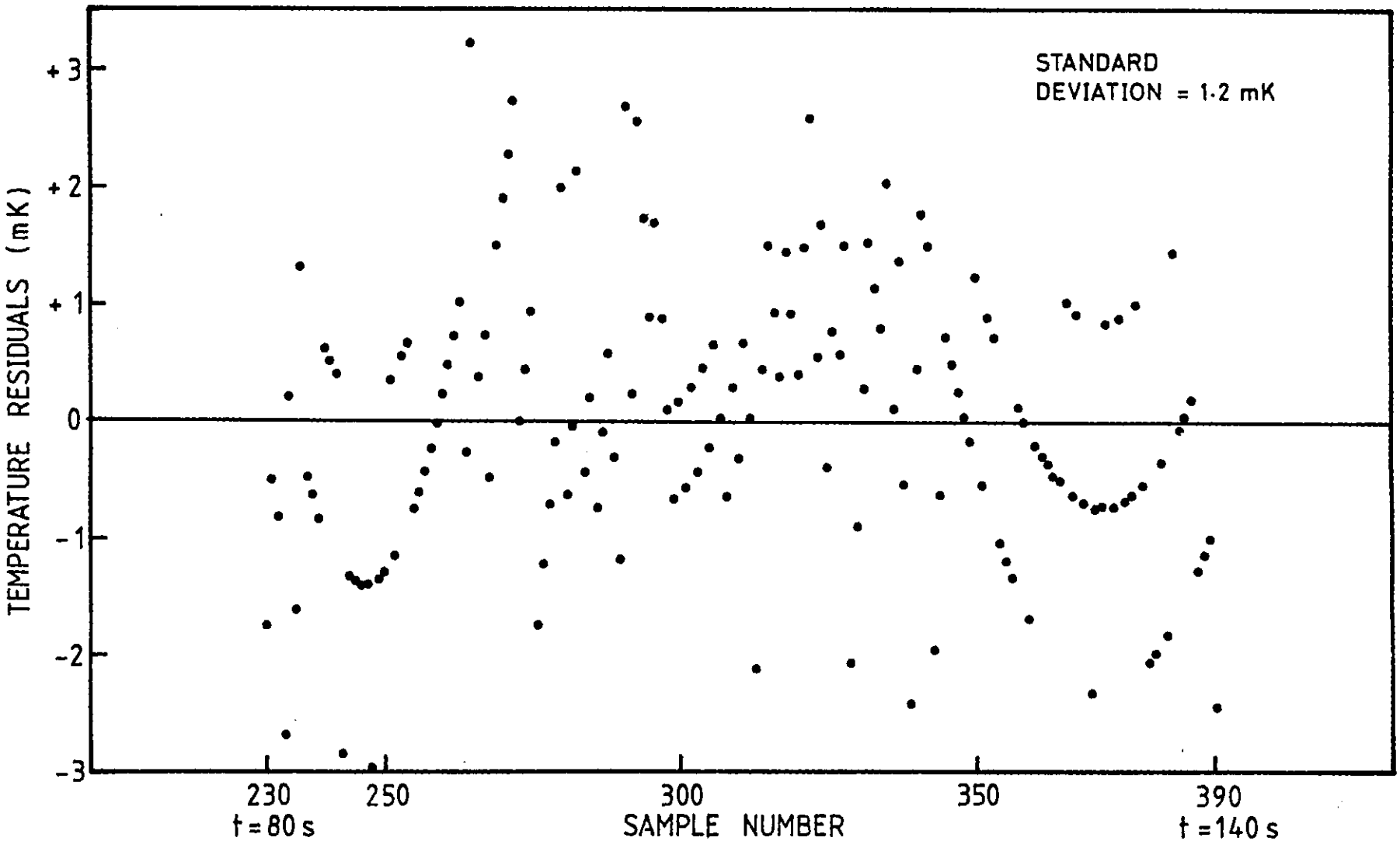

Fig. 5.2 Temperature residuals. Differences between measured temperatures and best fitted curve in the interval 80, 140 s for a typical measurement of sample T12 at room temperature. Sampling rate 0.36 s.

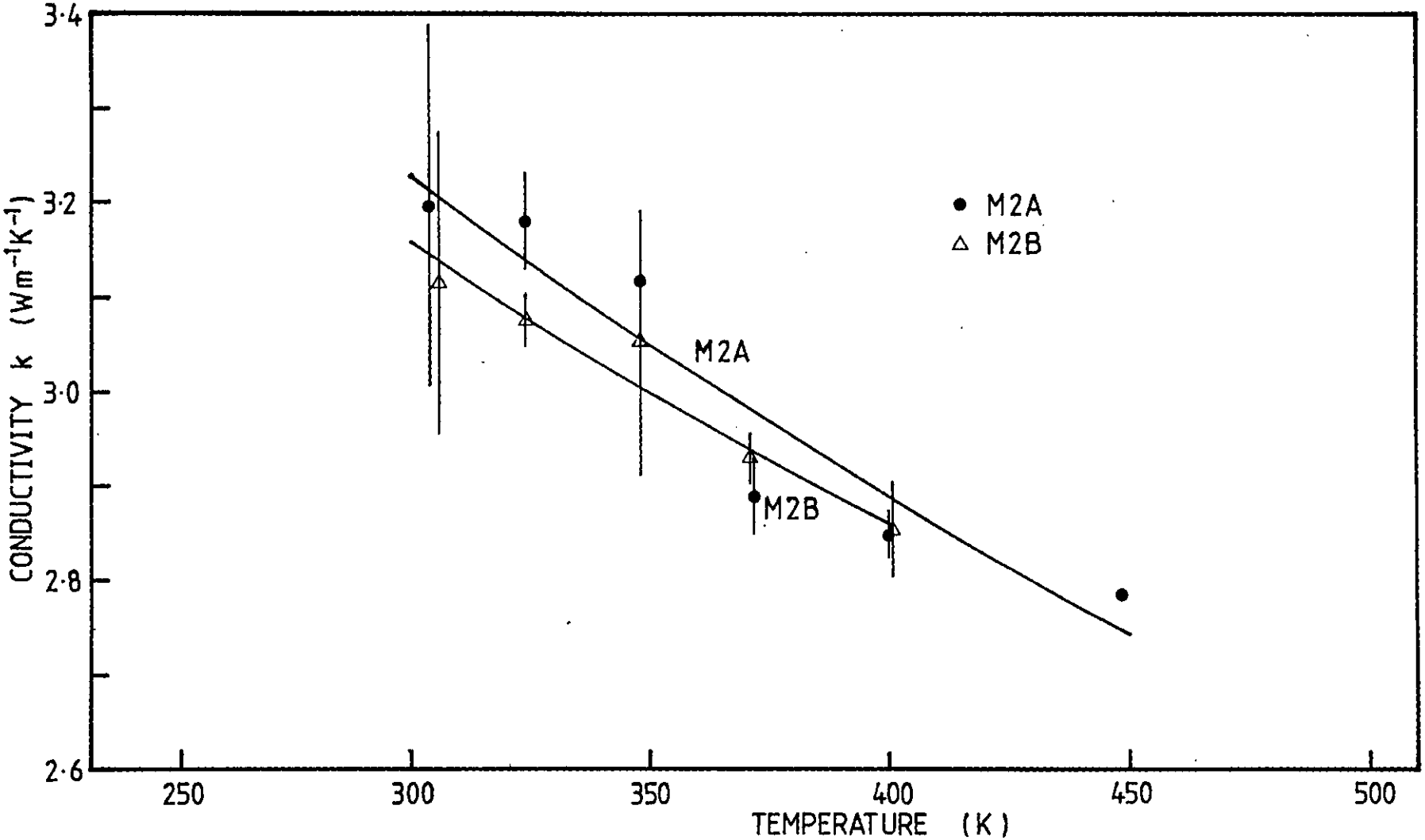

Fig. 5.3 Thermal conductivity of Merrivale granite sample M2. Suffixes A and B denote thermocouples A (offset r=2.85 mm) and B (r=4.27).

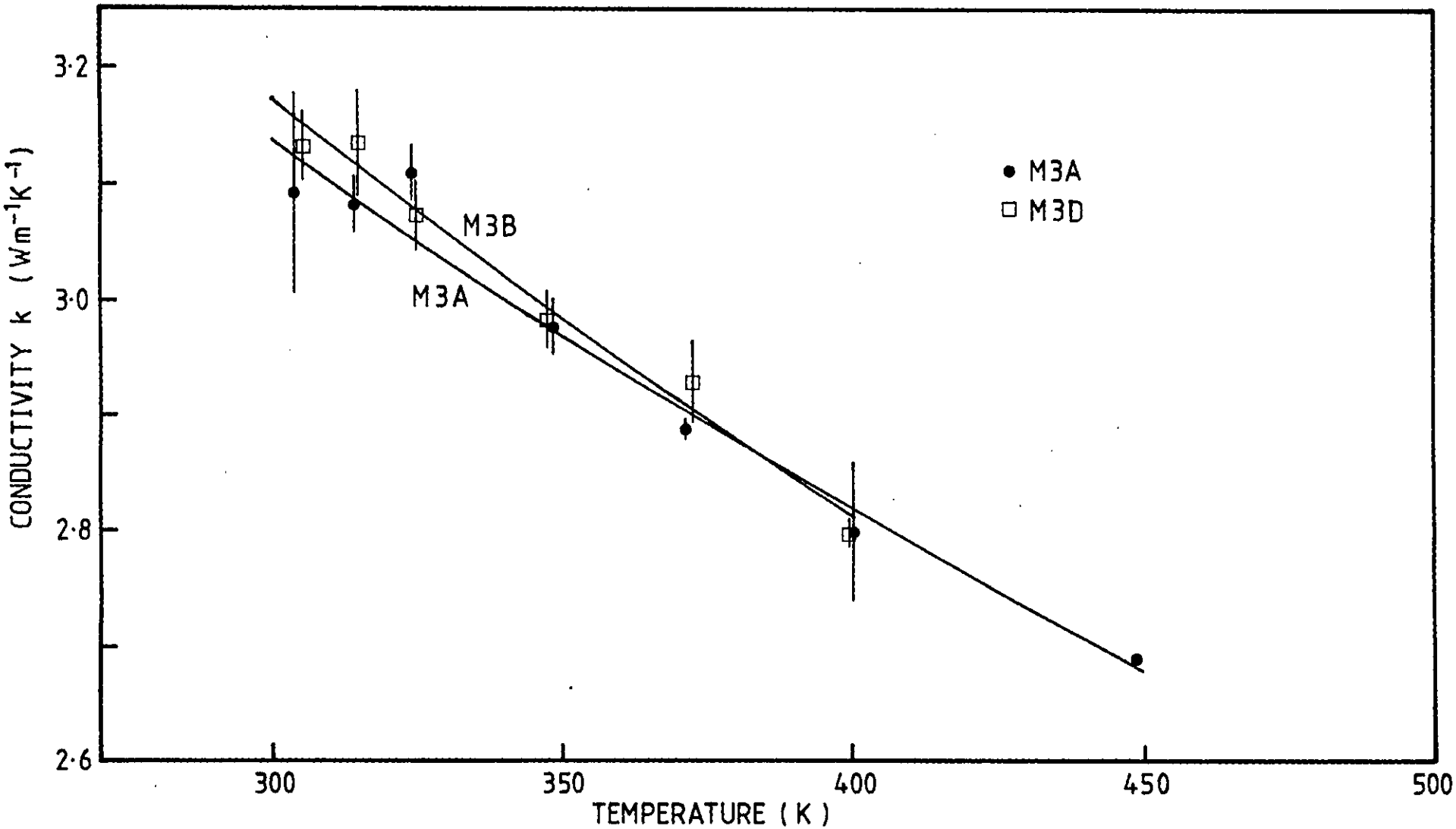

Fig. 5.4 Thermal conductivity of Merrivale granite sample M3. Offsets are 1.51 mm and 5.19 mm for thermocouples A and D respectively.

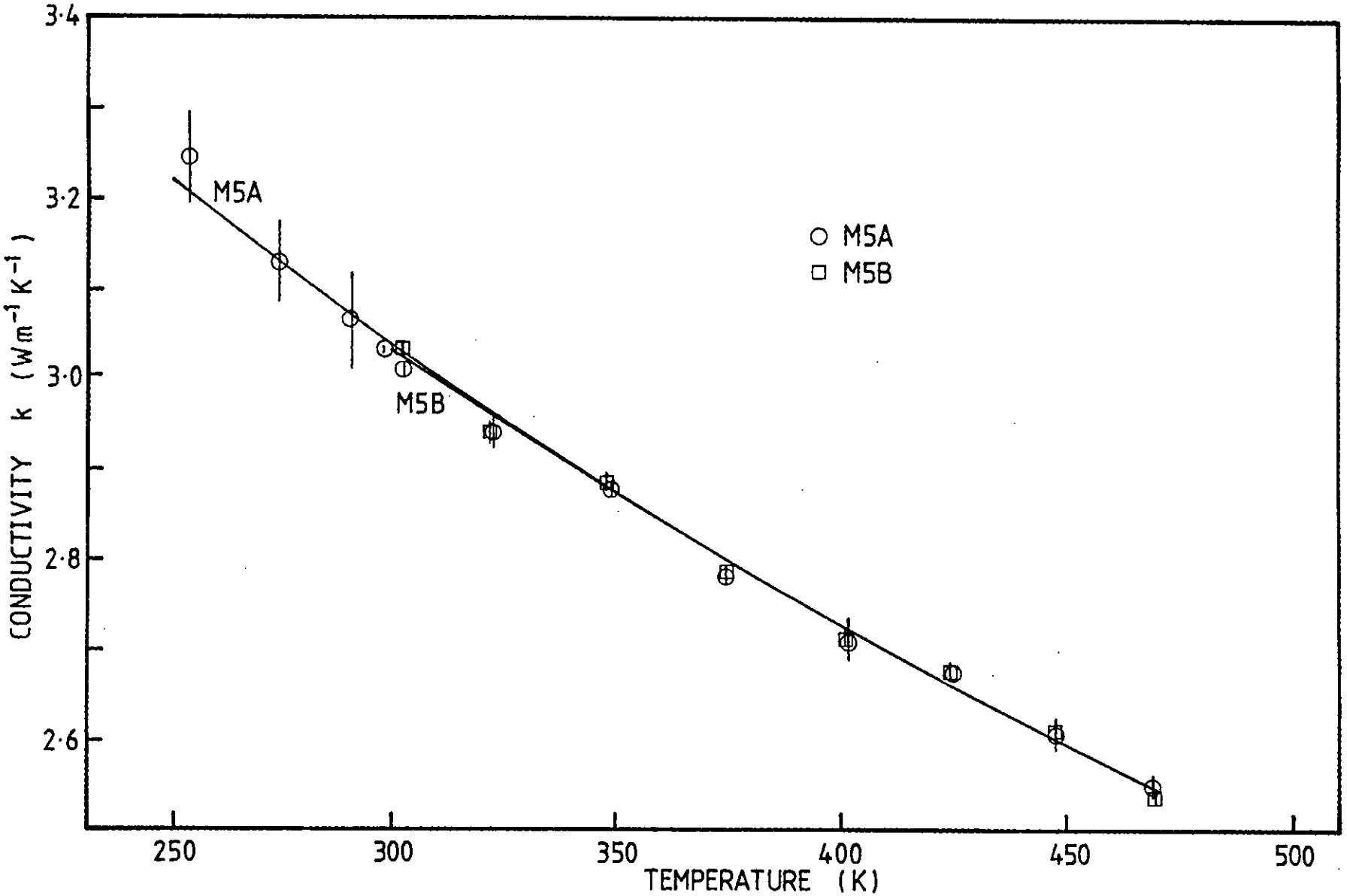

Fig. 5.5 Thermal conductivity of Merrivale granite sample M5. Offsets are 2.77 mm and 4.26 mm for thermocouples A and B respectively.

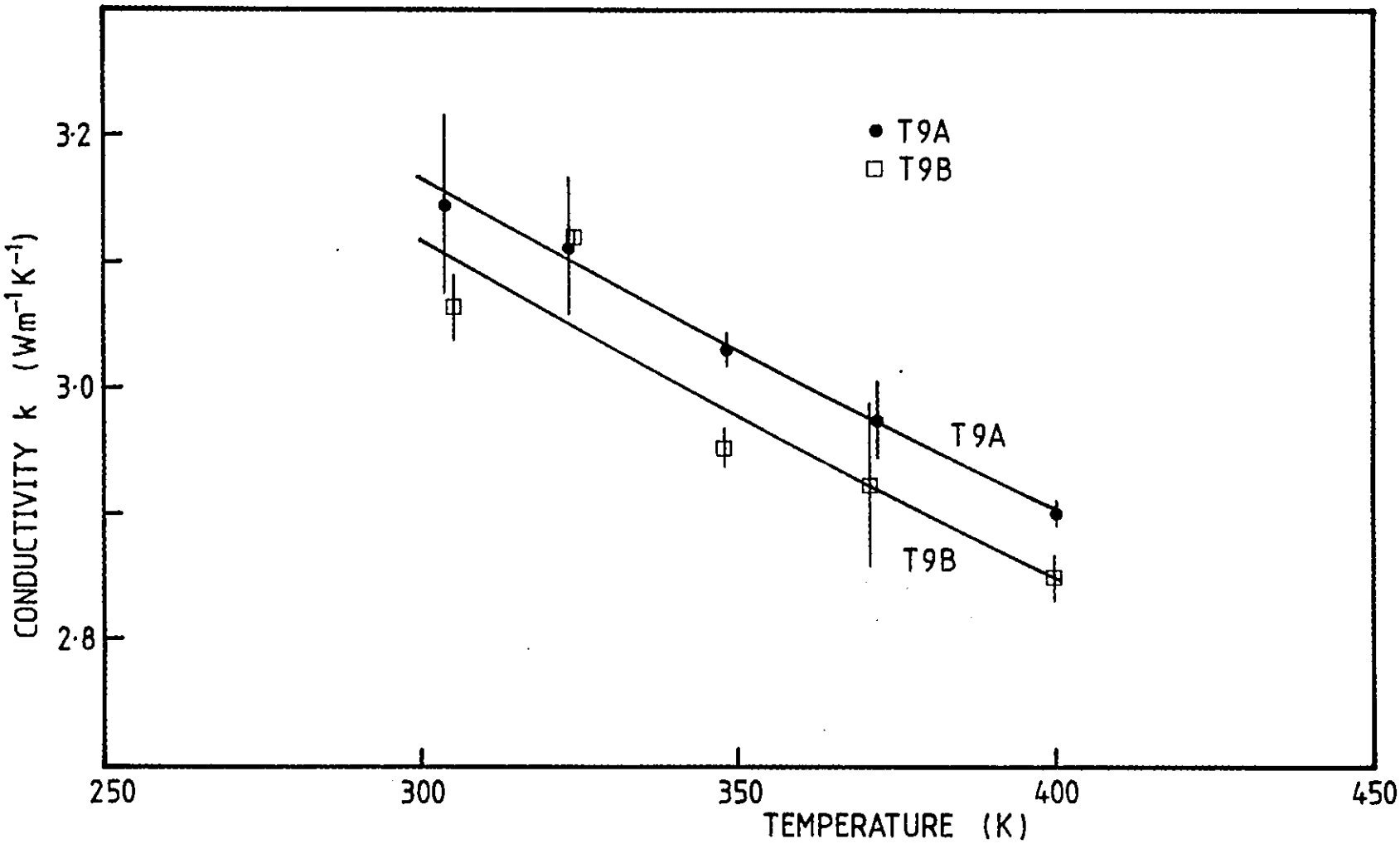

Fig. 5.6 Thermal conductivity of Troon granite sample T9. Offsets are 1.96 mm and 3.51 mm for thermocouples A and B respectively.

Robinson (1979) performed a set of tests to monitor the dependence of measured conductivity on the linear power, and detected no appreciable correlation.

During all the experimental runs, the resistance of the heater wire was calculated from the average measured voltage and current through the heater. This provided useful information on the resistance variations with temperature and time. The standard deviation of a set of measurements of wire resistance at a constant temperature was usually less than 0.2% of the mean value, but larger variations occurred at different temperatures due to the temperature dependence of the wire and other random effects (Appendix IV). Fig. 5.7 shows that for a typical constantan heater the random variation is larger than the temperature variation (which should have a slightly positive trend with increasing temperature). This suggests that the potentiometric method of power measurement is slightly more accurate than simple current measurements coupled with a single resistance determination at room temperature, and justifies the increased complexity of the wiring and apparatus.

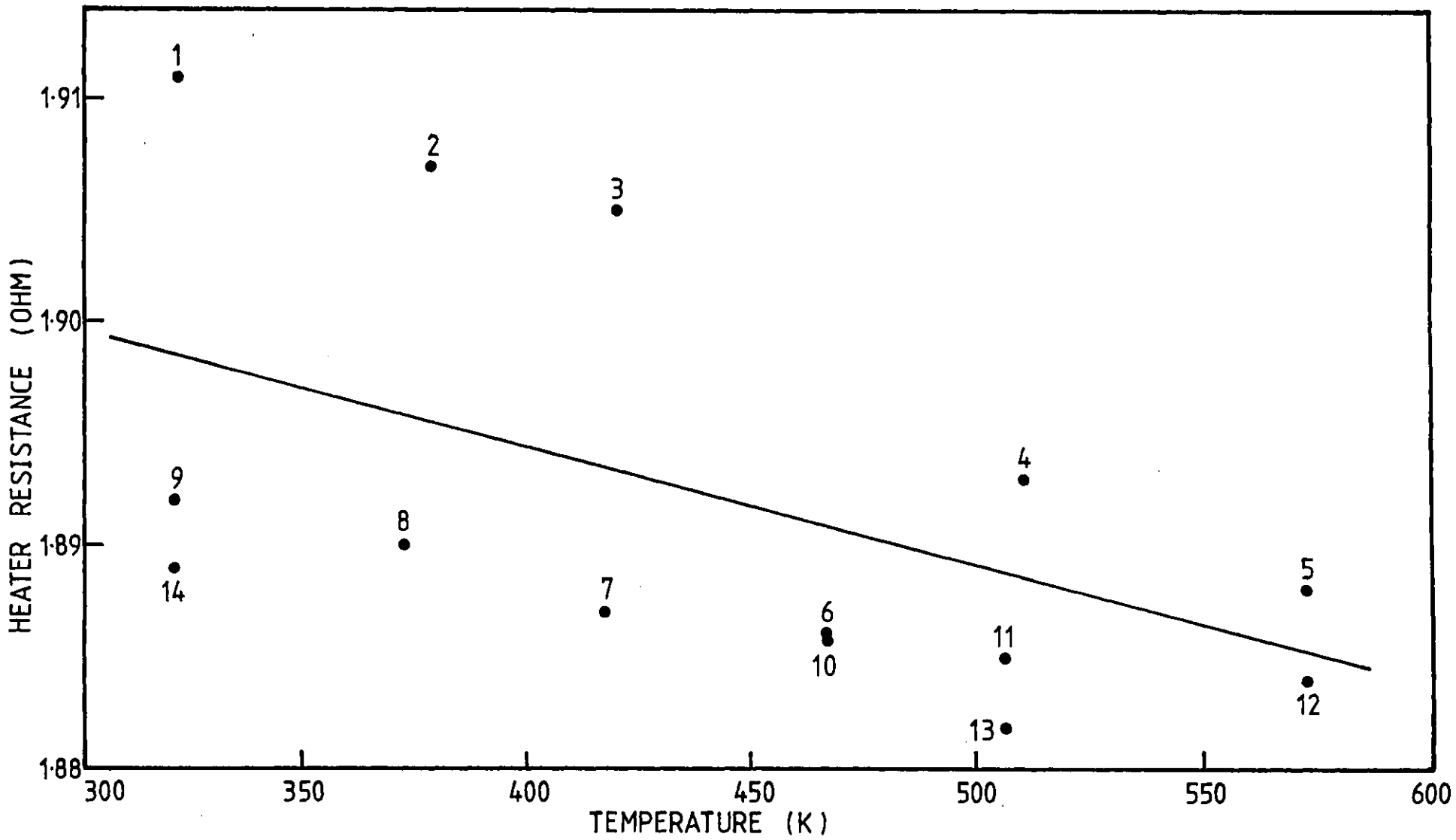

Fig. 5.7 Heater wire resistance as a function of temperature. The figures next to the points show the chronological order of the measurements.

5.2 Conductivity of fused silica and ceramic.

The conductivities of two standard materials were measured in order to compare the absolute accuracy of the present method against published results. The requirements on standard materials are high thermal stability over a wide temperature range and a conductivity value similar to those of most rocks. Fused silica is widely acknowledged to have very stable thermal characteristics over a wide temperature range (Sibbitt **et al.**, 1979). Conductivity measurements were performed in the range 300-470 K on a high-purity fused silica sample (supplied by Gooch & Housego Ltd.) with zinc oxide-loaded silicone grease as the contact material. A set of at least three readings was taken at each oven temperature in increasing steps of 25 K from 300 to 470 K. The effect of temperature cycling on the fused silica, silicone grease, sample thermocouple and heater was checked by repeated readings at 300 and 470 K, and found to be negligible. Fig. 5.8 compares the results with those of Ratcliffe (1963) and Birch and Clark (1940). Values of individual measurements are shown together with average values at every temperature as a measure of the scatter in the results. The larger scatter at the low and high ends of the range is probably attributable to poorer oven regulation in these regions. The average percentage standard deviation of the individual conductivity values is 1.5 %. The agreement with the published results is good in view of the limited length of the available sample (60.13 mm). As previously shown, the accuracy in the determination of the power input Q (and hence the conductivity) is inversely proportional to the sample length.

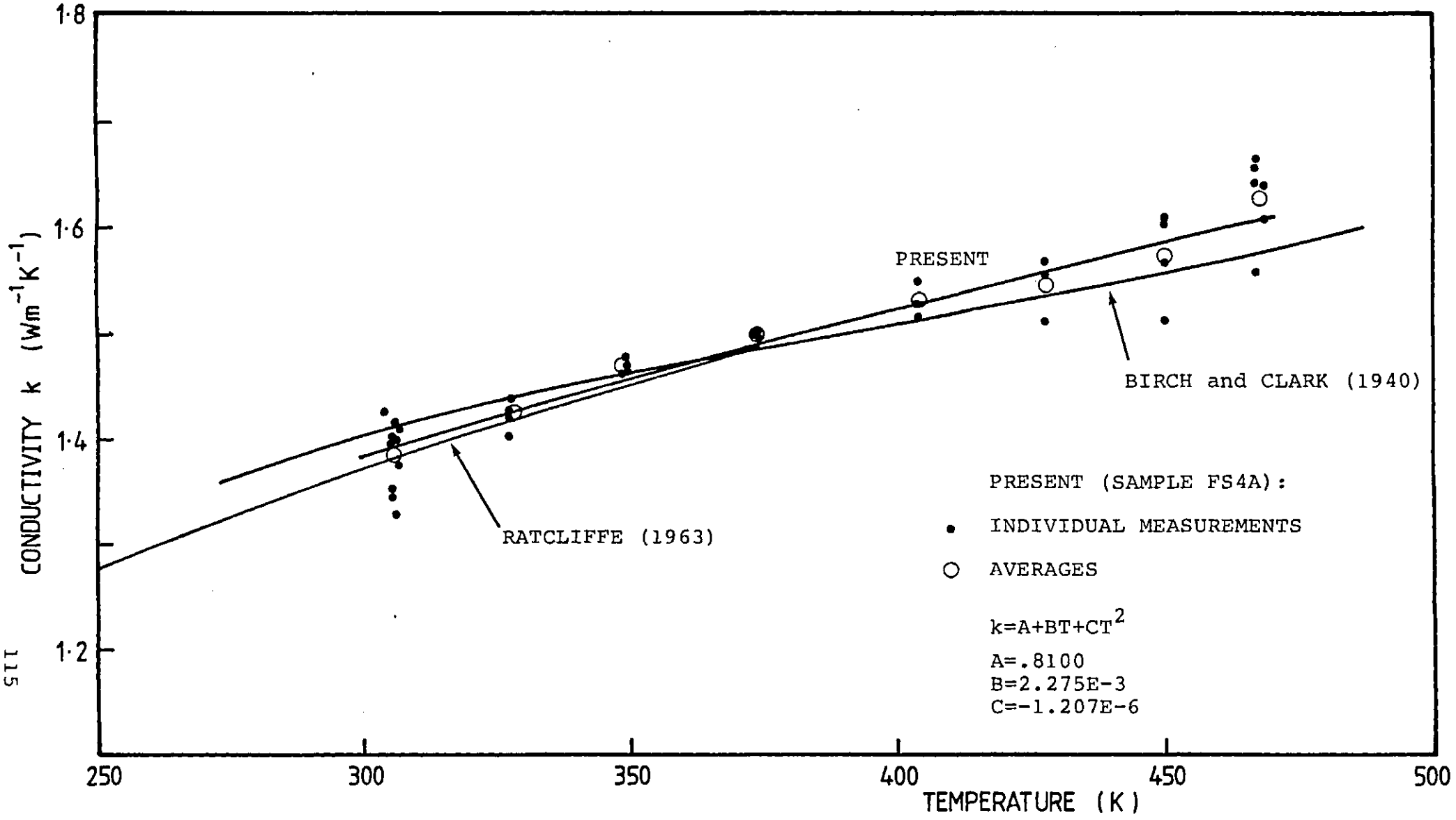

Fig. 5.8 Compariason of thermal conductivity measurements of fused silica.

The diffusivity results are plotted in Fig. 5.9 together with the values calculated from the equation $h=k/\rho c$, with k taken from the present experiments and ρ, c from Kanamori **et al.** (1968). The slopes of the h vs. T curves are in agreement, but the absolute values of the measured conductivities are 30% too low, probably because of the inaccuracy in the thermocouple offset measurement. Values of h from Kanamori **et al.** (1968) are also shown in Fig.5.9.

Fused silica is unsuitable for use as a standard in needle-probe measurements where a long and thin hole has to be drilled into the sample. A material which has been found to possess the required machinability in this application is zero-porosity Corning Macor 9658 ceramic (Bloomer, 1980). The results of a set of conductivity measurements on a Macor sample (supplied by McGeoch & Co. Ltd.) with zinc oxide-loaded silicone grease as the contact material are shown in Fig. 5.10. Each point is an average of three to seven experimental values and the error bars represent the standard deviations. The increase in conductivity with temperature is that expected for a glassy material. The value at room temperature (Table 5.2) is in good agreement with that from a divided bar apparatus on discs from the same Macor block and those reported by Bloomer (1980), measured by a divided-bar and by a needle-probe calibrated against a silica glass standard.

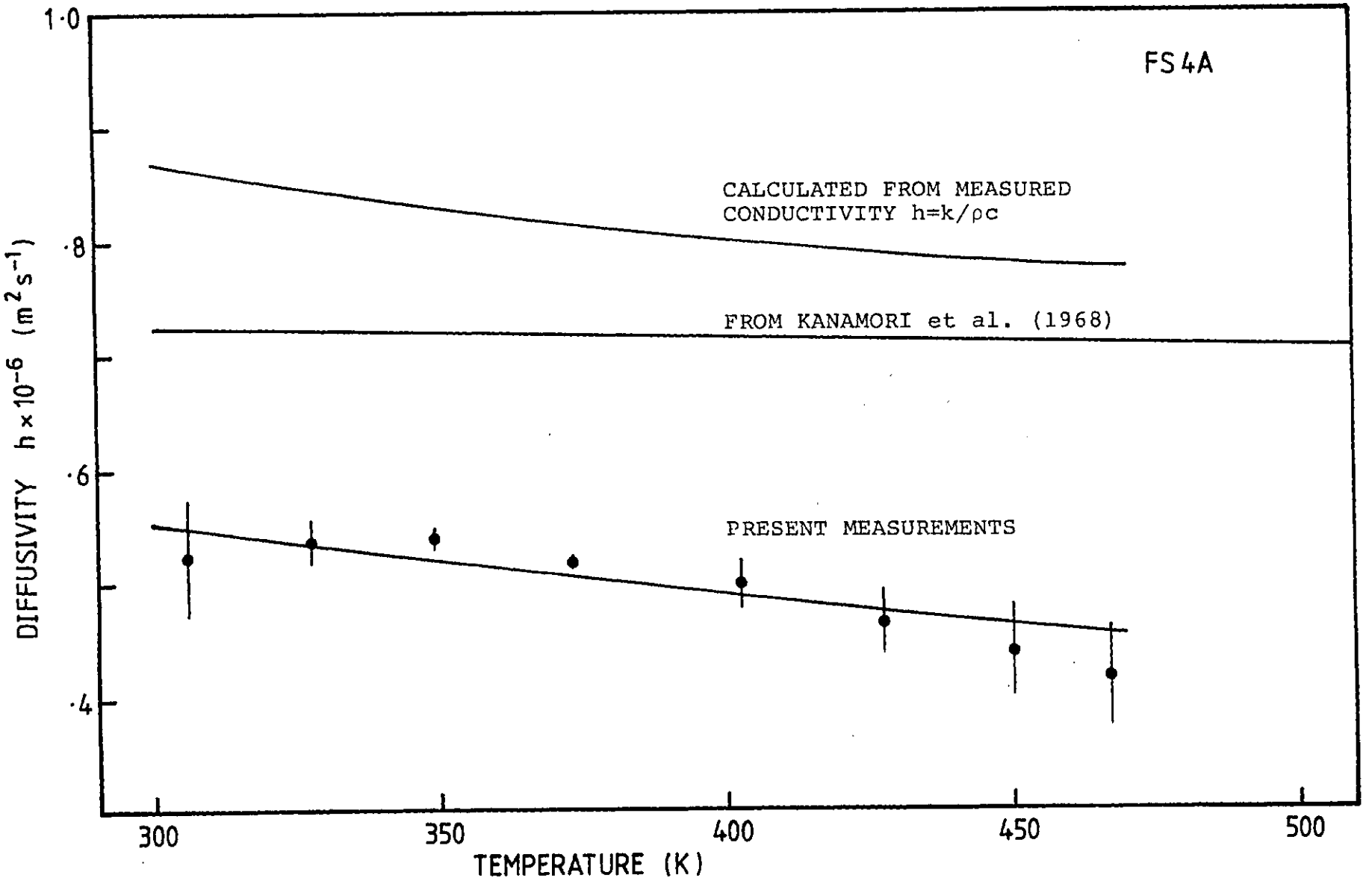

Fig. 5.9 Diffusivity of fused silica sample FS4A. The values of ρ and c in the equation h=k/ρc are from Kanamori et. al. (1968), k is from the present study.

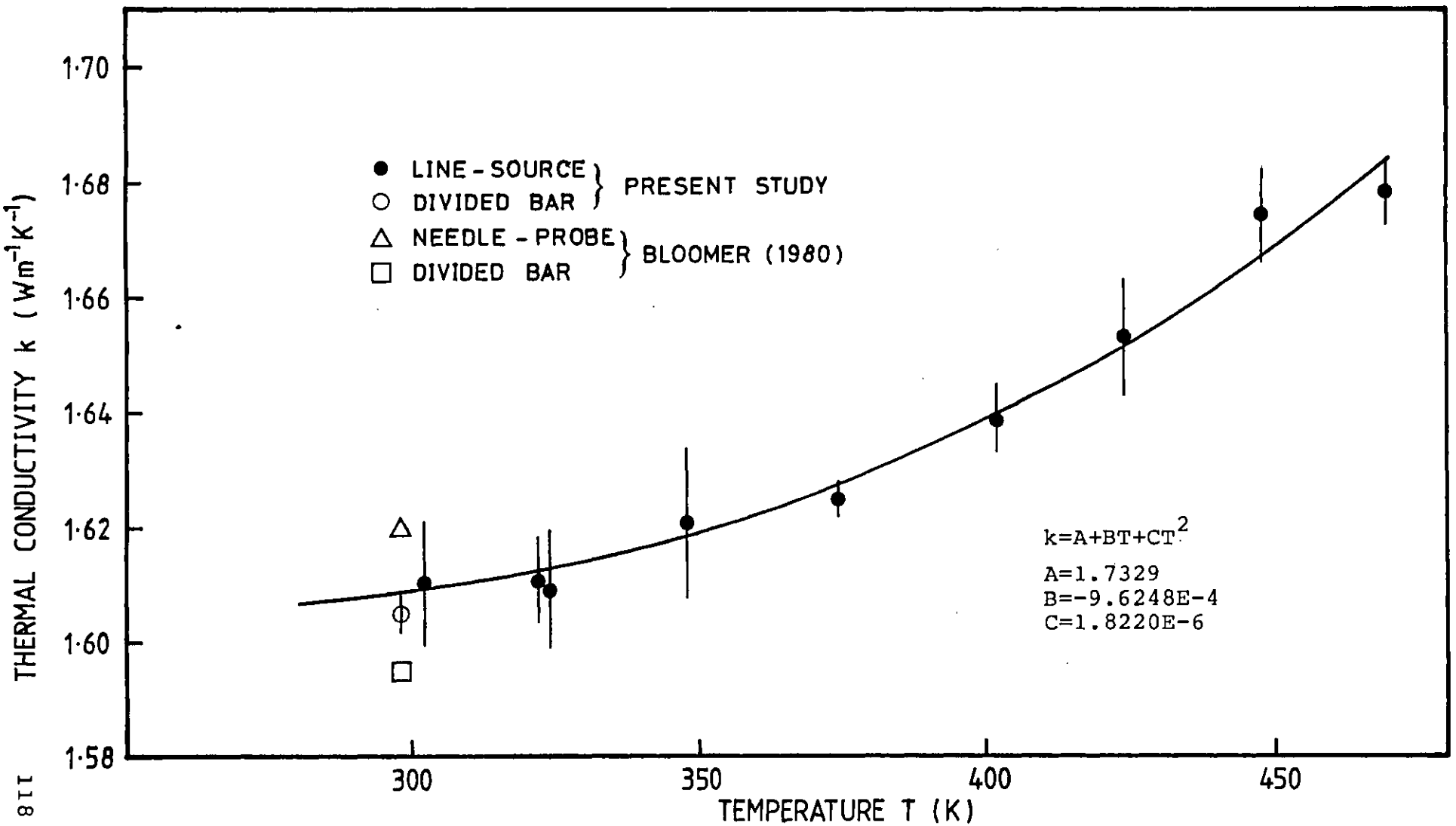

Fig. 5.10 Comparison of conductivity measurements of Macor ceramic, sample MAC 4A.

TABLE 5.2 Comparison of conductivity results of Macor ceramic at 298 K.

Source of data	No. of readings	k,S.D.
Line-source (at 302 K)	6	1.610±0.011
Divided-bar	24	1.605±0.003
Needle-probe (Bloomer, 1980)	39	1.62 ±0.03
Divided-bar (Bloomer, 1980)	13	1.59 ±0.04

One of the values at 325 K was obtained after dismantling and reassembling the sample with a new heater and thermocouple, and shows a negligible discrepancy in the measured conductivity. The smoothed curve of Fig. 5.10 is a second-order polynomial in T. Other curves could have been fitted to the experimental points with as good a justification, but the differences would have been negligible within the temperature range of the experiments. Good repeatability was observed after temperature cycling to 470 K.

The diffusivity results are plotted in Fig. 5.11. Tables of results for both standard materials are given in Appendix IV.

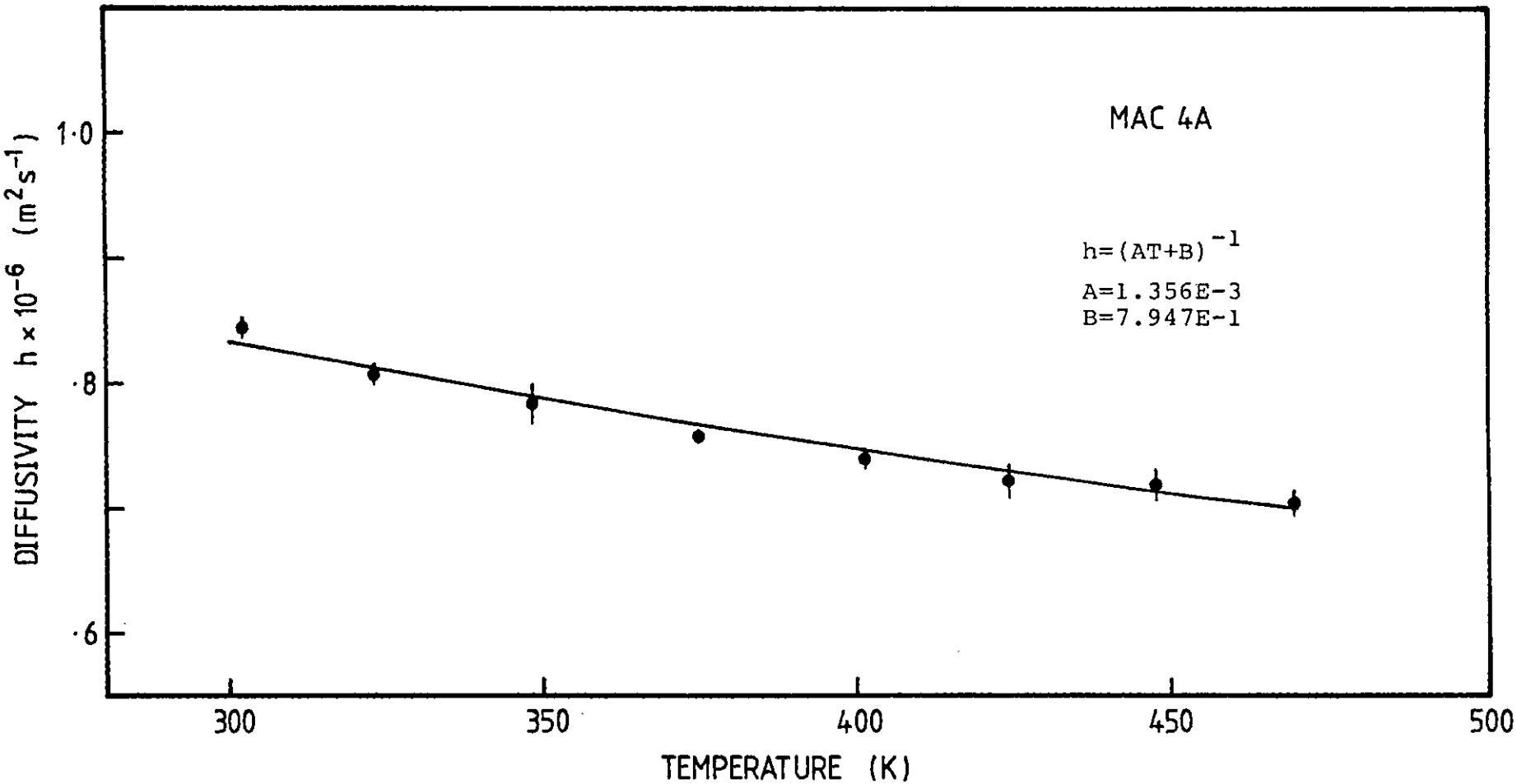

Fig. 5.11 Diffusivity of Macor ceramic sample MAC 4A.

5.3 Temperature dependence of conductivity.

A set of samples representative of the main geological suites found in S.W. England were investigated. The size of the samples was kept as large as possible, yet compatible with the attainment of thermal equilibrium in a reasonably short time, so as to minimize the effects of grain-size inhomogeneities and heat reflections at the boundaries. A description of the samples is given in Appendix V, and the conductivity and diffusivity results, together with other relevant sample parameters, are tabulated in Appendix IV. Each result in Appendix IV is an average of several experimental runs, the standard deviation giving a measure of the repeatability. Some spurious results (probably caused by bad oven regulation or noisy data sets) are not reported. The heater wire resistances are also shown for each measurement as a good standard deviation in the measured wire resistance was found to be associated with repeatability in the conductivity. Corrections to the conductivity results were attempted in some cases where the resistance variations were wide: the conductivity was scaled proportionally to the wire resistance at a given temperature (normally room temperature), and in general this was found to decrease the scatter in k. This procedure, however, is no substitute for good temperature sets, a reflection of the fact that high wire resistance variations are associated with a shape degradation in the input power step function.

Conductivity values of a set of granite samples from Merrivale (Dartmoor, Devon) are plotted against absolute temperature in Fig. 5.3, 5.4, 5.5 and 5.12. The samples

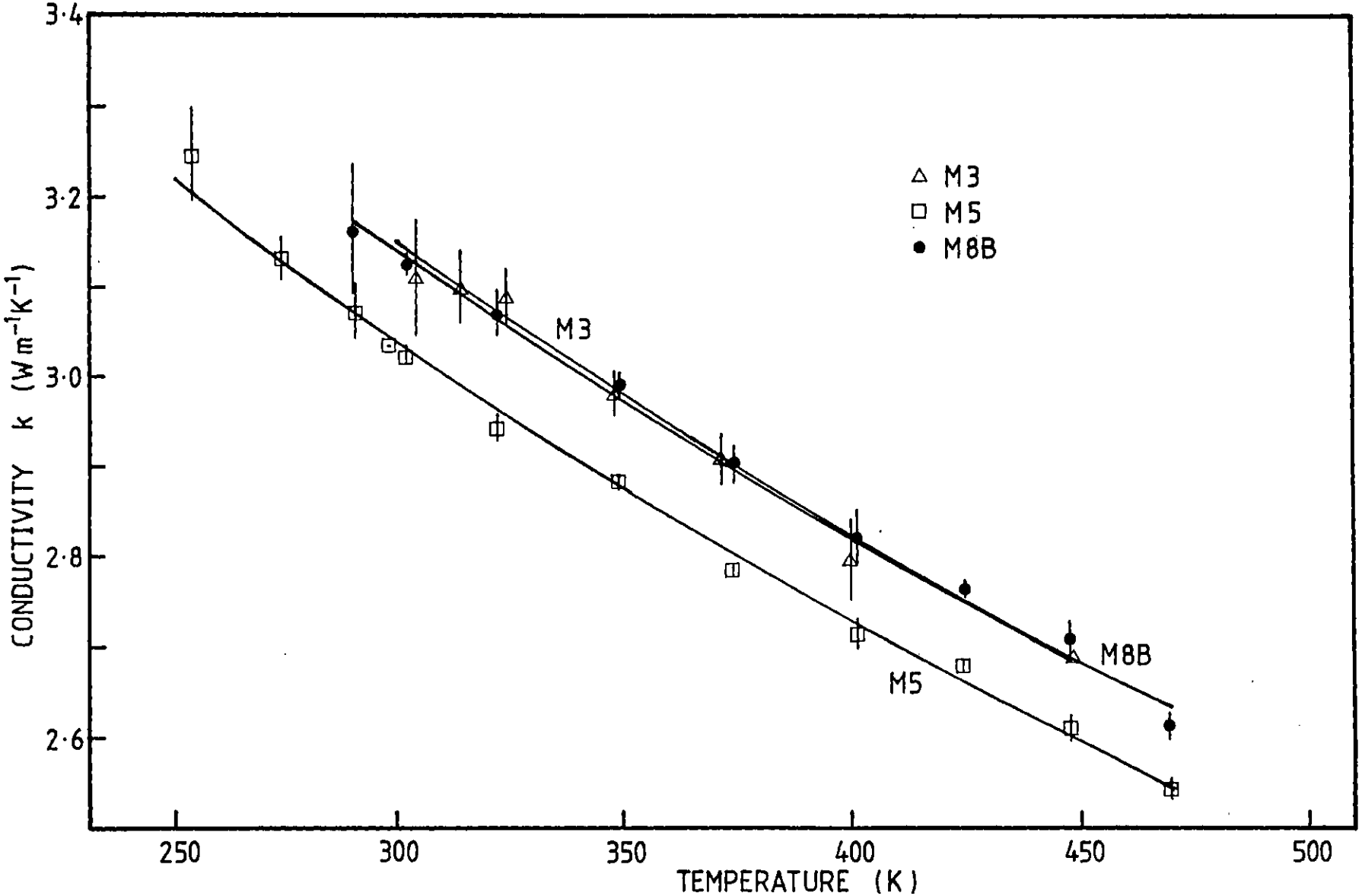

Fig. 5.12 Thermal conductivity of Merrivale granite samples M3, M5 and M8B. All least-squares curves are of the form k=(AT+B)-1

were cut from a single block of rock and with the same orientation thus allowing a study of grain-size related conductivity variations. Each point on the graphs is an average of several measurements with the error bars representing the standard deviations. All the samples were dried at 400 K for 24 hours prior to measurements. The temperature sequence was started at 400 K, then T was increased in steps of 25 K to 470 K, then decreased to room temperature and increased again to 375 K in steps of 25 K. Measurements at sub-ambient temperatures down to 250 K were then performed on samples M5 in the cryostat in order to verify the 1/T relationship in this range. Some measurements at 470 K were then repeated. It was thus hoped that conductivity variations caused by moisture loss from the samples would be minimized. The standard deviations at room temperature are considerably larger than the others, a consequence of poor oven regulation in this range. The absolute values of k also tend to be lower than expected at room T. The marginally poorer repeatabilty of measurements in the cryostat (sample M5) is not easily accounted for given the good intrinsic temperature stability of the ethyl glycol bath.

The curves on the diagrams are best least-squares fitted lines of the form $k=(A+BT)^{-1}$. This equation was chosen from the considerations of chapter 2, but the choice is rather arbitrary, as fits of lines of the form $k=A+BT^{-1}$ or even straight lines $k=A+BT$ led to similar correlation coefficients over the limited temperature range investigated. Fig. 5.13 shows a comparison of the smoothed

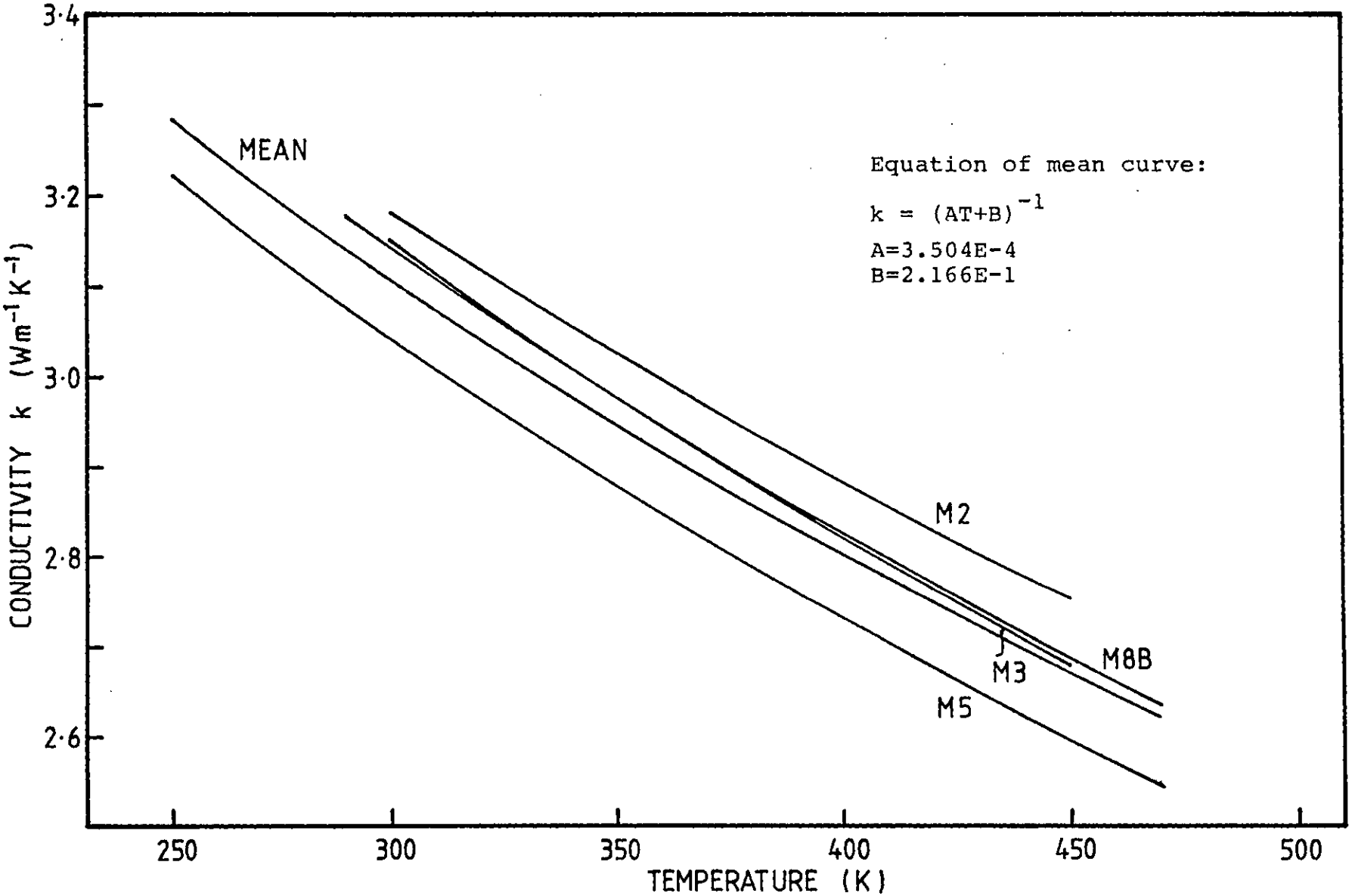

Fig. 5.13 Smoothed thermal conductivities of Merrivale granite.

k-values for all the Merrivale granite samples together with a mean curve calculated from a least-squares fit to all the conductivity points. The sample-to-sample spread of conductivities is within ±3% of the mean value at all temperatures. This is probably at least partly due to grain-size effects as it cannot be entirely accounted for by the inaccuracy in the linear input power measurements. Such differences are not uncommon in adjacent regions of coarse-grained rock (the average grain size of the orthoclase megacrysts in the Merrivale granite samples was 20 mm). The slopes of the curves were all very similar, suggesting an almost identical temperature dependence of conductivity.

Fig. 5.14 shows conductivity results from a set of samples from Troon (Carnmenellis, Cornwall) all cut from the same block together with least-squares fitted curves. The temperature sequence was the same as for the Merrivale samples (except that for T12 which is described later). The values for sample T12 at 250 K seems to be anomalously low, but it was included having proved repeatable. Fig. 5.15 is a plot of the smoothed values only together with the mean curve for all the samples. The range of conductivities at a fixed temperature is wider than in the Merrivale granite, even if the grain sizes were comparable. The mean conductivity is slightly lower at ambient and sub-ambient temperatures, becoming substantially equal at temperatures above 400 K. This similarity in conductivities was attributed to the similar compositions of the granites.

Values for a Cornish slate (Killas) specimen are shown in Fig. 5.16. The scatter in conductivities at a fixed

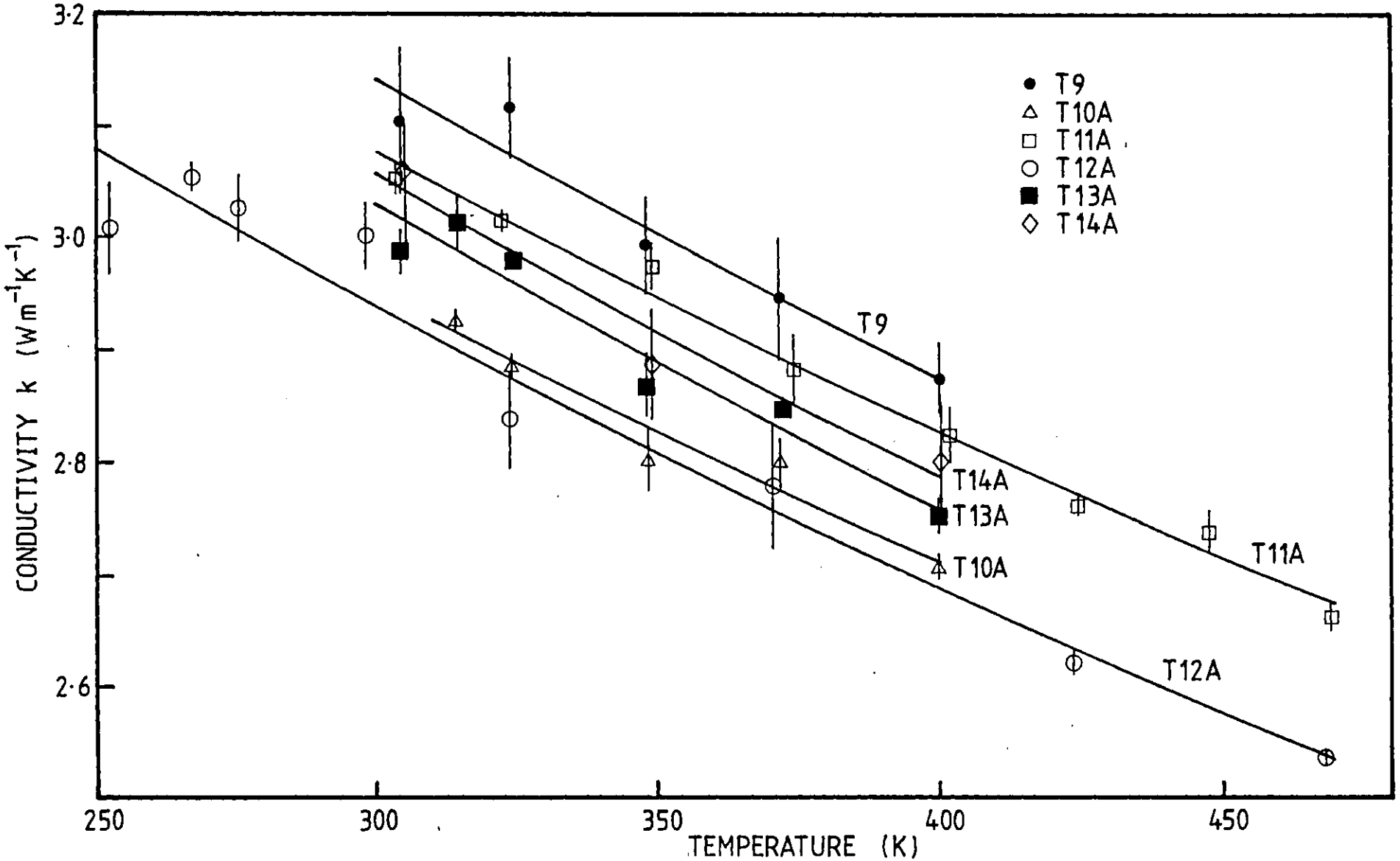

Fig. 5.14 Conductivity of Troon granite samples T9, T10A, T11A, T12, T13A and T14A.

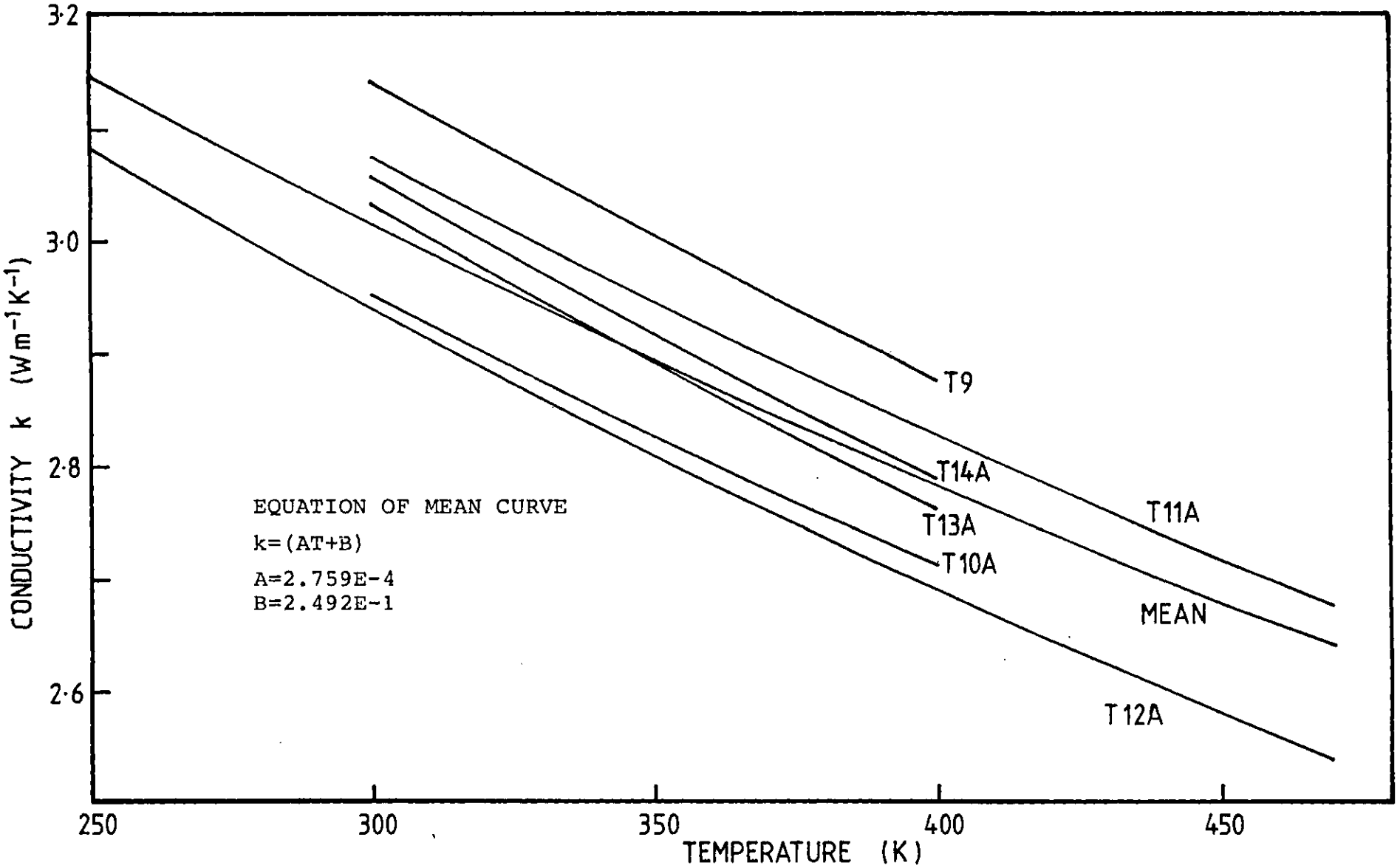

Fig. 5.15 Smoothed conductivities of Troon granite.

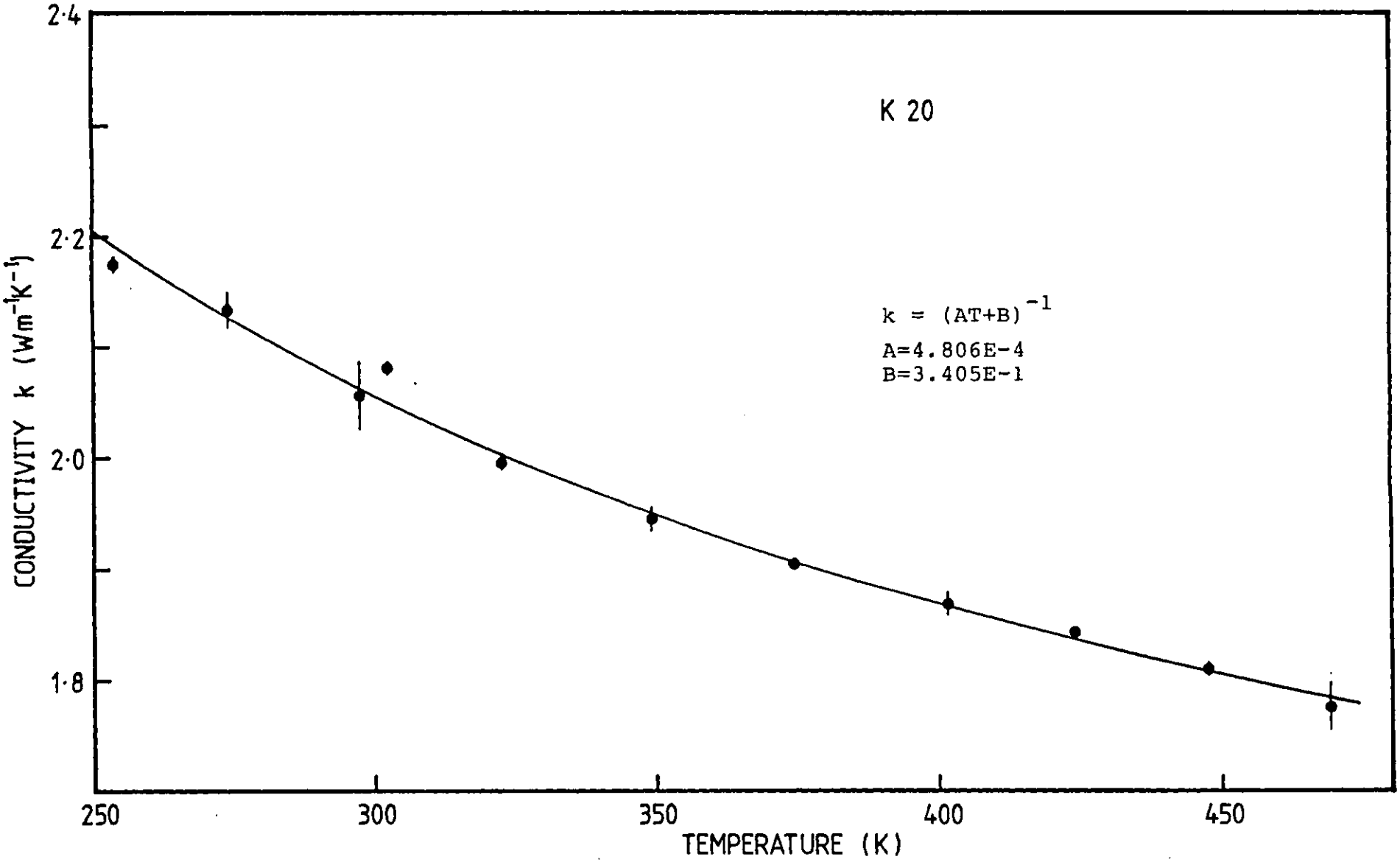

Fig. 5.16 Conductivity of Cornish slate sample K20.

temperature is small, reflecting the tendency of all line-source measurements to give better repeatability for lower conductivity materials. For the same input power, a low-conductivity material will cause a larger temperature increase at the sensor, leading to a lower experimental error.

A granite sample from Holman Mine (Troon, Carnmenellis, Cornwall), was investigated over the extended temperature range 320-570 K. The sample was initially dried at 370 K, then measured repeatedly at 320, 370, 420, 510 and 570 K in increasing steps of temperature, then at 510, 420, 370 and 320 K in decreasing steps. A similar second cycle from 320 to 570 K and back to 320 K was subsequently performed. The resulting conductivities plotted in Fig. 5.17 show that a considerable conductivity decrease took place between 420 and 500 K in the first T-cycle, which resulted in a lowered conductivity at the end of the cycle. The second cycle showed very similar conductivities at high temperatures, with a further decrease in the 320 K value at the end of the cycle. This behaviour was attributed to water loss and possibly some irreversible opening of microcracks in the quartz grains and at grain boundaries, and is within the limits predicted by the theory of section 2.3. Fig. 5.18 shows the averaged conductivities as functions of temperature, the large error bars reflecting real changes in rock conductivity rather than experimental scatter.

A similar procedure was applied to a dry Troon granite sample, Fig. 5.19. The conductivity of T12 was measured in increasing steps of oven temperature from 250 to 470 K.

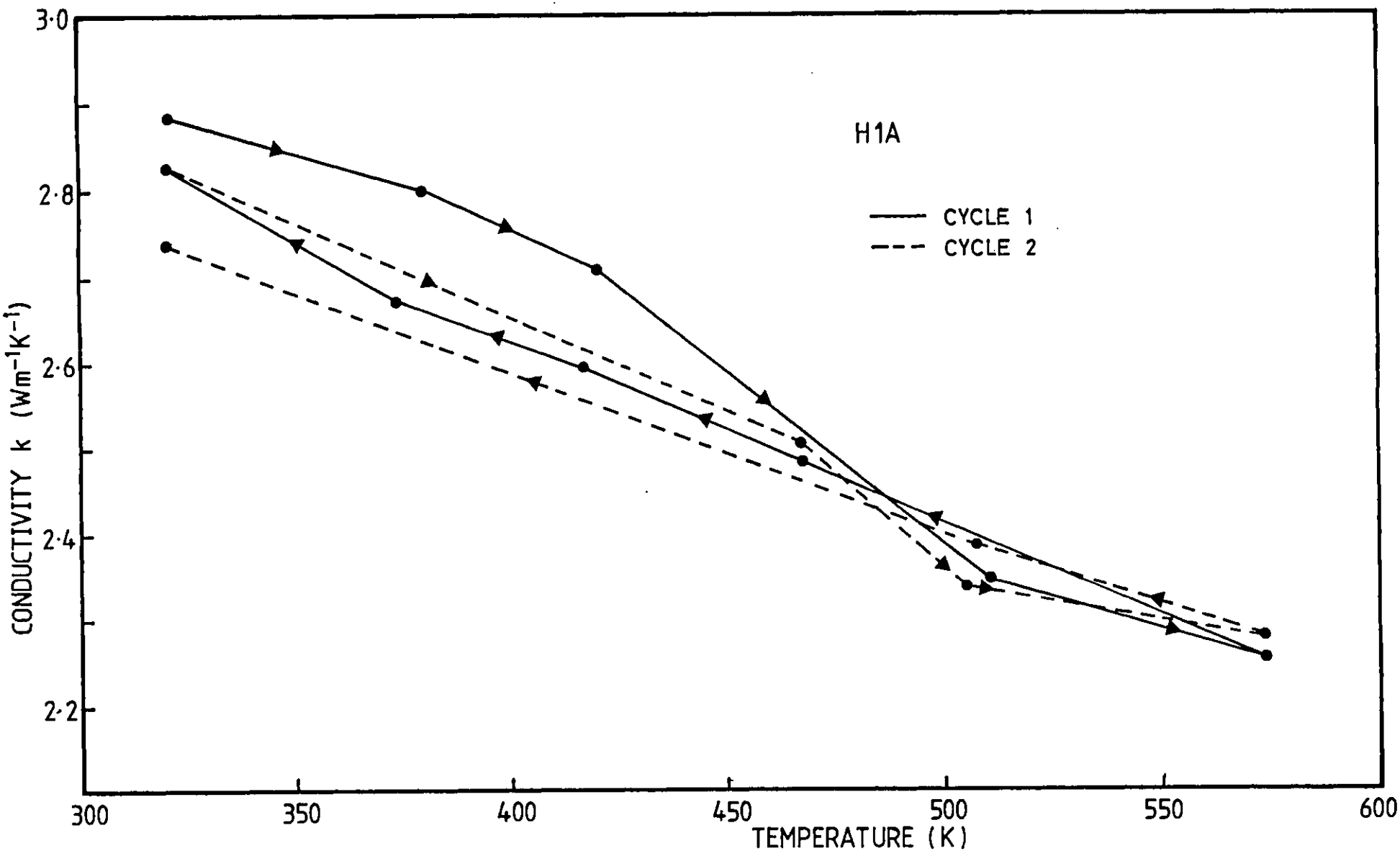

Fig. 5.17 Effect of temperature cycling on conductivity of Holman granite sample H1A.

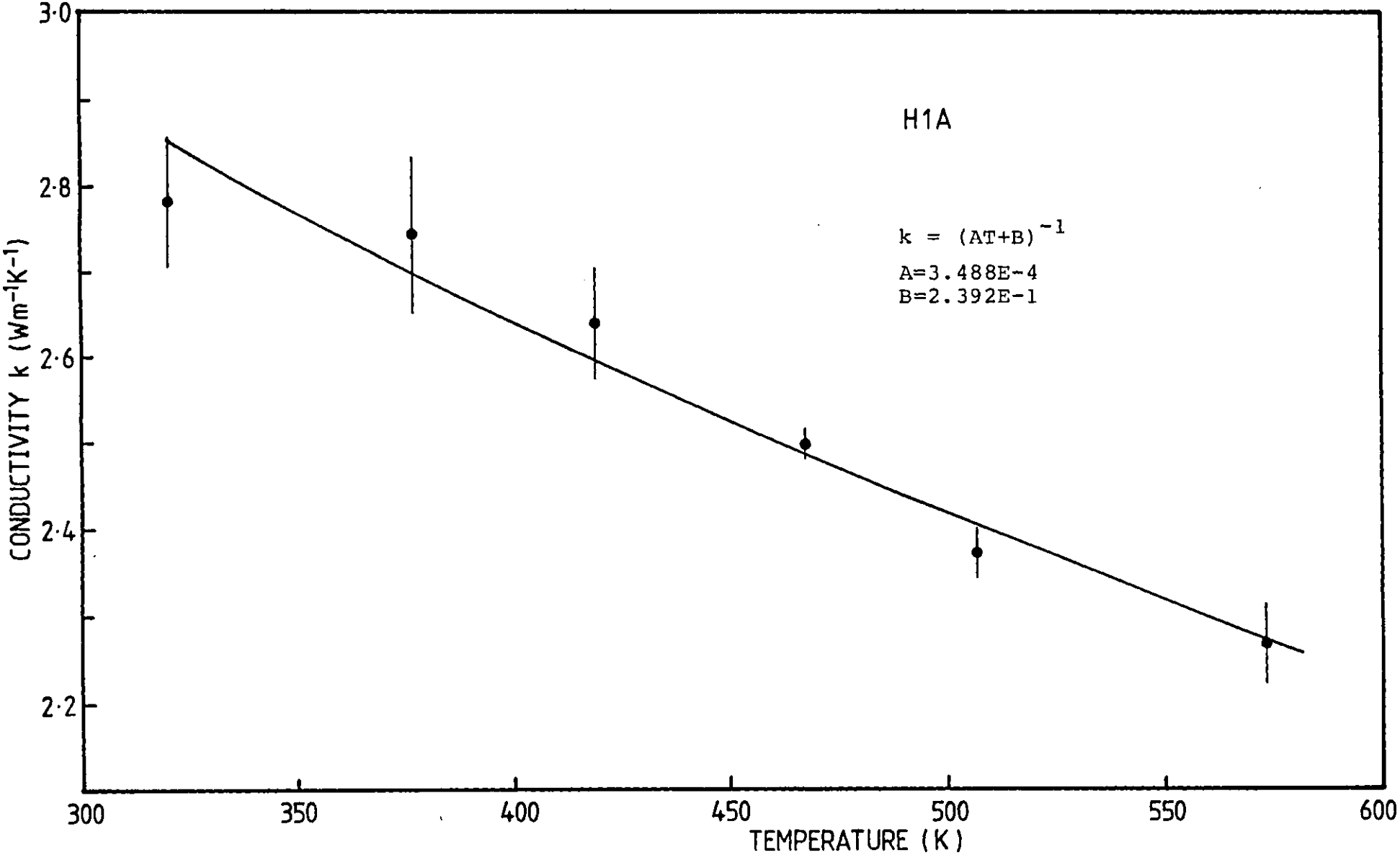

Fig. 5.18 Conductivity of Holman granite sample H1A.

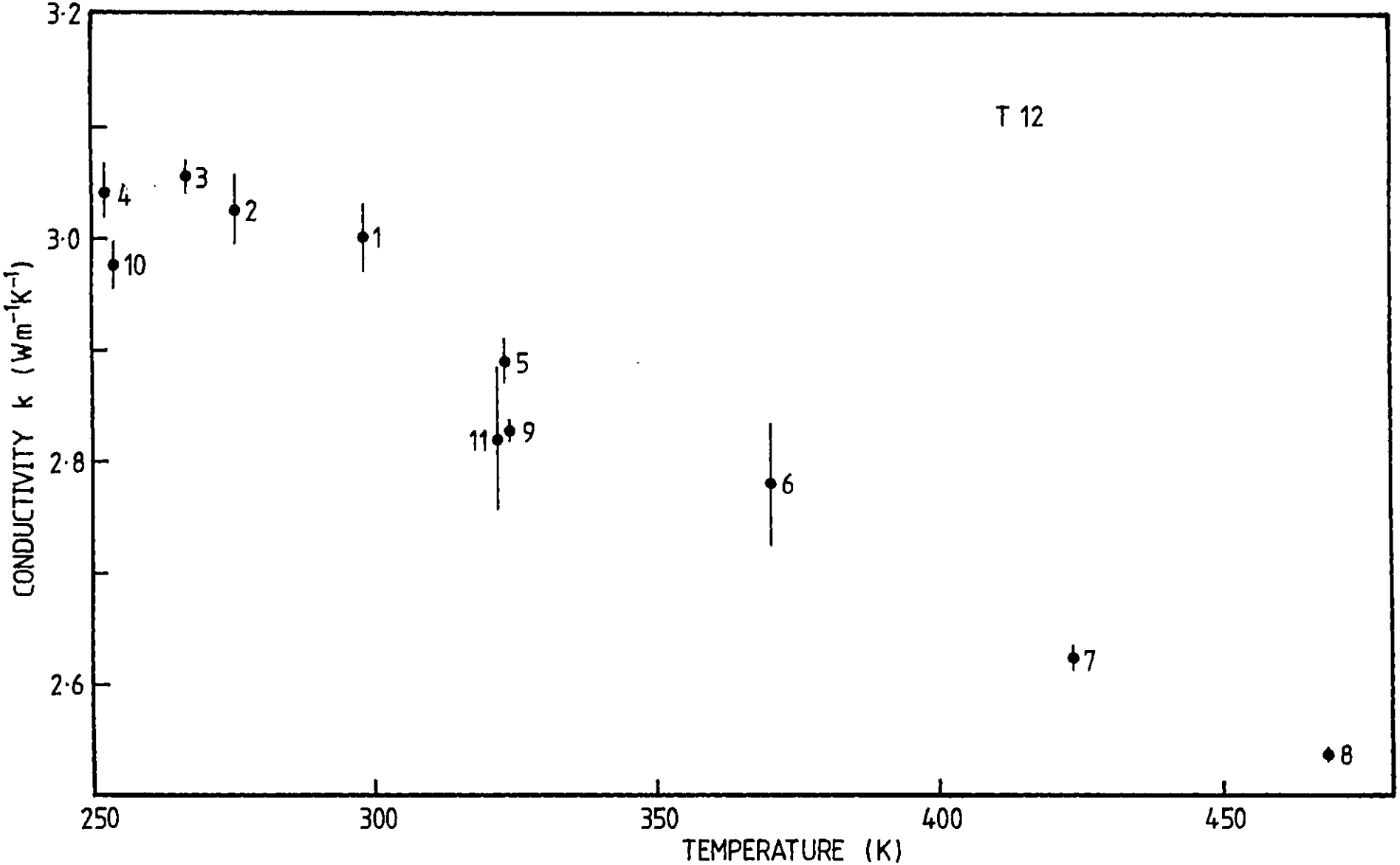

Fig. 5.19 Effect of temperature cycling on conductivity of Troon granite sample T12. The figures next to the points show the chronological order of the measurements.

Subsequent measurements at 320, 250 and 320 K showed a slight decrease in k, although point 11 at 320 K has too high a standard deviation to be conclusive.

Fig. 5.20 shows a comparison of the present results for the line-source temperature dependence of conductivity for the Merrivale, Troon and Holman granites with those of Dodson (1979) for a Cornish granite sample, and those of Birch and Clark (1940) for Rockport, Barre and Westerly granites. Also shown are room-temperature conductivities of water-saturated Merrivale granite from divided-bar measurements on 8 samples and two water-saturated Gaveriggan granites by the needle-probe method. The Troon and Gaveriggan values at room temperature, obtained after a compression cycle to 50 MPa, are discussed in section 5.5. The values for the dry samples are seen to be about 5% lower than those for wet samples, as fairly high-conductivity pore fluid is replced by air (with low conductivity), thus decreasing the apparent conductivity of the two-phase system.

The diffusivities of all the samples are tabulated in Appendix IV. The absolute values for some samples are lower than expected. It is suggested that in some cases the thermocouple wires, uninsulated in the proximity of the junction, may have come into contact thus forming a second junction at a larger offset from the heater. The measured offset would then tend to underestimate the real one, thus leading to an underestimate in the measured diffusivity. The temperature dependence of the diffusivity closely approaches the expected theoretical trend h~1/T for all the samples measured in conjunction with the new amplifier.

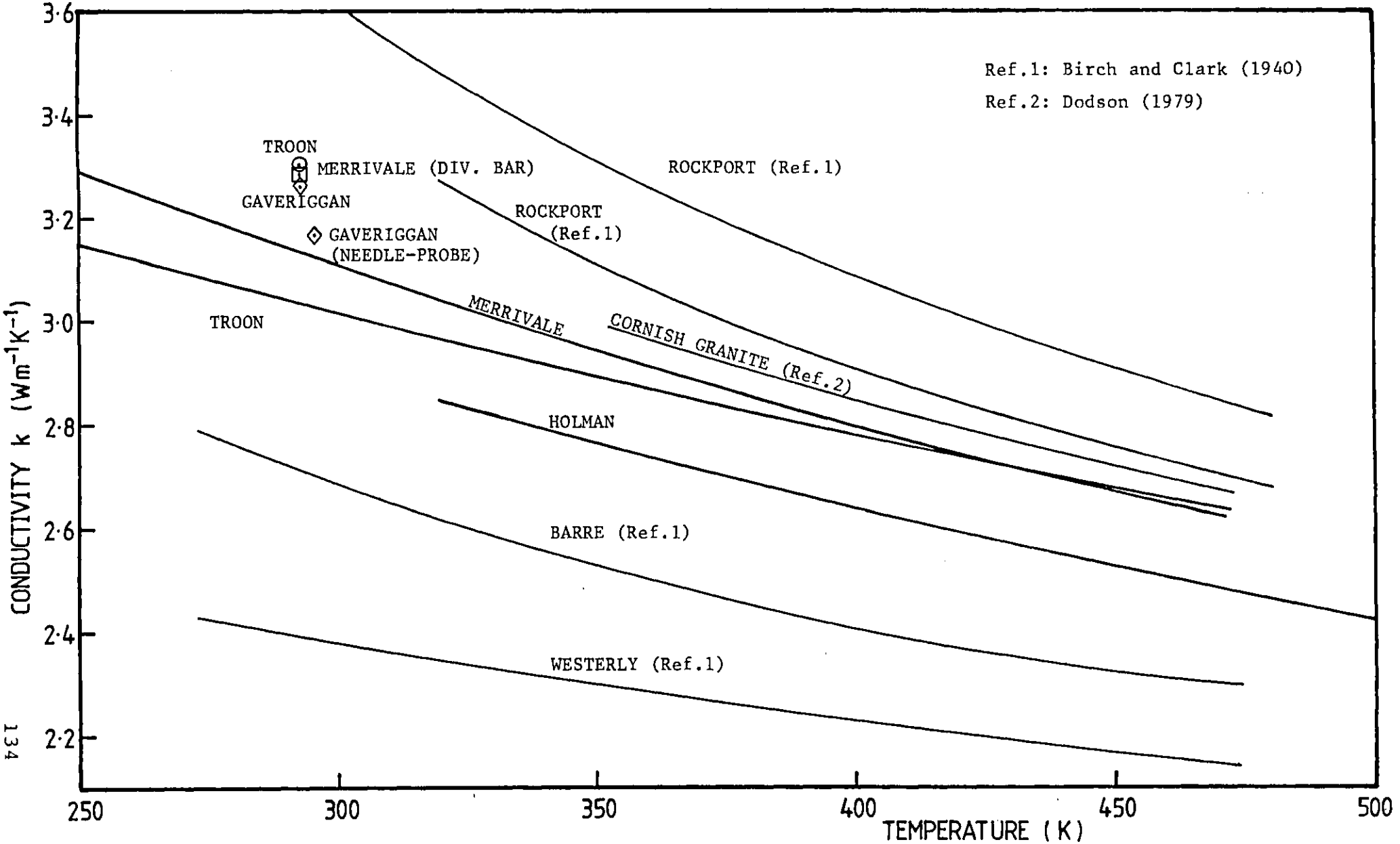

Fig. 5.20 Comparison of thermal conductivity measurements of granites.

5.4 Water saturation.

In order to relate the measured high-temperature conductivities of dry samples to those of water-saturated samples, which are more representative of the in situ conditions of the rock, several approaches can be adopted:

1) The samples are kept fluid-saturated over the entire temperature range. Birch and Clark (1940) used Helium and Nitrogen as the saturating fluids for temperatures up to 770 K, obtaining repeatable measuremnts after temperature cycling close to those for water-saturated samples (Clark, 1941). This method, however, is impractical and expensive for routine measurements, although high boiling-point liquids such as ethyl glycol or oil could be used as saturating fluids for temperatures up to 450-500 K.

2) The conductivity is measured under hydrostatic pressure, thus closely reproducing the in situ conditions of the rock. Water-saturation should be almost irrelevant in this case because at sufficiently high pressures all the penny-shaped cracks which most affect conductivity should be closed. This approach will be described in section 5.5 below.

3) The indirect method of section 2.3 is applied to relate dry to water-saturated conductivities by measuring the rock porosity. Alternatively, such a relationship can be determined experimentally by measuring (at room temperature) the conductivity of a sample after water-saturation and again after drying. All the high-temperature measurements can then be corrected by multiplying them by a constant factor equal to the ratio of the wet to the dry conductivities at room temperature. The latter method was

attempted and the results are described below.

The effect of water-saturation on two granite samples from adjacent core sections taken from Gaveriggan, Cornwall, was investigated at room temperature using a needle-probe technique. A 2 mm diameter hole was drilled in each of the samples by the Los Alamos Scientific Laboratory using an ultrasonic technique. The needle probe was calibrated against a Macor ceramic standard (k=1.605 at 300 K). Water-saturation was achieved by evacuating the air from the samples (vacuum down to~1 mm Hg for three hours), submerging the samples in water, and then allowing the water to penetrate the cracks under atmospheric pressure. Drying was performed at 450 K for 24 hours. The results are reported in Table 5.3. The conductivity of the water-saturated samples are substantially identical, but the percentage variations after drying differ markedly, suggesting that pore and crack patterns have a more marked effect on the conductivity of dry samples than on wet ones where the interstitial fluid short-circuits the crack thermal resistance. It is likely that the same effect may also partially account for the spread of conductivities in the Merrivale and Troon granites.

TABLE 5.3 Differences between thermal conductivities of water-saturated and dry Gaveriggan granite samples at 296 K. Units are $Wm^{-1}K^{-1}$. Figures in brackets are numbers of runs.

SAMPLE	k(WET)	k(DRY)	% CHANGE
G1	3.177±0.036 (12)	3.067±0.058 (70)	-3.5
G2	3.164±0.039 (75)	2.861±0.038 (19)	-9.6

5.5 Pressure dependence of conductivity.

The conductivities of two granite samples were measured over a range of hydrostatic pressures between normal pressure and 50 MPa, corresponding to in situ lithostatic pressures down to depths of about 2 Km. From the discussion of section 2.1, it is clear that pressure variations of up to 50 MPa do not directly affect the crystal lattice conductivity to a measurable extent. The present measurements were designed to investigate the effects of pressure on dry rocks, i.e. two-phase systems in which microcracks play a significant role in controlling the effective thermal conductivity.

Oil was used as the pressurizing agent in the autoclave to provide true hydrostatic compression. The samples were carefully coated with silicone rubber compound to prevent ingress of oil.

The results for a dry Troon granite sample (T12) at room temperature are shown in figures 5.21 and 5.22. The sample conductivity was measured at increasing pressure levels from 0 to 50 MPa and then re-measured in three subsequent

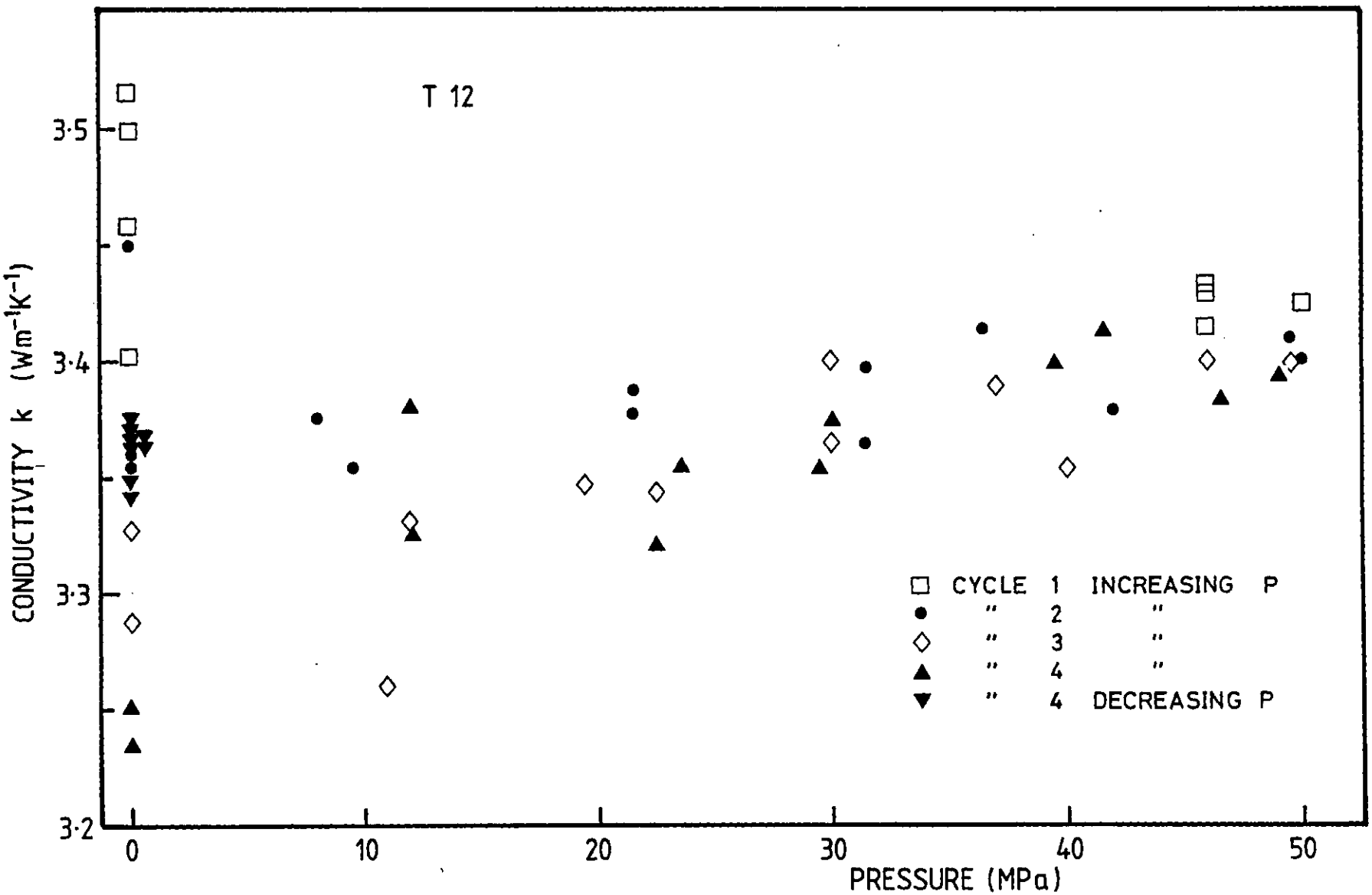

Fig. 5.21 Pressure dependence of conductivity for Troon Granite at 293 K. Points show results of individual runs.

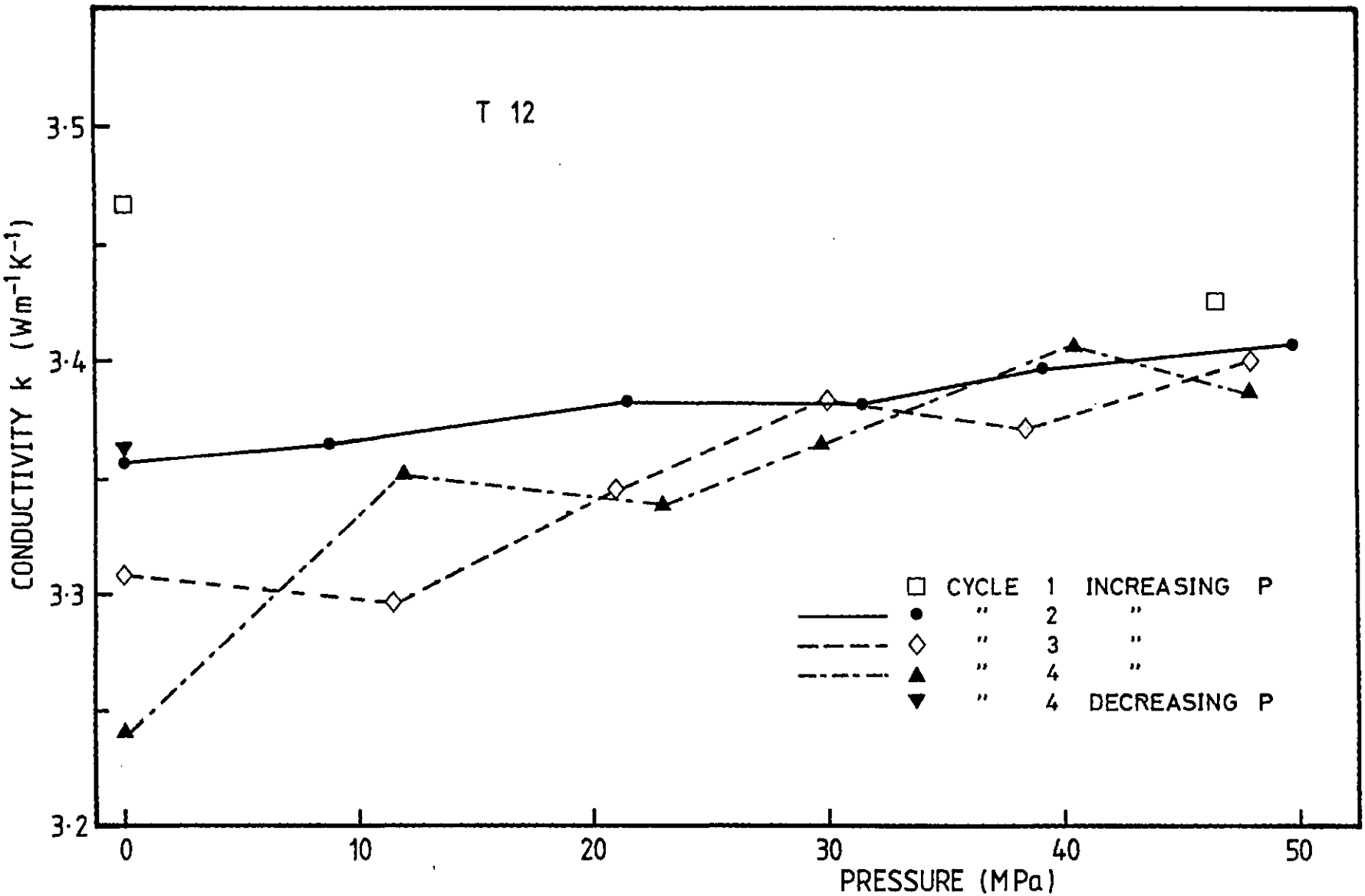

Fig. 5.22 Pressure cycling of Troon granite. Points shown are averages of 2-6 runs.

cycles after heating respectively to 370, 420 and 470 K for 24 hours. In the first pressure cycle the conductivity is seen to decrease slightly with pressure, but this result is not very conclusive given the considerable scatter in the values at normal pressure and their anomalously high values when compared to those for T12 at room temperature in Fig. 5.14. The possible causes of this anomaly are the following:

a) An experimental error whose causes remain unexplained - the equipment was checked against a Macor standard and gave accurate results.

b) A slight increase in the conductivity in the several months between the temperature and the pressure cycles, possibly associated with a gradual closing of the microcracks under internal stresses. A similar, if smaller effect was detected in sample H1A after the heating cycles. A more detailed investigation would be needed to confirm this effect.

In the second and third pressure cycles of Fig. 5.22, heating caused the conductivity to drop in direct proportion to the temperature, but after applying a moderate pressure of 20-30 MPa all the values seem to converge to the same slight direct linear dependence on pressure. The set of measurements at normal pressure at the end of the last cycle are about 3% higher than those at the beginning of the cycle, which implies a permanent closing of some of the cracks even after the pressure is released. This is not an uncommon effect (see for example Kappelmeyer and Haenel, 1974, p.216).

The pressure dependence for a Gaveriggan granite sample

(G3) is illustrated in figures 5.23 and 5.24. The sample was initially saturated with water, then measured at 0, 25, 50 MPa and again at normal pressure. Two more similar pressure cycles were performed after heating respectively to 370 and 450 K for 24 hours. Heating to 370 K had a negligible effect on the zero pressure conductivity, and heating to 450 K decreased it by about 2%. A pressure of 25 MPa was sufficient to bring the dry conductivity back to the water-saturated value at the same pressure.

The following conclusions were drawn from the high-pressure experiments:

1) The conductivity of both granite samples increases with increasing pressure. If a linear dependence is assumed, the average rate of increase is about 1.5×10^{-3} $Wm^{-1}K^{-1}MPa^{-1}$ for both the Troon and the Gaveriggan samples.

2) Pressures of the order of 20-25 MPa are sufficient to equalize the conductivities of the dry and water-saturated rocks.

3) The increase in conductivity is not totally reversed when the pressure is released.

4) Better stability is observed in the conductivities at elevated pressures than at normal pressure.

These cosiderations would appear to make conductivity determinations of dry granites at moderate pressures of 20-25 MPa a feasible alternative to measurements of water-saturated samples. Further experiments on a wider range of samples, which time limitations prevented in this study, are needed to confirm these results.

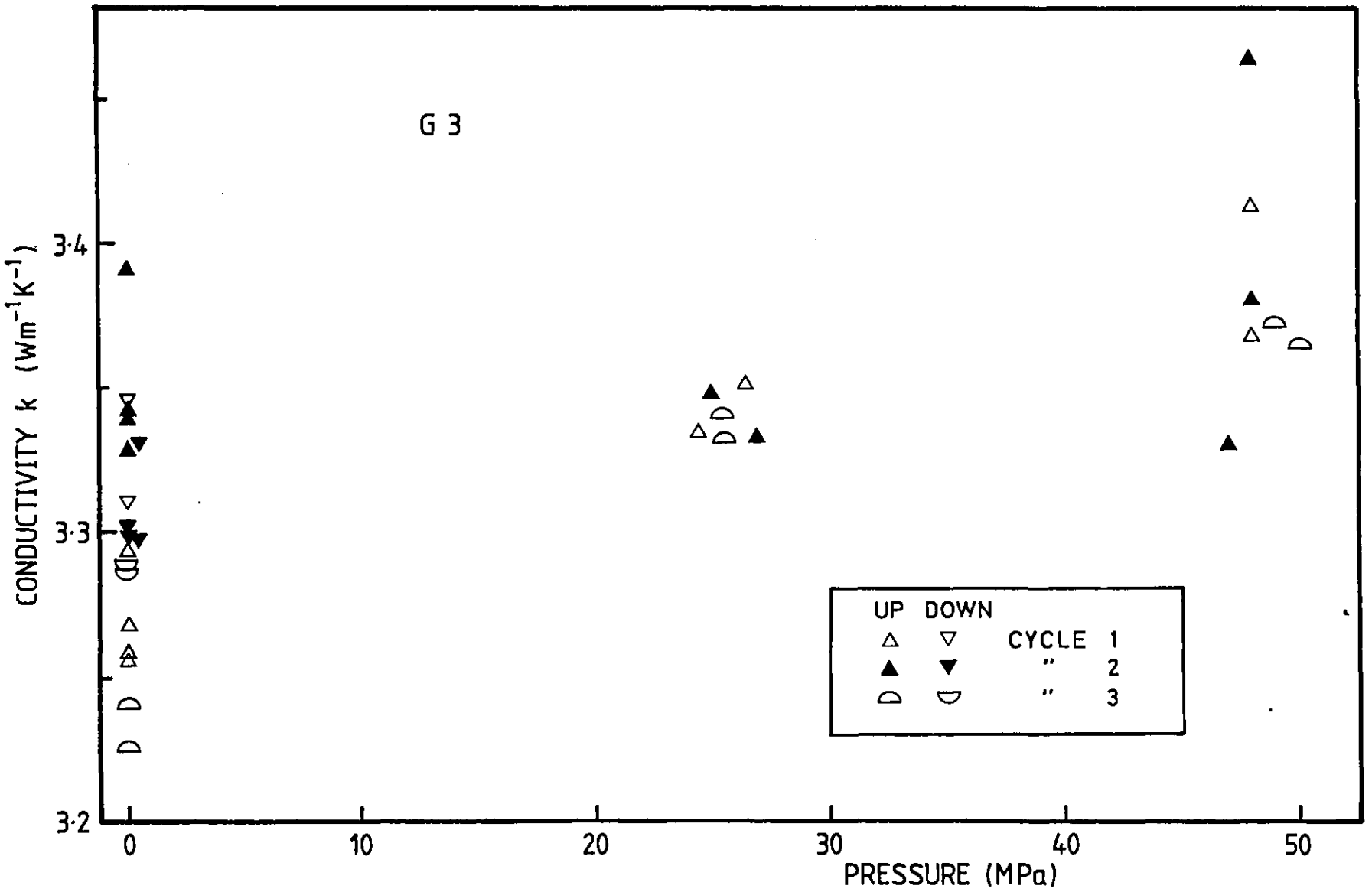

Fig. 5.23 Pressure dependence of conductivity for Gaveriggan granite at 293 K. Points show results of individual runs.

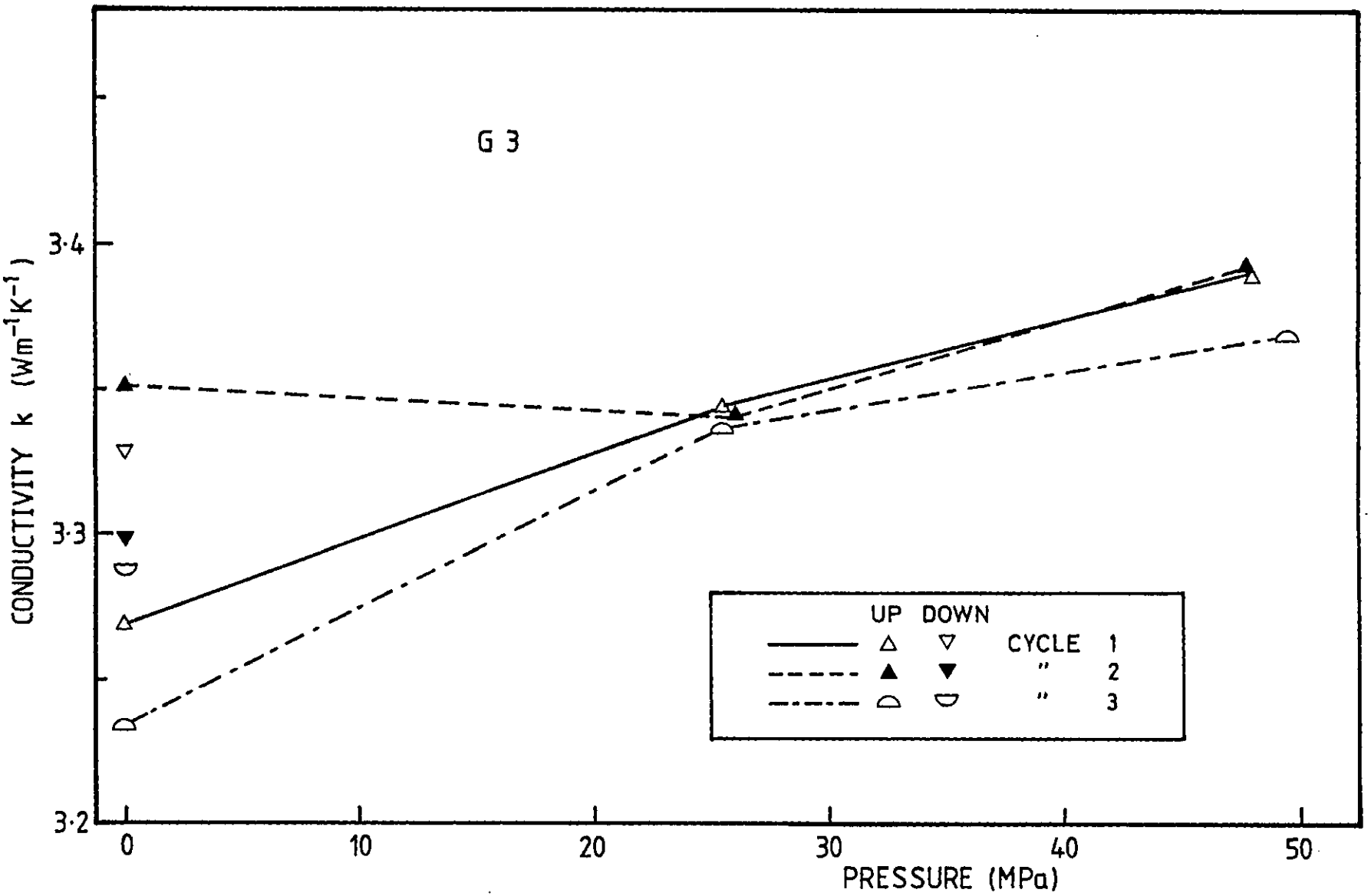

Fig. 5.24 Pressure cycling of Gaveriggan granite. Points shown are averages of 2-6 runs.

Chapter 6

CONCLUSION

The results presented in the previous chapter demonstrate the validity of this line-source method of rapid thermal conductivity measurement over a range of elevated temperatures and pressures. The high-temperature measurements highlighted the marked temperature-dependent decrease in thermal conductivity for rocks likely to be encountered in a typical geothermal resevoir, and showed good agreement with the theoretical predictions and with published results for similar rock types. The high-pressure experiments detected a weak positive pressure dependence in Cornish granite and proved a valuable tool for relating the conductivity of dry samples to those of water-saturated ones, more representative of the in situ rock conditions.

The use of the exponential integral solution within a well-defined sampling time window, though increasing the computational complexity, led to a satisfactory experimental accuracy. The statistical reliability was enhanced by the large size of the data sample obtainable using modern digital techniques. Local data processing by microcomputer resulted in a rapid detection of spurious results.

Some of the mathematical solutions, and much of the instrumentation described in chapters 3 and 4 can be employed in conjunction with needle-probes for the thermal conductivity determination of unconsolidated or soft sediments.

Some aspects of the line-source experiment could not be investigated in detail because of time limitations. Suggestions for improvements and extensions to the method are given below as guidelines for further work.

The improved availability of low-cost, fast 16 and 32 bit microcomputers will soon allow more complex mathematical computations to be carried out in real time. A quick determination of the conductivity, possibly by the logarithmic method, would enable a precise calculation of the upper and lower time bounds of the sampling window for every sample, based on parameters such as the thermal constants of the adhesive, sample dimensions and thermocouple offset. The conductivity would then be re-calculated to a better accuracy by the standard method based on the sampling window thus determined.

Automatic control by microcomputer of the oven and switching of sample thermocouples and heaters could easily be implemented. Temperature-sensing routines could be designed to continuously monitor the temperatures of the samples and start a measurement as soon as satisfactory temperature equilibrium is reached. This would allow concurrent measurement of up to 20-30 samples in the same oven over a range of temperatures and a period of several days, thus decreasing running costs and errors.

The bonding materials used here were considered to be satisfactory, thermal silicone grease being preferred for ease of sample dismantling and inspection after measurements. However, a selection of sample bonding materials with thermal parameters matched to those of the rock would result in a decreased lower time bound for the

sampling window, with a consequent improvement in the repeatability of the results.

Appendix I

CIRCUIT DIAGRAMS AND COMPONENT LAYOUTS OF LINE-SOURCE APPARATUS

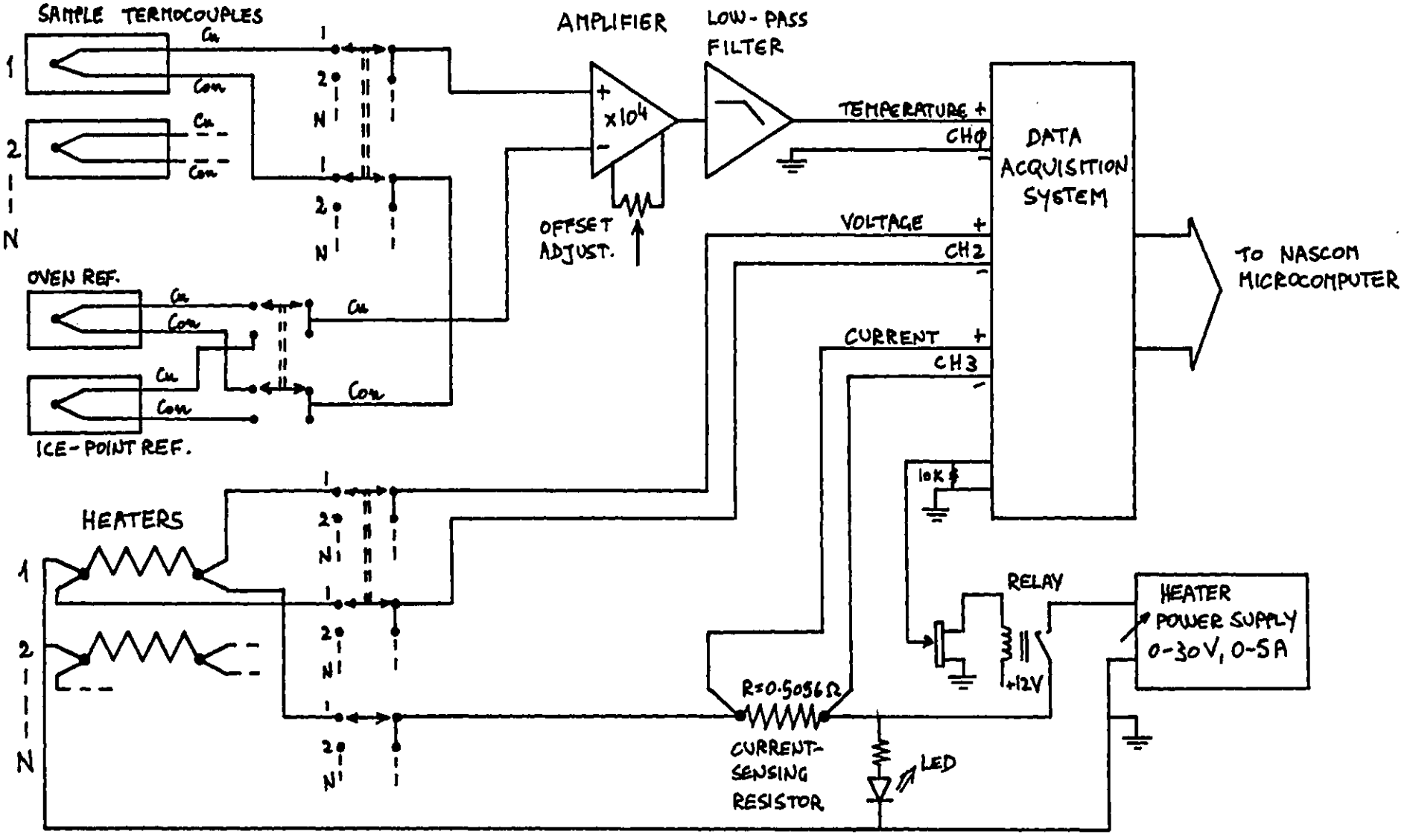

Fig. AI.1 ANALOGUE SECTION SCHEMATIC DIAGRAM

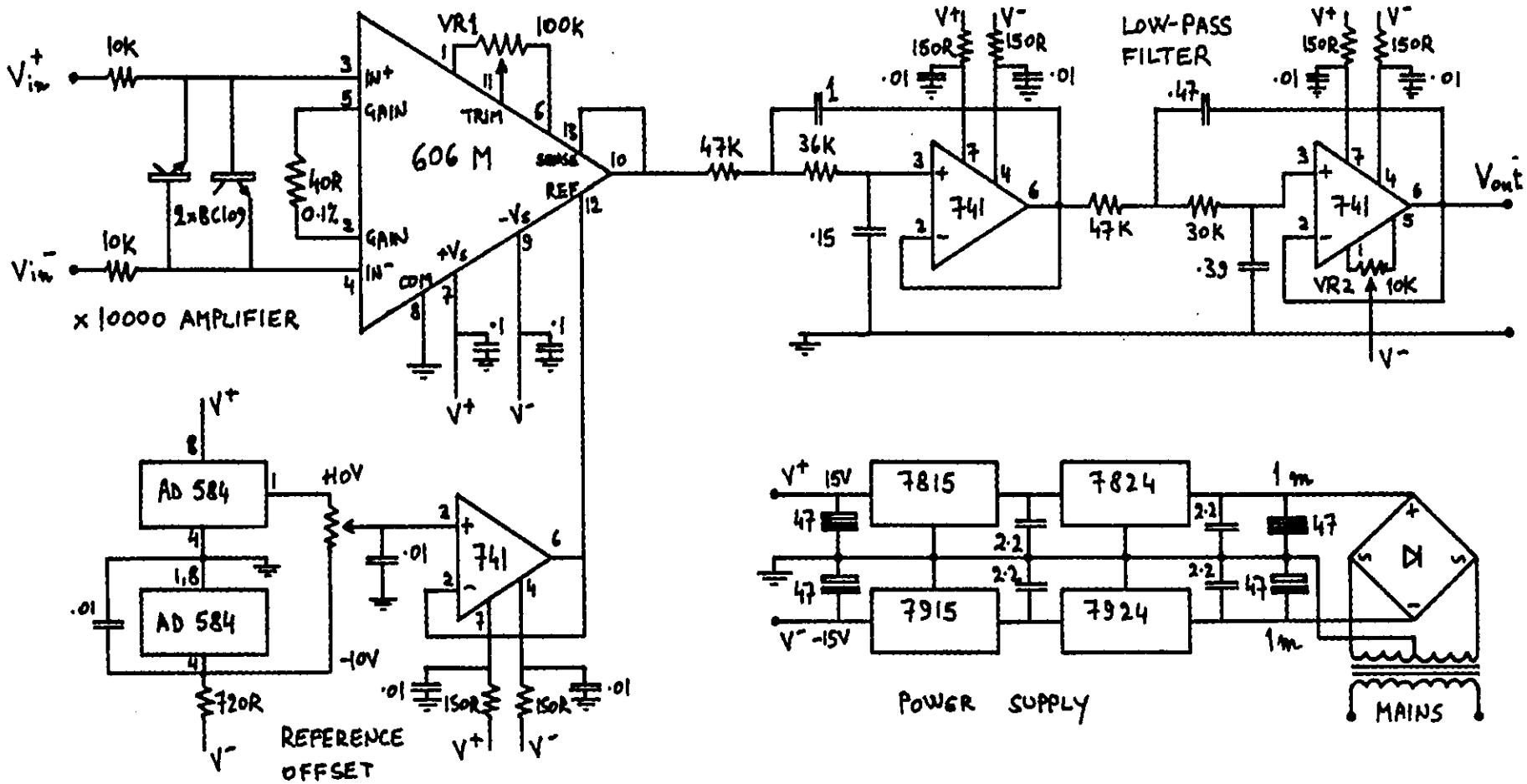

Fig. AI.2 THERMOCOUPLE AMPLIFIER AND FILTER

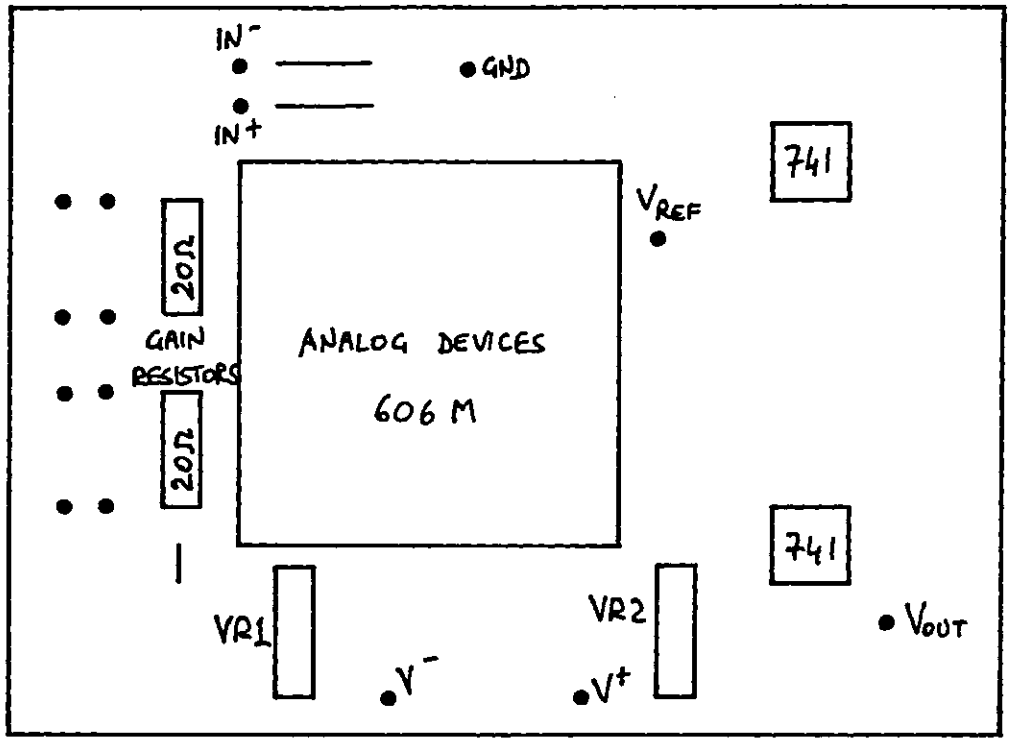

MAIN AMPLIFIER/FILTER BOARD

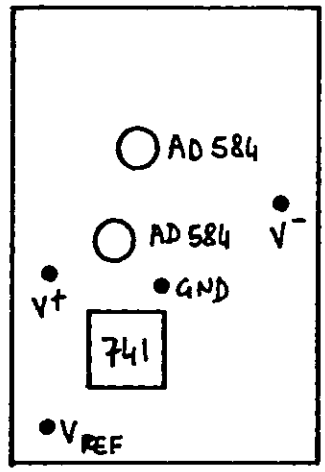

VOLTAGE REFERENCE
BOARD

Fig. AI.3 Layout of thermocouple amplifier.

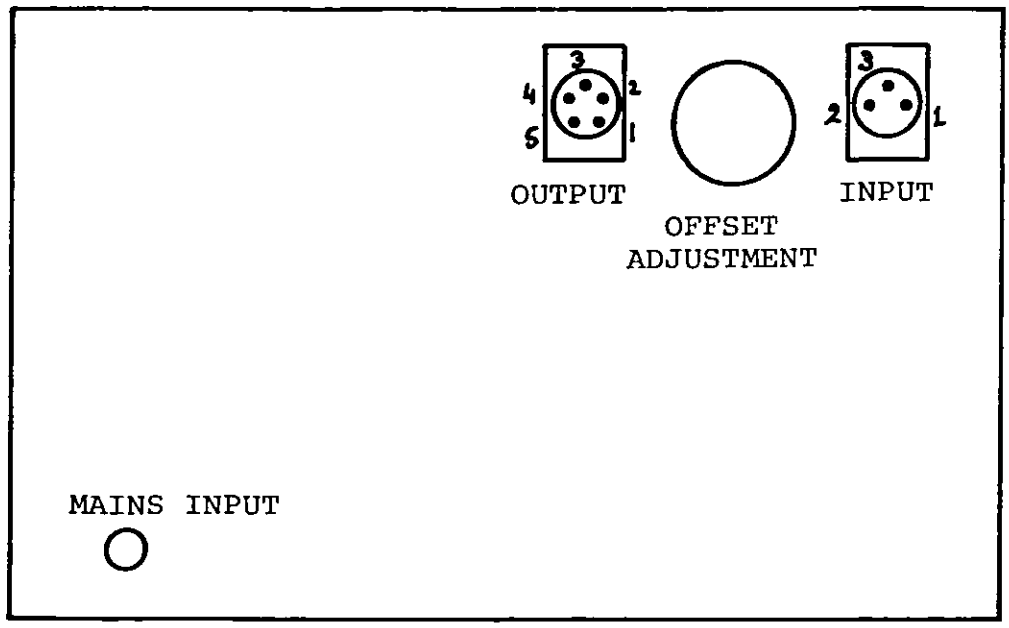

INPUT PLUG:	PIN 1	GND
	2	IN^+
	3	IN^-
OUTPUT PLUG:	PIN 1	N.C.
	2	N.C.
	3	GND
	4	V_{out}
	5	N.C.

OFFSET VOLTAGE = (DIAL POSITION - 500)/50 Volts

Fig. AI.4 Thermocouple amplifier front panel.

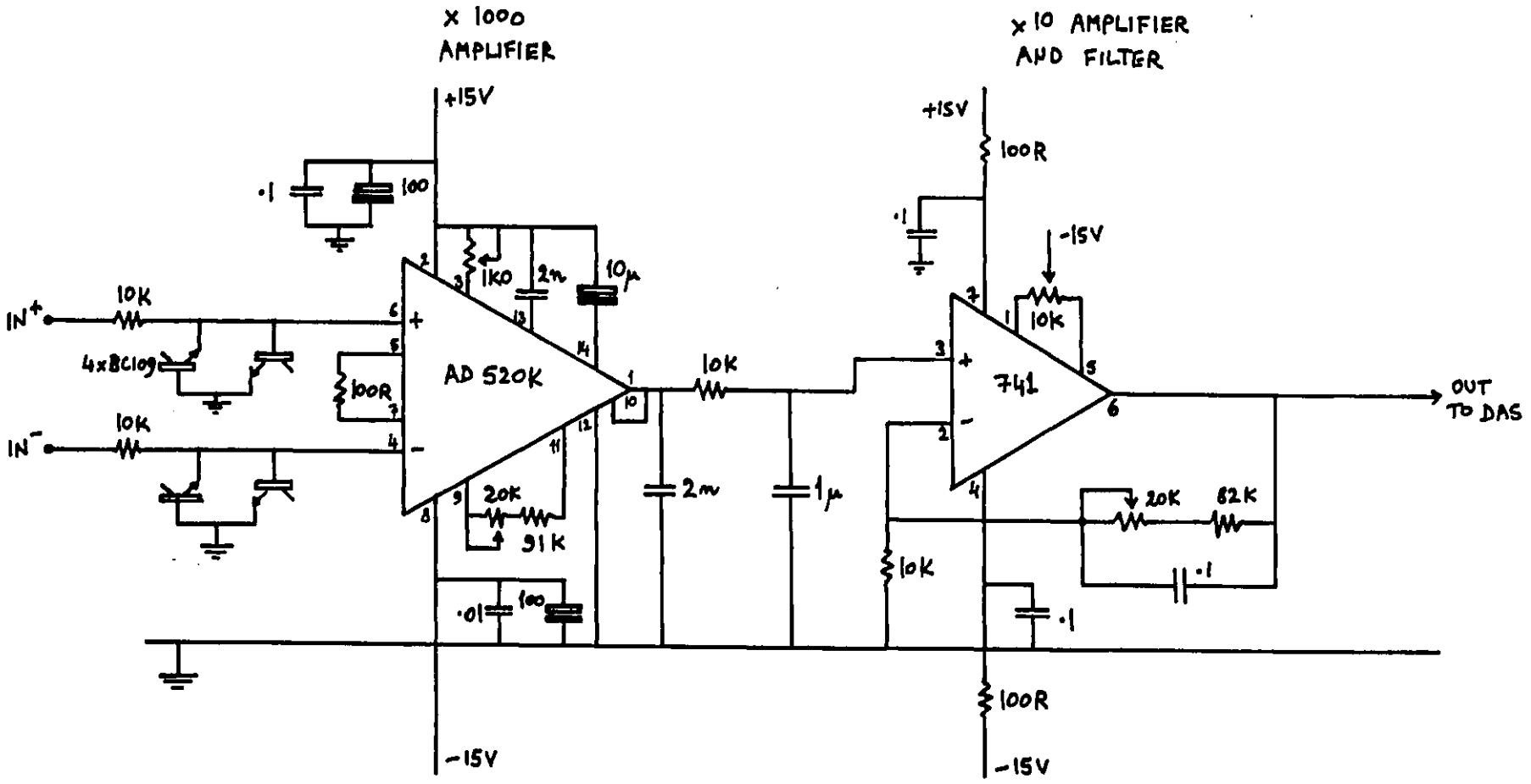

Fig. AI.5

OLD THERMOCOUPLE AMPLIFIER

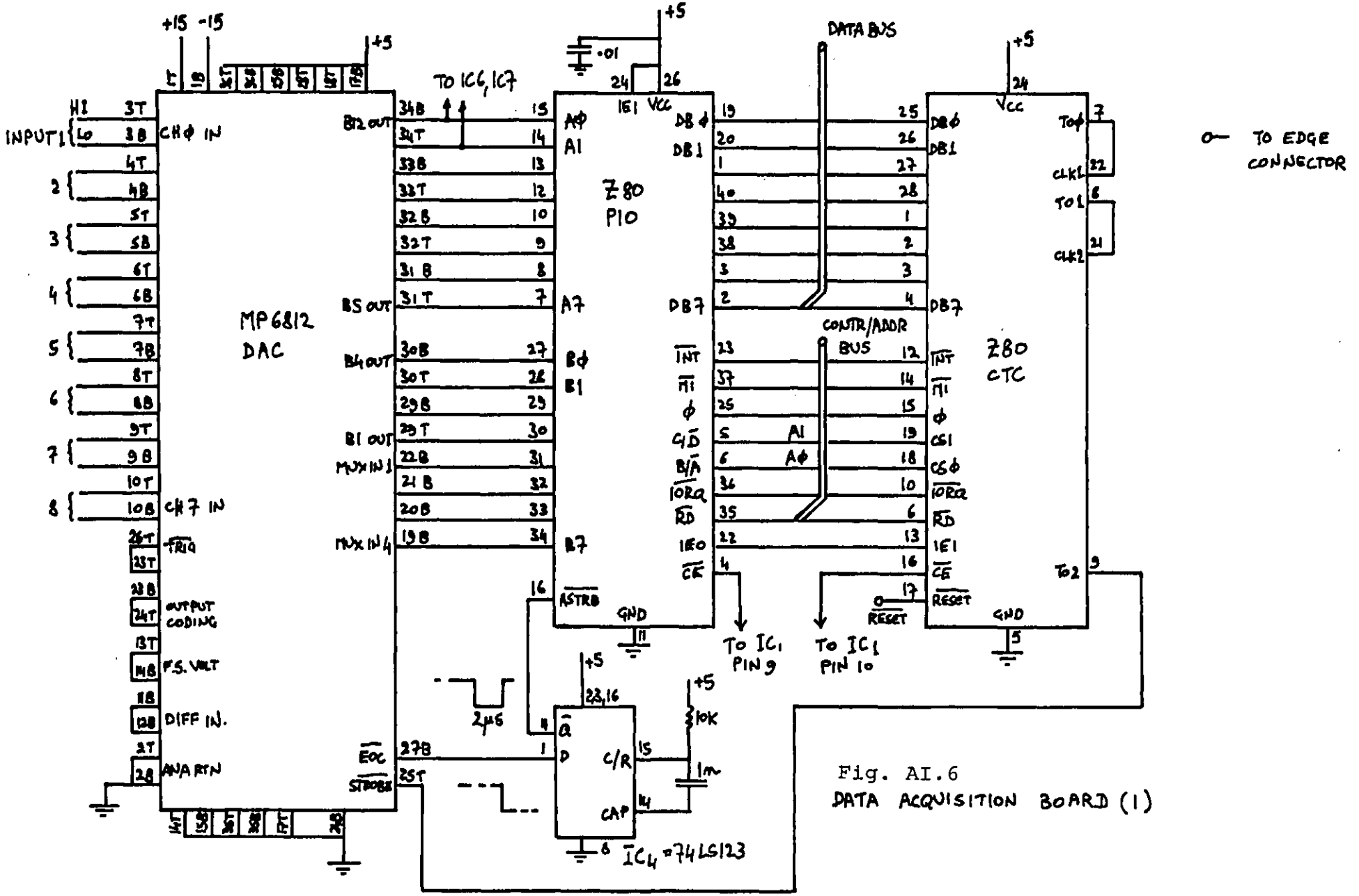

Fig. AI.6
DATA ACQUISITION BOARD (1)

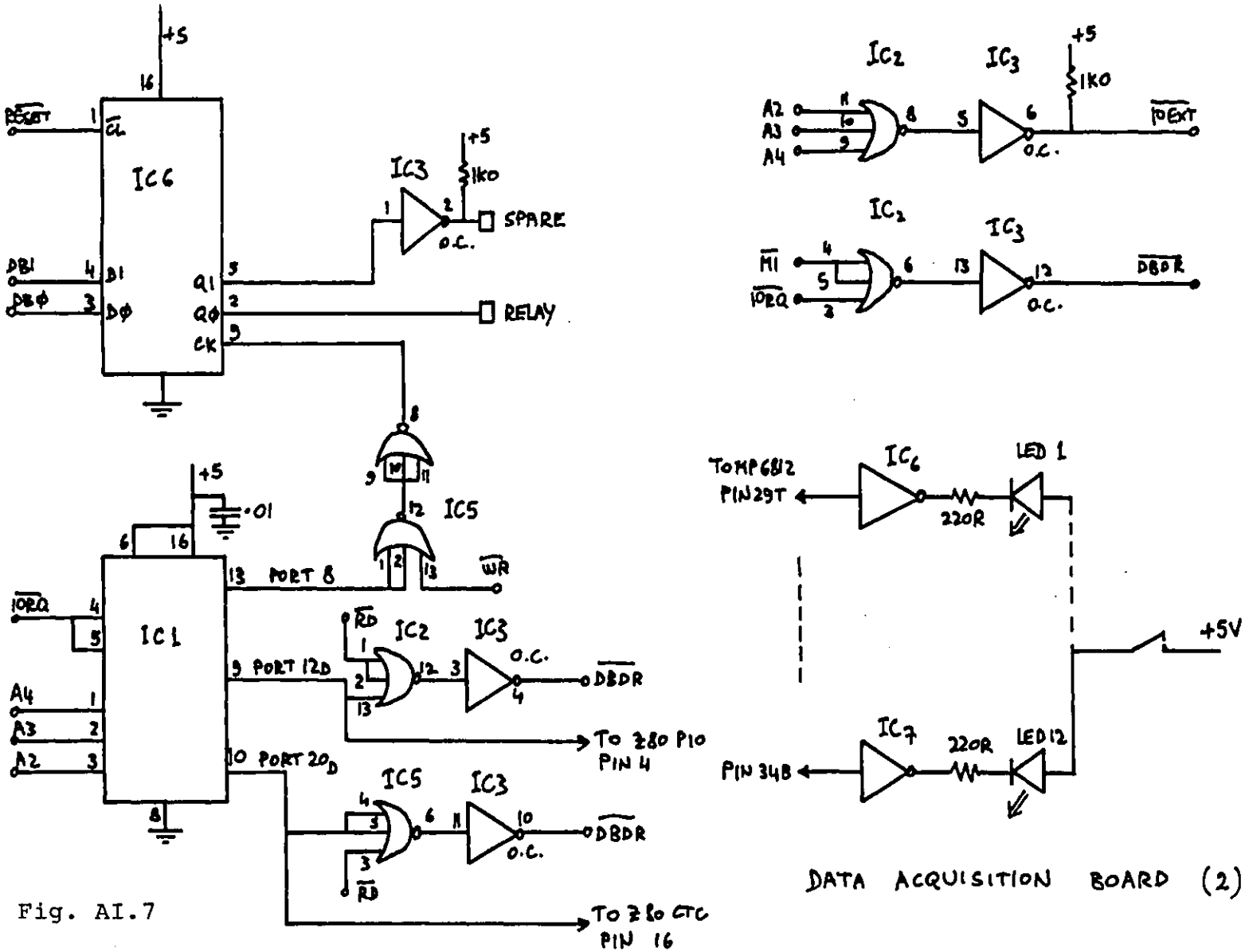

Fig. AI.7

IC1 = SN 74LS138
IC2, IC5 = SN 74LS27
IC3 = SN 7406
IC4 = SN 74LS123
IC6 = 74 C174
IC7, IC8 = SN 74LS04

DATA ACQUISITION BOARD (2)

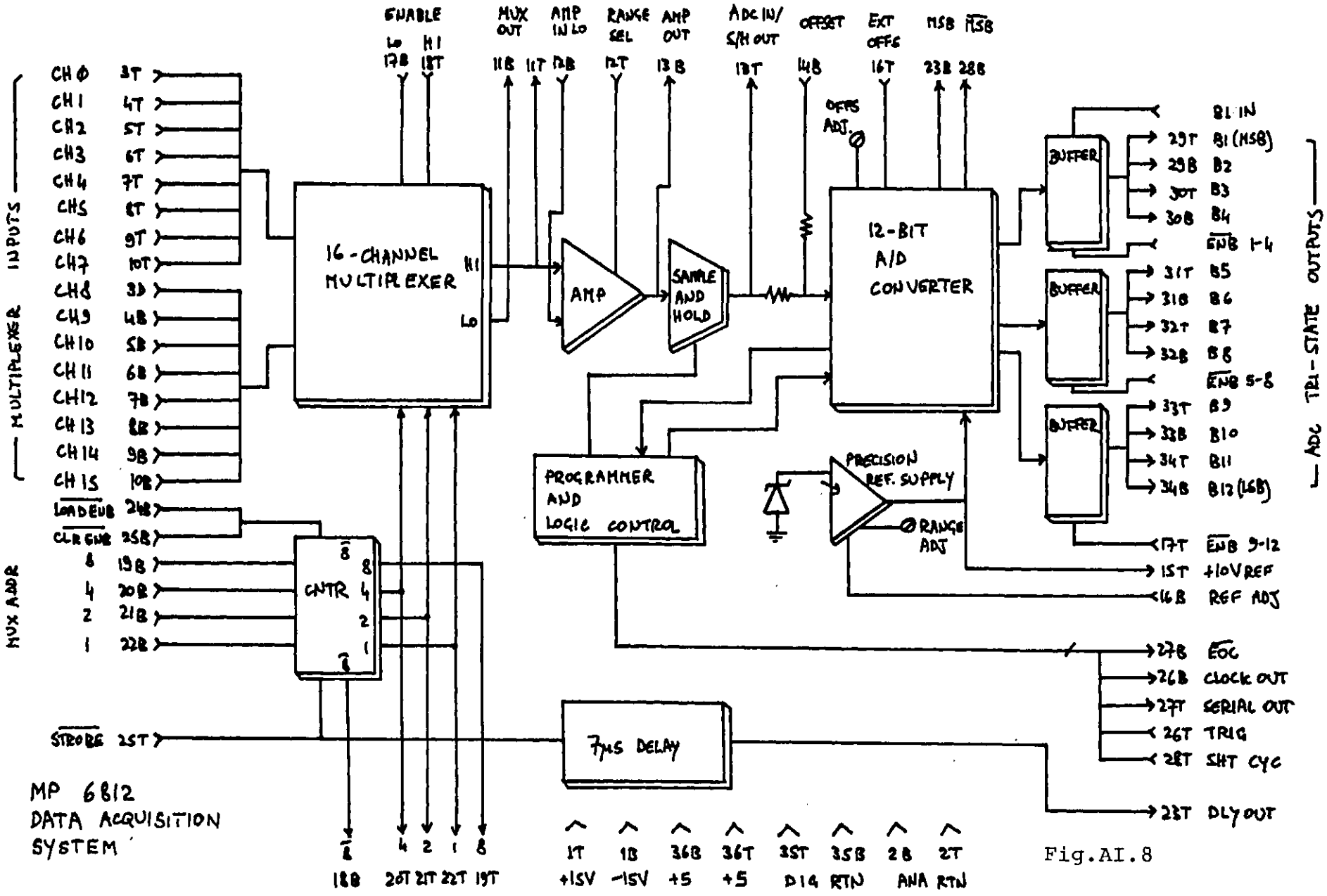

MP 6812
DATA ACQUISITION
SYSTEM

Fig.AI.8

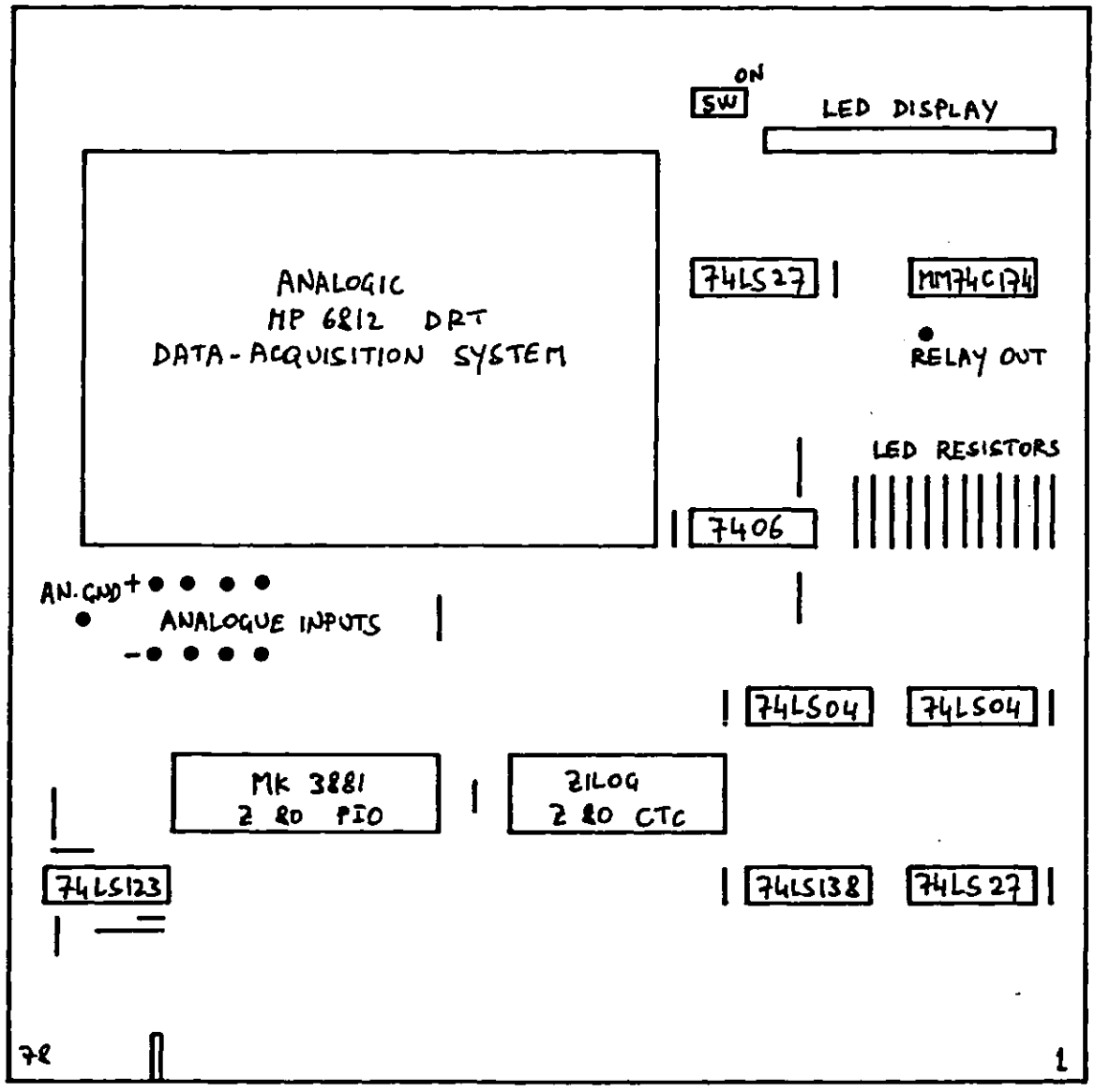

Fig. AI.9 Layout of data acquisition board.

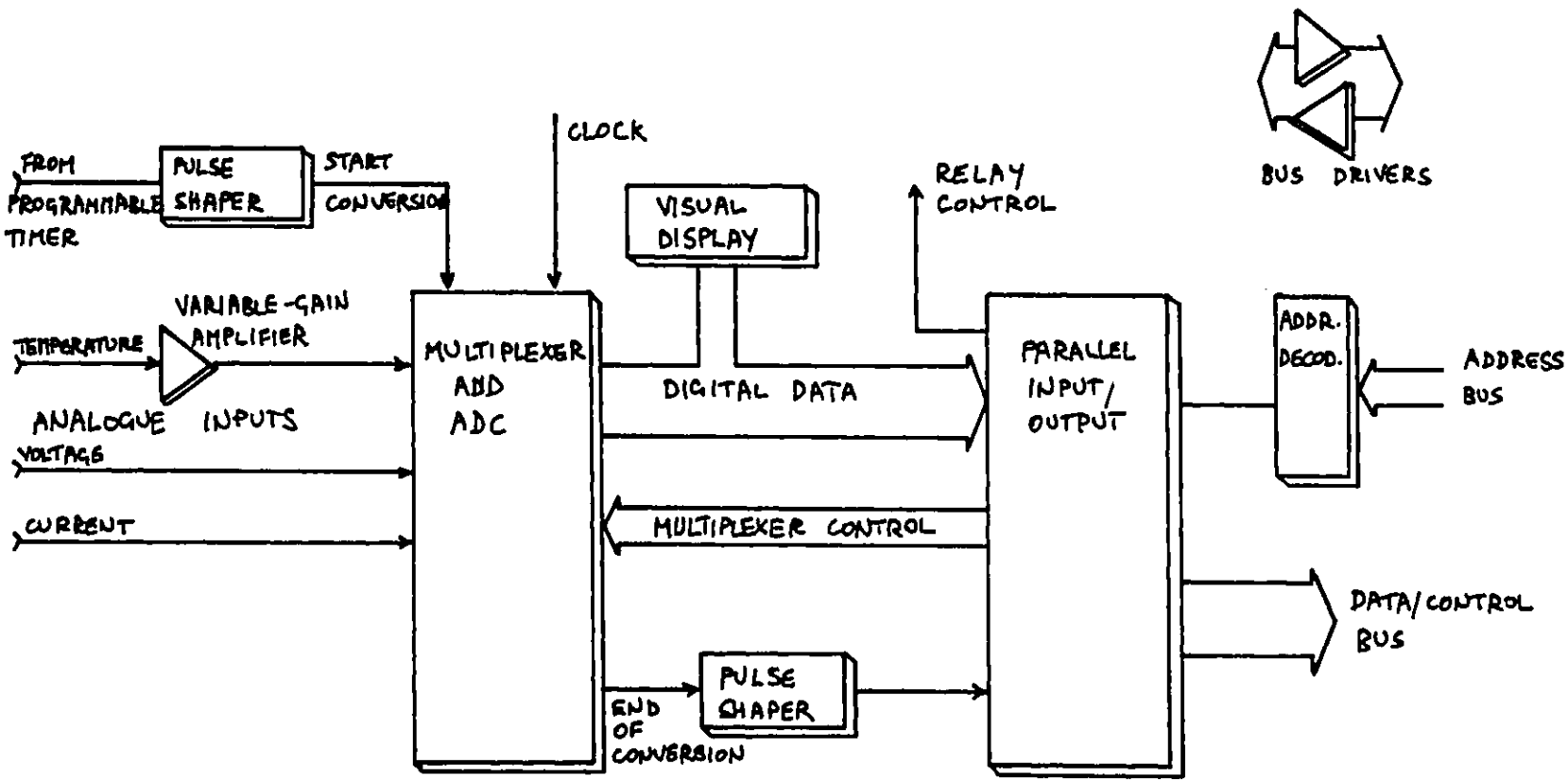

Fig. AI.10 OLD DATA ACQUISITION BOARD - BLOCK DIAGRAM

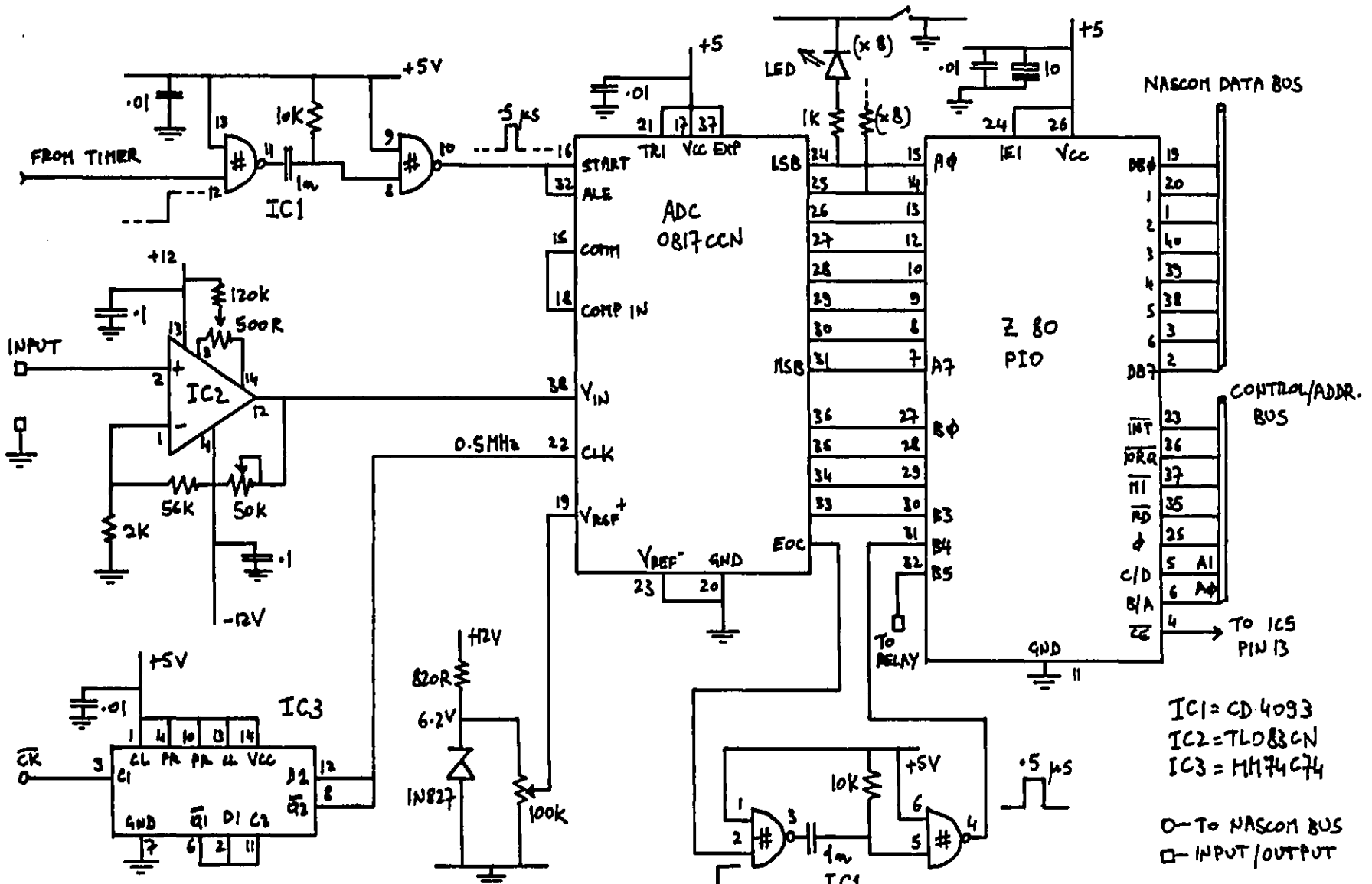

Fig. AI.11 OLD DATA ACQUISITION SYSTEM (1)

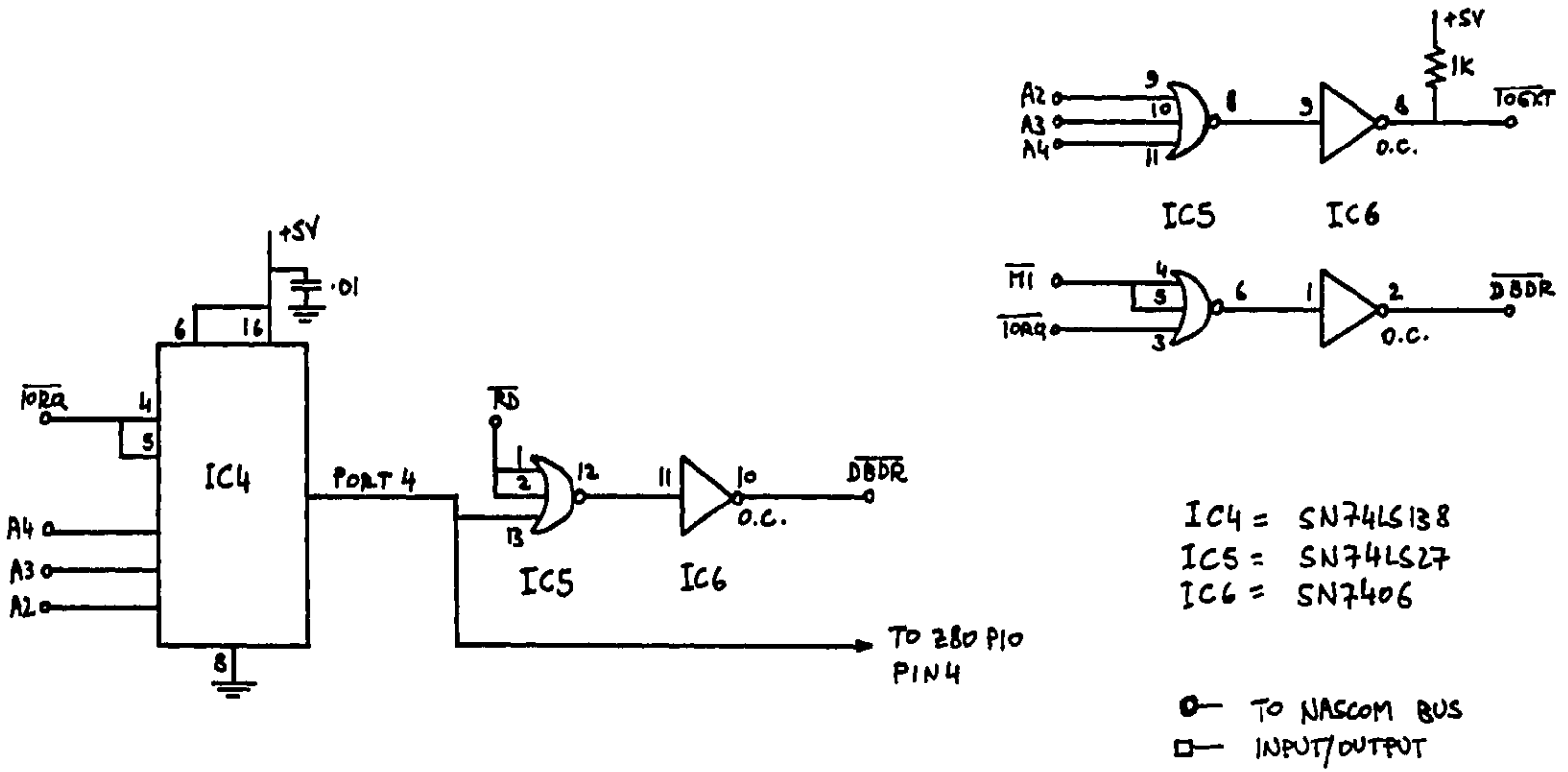

Fig. AI.12 OLD DATA ACQUISITION SYSTEM (2)

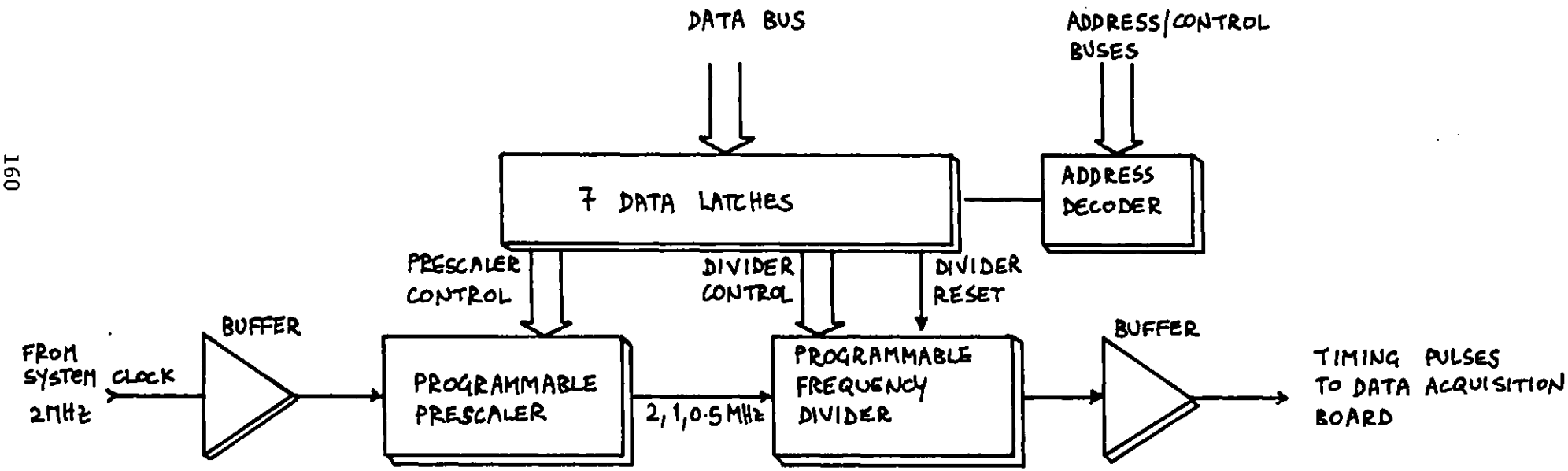

Fig. AI.13 TIMER BLOCK DIAGRAM

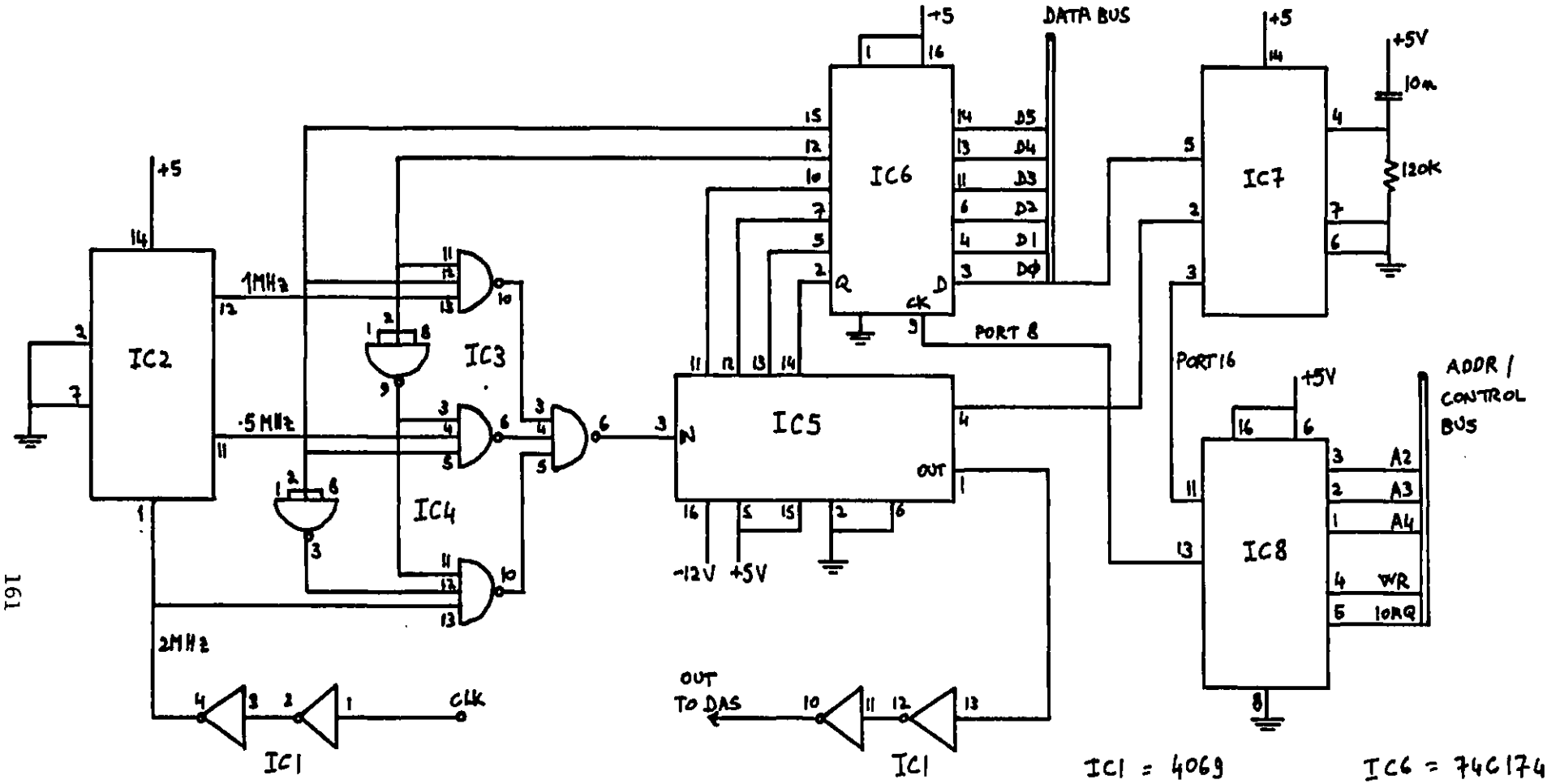

IC1 = 4069
IC2 = 4024
IC3 = 4023
IC4 = 4023
IC5 = MK 5009
IC6 = 74C174
IC7 = 4013
IC8 = 74LS138

Fig. AI.14 PROGRAMMABLE TIMER

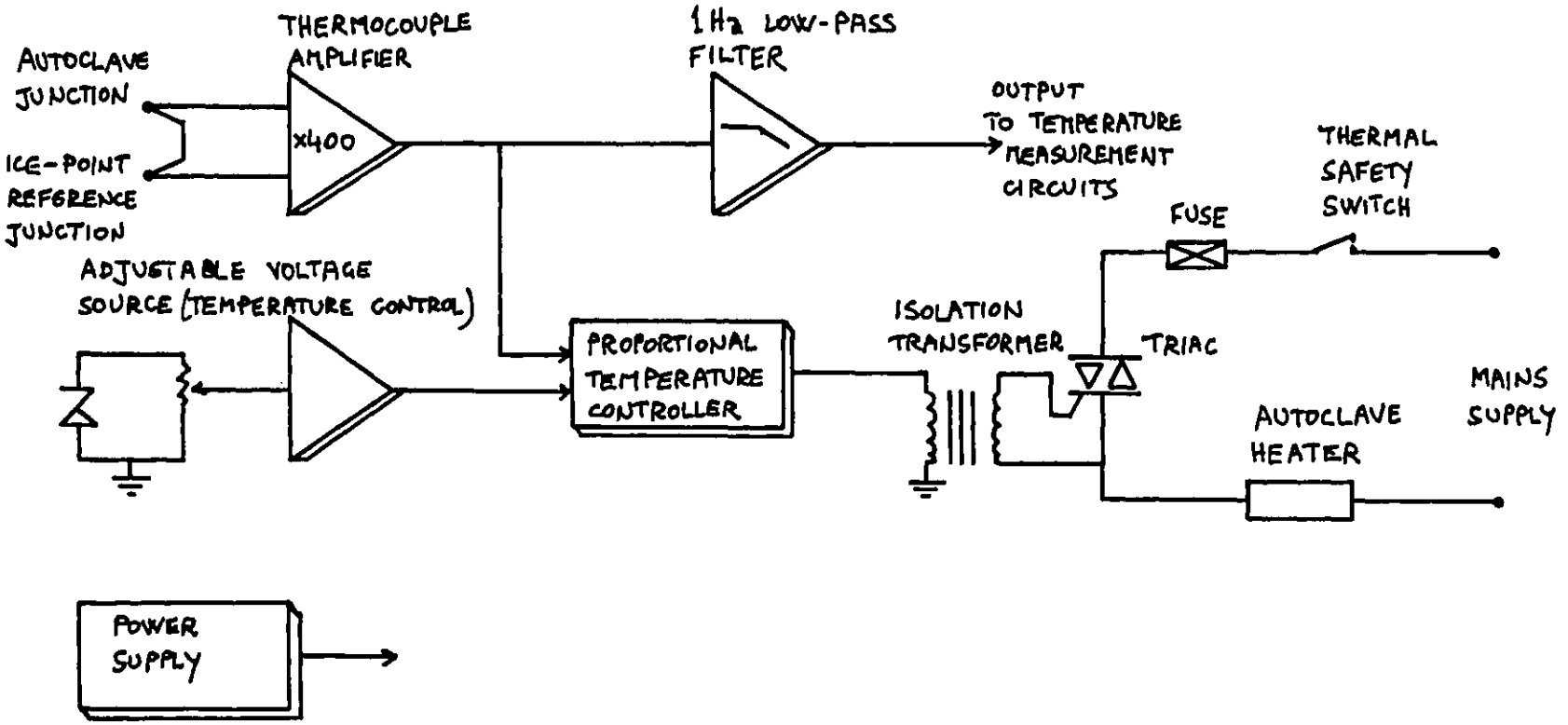

Fig. AI.15

AUTOCLAVE TEMPERATURE CONTROLLER (BLOCK DIAGRAM)

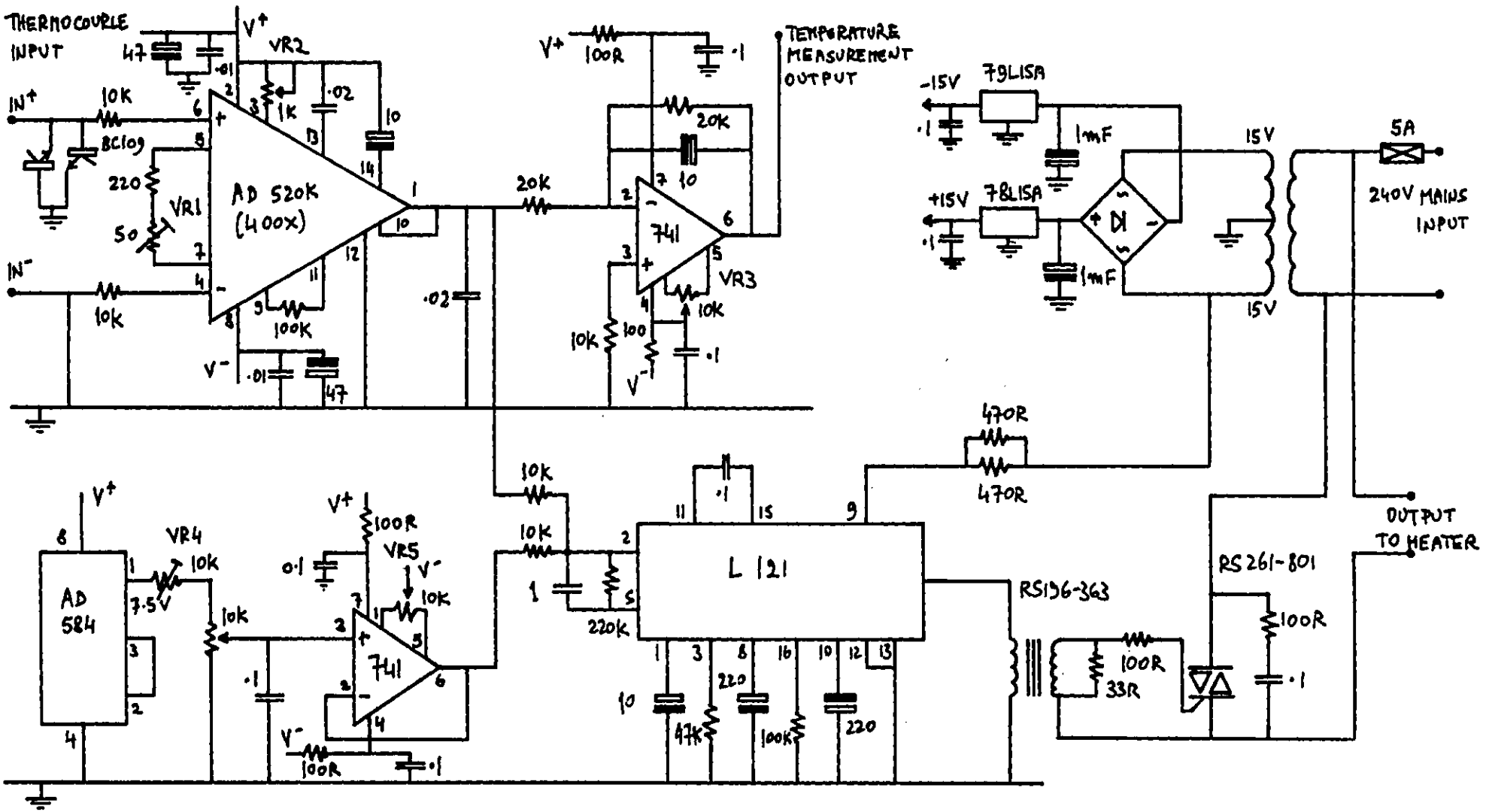

Fig. AI.16 AUTOCLAVE TEMPERATURE CONTROLLER

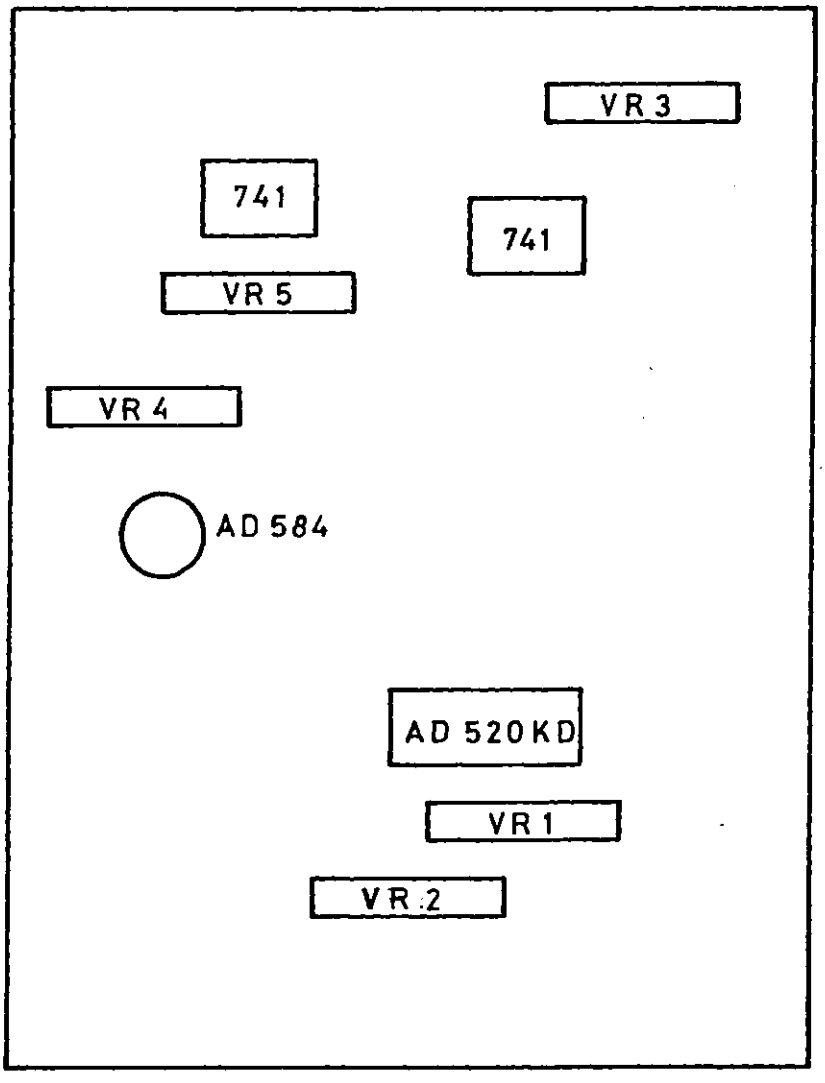

Fig. AI.17 Temperature controller layout.

Appendix II

LINE-SOURCE BASIC AND MACHINE LANGUAGE COMPUTER PROGRAM

LINE-SOURCE PROGRAM

```
10 REM - ALL REM STATEMENTS IN THIS PROGRAM SHOULD BE
20 REM - REMOVED PRIOR TO EXECUTION TO INCREASE EFFICIENCY
50 CLS:SCREEN 15,18:REM - CLEAR SCREEN
60 PRINT"LINE-SOURCE PROGRAM"
70 INPUT "OVEN TEMP. ";TE:REM - e.m.f. IN mV
75 TE=(SQR(1500.48+0.144*TE)-38.736)/0.072
78 PRINT "OVEN TEMP. =";TE;" C"
80 INPUT "RADIUS (mm) ";R:R=R/1000
85 REM - INITIAL VALUES OF CONDUCTIVITY AND DIFFUSIVITY
90 K=3.2:INPUT "COND. ";K
95 KS=.2:INPUT "DIFF. ";KS:KS=KS*1E-6
100 DATA 125,10,10:REM - CLOCK PERIOD WHEN HEATER OFF
110 DATA 125,10,10:REM - CLOCK PERIOD WHEN HEATER ON
120 UL=400:REM - TOTAL NO. OF SAMPLES
125 REM - V(N)=VOLTAGE, C(N)=CURRENT,T(N)=TEMPERATURE
127 REM - (ADC UNITS),VX(N)=TEMPERATURE (K), TI(N)=TIME
130 DIM V(UL+1),C(UL+1),T(UL+1)
140 DIM VX(UL),TI(UL),TL(UL)
150 GOSUB10000:REM - SET UP M/C CLOCK PERIOD TABLE
160 DOKE 4100,3332
170 A=USR(1): REM INITIALIZE PARALLEL PORTS,TIMERS -
175 REM - M/C ROUTINE AT 0D04H
180 GOSUB 1010
190 DOKE4100,3397:REM - ADDR. OF M/C READ ROUTINE
200 A=10:REM - NO. OF READINGS WITH HEATER OFF
205 REM - MAIN DATA-COLLECTION LOOP
210 FOR I=1 TO UL
220 OUT 13,0:REM - MUX ADDR. 0
230 T(I)=USR(1):REM - M/C SUBROUTINE READ
240 OUT 13,32
250 V(I)=USR(1)
260 OUT 13,48
270 C(I)=USR(A-I):REM - RELAY ON WHEN A=I
275 PRINT I;T(I);V(I);C(I)
280 NEXT
290 OUT 13,0
300 OUT8,0: REM RELAY OFF
310 REM - END OF DATA-COLLECTION ROUTINE
510 SN=38.736+0.072*TE
515 PRINT"THERMOCOUPLE SENSITIVITY=";SN;" uV/C"
520 ST=0.064/SN:REM - TEMPERATURE CONVERSION FACTOR
530 RESTORE
540 READ A,B,C,A,B,C
550 TI=A*B*C*24E-6+0.06
555 PRINT"TIMING INTERVAL=";TI;" s"
560 TJ=A*B*C*8E-6+0.01:REM - TIME OFFSET
570 A=0
580 B=0
590 T0=0
600 FOR I=1 TO 10
610 A=A+V(I)
620 B=B+C(I)
630 T0=T0+T(I)
640 NEXT
650 A=A/10:REM - V OFFSET
660 B=B/10:REM - I OFFSET
670 T0=T0/10:REM - TEMPERATURE OFFSET
```

```
680 V=0
690 C=0
695 REM - AVERAGE VOLTAGE, CURRENT
700 FOR I=11 TO UL
710 V=V+V(I)
720 C=C+C(I)
730 J=I-10
740 VX(J)=(T(I)-T0)*ST:REM - TEMP. ARRAY
750 TI(J)=(J-1)*TI+TJ:REM - TIME ARRAY
760 NEXT
770 V=V/(UL-10)-A
780 C=C/(UL-10)-B
790 RE=0.5056
800 PO=V*C*3.41333E-6/RE
810 PRINT"POWER= ";PO;" W/m"
815 PRINT"OFFS. =";T0
820 ZW=V*RE/C
830 PRINT"RES. =",ZW
1900 L1=230
1905 L2=390
1910 FOR N=L1 TO L2:REM - DISPLAY BAD POINTS
1920 D1=VX(N)-VX(N-1)
1930 IF(D1<0.04)AND(D1>0)GOTO1950
1940 PRINTN,D1
1950 NEXT
2000 REM - SIMOD ROUTINE- TO CALCULATE CONDUCTIVITY
2005 REM - AND DIFFUSIVITY BY NONLINEAR LEAST-SQUARES
2015 A=100:B=0.0001:C=05772
2030 PP-PO/(4*3.14159)
2040 FOR IT=1 TO 10
2050 S1=0:S2=0:S3=0:S4=0:S5=0
2055 D=R^2/(4*KS)
2060 FOR N=L1 TO L2
2070 X=D/TI(N):Y=X:XX=X
2100 FOR NN=2 TO A:XX=-XX*X*(NN-1)/NN^2:Y=Y+XX
2110 IF ABS(XX)<B GOTO 2150:NEXT
2150 VM=(-C-LOG(X)+Y)*PP/K:DE=VX(N)-VM
2170 V1=-VM/K:V2=PP/(K*KS)*EXP(-X)
2190 S1=S1+V1^2
2200 S2=S2+V2^2
2210 S3=S3+V1*V2
2220 S4=S4+V1*DE
2230 S5=S5+V2*DE
2240 NEXTN
2250 D0=S1*S2-S3^2
2260 D1=(S4*S2-S3*S5)/D0
2270 D2=(S5*S1-S3*S4)/D0
2280 K=K+D1
2290 KS=KS+D2
2300 PRINT K,KS
2305 IF ABS(D1)<0.001 GOTO 2320
2310 NEXT IT
2320 END
10000 REM -SUBROUTINE POKE-
10010 READ A,B,C
10020 POKE 3328,A
10030 POKE 3329,B
10040 POKE 3330,C
10050 RETURN
```

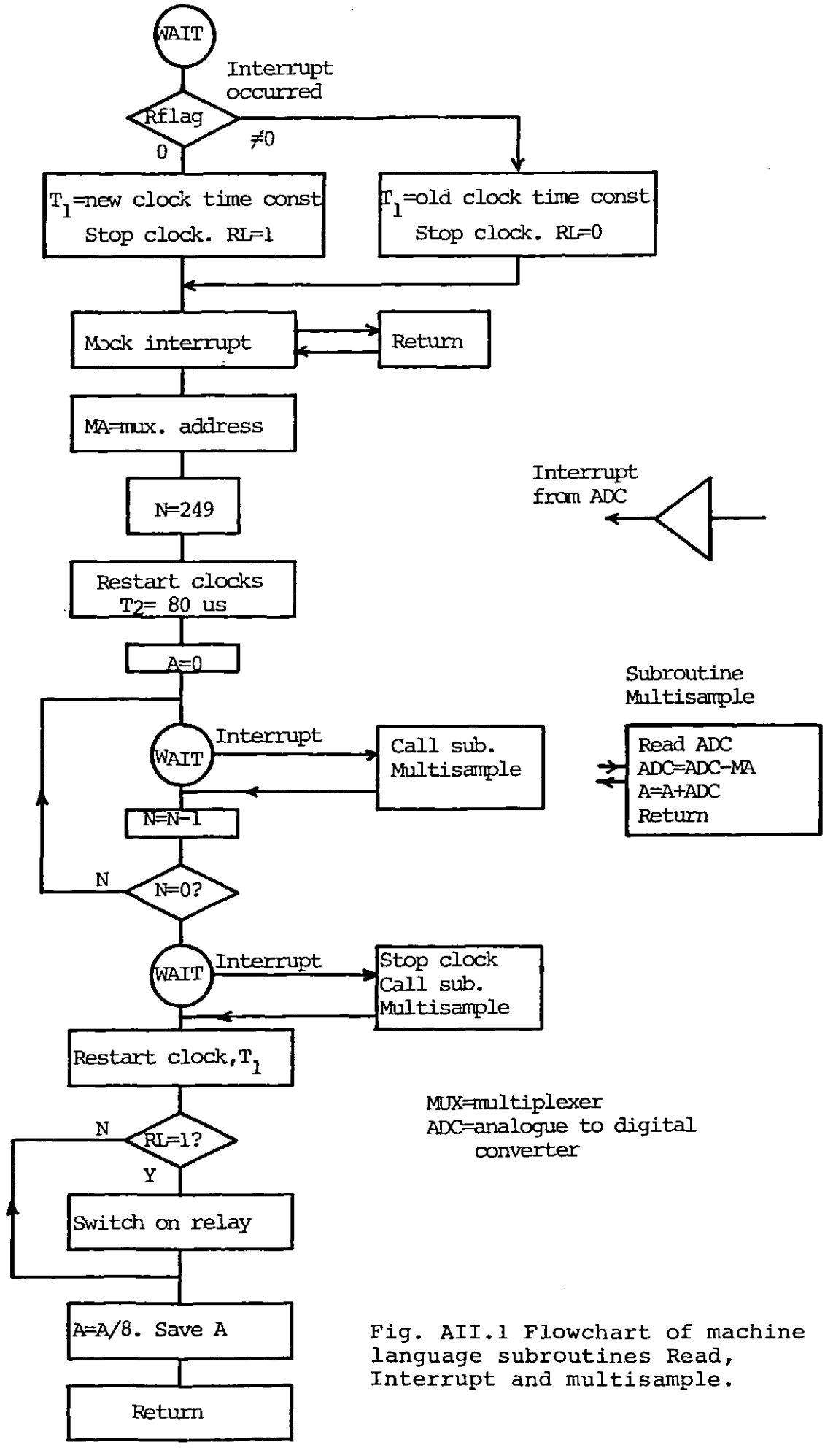

Fig. AII.1 Flowchart of machine language subroutines Read, Interrupt and multisample.

```
                ;
                ;LINE SOURCE PROGRAM - ASSEMBLER LISTING
                ;
ØDØØ                    ORG ØDØØH
ØØØC =                  PIODA EQU 12     ;PIO ADDRESSES
ØØØD =                  PIODB EQU 13
ØØØE =                  PIOCA EQU 14
ØØØF =                  PIOCB EQU 15
ØØ14 =                  RTCØ EQU 2Ø      ;TRC(CLOCKS) ADDR.
ØØ15 =                  RTC1 EQU 21
ØØ16 =                  RTC2 EQU 22
ØØ35 =                  KDEL EQU ØØ35H   ;DELAY SUBROTINE
E98B =                  DEINT EQU ØE98BH;GET ARG. FROM BASIC
FØF2 =                  SENDB EQU ØFØF2H;RET ARG. TO BASIC
                ;
ØDØØ ØØ         TCØ:   DEFB Ø           ;SPACE FOR CLOCK
ØDØ1 ØØ         TC1:   DEFB Ø           ;TIME CONSTANTS
ØDØ2 ØØ         TC2:   DEFB Ø           ;INITIAL. FROM BASIC
ØDØ3 ØØ                DEFB Ø
                ;
                ;SUBROUTINE INITIALIZE
                ;TO INITIALIZE PIO AND RTC
ØDØ4 3E4F       INIT:  LD   A,4FH       ;INITIALIZE PIO
ØDØ6 D3ØE              OUT  (PIOCA),A
ØDØ8 3ECF              LD   A,ØCFH
ØDØA D3ØF              OUT  (PIOCB),A
ØDØC 3EØF              LD   A,ØFH
ØDØE D3ØF              OUT  (PIOCB),A
ØD1Ø 3EØ7              LD   A,Ø7H       ;CLOCK MODE
ØD12 D314              OUT  (RTCØ),A
ØD14 3E47              LD   A,47H       ;COUNTER MODE
ØD16 D315              OUT  (RTC1),A
ØD18 D316              OUT  (RTC2),A    ;COUNTER MODE
ØD1A F3                DI               ;DISABLE CPU INTERRUPT
ØD1B ED5E              IM2              ;CPU INTERRUPT MODE 2
ØD1D CDC9ØD            CALL RETINT      ;FAKE RETURN FROM INT.
ØD2Ø 3EØE              LD   A,ØEH       ;CPU INT. VECTOR
ØD22 ED47              LD   I,A
ØD24 3E28              LD   A,28H       ;PIO INT. VECTOR (DUMMY)
ØD26 D3ØE              OUT  (PIOCA),A
ØD28 3E87              LD   A,87H
ØD2A D3ØE              OUT  (PIOCA),A   ;PIO INT. CONTROL WORD
ØD2C FB                EI               ;ENABLE CPU INTERRUPT
ØD2D CD3ØØ             CALL KDEL        ;WAIT ROUTINE
ØD3Ø 3E24              LD   A,24H       ;PIO READ INT. VECTOR
ØD32 D3ØE              OUT  (PIOCA),A
ØD34 3AØØØD            LD   A,(TCØ)     ;START CLOCKS
ØD37 D314              OUT  (RTCØ),A
ØD39 3AØ1ØD            LD   A,(TC1)
ØD3C D315              OUT  (RTC1),A
ØD3E 3AØ2ØD            LD   A,(TC2)
ØD41 D316              OUT  (RTC2),A
ØD43 F3                DI               ;DISABLE CPU INTERRUPT
ØD44 C9                RET
                ;
                ;SUBROUTINE READ
ØD45 CD8BE9            CALL DEINT       ;ARG. IN D,E
ØD48 3EØØ              LD   A,Ø
ØD4A BB                CP   A,E
```

```
ØD4B 2ØØ7            JR   NZ,HALT1
ØD4D BA              CP   A,D
ØD4E 2ØØ4            JR   NZ,HALT1
ØD5Ø 3E26            LD   A,26H       ;CHANGE INT. ADDR.
ØD52 D3ØE            OUT  (PIOCA),A
ØD54 FB       HALT1: EI
ØD55 76              HALT             ;WAIT FOR INTERRUPT
ØD56 C9              RET
                     ;
                     ;INTERRUPT SUBROUTINE
ØD8Ø                 ORG ØD8ØH
ØD8Ø 3EØ7            LD   A,Ø7        ;STOP CLOCKS
ØD82 D314            OUT  (RTCØ),A
ØD84 3E47            LD   A,47H
ØD86 D315            OUT  (RTC1),A
ØD88 D316            OUT  (RTC2),A
ØD8A D9              EXX              ;SAVE CLOCKS
ØD8B DB14            IN   A,(RTCØ)
ØD8D 67              LD   H,A
ØD8E DB15            IN   A,(RTC1)
ØD9Ø 6F              LD   L,A
ØD91 DB16            IN   A,(RTC2)
ØD93 47              LD   B,A
ØD94 ØE01            LD   C,1
ØD96 D9              EXX
ØD97 1827            JR   INT1
ØD99 ØØ              NOP
ØD9A ØØ              NOP
ØD9B ØØ              NOP
ØD9C ØØ              NOP
ØD9D ØØ              NOP
ØD9E ØØ              NOP
ØD9F ØØ              NOP
ØDAØ 3EØ7            LD   A,7         ;STOP CLOCKS
ØDA2 D314            OUT  (RTCØ),A
ØDA4 3E47            LD   A,47H
ØDA6 D315            OUT  (RTC1),A
ØDA8 D316            OUT  (RTC2),A
ØDAA D9              EXX              ;READ CLOCK TIME CONST.
ØDAB 3AØØØD          LD   A,(ØDØØH)
ØDAE 67              LD   H,A
ØDAF 3AØ1ØD          LD   A,(ØDØ1H)
ØDB2 6F              LD   L,A
ØDB3 3AØ2ØD          LD   A,(ØDØ2H)
ØDB6 47              LD   B,A
ØDB7 ØE00            LD   C,Ø
ØDB9 D9              EXX
ØDBA ØØ              NOP
ØDBB ØØ              NOP
ØDBC ØØ              NOP
ØDBD ØØ              NOP
ØDBE ØØ              NOP
ØDBF ØØ              NOP
ØDCØ 3E2Ø     INT1:  LD   A,2ØH       ;PIO INT. ADDRESS
ØDC2 D3ØE            OUT  (PIOCA),A   ;(MULTISAMPLE SUB.)
ØDC4 CDC9ØD          CALL RETINT      ;MOCK INT. CALL
ØDC7 18Ø2            JR   INT2
ØDC9 ED4D     RETINT:RETI
ØDCB DBØD     INT2:  IN   A,(PIODB)  ;GET MUX. ADDRESS
```

```
ØDCD 4F              LD   C,A
ØDCE CB81            RES  Ø,C          ;CLEAN MUX. ADDR.
ØDDØ CB89            RES  1,C
ØDD2 CB91            RES  2,C
ØDD4 CB99            RES  3,C
ØDD6 Ø6F9            LD   B,249        ;SET NO. OF READINGS
ØDD8 37              SCF               ;CLEAR HL
ØDD9 3F              CCF
ØDDA ED62            SBC  HL,HL
ØDDC 3EØA            LD   A,ØAH        ;CLOCKS TO 8Ø uS
ØDDE D314            OUT  (RTCØ),A
ØDEØ 3EØ1            LD   A,1
ØDE2 D315            OUT  (RTC1),A
ØDE4 D316            OUT  (RTC2),A
ØDE6 AF              XOR  A,A          ;CLEAR A
ØDE7 FB       HALT2: EI
ØDE8 76              HALT              ;WAIT FOR INTERRUPT
ØDE9 1ØFC            DJNZ HALT2
ØDEB Ø8              EX   AF,AF'
ØDEC 3E22            LD   A,22H
ØDEE D3ØE            OUT  (PIOCA),A    ;PIO INT. ADDR.
                                       ;(LAST CYCLE)
ØDFØ FB              EI
ØDF1 76              HALT
ØDF2 Ø8              EX   AF,AF'
ØDF3 D9              EXX
ØDF4 7C              LD   A,H          ;START CLOCKS
ØDF5 D314            OUT  (RTCØ),A
ØDF7 7D              LD   A,L
ØDF8 D315            OUT  (RTC1),A
ØDFA 78              LD   A,B
ØDFB D316            OUT  (RTC2),A
ØDFD CB41            BIT  Ø,C          ;RELAY ON?
ØDFF 2ØØ4            JR   NZ,INT3      ;NO
ØE01 3E01            LD   A,1          ;SWITCH RELAY ON
ØE03 D3Ø8            OUT  (Ø8H),A
ØE05 3E24     INT3:  LD   A,24H        ;PIO INT. ADDR.
ØE07 D3ØE            OUT  (PIOCA),A
ØE09 Ø8              EX   AF,AF'
ØE0A D9              EXX
ØE0B CB15            RL   L            ;RESULT / 8
ØE0D CB14            RL   H
ØE0F 17              RLA
ØE10 44              LD   B,H
ØE11 CDF2FØ          CALL SENDB        ;SEND DATA BACK TO BASIC
                                       ;ARG. IN A,B
ØE14 ED4D            RETI
                ;
                ;INTERRUPT ADDRESS TABLE
ØE2Ø            ORG ØE2ØH
ØE2Ø 3CØE            DEFW ØE3CH        ;MULTISAMPLE
ØE22 3ØØE            DEFW ØE3ØH        ;    " (CHANGE CLOCK)
ØE24 8ØØD            DEFW ØD8ØH        ;READ
ØE26 AØØD            DEFW ØDAØH        ;READ (CHANGE CLOCK)
ØE28 C9ØD            DEFW ØDC9H        ;DUMMY SUB
ØE2A ØØØØ            DEFW ØØØØ
ØE2C ØØØØ            DEFW ØØØØ
ØE2E ØØØØ            DEFW ØØØØ
                ;
```

```
                ;SUBROUTINE MULTISAMPLE
                ;FOR FAST DATA ACQUISITION (80 us)
ØE3Ø 3E07           LD   A,7          ;STOP CLOCKS
ØE32 D314           OUT  (RTCØ),A
ØE34 3E47           LD   A,47H
ØE36 D315           OUT  (RTC1),A
ØE38 D316           OUT  (RTC2),A
ØE3A Ø8             EX   AF,AF'
ØE3B ØØ             NOP
ØE3C Ø8             EX   AF,AF'       ;COLLECT ADC DATA
ØE3D DBØC           IN   A,(PIODA)    ;LO BYTE
ØE3F 5F             LD   E,A
ØE4Ø DBØD           IN   A,(PIODB)    ;HI BYTE
ØE42 A9             XOR  A,C          ;CLEAN HI BYTE
ØE43 57             LD   D,A
ØE44 Ø8             EX   AF,AF'
ØE45 19             ADD  HL,DE        ;SUM IN HL AND A
ØE46 CEØØ           ADC  A,Ø
ØE48 ED4D           RETI
```

```
E98B DEINT    ØD54 HALT1    ØDE7 HALT2    ØDØ4 INIT     ØDCØ INT1
ØDCB INT2     ØE05 INT3     ØØ35 KDEL     ØØØE PIOCA    ØØØF PIOCB
ØØØC PIODA    ØØØD PIODB    ØDC9 RETINT   ØØ14 RTCØ     ØØ15 RTC1
ØØ16 RTC2     FØF2 SENDB    ØDØØ TCØ      ØDØ1 TC1      ØDØ2 TC2

No errors
```

Appendix III

Inverse Laplace transform of $K_o \ln(p)$

To find the inverse Laplace transform of

$$F(p) = K_o(qr)\ln(\beta p) \ , \tag{1}$$

set

$$G(p) = dF(p)/dp = -r\ (4hp)^{-1/2}\ K_1(qr)\ln(\beta p)+K_o(qr)/p$$

$$= H(p) + K_o(qr)/p \ . \tag{2}$$

The second term is easily transformed. H can be written as

$$H(p) = -rp^{1/2}/(2h^{1/2})\ K_1(qr)\ \ln(\beta p)/p \tag{3}$$

and the two terms $p^{1/2}K_1$ and $\ln(p)/p$ transformed separately. From standard tables (Bateman Manuscript Project, 1954)

$$L^{-1}\{p^{1/2}K_1(qr)\} = r\ \exp(-a/t)/(4h^{1/2}t^2) \tag{4}$$

$$L^{-1}\{\ln(\beta p)/p\} = -\ln(Ct)/\beta \tag{5}$$

where $a=r^2/4h$ and $\ln C=j$.

Using the convolution theorem

$$L^{-1}\{X(p)Y(p)\} = L^{-1}\{X(p)\} * L^{-1}\{Y(p)\}, \tag{6}$$

gives

$$h(t) = L^{-1}\{H(p)\} = \int_0^t a\ \exp(-a/\tau)/(2\tau^2)\ \ln[C(t-\tau)/\beta]\ d\tau \tag{7}$$

Setting $\tau=1/x$,

$$h(t) = a/2\ \ln(C/\beta)\int_{1/t}^{\infty} e^{-ax}\ dx + a/2\int_{1/t}^{\infty} e^{-ax}\ \ln(tx-1)\ dx$$

$$- a/2\int_{1/t}^{\infty} e^{-ax}\ \ln(x)\ dx \ . \tag{8}$$

The second integral is evaluated using

$$\int_0^{\infty} e^{-x}\ \ln(x)\ dx = -j \ . \tag{9}$$

Then

$$h(t) = e^{-\alpha}/2\ \ln[t/(\alpha\beta)] - 1/2\int_{\alpha}^{\infty} e^{-x}/x\ dx, \tag{10}$$

where $\alpha=r^2/(4ht)$

and

$$g(t) = L^{-1}\{G\} = e^{-\alpha}/2 \ln[t/(\alpha\beta)] . \qquad (11)$$

Finally, using

$$\int_p^\infty G(s)\, ds = - F(p) \qquad (12)$$

and the theorem

$$L^{-1}\{\int_p^\infty G(s)ds\} = g(t)/t \qquad (13)$$

gives

$$L^{-1}\{K_o(qr)\ln(\beta p)\} = -e^{-\alpha}/(2t) \ln[t/(\alpha\beta)] . \qquad (14)$$

It is found that if the Laplace transforms of $K_o(qr)$ and $\ln(\beta p)$ in (1) are evaluated separately and the results convolved, the convolution integral diverges.

Appendix IV

TABLES OF RESULTS

The experimental results of the temperature cycles are tabulated in the following form:

Sample identifier (e.g. M2A): type of rock (first letter(s)),sample number,thermocouple number (A-D)

T Oven temperature (K)

k Conductivity ($Wm^{-1}K^{-1}$). Average of N readigs

S.D.(k) Standard deviation of conductivity

h Diffusivity (10^{-6} m^2s^{-1}). Average of N readings

S.D.(h) Standard deviation of diffusivity (10^{-6} m^2s^{-1})

R Wire electrical resistance (Ohm). Average of N readings

S.D.(R) Standard deviation of wire resistance

N Number of readings

Average resistance: mean of all wire resistances $\pm$S.D.

Average errors in k and h: mean of all standard deviations shown in table

r Thermocouple offset (mm)

l,d Sample length, diameter

In the pressure dependence tables, the results of individual runs are quoted as follows:

P Pressure (MPa)

k Conductivity ($Wm^{-1}K^{-1}$)

R Heater wire resistance (Ohm)

The sampling window for v is 80,140 s (161 points); for linear power, resistance measurements 0,140 s (390 points). Sampling rate 0.36 s.

The results are quoted to four significant figures to ease mathematical manipulation. This does not reflect their true statistical reliability.

MERRIVALE GRANITE SAMPLE M2A

T	k	SD(k)	h	SD(h)	R	SD(R)	N
304.1	3.197	0.190	2.053	0.000	3.316	0.006	2
324.6	3.182	0.052	1.990	0.106	3.336	0.003	3
348.1	3.121	0.000	1.590	0.000	3.318	0.000	1
372.0	2.890	0.038	1.540	0.099	3.328	0.007	4
400.1	2.849	0.022	1.335	0.025	3.334	0.004	3
448.8	2.788	0.000	1.258	0.000	3.340	0.000	1

LEAST-SQUARES CURVES

1/k=AT+B
A= 3.641E-04+- 6.297E-05
B= 2.005E-01+- 2.326E-02

1/h=AT+B
A= 2.296E-03+- 2.952E-04
B=-2.058E-01+- 1.091E-01

R=AT+B
A= 1.284E-04+- 6.777E-05
B= 3.282E+00+- 2.504E-02

NUMBER OF RUNS= 14
NUMBER OF POINTS= 6
AVERAGE RESISTANCE= 3.329+-0.010
AVERAGE ERROR IN k= 2.4%
AVERAGE ERROR IN h= 4.5%

r=2.85, l=120, d=75 mm

MERRIVALE GRANITE SAMPLE M2B

T	k	SD(k)	h	SD(h)	R	SD(R)	N
306.2	3.119	0.162	0.000	0.000	3.311	0.000	2
324.0	3.078	0.025	1.172	0.016	3.337	0.004	3
348.4	3.053	0.138	0.994	0.096	3.320	0.001	2
371.9	2.932	0.023	1.043	0.019	3.327	0.006	3
400.2	2.853	0.051	0.839	0.014	3.334	0.004	3

LEAST-SQUARES CURVES

1/k=AT+B
A= 3.248E-04+- 4.236E-05
B= 2.192E-01+- 1.490E-02

1/h=AT+B
A= 3.904E-03+- 1.348E-03
B=-4.072E-01+- 4.883E-01

R=AT+B
A= 1.437E-04+- 1.405E-04
B= 3.275E+00+- 4.940E-02

NUMBER OF RUNS= 13
NUMBER OF POINTS= 5
AVERAGE RESISTANCE= 3.326+-0.011
AVERAGE ERROR IN k= 2.6%
AVERAGE ERROR IN h= 3.6%

r=4.265, l=120, d=75 mm

MERRIVALE GRANITE SAMPLE M2

T	k	SD(k)	h	SD(h)	R	SD(R)	N
305.1	3.158	0.151	0.000	0.000	3.313	0.005	4
324.3	3.130	0.068	0.000	0.000	3.336	0.003	6
348.2	3.075	0.105	0.000	0.000	3.319	0.002	3
372.0	2.908	0.037	0.000	0.000	3.327	0.006	7
400.1	2.851	0.035	0.000	0.000	3.334	0.002	6
448.8	2.788	0.000	0.000	0.000	3.340	0.000	1

LEAST-SQUARES CURVES

1/k=AT+B
A= 3.248E-04+- 4.250E-05
B= 2.168E-01+- 1.571E-02

1/h=AT+B
A= 0.000E+00+- 0.000E+00
B= 0.000E+00+- 0.000E+00

R=AT+B
A= 1.398E-04+- 7.127E-05
B= 3.277E+00+- 2.634E-02

NUMBER OF RUNS= 27
NUMBER OF POINTS= 6
AVERAGE RESISTANCE= 3.328+-0.010
AVERAGE ERROR IN k= 2.6%
AVERAGE ERROR IN h= 0.0%

l=120, d=75 mm

MERRIVALE GRANITE SAMPLE M3A

T	k	SD(k)	h	SD(h)	R	SD(R)	N
304.3	3.095	0.083	0.754	0.130	3.329	0.003	4
314.3	3.082	0.025	0.860	0.031	3.335	0.001	4
324.1	3.109	0.026	0.932	0.027	3.322	0.005	3
348.8	2.978	0.025	0.702	0.025	3.336	0.001	3
372.1	2.889	0.006	0.759	0.016	3.338	0.008	3
400.0	2.799	0.060	0.653	0.024	3.341	0.001	4
448.7	2.691	0.000	0.581	0.000	3.358	0.000	1

LEAST-SQUARES CURVES

1/k=AT+B
A= 3.656E-04+- 2.489E-05
B= 2.088E-01+- 9.012E-03

1/h=AT+B
A= 3.633E-03+- 9.559E-04
B= 6.139E-02+- 3.462E-01

R=AT+B
A= 1.926E-04+- 4.315E-05
B= 3.268E+00+- 1.563E-02

NUMBER OF RUNS= 22
NUMBER OF POINTS= 7
AVERAGE RESISTANCE= 3.337+-0.011
AVERAGE ERROR IN k= 1.3%
AVERAGE ERROR IN h= 5.5%

r=1.505, l=120, d=75 mm

MERRIVALE GRANITE SAMPLE M3D

T	k	SD(k)	h	SD(h)	R	SD(R)	N
305.5	3.133	0.028	1.281	0.018	3.327	0.001	3
314.5	3.135	0.045	1.503	0.060	3.330	0.001	2
324.2	3.073	0.027	1.477	0.019	3.326	0.003	3
348.4	2.983	0.026	1.209	0.012	3.336	0.001	3
371.8	2.929	0.033	1.352	0.035	3.339	0.009	3
400.0	2.798	0.012	1.089	0.010	3.342	0.002	3

LEAST-SQUARES CURVES

1/k=AT+B
A= 4.055E-04+- 2.657E-05
B= 1.934E-01+- 9.184E-03

1/h=AT+B
A= 1.833E-03+- 9.371E-04
B= 1.374E-01+- 3.239E-01

R=AT+B
A= 1.711E-04+- 2.992E-05
B= 3.274E+00+- 1.034E-02

NUMBER OF RUNS= 17
NUMBER OF POINTS= 6
AVERAGE RESISTANCE= 3.333+-0.006
AVERAGE ERROR IN k= 0.9%
AVERAGE ERROR IN h= 1.9%

r=5.185, l=120, d=75

MERRIVALE GRANITE SAMPLE M3

T	k	SD(k)	h	SD(h)	R	SD(R)	N
304.8	3.111	0.064	0.000	0.000	3.328	0.002	7
314.4	3.100	0.039	0.000	0.000	3.333	0.003	6
324.2	3.091	0.031	0.000	0.000	3.324	0.004	6
348.6	2.981	0.023	0.000	0.000	3.336	0.001	6
371.9	2.909	0.030	0.000	0.000	3.339	0.008	6
400.0	2.799	0.044	0.000	0.000	3.342	0.001	7
448.7	2.691	0.000	0.000	0.000	3.358	0.000	1

LEAST-SQUARES CURVES

1/k=AT+B
A= 3.715E-04+- 1.648E-05
B= 2.060E-01+- 5.967E-03

1/h=AT+B
A= 0.000E+00+- 0.000E+00
B= 0.000E+00+- 0.000E+00

R=AT+B
A= 2.010E-04+- 3.245E-05
B= 3.265E+00+- 1.175E-02

NUMBER OF RUNS= 39
NUMBER OF POINTS= 7
AVERAGE RESISTANCE= 3.337+-0.011
AVERAGE ERROR IN k= 1.3%
AVERAGE ERROR IN h= 0.0%

l=120, d=75 mm

MERRIVALE GRANITE SAMPLE M5A

T	k	SD(k)	h	SD(h)	R	SD(R)	N
253.9	3.248	Ø.Ø5Ø	1.521	Ø.Ø71	3.264	Ø.ØØ1	4
274.2	3.131	Ø.Ø45	1.419	Ø.Ø62	3.267	Ø.ØØ1	6
29Ø.8	3.Ø7Ø	Ø.Ø56	1.293	Ø.128	3.262	Ø.ØØØ	3
298.2	3.Ø35	Ø.ØØ1	1.335	Ø.ØØ7	3.272	Ø.ØØ1	3
3Ø2.7	3.Ø11	Ø.ØØ3	1.314	Ø.ØØ2	3.263	Ø.ØØ1	2
322.4	2.942	Ø.Ø12	1.25Ø	Ø.Ø12	3.268	Ø.ØØ1	2
349.Ø	2.881	Ø.ØØ4	1.138	Ø.Ø59	3.272	Ø.ØØ2	2
374.8	2.785	Ø.ØØ7	1.Ø95	Ø.ØØ5	3.277	Ø.ØØ1	2
4Ø1.7	2.713	Ø.Ø26	1.Ø24	Ø.Ø21	3.282	Ø.ØØ1	2
424.6	2.677	Ø.ØØ3	Ø.977	Ø.Ø1Ø	3.284	Ø.ØØØ	2
447.7	2.61Ø	Ø.Ø11	Ø.927	Ø.Ø14	3.29Ø	Ø.ØØ1	3
469.5	2.553	Ø.Ø11	Ø.891	Ø.Ø1Ø	3.3Ø1	Ø.ØØ2	3

LEAST-SQUARES CURVES

1/k=AT+B
A= 3.726E-Ø4+- 8.348E-Ø6
B= 2.174E-Ø1+- 2.984E-Ø3

1/h=AT+B
A= 2.122E-Ø3+- 5.Ø79E-Ø5
B= 1.256E-Ø1+- 1.815E-Ø2

R=AT+B
A= 1.584E-Ø4+- 1.743E-Ø5
B= 3.22ØE+ØØ+- 6.231E-Ø3

NUMBER OF RUNS= 34
NUMBER OF POINTS= 12
AVERAGE RESISTANCE= 3.275+-Ø.Ø12
AVERAGE ERROR IN k= Ø.6%
AVERAGE ERROR IN h= 2.7%

r=2.77, l=12Ø, d=75 mm

MERRIVALE GRANITE SAMPLE M5B

T	k	SD(k)	h	SD(h)	R	SD(R)	N
302.5	3.036	0.001	1.103	0.005	3.263	0.001	2
322.3	2.944	0.020	1.061	0.031	3.268	0.002	3
349.4	2.887	0.008	1.006	0.007	3.271	0.001	2
374.0	2.787	0.001	0.938	0.003	3.276	0.001	2
401.7	2.716	0.009	0.896	0.012	3.283	0.000	2
424.2	2.682	0.006	0.864	0.009	3.284	0.000	2
447.6	2.613	0.018	0.816	0.020	3.290	0.000	2
469.1	2.540	0.000	0.779	0.001	3.302	0.002	2

LEAST-SQUARES CURVES

1/k=AT+B
A= 3.684E-04+- 1.238E-05
B= 2.191E-01+- 4.834E-03

1/h=AT+B
A= 2.245E-03+- 6.166E-05
B= 2.191E-01+- 2.407E-02

R=AT+B
A= 2.089E-04+- 1.829E-05
B= 3.199E+00+- 7.141E-03

NUMBER OF RUNS= 17
NUMBER OF POINTS= 8
AVERAGE RESISTANCE= 3.280+-0.013
AVERAGE ERROR IN k= 0.3%
AVERAGE ERROR IN h= 1.2%

r=4.255, l=120, d=75 mm

MERRIVALE GRANITE SAMPLE M5

T	k	SD(k)	h	SD(h)	R	SD(R)	N
253.9	3.248	Ø.Ø5Ø	Ø.ØØØ	Ø.ØØØ	3.264	Ø.ØØ1	4
274.2	3.131	Ø.Ø45	Ø.ØØØ	Ø.ØØØ	3.267	Ø.ØØ1	6
29Ø.8	3.Ø7Ø	Ø.Ø56	Ø.ØØØ	Ø.ØØØ	3.262	Ø.ØØØ	3
298.2	3.Ø35	Ø.ØØ1	Ø.ØØØ	Ø.ØØØ	3.272	Ø.ØØ1	3
3Ø2.6	3.Ø23	Ø.Ø15	Ø.ØØØ	Ø.ØØØ	3.263	Ø.ØØ1	4
322.3	2.943	Ø.Ø15	Ø.ØØØ	Ø.ØØØ	3.268	Ø.ØØ1	5
349.2	2.884	Ø.ØØ6	Ø.ØØØ	Ø.ØØØ	3.271	Ø.ØØ2	4
374.6	2.786	Ø.ØØ4	Ø.ØØØ	Ø.ØØØ	3.276	Ø.ØØ1	4
4Ø1.7	2.714	Ø.Ø16	Ø.ØØØ	Ø.ØØØ	3.283	Ø.ØØ1	4
424.4	2.68Ø	Ø.ØØ5	Ø.ØØØ	Ø.ØØØ	3.284	Ø.ØØØ	4
447.6	2.611	Ø.Ø12	Ø.ØØØ	Ø.ØØØ	3.29Ø	Ø.ØØ1	5
469.3	2.548	Ø.Ø11	Ø.ØØØ	Ø.ØØØ	3.3Ø1	Ø.ØØ2	5

LEAST-SQUARES CURVES

1/k=AT+B
A= 3.747E-Ø4+- 8.Ø61E-Ø6
B= 2.166E-Ø1+- 2.881E-Ø3

1/h=AT+B
A= Ø.ØØØE+ØØ+- Ø.ØØØE+ØØ
B= Ø.ØØØE+ØØ+- Ø.ØØØE+ØØ

R=AT+B
A= 1.591E-Ø4+- 1.795E-Ø5
B= 3.219E+ØØ+- 6.417E-Ø3

NUMBER OF RUNS= 51
NUMBER OF POINTS= 12
AVERAGE RESISTANCE= 3.275+-Ø.Ø12
AVERAGE ERROR IN k= Ø.7%
AVERAGE ERROR IN h= Ø.Ø%

l=12Ø, d=75 mm

MERRIVALE GRANITE SAMPLE M8B

T	k	SD(k)	h	SD(h)	R	SD(R)	N
290.8	3.162	0.068	1.256	0.040	3.277	0.002	2
302.7	3.125	0.009	1.244	0.008	3.280	0.001	3
322.3	3.066	0.019	1.202	0.018	3.285	0.006	5
349.5	2.993	0.012	1.127	0.010	3.288	0.002	3
374.5	2.900	0.018	1.047	0.017	3.292	0.001	3
401.7	2.818	0.030	0.977	0.024	3.298	0.001	4
424.4	2.766	0.007	0.925	0.003	3.299	0.001	4
447.6	2.707	0.018	0.879	0.008	3.305	0.001	3
469.5	2.613	0.016	0.818	0.008	3.317	0.003	5

LEAST-SQUARES CURVES

1/k=AT+B
A= 3.599E-04+- 1.021E-05
B= 2.103E-01+- 3.889E-03

1/h=AT+B
A= 2.387E-03+- 1.037E-04
B= 7.388E-02+- 3.947E-02

R=AT+B
A= 1.935E-04+- 1.549E-05
B= 3.221E+00+- 5.898E-03

NUMBER OF RUNS= 32
NUMBER OF POINTS= 9
AVERAGE RESISTANCE= 3.293+-0.013
AVERAGE ERROR IN k= 0.7%
AVERAGE ERROR IN h= 1.4%

r=4.915, l=120, d=75 mm

TROON GRANITE SAMPLE T9A

T	k	SD(k)	h	SD(h)	R	SD(R)	N
304.4	3.145	0.071	1.143	0.110	3.404	0.000	3
323.9	3.112	0.053	1.419	0.036	3.388	0.040	3
348.2	3.031	0.012	1.192	0.011	3.418	0.005	3
372.1	2.976	0.031	1.380	0.051	3.416	0.003	3
400.1	2.900	0.009	1.215	0.035	3.431	0.009	3

LEAST-SQUARES CURVES

1/k=AT+B
A= 2.865E-04+- 1.304E-05
B= 2.298E-01+- 4.582E-03

1/h=AT+B
A=-2.635E-04+- 1.123E-03
B= 8.854E-01+- 3.945E-01

R=AT+B
A= 3.506E-04+- 1.409E-04
B= 3.289E+00+- 4.950E-02

NUMBER OF RUNS= 15
NUMBER OF POINTS= 5
AVERAGE RESISTANCE= 3.411+-0.016
AVERAGE ERROR IN k= 1.1%
AVERAGE ERROR IN h= 3.9%

r=1.955, l=120, d=60 mm

TROON GRANITE SAMPLE T9B

T	k	SD(k)	h	SD(h)	R	SD(R)	N
305.2	3.063	0.023	0.966	0.087	3.403	0.002	3
324.1	3.120	0.000	1.158	0.000	3.411	0.000	1
348.3	2.953	0.015	0.885	0.009	3.415	0.001	3
371.8	2.922	0.064	0.970	0.048	3.431	0.024	3
400.2	2.848	0.021	0.821	0.017	3.435	0.013	3

LEAST-SQUARES CURVES

1/k=AT+B
A= 3.027E-04+- 7.053E-05
B= 2.299E-01+- 2.479E-02

1/h=AT+B
A= 2.357E-03+- 1.499E-03
B= 2.308E-01+- 5.271E-01

R=AT+B
A= 3.516E-04+- 4.493E-05
B= 3.296E+00+- 1.579E-02

NUMBER OF RUNS= 13
NUMBER OF POINTS= 5
AVERAGE RESISTANCE= 3.419+-0.014
AVERAGE ERROR IN k= 1.0%
AVERAGE ERROR IN h= 4.3%

r=3.51, l=120, d=60 mm

TROON GRANITE SAMPLE T9

T	k	SD(k)	h	SD(h)	R	SD(R)	N
304.8	3.104	0.065	0.000	0.000	3.404	0.001	6
323.9	3.114	0.043	0.000	0.000	3.394	0.035	4
348.4	2.992	0.044	0.000	0.000	3.417	0.003	6
371.9	2.949	0.054	0.000	0.000	3.424	0.017	6
400.1	2.874	0.032	0.000	0.000	3.433	0.010	6

LEAST-SQUARES CURVES

1/k=AT+B
A= 2.939E-04+- 3.943E-05
B= 2.301E-01+- 1.386E-02

1/h=AT+B
A= 0.000E+00+- 0.000E+00
B= 0.000E+00+- 0.000E+00

R=AT+B
A= 3.744E-04+- 9.889E-05
B= 3.283E+00+- 3.476E-02

NUMBER OF RUNS= 28
NUMBER OF POINTS= 5
AVERAGE RESISTANCE= 3.414+-0.016
AVERAGE ERROR IN k= 1.6%
AVERAGE ERROR IN h= 0.0%

l=120, r=60 mm

TROON GRANITE SAMPLE T1ØA

T	k	SD(k)	h	SD(h)	R	SD(R)	N
314.4	2.925	Ø.ØlØ	1.277	Ø.Ø12	3.341	Ø.ØØ2	4
324.Ø	2.889	Ø.ØlØ	1.245	Ø.Ø17	3.346	Ø.ØØl	3
348.4	2.8Ø4	Ø.Ø28	1.Ø91	Ø.Ø47	3.324	Ø.ØØl	3
372.Ø	2.8ØØ	Ø.Ø19	1.233	Ø.Ø3Ø	3.354	Ø.ØØl	3
4ØØ.1	2.7Ø7	Ø.ØlØ	1.Ø8Ø	Ø.ØØ8	3.336	Ø.ØØ5	3

LEAST-SQUARES CURVES

l/k=AT+B
A= 2.987E-Ø4+- 3.983E-Ø5
B= 2.492E-Ø1+- 1.4Ø7E-Ø2

l/h=AT+B
A= 1.311E-Ø3+- 8.185E-Ø4
B= 3.867E-Ø1+- 2.891E-Ø1

R=AT+B
A=-1.222E-Ø5+- 1.847E-Ø4
B= 3.345E+ØØ+- 6.524E-Ø2

NUMBER OF RUNS= 16
NUMBER OF POINTS= 5
AVERAGE RESISTANCE= 3.34Ø+-Ø.Ø11
AVERAGE ERROR IN k= Ø.5%
AVERAGE ERROR IN h= 2.Ø%

r=2.49, l=12Ø, d=6Ø mm

TROON GRANITE SAMPLE T11A

T	k	SD(k)	h	SD(h)	R	SD(R)	N
302.7	3.053	0.016	1.457	0.019	3.355	0.000	3
322.3	3.015	0.010	1.525	0.088	3.360	0.002	3
349.4	2.975	0.019	1.455	0.036	3.363	0.001	4
374.6	2.882	0.032	1.365	0.050	3.367	0.001	4
401.7	2.823	0.023	1.336	0.050	3.374	0.001	4
424.3	2.763	0.007	1.244	0.015	3.376	0.001	4
447.6	2.737	0.020	1.231	0.029	3.382	0.001	3
469.5	2.663	0.013	1.166	0.017	3.395	0.002	5

LEAST-SQUARES CURVES

1/k=AT+B
A= 2.878E-04+- 1.206E-05
B= 2.387E-01+- 4.710E-03

1/h=AT+B
A= 1.150E-03+- 1.306E-04
B= 3.037E-01+- 5.099E-02

R=AT+B
A= 2.121E-04+- 2.070E-05
B= 3.290E+00+- 8.083E-03

NUMBER OF RUNS= 30
NUMBER OF POINTS= 8
AVERAGE RESISTANCE= 3.372+-0.013
AVERAGE ERROR IN k= 0.6%
AVERAGE ERROR IN h= 2.7%

r=2.265, l=120, d=60 mm

TROON GRANITE SAMPLE T12A

T	k	SD(k)	h	SD(h)	R	SD(R)	N
253.4	3.008	0.039	1.364	0.020	3.346	0.008	6
266.9	3.054	0.013	1.451	0.023	3.341	0.001	3
275.6	3.025	0.029	1.444	0.045	3.342	0.001	5
298.3	3.001	0.030	1.497	0.062	3.345	0.001	7
323.4	2.838	0.045	1.358	0.074	3.362	0.007	13
370.6	2.780	0.054	1.288	0.037	3.360	0.001	8
423.6	2.622	0.009	1.171	0.014	3.371	0.001	3
468.5	2.537	0.005	1.079	0.007	3.390	0.003	3

LEAST-SQUARES CURVES

1/k=AT+B
A= 3.176E-04+- 2.276E-05
B= 2.450E-01+- 7.806E-03

1/h=AT+B
A= 1.060E-03+- 1.713E-04
B= 4.043E-01+- 5.877E-02

R=AT+B
A= 2.084E-04+- 2.680E-05
B= 3.287E+00+- 9.192E-03

NUMBER OF RUNS= 48
NUMBER OF POINTS= 8
AVERAGE RESISTANCE= 3.357+-0.017
AVERAGE ERROR IN k= 1.0%
AVERAGE ERROR IN h= 2.6%

r=4.025, l=120, d=60 mm

TROON GRANITE SAMPLE T13A

T	k	SD(k)	h	SD(h)	R	SD(R)	N
304.6	2.989	0.019	0.929	0.021	3.437	0.003	3
314.5	3.013	0.023	1.025	0.023	3.493	0.002	4
324.0	2.980	0.006	1.010	0.005	3.487	0.001	3
348.4	2.868	0.028	0.842	0.024	3.439	0.002	3
372.0	2.847	0.005	0.894	0.009	3.497	0.001	3
400.0	2.754	0.014	0.745	0.010	3.479	0.004	3

LEAST-SQUARES CURVES

1/k=AT+B
A= 3.241E-04+- 3.644E-05
B= 2.327E-01+- 1.259E-02

1/h=AT+B
A= 3.147E-03+- 9.901E-04
B= 3.293E-02+- 3.421E-01

R=AT+B
A= 2.080E-04+- 3.525E-04
B= 3.400E+00+- 1.218E-01

NUMBER OF RUNS= 19
NUMBER OF POINTS= 6
AVERAGE RESISTANCE= 3.472+-0.027
AVERAGE ERROR IN k= 0.5%
AVERAGE ERROR IN h= 1.7%

r=2.94, l=120, d=60 mm

TROON GRANITE SAMPLE T14A

T	k	SD(k)	h	SD(h)	R	SD(R)	N
305.2	3.062	0.066	1.079	0.066	3.435	0.006	3
348.4	2.887	0.048	0.958	0.053	3.450	0.002	3
400.0	2.801	0.050	0.921	0.047	3.490	0.001	4

LEAST-SQUARES CURVES

1/k=AT+B
A= 3.173E-04+- 7.203E-05
B= 2.319E-01+- 2.545E-02

1/h=AT+B
A= 1.649E-03+- 5.419E-04
B= 4.395E-01+- 1.915E-01

R=AT+B
A= 5.864E-04+- 1.223E-04
B= 3.252E+00+- 4.320E-02

NUMBER OF RUNS= 10
NUMBER OF POINTS= 3
AVERAGE RESISTANCE= 3.458+-0.028
AVERAGE ERROR IN k= 1.9%
AVERAGE ERROR IN h= 5.6%

r=3.15, l=120, d=60 mm

CORNISH SLATE SAMPLE K20

T	k	SD(k)	h	SD(h)	R	SD(R)	N
253.7	2.175	0.006	0.871	0.013	3.386	0.002	3
274.2	2.134	0.016	0.825	0.011	3.388	0.000	3
297.9	2.057	0.027	0.755	0.021	3.394	0.001	3
302.7	2.082	0.005	0.677	0.005	3.379	0.001	3
322.4	1.997	0.004	0.627	0.003	3.384	0.001	3
349.5	1.946	0.011	0.585	0.006	3.389	0.002	3
374.6	1.905	0.004	0.556	0.002	3.393	0.001	3
401.7	1.867	0.009	0.529	0.005	3.400	0.001	3
424.3	1.842	0.003	0.506	0.004	3.401	0.001	3
447.7	1.810	0.006	0.486	0.003	3.407	0.001	3
469.2	1.775	0.022	0.460	0.008	3.420	0.002	6

LEAST-SQUARES CURVES

1/k=AT+B
A= 4.806E-04+- 1.829E-05
B= 3.405E-01+- 6.636E-03

1/h=AT+B
A= 4.718E-03+- 2.592E-04
B=-1.115E-02+- 9.405E-02

R=AT+B
A= 1.389E-04+- 2.736E-05
B= 3.345E+00+- 9.926E-03

NUMBER OF RUNS= 36
NUMBER OF POINTS= 11
AVERAGE RESISTANCE= 3.395+-0.012
AVERAGE ERROR IN k= 0.5%
AVERAGE ERROR IN h= 1.1%

r=4.58, l=120, d=60 mm

HOLMAN GRANITE SAMPLE H1A

T	k	SD(k)	h	SD(h)	R	SD(R)	N
32Ø.6	2.783	Ø.Ø74	1.523	Ø.123	1.891	Ø.ØØ5	23
377.Ø	2.744	Ø.Ø91	1.44Ø	Ø.179	1.899	Ø.ØØ9	13
418.9	2.639	Ø.Ø65	1.319	Ø.Ø48	1.895	Ø.Ø1Ø	8
467.3	2.5Ø1	Ø.Ø16	1.2Ø4	Ø.Ø36	1.886	Ø.ØØØ	8
5Ø7.6	2.374	Ø.Ø27	1.Ø97	Ø.Ø4Ø	1.884	Ø.ØØ5	6
573.2	2.27Ø	Ø.Ø46	Ø.ØØØ	Ø.ØØØ	1.885	Ø.ØØ2	6

LEAST-SQUARES CURVES

1/k=AT+B
A= 3.488E-Ø4+- 3.298E-Ø5
B= 2.392E-Ø1+- 1.49ØE-Ø2

1/h=AT+B
A= 1.378E-Ø3+- 1.442E-Ø4
B= 1.939E-Ø1+- 6.1Ø8E-Ø2

R=AT+B
A=-4.739E-Ø5+- 2.332E-Ø5
B= 1.911E+ØØ+- 1.Ø53E-Ø2

NUMBER OF RUNS= 64
NUMBER OF POINTS= 6
AVERAGE RESISTANCE= 1.89Ø+-Ø.ØØ6
AVERAGE ERROR IN k= 2.Ø%
AVERAGE ERROR IN h= 6.2%

r=2.67, l=12Ø, d=6Ø mm

SOUTH AFRICAN NORITE SAMPLE N7A

T	k	SD(k)	h	SD(h)	R	SD(R)	N
253.9	2.356	Ø.Ø27	1.326	Ø.Ø45	1.988	Ø.ØØ1	4
274.5	2.32Ø	Ø.Ø16	1.277	Ø.Ø24	1.986	Ø.ØØØ	4
322.Ø	2.252	Ø.Ø17	1.155	Ø.Ø25	1.983	Ø.ØØ1	6
374.5	2.241	Ø.ØØ9	1.Ø67	Ø.Ø14	1.985	Ø.ØØ1	3
427.9	2.232	Ø.Ø17	1.Ø25	Ø.Ø2Ø	1.981	Ø.ØØ1	4
467.6	2.237	Ø.Ø14	1.ØØ5	Ø.Ø18	1.976	Ø.ØØØ	3

LEAST-SQUARES CURVES

1/k=AT+B
A= 1.Ø12E-Ø4+- 2.889E-Ø5
B= 4.Ø44E-Ø1+- 1.Ø45E-Ø2

1/h=AT+B
A= 1.164E-Ø3+- 1.156E-Ø4
B= 4.738E-Ø1+- 4.183E-Ø2

R=AT+B
A=-4.538E-Ø5+- 1.Ø65E-Ø5
B= 1.999E+ØØ+- 3.853E-Ø3

NUMBER OF RUNS= 24
NUMBER OF POINTS= 6
AVERAGE RESISTANCE= 1.983+-Ø.ØØ4
AVERAGE ERROR IN k= Ø.7%
AVERAGE ERROR IN h= 2.1%

r=3.94, l=12Ø, d=6Ø mm

FUSED SILICA SAMPLE FS4A

T	k	SD(k)	h	SD(h)	R	SD(R)	N
305.9	1.385	0.034	0.524	0.051	0.989	0.000	10
327.3	1.425	0.014	0.537	0.017	0.988	0.000	4
349.1	1.470	0.007	0.541	0.009	0.987	0.000	4
373.8	1.498	0.001	0.519	0.003	0.987	0.000	3
402.7	1.532	0.017	0.500	0.019	0.986	0.000	3
427.5	1.546	0.030	0.466	0.027	0.986	0.000	3
449.9	1.574	0.045	0.441	0.042	0.985	0.000	4
467.4	1.628	0.040	0.467	0.043	0.983	0.001	6

LEAST-SQUARES CURVES

$k=A+BT+CT^2$
A= .810044
B= 2.27493E-3
C= -1.20741E-6

$1/n=AT+B$
A= 2.344E-03+- 4.937E-04
B= 1.103E+00+- 1.934E-01

$R=AT+B$
A=-2.997E-05+- 3.972E-06
B= 9.980E-01+- 1.556E-03

NUMBER OF RUNS= 37
NUMBER OF POINTS= 8
AVERAGE RESISTANCE= 0.986+-0.002
AVERAGE ERROR IN k= 1.5%
AVERAGE ERROR IN h= 5.4%

r=2.0, l=60.13, d=64 mm

MACOR CERAMIC SAMPLE MAC4A

T	k	SD(k)	h	SD(h)	R	SD(R)	N
302.3	1.610	0.011	0.846	0.007	2.354	0.011	6
323.3	1.610	0.008	0.809	0.008	2.356	0.010	7
348.5	1.621	0.013	0.785	0.014	3.355	0.005	4
374.5	1.625	0.003	0.758	0.005	3.359	0.003	3
401.6	1.639	0.006	0.742	0.007	3.364	0.003	3
424.3	1.653	0.010	0.722	0.014	3.342	0.003	4
447.7	1.674	0.008	0.721	0.013	3.370	0.001	3
469.3	1.678	0.006	0.705	0.009	3.393	0.004	5

LEAST-SQUARES CURVES

$k=A+BT+CT^2$
A= 1.73292
B= -9.62481E-4
C= 1.82204E-6

1/h=AT+B
A= 1.356E-03+- 1.007E-04
B= 7.947E-01+- 3.934E-02

R=AT+B
A= 6.055E-03+- 2.026E-03
B= 7.716E-01+- 7.910E-01

NUMBER OF RUNS= 35
NUMBER OF POINTS= 8
AVERAGE RESISTANCE= 3.112+-0.467
AVERAGE ERROR IN k= 0.5%
AVERAGE ERROR IN h= 1.3%

r=3.0, l=120.4, d=75 mm

PRESSURE DEPENDENCE OF CONDUCTIVITY
TROON GRANITE SAMPLE T12

Temperature 297 K

P	k	R	Notes
Ø	3.499	3.362	Cycle 1: Increasing P
Ø	3.514	3.361	
Ø	3.402	3.358	
Ø	3.457	3.358	
50.Ø	3.427	3.358	
46.Ø	3.430	3.359	
46.Ø	3.432	3.357	
44.Ø	3.415	3.358	
Ø	3.450	3.360	Cycle 2: After heating to 370
Ø	3.360	3.361	K for 24 h. Increasing P
Ø	3.354	3.362	
8.Ø	3.376	3.362	
9.5	3.354	3.361	
21.5	3.387	3.361	
21.5	3.377	3.362	
31.5	3.397	3.362	
31.5	3.365	3.362	
36.5	3.415	3.360	
42.Ø	3.380	3.360	
49.5	3.410	3.362	
50.Ø	3.403	3.362	
Ø	3.327	3.364	Cycle 3: After heating to 420
Ø	3.288	3.364	K for 24 h. Increasing P
12.Ø	3.331	3.364	
11.Ø	3.260	3.363	
19.5	3.348	3.364	
22.5	3.344	3.364	
30.Ø	3.401	3.362	
30.Ø	3.364	3.363	
40.Ø	3.354	3.362	
37.Ø	3.390	3.362	
50.Ø	3.399	3.360	
46.Ø	3.401	3.361	
Ø	3.250	3.367	Cycle 4: After heating to 470
Ø	3.235	3.367	K for 24 h. Increasing P
12.Ø	3.379	3.365	
12.Ø	3.327	3.365	
23.5	3.356	3.365	
22.5	3.322	3.365	
29.5	3.356	3.363	
30.Ø	3.374	3.363	
39.5	3.399	3.363	
41.5	3.414	3.364	
46.5	3.384	3.364	
49.Ø	3.394	3.364	

P	k	R	Notes
Ø	3.342	3.365	Decreasing P
Ø	3.362	3.365	
Ø	3.37Ø	3.365	
Ø	3.368	3.365	
Ø	3.368	3.366	
Ø	3.349	3.364	
Ø	3.363	3.364	
Ø	3.375	3.364	

PRESSURE DEPENDENCE OF CONDUCTIVITY
GAVERIIGAN GRANITE SAMPLE G3

Temperature 297 K

P	k	R	Notes
Ø	3.295	2.Ø23	Cycle 1:
Ø	3.268	2.Ø23	Sample water-saturated
Ø	3.256	2.Ø23	Increasing P
Ø	3.258	2.Ø19	
26.5	3.352	2.Ø33	
24.5	3.335	2.Ø28	
48.Ø	3.368	2.Ø48	
48.Ø	3.413	2.Ø27	
Ø	3.31Ø	2.Ø18	Decreasing P
Ø	3.346	2.Ø17	
Ø	3.329	2.Ø61	Cycle 2: After heating to 37Ø
Ø	3.39Ø	2.Ø62	K for 24 h. Increasing P
Ø	3.34Ø	2.Ø63	
Ø	3.343	2.Ø63	
25.Ø	3.348	2.1Ø9	
27.Ø	3.333	2.137	
48.Ø	3.464	2.167	
48.Ø	3.381	2.196	
Ø	3.295	2.182	Decreasing P
Ø	3.294	2.179	
Ø	3.3Ø4	2.178	
47.Ø	3.33Ø	2.196	Increasing P
Ø	3.241	1.943	Cycle 3: After heating to 45Ø
Ø	3.226	1.943	K for 24 h. Increasing P
25.5	3.333	1.942	
25.5	3.341	1.941	
5Ø.Ø	3.365	1.94Ø	
49.Ø	3.372	1.941	
Ø	3.286	1.942	Decreasing P
Ø	3.288	1.942	

Conductivities were corrected for heater resistance variations.

Appendix V

DESCRIPTIONS OF ROCK SAMPLES

The following description was kindly supplied by J.R. Hawkes of the Institute of Geological Sciences.

Generalized description of SW England granites.

The principal constituents are orthoclase, quartz, plagioclase and a fairly iron-rich biotite mica. The mineral contents are broadly as follows:

	Approximate volume per cent
Alkali feldspar	40
Quartz	32
Plagioclase	20
Biotite	6
Others	2

Most samples contain a little muscovite which may partly replace biotite, and/or some of the plagioclase. Finely divided sericitic muscovite is a common feature in large numbers of plagioclase crystals. Another alteration product of biotite is chlorite. Except where the granite has been greisened and/or affected by vein mineralization, the amounts of muscovite and chlorite are small; generally of the order of 1 or 2 per cent. Since they replace either biotite or plagioclase, the approximate modal figures shown above would be modified only by these small percentage amounts.

Accessory minerals account on average for a further two per cent. The chief of these is commonly schorlite tourmaline; others include apatite, zircon, ilmenite,

uraninite, rutile, fluorite and monazite. Monazite occurs along with the rutile and fluorite in biotite and is responsible for numerous "pleochroic haloes" of α-partical damage seen in such crystals.

The granites have a hypidiomorphic texture. Mean matrix grain sizes are of the order of 1-3 mm and most specimens contain scatterd quartz and orthoclase megacrysts. The orthoclase megacrysts range in size from 5 mm up to nearly 200 mm. Their mean size varies considerably according to location within the granite intrusions.

Holman Mine granite.

(Carnmenellis. National Grid Reference SW 6580 3670).

Troon granite.

(Carnmenellis. National Grid Reference SW 6570 3677).

Granite at this locality has the general characteristics outlined above. Orthoclase megacrysts account for 5-10 per cent of the rock with a mean size of around 20 mm.

Merrivale Granite.

(Dartmoor. National Grid Reference SX 5660 7350).

The generalized description again fits, but muscovite replaces more of the biotite than is the usual case, forming about 3 per cent of the rock by volume. Orthoclase megacrysts account for only 1-5 per cent, with a mean size a little over 20 mm.

The visual difference between the ordinary and heated samples may be due to oxidation of dispersed limonite present chiefly in feldspathic areas.

Gaveriggan granite.

(St. Austell. National Grid Reference SW 9316 5916. 317 m depth).

A finer-grained type of granite commonly developed near the margins of the St. Austell main intrusion. Mineralogically similar to that given in the general description, but with a mean matrix grain size nearer to 1 mm. Orthoclase megacrysts scarce.

Simplified description of the Killas specimen.

(From Gaveriggan, St.austell. National Grid Reference SW 9316 5916).

Microscope examination of this very fine-grained material indicates that quartz, sericite and chlorite are the chief constituents. Accessory minerals include tourmaline and a dispersed opaque material that may be ilmenite. There is a good deal of limonitic staining in the rock, particularly near the quartz-sericite-plagioclase veins that cut this particular sample.

International Conference on

geothermal energy

Florence, Italy: May 11-14, 1982

PAPER J6

A LINE-SOURCE METHOD FOR THE MEASUREMENT OF TEMPERATURE DEPENDENCE OF THERMAL CONDUCTIVITY OF ROCKS

A. Sartori and M.F. Francis

Imperial College, U.K.

Summary

Hot Dry Rock technology requires a thorough knowledge of the variation of the thermal properties of crystalline rocks up to depths of the order of five kilometres. This paper describes a transient method for fast laboratory measurements of the temperature dependence of the thermal conductivity of rock and other poor conductors. A cylindrical sample of rock is heated by a thin axial heater wire, the resulting temperature increase at points within the rock being monitored by a microcomputer. A new line-source solution to the heat equation, derived to take into account contact resistance between heater and specimen, is fitted to the experimental temperature data to yield values of conductivity and diffusivity in just a few minutes. Conductivity values of several Cornish granite specimens are presented in the temperature range 250-470 K. They exhibit a T^{-1} dependence on temperature as expected for this type of rock, and show good agreement with conductivities from a steady-state apparatus at room temperature and with published results for similar types of rock over the whole temperature range. The method yields absolute values of conductivity, thus requiring no calibrations. The absolute accuracy is estimated at better than 2.5%, which compares favourably with that obtainable with steady-state methods. Sample preparation is simple and not critical. The method described is well suited for measurements of the variation of thermal properties with pressure.

Held at the Centro Affari Firenze
Organised and sponsored by
BHRA Fluid Engineering, Cranfield, Bedford MK43 0AJ, England
in conjunction with Ente Nazionale per l'Energia Elettrica (ENEL), Italy

NOMENCLATURE

b	radius of cement cylinder
d	radius of sample
h	thermal diffusivity of rock
h_1	thermal diffusivity of cement
I_n	modified Bessel function of the first kind and order n
k	thermal conductivity of rock
k_1	thermal conductivity of cement
K_n	modified Bessel function of the second kind and order n
p	Laplace transformation variable
q	$=(p/h)^{\frac{1}{2}}$
q_1	$=(p/h_1)^{\frac{1}{2}}$
Q	line-source linear power
r	radial coordinate in cylindrical polar coordinates
t	time
T	absolute temperature
v	rock temperature
$\bar{v}$	$=L\{v\}$, Laplace transform of temperature
α	$=r^2/4ht$
β	$=b^2e^{2\gamma}/4h$
γ	Euler's constant $=0.5772$

1. INTRODUCTION

Hot Dry Rock (HDR) technology requires detailed information on the dependence of the thermal properties of crustal crystalline rocks on temperature, pressure, moisture and mineralogy up to depths of the order of 5 km. For a given regional heat flow, the crustal thermal conductivity controls the geothermal gradient. Thus the drilling depth required to reach a rock at a given temperature will vary in direct proportion to the mean thermal conductivity of the formation (Ref. 1). Fig. 1 shows a plot of an extrapolated temperature profile based on observed surface values of conductivity with two different published values for the temperature dependence of conductivity of Westerly and Rockport granites (Ref. 2). It will be noticed that for temperatures of 450-500 K (180-230°C), the drilling depth is critically dependent on the temperature dependence of the conductivity. Because drilling costs increase exponentially with depth (Ref. 3), thermal conductivity characteristics are important in determining costs associated with developing a reservoir. In the performance modelling of a HDR reservoir, the thermal conductivity of the formation will strongly affect the lifetime of the reservoir and the maximum rate of heat extraction (Ref. 3).

The objective of this work was to test a simple line-source transient method for fast measurements of rock thermal conductivities over a range of ordinary and elevated temperatures. Cylindrical samples of rock, which had reached temperature equilibrium in an oven, were heated by means of an axial heater wire (Ref. 4). The resulting transient temperature increase at points inside the rock was interpreted to yield values of conductivity and diffusivity in just a few minutes. In the development of the method an attempt was made to overcome some of the shortcomings of the well-established divided-bar and needle-probe methods (Ref. 5), such as the need for carefully characterized reference materials over a wide temperature range. In the present method, absolute values of the thermal parameters are obtained, thus no calibrations being required. The expensive drilling of long and narrow holes in the samples needed to accommodate needle-probes was avoided, and the reduced thickness of the heater contributed to minimizing contact-resistance effects. Although all the samples tested to date were cylindrical, their shape is not critical, which simplifies preparation. The experiments described in this paper were performed at atmospheric pressure, but extension to a range of high pressures does not require major modifications and will be undertaken in the near future.

2. THEORETICAL ANALYSIS

2.1. Line-source solution with contact resistance.

It became apparent early in the investigation that the existing mathematical treatments of the needle-probe method (Ref. 6) could not be adapted to the line-source method. Unlike needle-probes, the heaters used in the present work were very thin and could be treated as ideal line sources. A new mathematical treatment was developed to account for the contact resistance of a thin layer of cement between heater and rock. An analytical solution to the equation of conduction of heat was sought in cylindrical polar coordinates using the following boundary conditions:

1) An infinitely long line-source along the z-axis emits heat at a constant rate Q per unit length into an infinite mass of rock of conductivity k and diffusivity h for t>0. The initial temperature is zero everywhere.

2) The cement is modelled as a solid cylinder of radius b concentric with the heater, having conductivity k_1 and diffusivity h_1. This is only an approximation to the actual shape of the cement, but it simplifies the solution.

It is shown in Appendix I that an approximate solution in the region $r \geq b$ is given by

$$v = \frac{Q}{4\pi k}\left\{\int_{\alpha}^{\infty} e^{-u}/u \; du + \frac{b^2}{4k}\left(k/h - k_1/h_1\right)\frac{e^{-\alpha}}{t}\ln(t/\alpha\beta) - \frac{b^2}{4}\left(1/h_1 - 1/h\right)\frac{e^{-\alpha}}{t}\right\}. \quad (1)$$

If b=0, or $k=k_1$, $h=h_1$, the second and third terms vanish, and Eq. (1) reduces to a simpler line source solution already in the literature (Ref. 7). The approximation

is valid for $b^2/ht<<1$ and arbitrary r, which can be regarded as either the large time solution, or a case of a thin layer of cement. Both these requirements were satisfied in the present experiments. A more complex solution which takes into account a thin layer of cement between two semi-cylinders of rock is now under study.

2.2. Application of theoretical results.

The parameters k (thermal conductivity) and h (thermal diffusivity) can be calculated from a least-squares fit of equation (1) to a graph of temperature against elapsed time assuming approximate values of the thermal properties and thickness of the cement. In the present study, however, the following simpler approach was adopted which is more suitable for fast data reduction by microcomputer. Equation (1) can be rewritten as

$$v = v_I + v_E \tag{2}$$

where v_I is the first term, corresponding to the ideal solution for no contact resistance, and v_E is the sum of the second and third terms, the "error" caused by the contact resistance. A graph of v_E/v_I versus ht/b^2 is plotted in Fig. 2 for various values of r/b and typical values of conductivity and diffusivity for a granite sample/fire cement contact. The value t_{MIN} of the time for which the term v_E becomes negligible can be determined from this graph. At larger times, boundary effects at the surfaces of the samples become important. Using Laplace transformation techniques, the effects of keeping the surfaces of finite cylinders of radius d at zero temperature were calculated to be less than 1% when $d/r \geq 10$ and $ht/d^2 \leq 0.3$ for a sample of radius d. For a typical granite sample with $k=1.5\times10^{-6}$ m^2s^{-1}, $d=3\times10^{-2}$m, the minimum and maximum acquisition times t_{MIN} and t_{MAX} are of the order of 60-80 and 150 s respectively.

An iterative nonlinear least-squares method due to Box (Ref. 8) was used to fit v_I to the experimental temperatures over the range $t_{MIN} < t < t_{MAX}$ to obtain the parameters k and h. The number of iterations is not strongly dependent on the initial values of k and h chosen and convergence to the final values is fast. The well-known logarithmic approximation (Ref. 7) to the exponential integral in Eq. (1) was not used here as the requirement $r^2/ht<<1$ for the approximation to hold was not satisfied to the desired accuracy. The consequent increased complexity of the calculations was offset by the availability of a microcomputer for the fast computations of the nonlinear least-squares routines. A better accuracy could thus be obtained than in previous methods.

3. LINE SOURCE APPARATUS

3.1. Apparatus description.

The preparation of the samples involved cutting the rock into cylinders 90 to 120 mm long and 60 to 75 mm in diameter. Each cylinder was then cut longitudinally into two halves, thin grooves were scribed into one half of the cylinder to accommodate a copper-constantan thermocouple and an axial constantan heater wire (diameter 0.2 mm), at a separation of 1 to 4 mm. The other half of the sample was cemented back on with hot-cure epoxy resin or fire cement (Fig. 3). The small diameter of the thermocouple wires (0.12 mm) and their position parallel to the heater reduce conductive heat losses along the wires. Also, the leads lie roughly parallel to equithermal planes in this arrangement, thereby reducing the distortion of the temperature field within the rock. The cold junction of the thermocouple was placed in an aluminium block within the oven (Fig. 4) and had a short time temperature stability similar to that of the oven (0.1 K). This allowed the differential temperature between sample and oven to be measured directly and independently of oven temperature. High temperature cables were welded to the ends of the heaters for current supply with separate cables for potentiometric measurement of power input. Typical power inputs were of the order of 30 to 40 W/m, with a time stability of about 0.1% in each individual experiment. The absolute accuracy of the temperature measurements is not critical in this type of experiment, but the sensitivity of a thermocouple at a given temperature has a direct effect on the results. Thermocouple sensitivity was determined by calibration of several random thermocouples from the same batch of wire as that used in the conductivity measurements. The standard deviation was found to be less than 1% of the average sensitivity. The reference

thermometer was a platinum resistance thermometer calibrated by the National Physical Laboratory to an accuracy of 0.01 K.

Amplification of the dynamic microvolt-level signals required a low-noise (1.0 μV peak-to-peak between 0.01 and 10 Hz) instrumentation amplifier followed by a low-pass filter with a cutoff frequency of 10 Hz and a slope of -24 dB/octave for reduction of mains-borne electromagnetic interference and high frequency noise. This frequency response was a compromise between the requirement for fast response and noise reduction. The delay introduced by the filter was calculated to be 0.2 s for 1% accuracy, with a negligible effect on the final values of conductivity. A 12-bit multichannel data acquisition system provided the interface with an 8-bit microcomputer, which performed all the control functions, data acquisition and data reduction. After power to the heater was switched on, the heater voltage and current and the sample temperature were digitized at 0.3 intervals for about 140 s. A digital filter provided a further improvement in the signal-to-noise ratio: each signal was sampled 250 times in rapid succession and averaged over a 20 ms time interval, thus eliminating periodic signals with a period of 20 ms such as 50 Hz electromagnetic interference and its harmonics. The resolution of the system was 2 mK with drift of less than 0.1 K in a 150 s interval. On this apparatus, the determination of the thermal parameters took 2 to 6 minutes depending on the number of iterations required in the least-squares routine. Temperature equilibrium to better than 0.1 K between oven and a rock sample was established in 8-12 hours. Measurements of the same sample could be repeated at 60-90 minutes intervals. Up to twenty samples were measured in rapid succession in the same oven.

3.2 Discussion of errors.

Mis-positioning of the voltage-sensing leads by just ±1 mm can lead to a systematic error of ± 1% in the conductivity values. This was taken as the average error in the power measurements. The sensitivity tolerance of the thermocouples introduced an uncertainty of about ± 1% in the slope of the temperature versus time curve, and hence in the final results. The approximations of the mathematical model are probably responsible for a further uncertainty of ± 0.5% in the results, bringing the total error to about ± 2.5%. Careful preparation of the samples is paramount in keeping this figure low. One sample was measured, dismantled, provided with a new heater and thermocouple, and re-measured, with a negligible shift in the measured conductivity. All the measurements were repeated at least three times at the same temperature as a check on the repeatability. It was found that temperature fluctuations in the oven and reference junction caused a scatter in the results. This was a function of the temperature increases measured and therefore of the thermal conductivity, varying between a fraction of a percent at $k=1.6 Wm^{-1}K^{-1}$ to 1-2% at k=3.2.

4. RESULTS

A set of samples representative of the main geological suites found in S.W. England and one ceramic sample were investigated. A set of comparative measurements of a zero porosity Corning Macor 9658 ceramic sample were performed to test the absolute accuracy of the method. Table 1 shows that at room temperature the measured conductivity was in good agreement with that obtained with a divided-bar apparatus and with those reported by Bloomer (Ref. 9) and measured by a divided-bar and by a needle-probe calibrated against a silica glass standard. The good agreement with the values from the divided-bar apparatus was explained by the fact that the samples were cut from the same block of material. In Fig. 5 the conductivity is shown to increase with increasing temperature, as expected from this type of material. Each point in Fig. 5 is an average of three to seven experimental values. The standard deviations of the individual readings, represented by the error bars in Fig. 5 suggest good repeatability. One of the values at 325K (52°C) was obtained after dismantling and reassembling the sample with a new heater and thermocouple, and shows a negligible change in the measured conductivity. The smoothed curve is a second-order polynomial in T. Other curves could have been fitted to the experimental points with as good a justification, but the differences would be negligible within the temperature range of the experiments. The smoothed conductivity values are tabulated in Table 2, which also shows smoothed conductivity values for ten selected rock samples. Samples M2B through M8B were taken from the same block of granite from Merrivale (Dartmoor), samples T9 through T14A are granites from Troon (Carnmenellis), K20 is a Cornish slate

sample, and MAC-4A is the ceramic sample. The sample-to-sample conductivity differences are not entirely due to experimental errors, and are probably real differences due to the large grain size of the samples. Fig. 6 shows a comparison of smoothed results for two representative Cornish samples (M5 and M8B) from this study with the results by other workers on similar rocks. The thermal conductivity exhibits a 1/T variation consistent with the anharmonic phonon scattering region. The divided-bar measurement at room temperature was performed on a water-saturated sample, which probably accounts for the marginally higher thermal conductivity. A description of the rock samples is given in Appendix III.

5. CONCLUSIONS

The results obtained confirm the accuracy of the theoretical predictions and demonstrate the validity of this method of rapid thermal conductivity measurement. Fig. 6 highlights the marked temperature-dependent decrease in thermal conductivity for rocks likely to be encountered in a HDR reservoir. The statistical reliability was enhanced by the large size of the data sample obtainable using modern digital techniques. The same apparatus used in the experimental measurements described may be easily employed in conjunction with a needle-probe for the thermal conductivity determination of unconsolidated or soft sediments. The use of more realistic boundary conditions, though increasing the computational complexity, allowed an improved repeatability. One of the advantages of the method is that the calculated thermal conductivity is less dependent on the time window over which the rock temperature is sampled than with methods involving less rigorous analyses. A possible further application would involve measurements over a range of elevated temperatures and pressures and including the effects of more realistic levels of water-saturation such as are likely to be encountered in a typical HDR reservoir.

6. ACKNOWLEDGEMENTS

The authors wish to acknowledge the assistance of A. Chayne, A. Jackson, J. Robinson, N. Bassett, K. Jason and L. Zapalowski in the experimental work. Sincere thanks are accorded also to the Geology Department of Imperial College for the use of their facilities, Mr. J. Wheildon and Dr. A. Thomas-Betts for much helpful advice and the SEG for financial assistance to one of the authors.

7. REFERENCES

1. Wheildon, J., Francis, M.F., Ellis, J.R.L. and Thomas-Betts, A.: "Exploration and interpretation of the S.W. England geothermal anomaly". In: Commission of the European Communities. Proceedings of the second international seminar on the results of the EC geothermal energy research (Strasbourg, France: Mar. 4-6, 1980), pp. 456-465.

2. Birch, F. and Clark, H.: "The thermal conductivity of rocks and its dependence upon temperature and composition", 1,2. Am. J. Sci., 238, pp.529-558, 613-635.

3. Sibbitt, W.I. Dodson, J.G. and Tester, J.W.: Thermal conductivity of crystalline rocks associated with energy extraction from hot dry rock geothermal systems". J. geophys. Res., 24, B3, 1979, pp.1117-1124.

4. Cull, J.P.: "Thermal conductivity probes for rapid measurements in rocks". J. Phys. E, 7, 1974, pp.771-774.

5. Tye, R.P. (Ed.): "Thermal conductivity". Vols. 1 and 2, Academic, New York, 1969.

6. Von Herzen, R. and Maxwell, A.E.: "The measurement of thermal conductivity of deep-sea sediments by a needle-probe method". J. geophys. Res., 64, 10, 1959, pp. 1557-1563.

7. Carslaw, H.S. and Jaeger, J.C.: "Conduction of heat in solids" (2nd Ed.).Oxford University Press, 1959, pp. 261-262.

8. Box, G.E.P.: "Fitting empirical data". Ann. N.Y. Acad. Sci., 86, 3, 1960, pp. 792-816.

9. Bloomer, J.R.: "Methods of geothermal exploration with application to the Hampshire basin". Ph.D. Thesis, University of Oxford, 1980, p. 108.

10. Ref. 7: pp. 297-304.

11. Blackwell, J.H.: "A transient flow method for determination of thermal constants of insulating materials in bulk". J. appl. Phys., 25, 137, 1954, pp. 137-144.

12. California Institute of Technology: "Tables of integral transforms". McGraw-Hill, 1954, pp. 227-301.

APPENDIX I

The general form of the one-dimensional heat equation in cylindrical polars is

$$\frac{\partial^2 v}{\partial r^2} + \frac{1}{r}\frac{\partial v}{\partial r} = \frac{1}{h}\frac{\partial v}{\partial t} \tag{1}$$

Laplace transformation (Ref.10) with respect to time of this equation and of the boundary conditions in the two media gives the subsidiary equations

$$\frac{d^2\bar{v}_1}{dr^2} + \frac{1}{r}\frac{d\bar{v}_1}{dr} = q_1^2\bar{v}_1 \qquad \text{for } 0<r<b \tag{2}$$

$$\frac{d^2\bar{v}}{dr^2} + \frac{1}{r}\frac{d\bar{v}}{dr} = q^2\bar{v} \qquad \text{For } r\geq b \tag{3}$$

subject to the boundary conditions

$$\bar{v}_1 = \bar{v} \quad \text{and} \quad k_1\frac{d\bar{v}_1}{dr} = k\frac{d\bar{v}}{dr} \qquad \text{at } r=b, \tag{4}$$

$$\lim_{r\to 0}\left(r\frac{d\bar{v}_1}{dr}\right) = -Q/(2\Pi k_1 p) \tag{5}$$

and $\bar{v}$ bounded as $r\to\infty$, (6)

where $\bar{v}$ is defined as $\bar{v}(p)=L\{v(t)\}$. (7)

Equation (5) is the boundary condition at the wire.

Solution of Eqs. (2) and (3) subject to (4), (5) and (6) gives

$$\bar{v} = \frac{Q}{2\Pi b}\frac{K_o(qr)}{p\Delta} \tag{8}$$

where

$$\Delta = q_1 k_1 K_o(qb) I_1(q_1 b) + qkK_1(qb) I_o(q_1 b) , \tag{9}$$

with a similar expression for $\bar{v}_1$.

An exact solution for v can be derived from Eq. (8) by the inversion theorem of the Laplace transformation. For the purposes of the present work, however, an approximate expression for small values of (qb) and arbitrary r suffices (Ref. 11). Approximating the modified Bessel functions in Δ by the first few terms of series in ascending powers of p, we obtain

$$\Delta = \frac{k}{b}\{1+Ap\ln(\beta p) + Bp + O(p^2)\} \tag{10}$$

where $A=b^2(k/h-k_1/h_1)/4k$, $B=b^2(1/h_1-1/h)/4$, and $O(p^2)$ represents the terms of order p^2 and higher. Making use of the binomial theorem to find Δ^{-1},

$$\bar{v} = \frac{QK_o(qr)}{2\Pi pk} \{1-Ap \ln(\beta p)-Bp\} \tag{11}$$

to the first order in p.
v is found by applying the inversion theorem to each term of the series. From standard tables (Ref. 12),

$$L^{-1} \{K_o(qr)/p\} = \frac{1}{2}\int_{\alpha}^{\infty} e^{-u}/u \, du \tag{12}$$

$$L^{-1} \{K_o(qr)\} = e^{-\alpha}/2t \tag{13}$$

for the first and last terms respectively. In Appendix II, the inverse Laplace transform of the middle term is shown to be

$$L^{-1}\{K_o(qr)\ln(\beta p)\} = -e^{-\alpha}\ln(t/\alpha\beta)/2t. \tag{14}$$

The final result (equation (1) of section 2) follows from (11), (12), (13) and (14).

APPENDIX II

To find the inverse Laplace transform of

$$F(p)=K_o(qr) \ln(\beta p), \tag{1}$$

set $$G(p)= \frac{dF}{dp} = -(r/2h^{\frac{1}{2}}p^{\frac{1}{2}}) K_1(qr) \ln(\beta p)+K_o(qr)/p = H(p)+K_o(qr)/p \tag{2}$$

The second term is easily transformed.

H can be written as

$$H=-\{rp^{\frac{1}{2}}/(2h^{\frac{1}{2}})K_1(qr)\} \{\ln(\beta p)/p\} \tag{3}$$

and the two terms transformed separately.

From standard tables (Ref. 12),

$$L^{-1}\{p^{\frac{1}{2}} K_1(qr)\} = re^{-a/t}/(4h^{\frac{1}{2}}t^2) \tag{4}$$

$$L^{-1}\{\ln(\beta p)/p\} = -\ln(ct)/\beta \tag{5}$$

where $a=r^2/4h$ and $\ln c = \gamma$.

Using the convolution theorem of the Laplace transform

$$L^{-1}\{X(p)Y(p)\} = L^{-1}\{X(p)\} * L^{-1}\{Y(p)\}$$

gives

$$h(t)=L^{-1}\{H(p)\} = \int_0^t ae^{-a/\tau}/(2\tau^2) \ln\{c(t-\tau)/\beta\}d\tau \tag{6}$$

This integral is evaluated using

$$\int_0^{\infty} e^{-x} \ln x \, dx = -\gamma .$$

Then, from (2) and (6),

$$g(t)=L^{-1}\{G(p)\} = e^{-\alpha}\ln(t/\alpha\beta)/2. \tag{7}$$

Finally, using

$$\int_p^{\infty} G(s) \, ds = -F(p) \tag{8}$$

and the theorem

$$L^{-1}\{\int_p^\infty G(s)ds\} = g(t)/t, \tag{9}$$

we obtain

$$L^{-1}\{K_o(qr)\ \ln(\beta p)\ \} = -e^{-\alpha}\ln(t/\alpha\beta)/2t. \tag{10}$$

It is found that if the Laplace transforms of $K_o(qr)$ and $\ln(\beta p)$ are evaluated separately and the results convolved, the convolution integral diverges.

APPENDIX III

Descriptions of rock samples from Cornwall.

The principal constituents of the granite samples are orthoclase, quartz, plagioclase and a fairly iron-rich biotite mica. The mineral contents are broadly as follows (in percentage volumes):

Alkali feldspar	40
Quartz	32
Plagioclase	20
Biotite	6
Others	2

The granites have a hypiodiomorphic texture. Mean matrix grain sizes are of the order of 1-3 mm. In the Troon samples (T9A-T14A) orthoclase megacrysts account for 5-10% of the rock with a mean size of around 20 mm. In the Merrivale samples (M2B-M8B), muscovite partly replacing biotite forms about 3% of the rock by volume. Orthoclase megacrysts account for only 1-5%, with a mean size a little over 20 mm. In the Cornish slate specimen (K20), the chief constituents are quartz, sericite and chlorite. Accessory minerals include tourmaline and ilmenite, with a good deal of limonitic staining in the rock, particularly near the quartz-sericite-plagioclase veins which cut this particular sample (J.R. Hawkes, pers. comm.).

TABLE 1. Comparison of conductivity results of ceramic (Macor) at 298 K (25°C).

Source of data	No. of readings	Conductivity ($Wm^{-1}K^{-1}$)
Line-source (at 302 K - 29°C)	6	1.610±0.011
Divided-bar	24	1.605±0.003
Needle-probe (Bloomer, Ref. 9)	39	1.62±0.03
Divided-bar (Bloomer, Ref. 9)	13	1.59±0.04

TABLE 2. Conductivity results. Smoothed values, in $Wm^{-1}K^{-1}$.

Sample number	250K	300K	350K	400K	450K	470K
M2B	-	3.165	2.998	2.878	-	-
M3	-	3.166	2.965	2.813	2.696	-
M5	3.278	3.029	2.851	2.717	2.613	2.578
M8B	-	3.149	2.956	2.812	2.699	2.661
T9	-	3.198	3.010	2.869	-	-
T10A	-	2.955	2.828	2.733	-	-
T11A	-	3.090	2.933	2.816	2.724	2.693
T13A	-	3.066	2.890	2.759	-	-
T14A	-	3.068	2.908	2.788	-	-
K20	2.207	2.056	1.949	1.869	1.806	1.784
MAC-4A	-	1.608	1.619	1.639	1.669	1.683

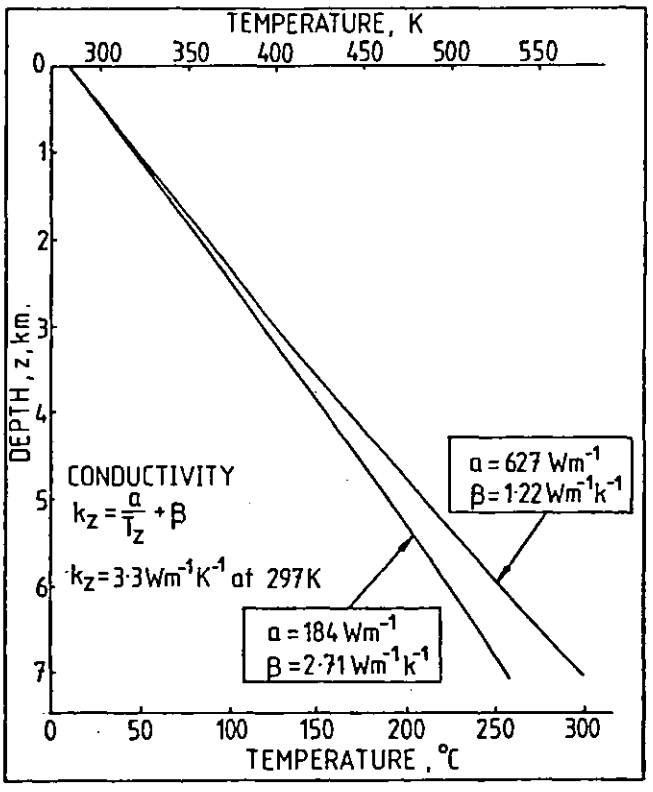

Figure 1. Crustal temperature profiles. Extrapolations are based on surface values of heat flow and thermal conductivity. Temperature dependence values of conductivity are from Birch and Clark (Ref.2).

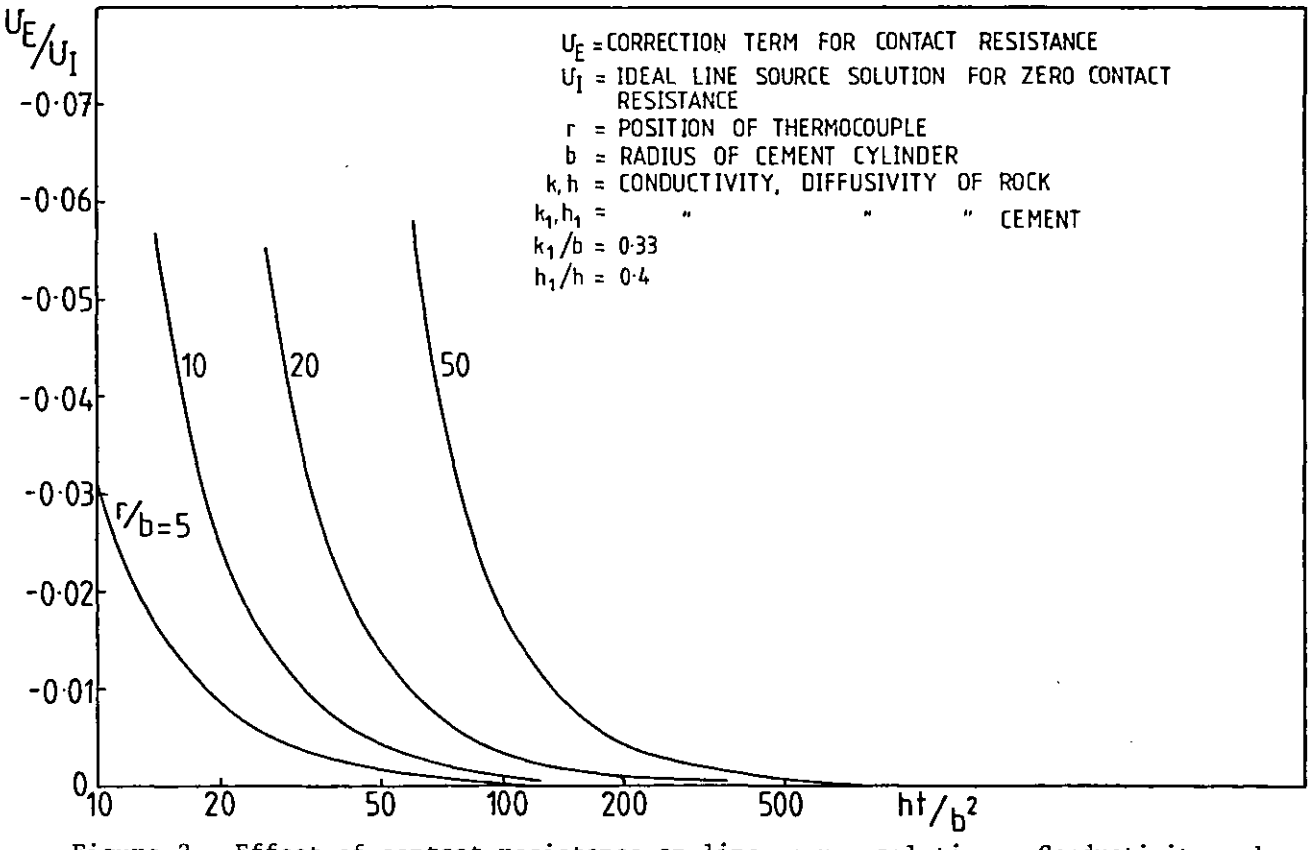

Figure 2. Effect of contact resistance on line-source solution. Conductivity and diffusivity values are for a typical granite/fire cement interface.

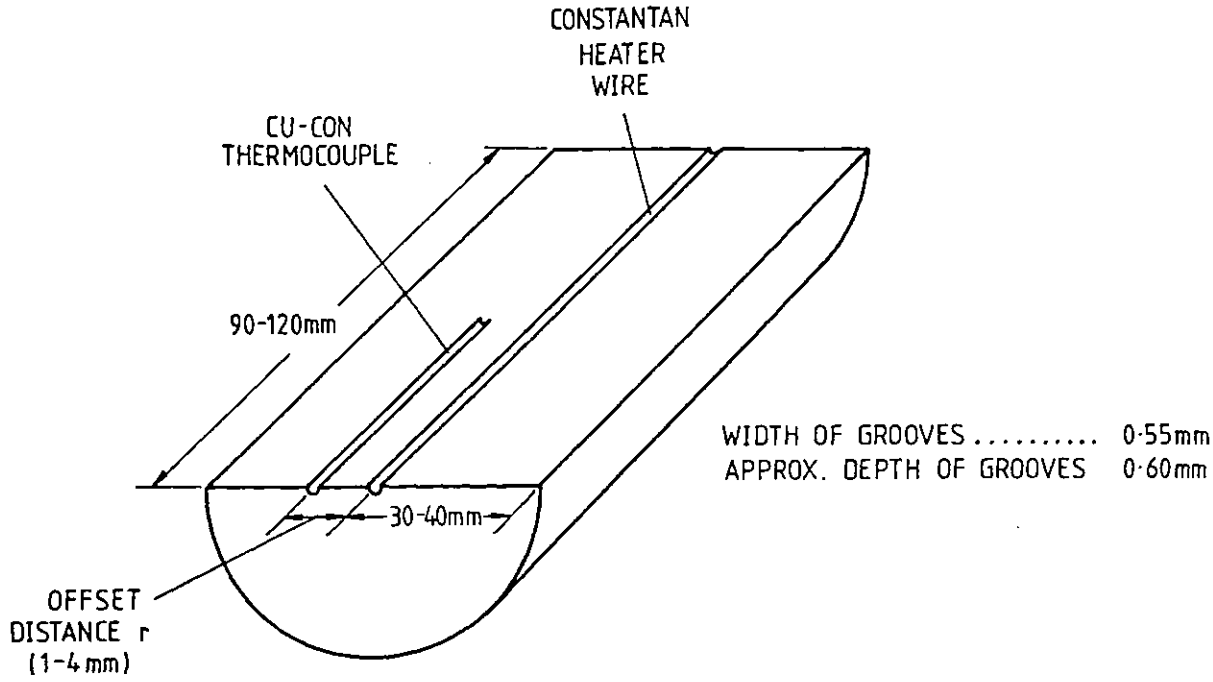

Figure 3. Section of a rock sample. The thermocouple junction is located at the mid-point of the sample. The grooves are scribed with a rotating diamond wheel. The top semicylinder of rock (not grooved) is cemented back on after emplacement of thermocouple and heater.

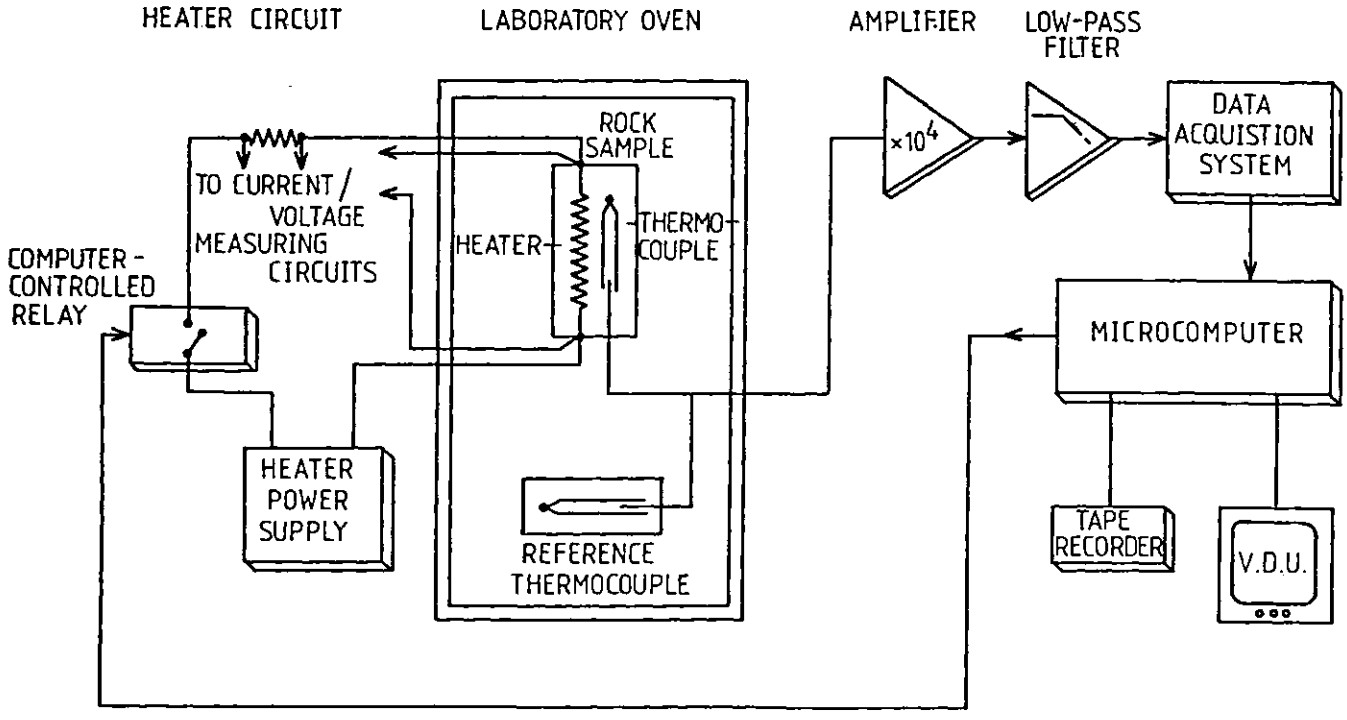

Figure 4. Line source apparatus. Only one sample is shown for simplicity. Appropriate switching of the power and thermocouple lines allowed measurements of up to twenty samples in rapid succession. Data were recorded on magnetic tape for further analysis.

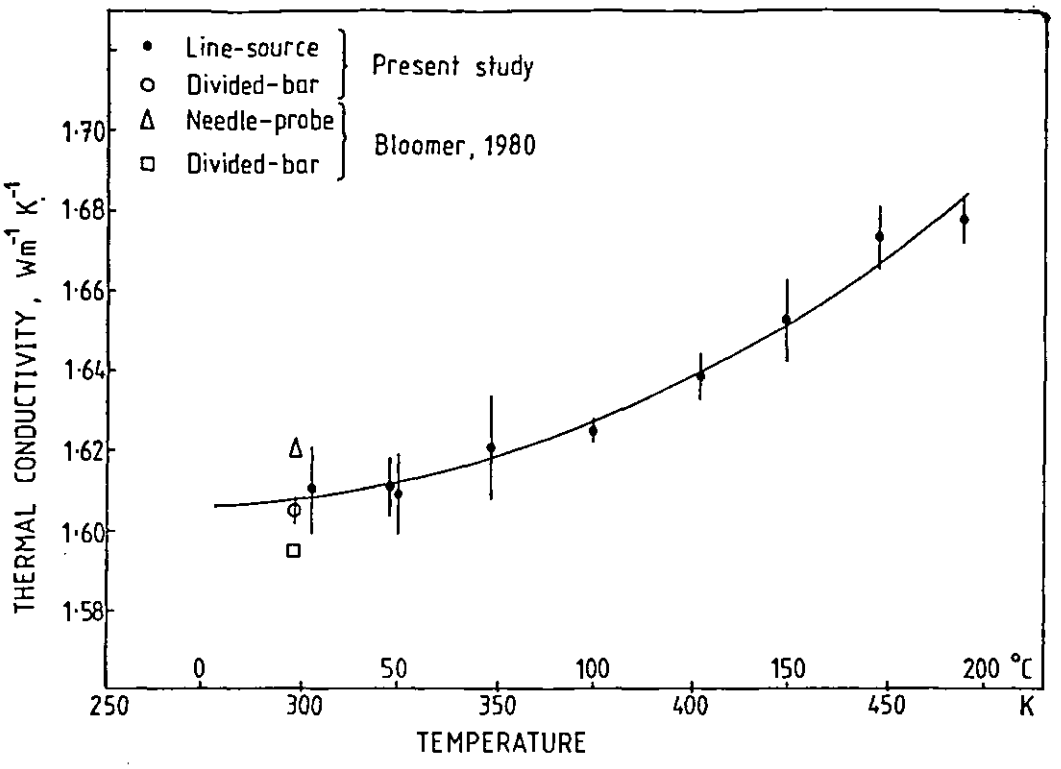

Figure 5. Thermal conductivity of ceramic (Macor). Points shown are averages of several experimental values. The error bars indicate the standard deviations of the individual readings. The curve is a second-order polynomial in T.

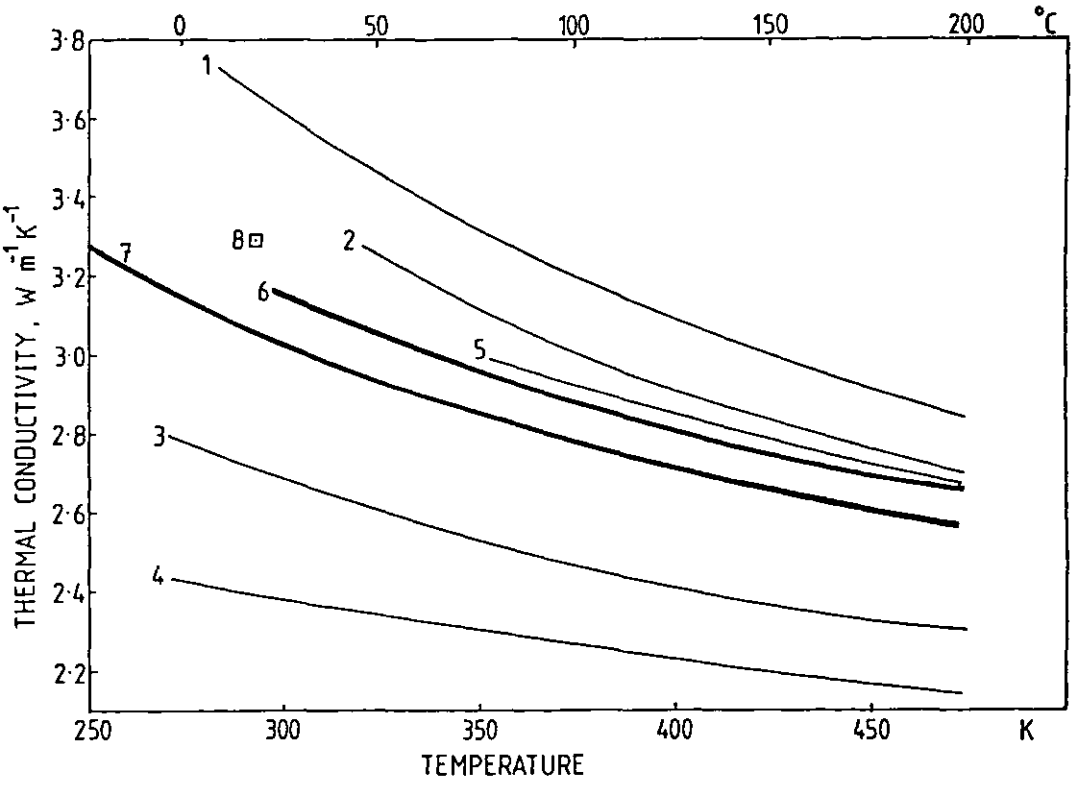

Figure 6. Comparison of thermal conductivity of granites. Curves are smoothed values. Lines 6 and 7 and point 8 refer to the present study.
1, 2: Rockport granite (Birch and Clark, Ref.2). 3: Barre granite (Ref.2). 4: Westerly granite (Ref.2). 5: Cornish granite (Dodson, pers. comm.). 6: Merrivale granite, sample M8B. 7: Merrivale granite, sample M5. 8: Merrivale granite, divided-bar measurement.

REFERENCES

ADAM, A.M. (1983) A micro-computer controlled thermal conductivity measurement using the line-source method. D.I.C. Dissertation, Imperial College, London.

ANALOG DEVICES, INC. (1975) Data acquisition products catalog.

ANALOG DEVICES, INC. (1979) Data acquisition products catalog supplement.

ARAKAWA, Y. and A. SHINOHARA (1980) Quick thermal conductivity meter. European Geophysical Society Meeting, Budapest, August 1980.

BASSETT, N.D. (1979) Temperature dependence of thermal conductivity in granites. M.Sc. Thesis, Imperial College, London.

BATEMAN MANUSCRIPT PROJECT. CALIFORNIA INSTITUTE OF TECHNOLOGY (1954) Tables of integral transforms, vol.1, McGraw-Hill.

BAXTER, W.G., D.E. CONNER and W. RAUCH (1969) Life testing small diameter thermocouples as a function of thermal cycling. General Electric Co., GEMP-737.

BECK, A. (1957) A steady-state method for the rapid measurement of the thermal conductivity of rock. J. **scient. Instrum., 34:** pp.186-189.

BECK, A.E., F.M. ANGLIN and J.H. SASS (1971) Analysis of heat flow data - in situ thermal conductivity measurements. **Can. J. Earth Sci., 8:** pp.1-19.

BERMAN, R. (1976) Thermal conduction in solids. Oxford University Press.

BEYER, W.H. (1981) Standard mathematical tables, 26th ed. CRC Press, Boca Raton, Florida.

BIRCH, F. and H. CLARK (1940) The thermal conductivity of rocks and its dependence upon temperature and composition, 1, 2. **Am. J. Sci., 238:** pp.529-558, 613-635.

BLACKWELL, J.H. (1953) Radial-axial heat flow in regions bounded internally by circular cylinders. **Can. J. Phys., 31:** pp.472-479.

BLACKWELL, J.H. (1954) A transient flow method for determination of thermal costants of insulating materials in bulk. **J. appl. Phys., 25:** pp.137-144.

BLACKWELL, J.H. (1956) The axial-flow error in the thermal conductivity probe. **Can. J. Phys.,34:** pp.412-417.

BLOOMER, J.R. (1980) Methods of geothermal exploration with application to the Hampshire basin. D. Phil. Thesis, Oxford University.

BLOOMER, J.R. and J. WARD (1979) A semi-automatic field apparatus for the measurement of thermal conductivities of sedimentary rocks. **J. Phys. E: Sci. Instrum., 12:** pp.1033-1035.

BOX, G.E.P. (1960) Fitting empirical data. **Ann. N.Y. Acad. Sci., 86:** pp.792-816.

CALLAWAY, J. and H.C. VON BAYER (1960) Effect of point imperfections on lattice thermal conductivity. **Phys. Rev., 120:** p.1149.

CAMERON, A. (1981) A model of the line source method of thermal conductivity measurement. Imperial College, London.

CARSLAW, H.S. and J.C. JAEGER (1940) Some two-dimensional problems in conduction of heat with circular symmetry.

Proc. London math. Soc., 46: p.361.

CARSLAW, H.S. and J.C. JAEGER (1959) Conduction of heat in solids, 2nd ed. Clarendon Press,Oxford.

CHAYNE, A. (1978) The temperature dependence of the thermal conductivity of geological materials. Imperial College, London.

CLARK, H. (1941) The effects of simple compression and wetting on the thermal conductivity of rocks. **Trans. Am. geophys. Union, II:** pp.543-544.

CLARK, S.P. (1957) Radiative heat transfer in the earth's mantle. **Trans. Am. geophys. Union, 38:** 931.

CULL, J.P. (1974) Thermal conductivity probes for rapid measurements in rock. **J. Phys. E: Sci. Instrum.,7:** 771.

CULL, J.P. (1975) The pressure and temperature dependence of thermal conductivity within the earth. Ph.D. Thesis, University of Oxford.

DARYANANI, G. (1976) Principles of active network synthesis and design. J. Wiley & Sons.

DODSON, J.G. (1979) Thermal conductivity of granite from Cornwall, England. Priv. Comm.

FRANCIS, M.F. (1980) Investigation of the South West England thermal anomaly zone. Ph.D. Thesis, Imperial College, London.

HAWKES, J.R. (1981) Description of samples from Cornwall. Pers. Comm.

INTERSIL (1982) Semiconductors data book.

JACKSON, A. (1978) Temperature dependence of thermal conductivity in granite samples taken from South West England. M.Sc. Thesis, Imperial College, 1978.

JAEGER, J.C. (1955) Conduction of heat in a solid in contact with a thin layer of a good conductor. **Quart. Jl. Mech. appl. Math., 8:** p.101.

JAEGER, J.C. (1956) Conduction of heat in an infinite region bounded internally by a circular cylinder of a perfect conductor. **Aust. J. Phys.,9:** pp.167-179.

JAEGER, J.C. (1958) The measurement of thermal conductivity and diffusivity with cylindrical probes. **Trans. Am. geophys. Union, 39:** pp.708-710.

JAEGER, J.C. and J.H. SASS (1964) A line source method for measuring the thermal conductivity and diffusivity of cylindrical specimens of rock and other poor conductors. **Brit. J. appl. Phys., 15:** pp.1187-1194.

JASON, K. (1980) The temperature dependence of thermal conductivity of rock. Imperial College, London.

JENKINS, G.M. and D.G. WATTS (1968) Spectral analysis and its applications. Holden-Day Publ.

KANAMORI, H., N. FUJII and H. MIZUTANI (1968) Thermal diffusivity measurement of rock-forming minerals from 300 to 1100 K. **J. geophys. Res., 73:** pp.595-605.

KAPPELMEYER, O. and R. HAENEL (1974) Geothermics with special reference to application. Geoexploration Monographs, Gebrueder Borntraeger, Berlin.

KAYE, G.W.C. and T.H. LABY (1948) Tables of physical and chemical constants. 10th ed. Longmans Green and Co., London.

KIEFFER, S.W., I.C. GETTING and G.C. KENNEDY (1976) Experimental determination of the pressure dependence of the thermal diffusivity of teflon, sodium chloride, quartz and silica. **J. geophys. Res. 81:** pp.3018-3024.

KING, R. (1966) Electrical Noise. Chapman & Hall Publ.

KINZIE, P.A. (1973) Thermocouple temperature measurement. Wiley and Sons, London.

KITTEL, C. (1949) Interpretation of the thermal conductivity of glasses. **Phys. Rev.,75:** p.972.

KITTEL, C. (1976) Introduction to solid state physics. 5th ed. J. Wiley Publ., London.

LEE, T.C. (1982) Estimation of formation temperature and thermal property from dissipation of heat generated by drilling. **Geophysics, 47:** pp.1577-1589.

McLACHLAN, N.W. (1955) Bessel functions for engineers. Oxford University Press.

MILLMAN, J. and C.C. HALKIAS (1972) Integrated electronics: analog and digital circuits and systems. McGraw-Hill, London.

MOONEY, D.L. and R.G. STEG (1969) Pressure dependence of the thermal conductivity and ultrasonic attenuation of non-metallic solids. **High Temp.- High Press., 1:** p.237.

MOSCHYTZ, G.S. (1975) Linear integrated networks - Design. Van Nostrand Reinhold Co.

MOTCHENBACHER, C.D. and F.C. FITCHEN (1973) Low-noise electronic design. Wiley & Sons Publ.

MURPHY, H.D. and R.G. LAWTON (1977) Downhole measurements of thermal conductivity in geothermal reservoirs. 1977 Energy Technology Conference, Houston, Texas.

RATCLIFFE, E.H. (1959) Thermal conductivities of fused and crystalline quartz. **Brit. J. appl. Phys., 10:** pp.22-25.

RATCLIFFE, E.H. (1963) A survey of most probable values for the thermal conductivities of glasses between about -150

and 100 °C, including new data on twenty-two glasses and a working formula for the calculation of conductivity from composition. **Glass. Technol., 4:** pp.113-128.

RISKIN, J.R. (1979) A user's guide to IC instrumentation amplifiers. Analog Devices Application Note.

ROBERTSON, E.C., R. RASPET, J.H. SWARTZ and M.E. LILLARD (1966) Properties of thermistors used in geothermal investigations. **Bull. U.S. Geol. Surv., 1203-B.**

ROBINSON, J. (1979) The temperature dependence of thermal conductivity in granite. Imperial College, London.

ROESER, W.F. and A.I. DAHL (1938) Reference tables for iron-constantan and copper-constantan thermocouples.**J. Res. natn. Bur. Stand. (US), 20:** p.337.

ROESER, W.F. and S.T. LONBERGER (1958) Methods of testing thermocouples and thermocouple materials. **J. Res. natn. Bur. Stand. (US), 14:** p.239.

ROSENBERG, H.M. (1975) The solid state. Clarendon Press, Oxford.

ROUFUSSE, M.C. and P.G. KLEMENS (1974) Lattice thermal conductivity of minerals at high temperatures. **J. geophys. Res., 79:** p.703.

SACHSE, H.B. (1975) Semiconducting temperature sensors and their applications. Wiley and Sons, London.

SARTORI, A. and M.F. FRANCIS (1982) A line-source method for the measurement of temperature dependence of thermal conductivity of rocks. International conference on geothermal energy, Florence, May 1982.

SCOTT, R.W., J.A. FOUNTAIN and E.A. WEST (1973) A comparison of two transient methods of measuring conductivity of particulate samples. **Rev. Scient.**

Instrum., 44: pp.1058-1063.

SIBBITT, W.L., J.G. DODSON and J.W. TESTER (1979) Thermal conductivity of crystalline rocks associated with energy extraction from hot dry rock geothermal systems. **J. geophys. Res., 84:** pp.1117-1124.

SLACK, G.A. (1977) In Solid State Physics (Eds. H. Eherenreich, F. Satz and D. Turnbull). Academic Press, New York.

TAUB, T. and D. SCHILLING (1977) Digital integrated electronics. McGraw-Hill, London.

TYE, R.P. (1969) Thermal conductivity, vol. 1 and 2. Academic Press, London & New York.

VAN DER HELD, E.F.M. and F.G. VAN DRUNEN (1949) A method of measuring the thermal conductivity of liquids. **Physica XV:** pp.865-881.

VAN DER HELD, E.F.M., J. HARDEBOL and J. KALSHOVEN (1953) On the measurement of the thermal conductivity of liquids by a non-stationary method. **Physica XIX:** pp.208-216.

VON HERZEN, R. and A.E. MAXWELL (1959) The measurement of thermal conductivity of deep sea sediments by a needle-probe method. **J. geophys. Res., 64:** p.1557.

WALSH, J.B. (1965) The effect of cracks on the compressibility of rocks. **J. geophys. Res., 70:** pp.381-389.

WALSH, J.B. and E.R. DECKER (1966) Effect of pressure and saturating fluid on the thermal conductivity of compact rock. **J. geophys. Res., 71:** pp.3053-3061.

WATSON, G.N. (1952) A treatise on the theory of Bessel functions, 2nd. ed. Cambridge University Press.

WHEILDON, J., M.F. FRANCIS, J.R.L. ELLIS and A. THOMAS-BETTS (1980) Exploration and interpretation of the S.W. England thermal anomaly. Commission of the European Communities second international seminar on the results of the EC Geothermal Energy Research. March, 1980.

WOODSIDE, W. and J.H. MESSMER (1961) Thermal conductivity of porous media: II. Consolidated rocks. **J. appl. Phys., 32:** pp. 1699-1706.

ZAPALOWSKI, L. (1980) Determination of thermal conductivities using the line source method. Imperial College, London.